Catalytic Conversion of Biomass-Derived Polyols to Value-Added Chemicals: Catalysis and Kinetics

Xin Jin

Submitted to the graduate degree program in Chemical & Petroleum Engineering and the Graduate Faculty of the University of Kansas School of Engineering in partial fulfillment of the requirements for the degree of Doctor of Philosophy

Chairperson: Raghunath V. Chaudhari

Bala Subramaniam

Laurence Weatherley

Aaron Scurto

Shenqiang Ren

Date Defended: 03-13-2014

The Dissertation Committee for Xin Jin certifies
that this is the approval version of the following dissertation:

Catalytic Conversion of Biomass-Derived Polyols to Value-Added Chemicals: Catalysis and Kinetics

_____

Chairperson: Raghunath V. Chaudhari

Date approved:

Abstract

Replacing fossil-based feedstocks with biomass to produce renewable fuels and chemicals is one of the major sustainability challenges facing human society. In this context, catalytic upgrading of non-food bio-derived polyols, including glycerol, erythritol, xylitol, sorbitol and mannitol, on heterogeneous catalysts attracts increasing attentions, because it will provide alternative routes for the production of fuels and chemicals. However, several issues are plaguing current technologies: (a) high oxygen contents in these $C_{3\sim6}$ polyols demand several difficult steps of deoxygenation, which require elevated reaction temperature (T = 220~300 ^{o}C) and high operating pressure of hydrogen; (b) conversion under such harsh conditions involving multi-phase, multi-step and multi-component reactions results in low selectivity towards desired products, loss of large quantities of carbon to less valuable wastes and (c) fast deactivation of catalysts due to poor intrinsic activity and stability.

The present work successfully demonstrates that, by rational design of multi-functional metal-based catalytic systems, conversion of various biopolyols to valuable megaton everyday chemicals, such as 1,2-propanediol, ethylene glycol, lactic acid and alcohols, can occur in one pot process under significantly milder reaction conditions with improved efficiency.

Detailed investigation on C-C/C-O cleavage revealed possible reaction pathways and mechanism of polyols on metal based catalysts. Therefore design of multi-

functional metal catalysts was achieved. It was for the first time to demonstrate that Cu catalysts exhibited an excellent C-C and C-O cleavage activity by immobilizing active sites for retro-aldol, dehydration and hydrogenolysis on one single catalyst, leading to >98% yield towards liquid products. Studies on reaction parameters and surface characterization enabled the establishment of activity-performance correlation for polyol conversion.

Further, by rational combining hydrogen generation and hydrogenolysis functionality to one metal catalyst, conversion of biopolyols occurred at only 115~160 ^{o}C even without adding external hydrogen, with 95%+ overall atom efficiency. Detailed kinetic modeling revealed that the reaction potential for hydrogen generation and hydrogenolysis is much lower on Pt/C catalyst. This is a significant advancement compared with conventional technologies. In collaboration with material scientists, mono and bimetallic Cu-based catalysts with predominant active [111] surface plane were also designed *via* lattice match engineering. The Cu nanocatalysts exhibited more than five-fold enhancement in activity compared to traditional ones and selectivity promoted dehydrogenation thus lactic acid was favorably formed in our system.

The methodologies and achieved results in this work will provide insights on the further studies on rational design of biomass conversion as well as other chemical processes.

DEDICATED TO

My wife Wenjuan and my son Kevin

Acknowledgement

I would like to express my sincere gratitude to my advisor Dr. Raghunath V. Chaudhari, distinguished professor of chemical and petroleum engineering for his guidance, support and encouragement during my PhD life. His optimistic, enthusiastic, and meticulously hard-working attitude has been and will always be inspiring me during the course of my scientific life. He is not only my advisor. In my mind, he is also my partner and close friend.

I would like to acknowledge Dr. Bala Subramaniam, director of Center for Environmentally Beneficial Catalysis (CEBC) and my committee member, for his valuable suggestions and critical review for my research and teaching. I would like to thank Dr. Shenqiang Ren, my project collaborator and committee member, for his insightful advice during our collaboration. I would also like to thank my committee members Dr. Laurence Weatherley and Dr. Aaron Scurto for their precious time and wonderful inputs during my comprehensive examination and my research work.

I would like to thank my friends and colleagues from the CEBC family, Dr. Debdut Roy for his patient guidance when I started my research work, Dr. Haijun Wan for his wonderful suggestions to my experiment design, Dr. Juan Bravo for his insightful advice on catalyst design and characterization, Dr. Fenghui Niu for kind assistance in instrumentation and Ms. Arely Torres for her warm-hearted help with my experimental work.

Also I want to gratefully acknowledge Dr. Claudia Bode and Dr. Darryl Fahey for their patient guidance and wonderful ideas for my research work, particularly on the preparation of research posters. I want to thank Dr. Christopher Lyon for the detailed instructions for my poster preparation and my comprehensive exam.

To Dr. William Kirk Snavely, Mr. Ed Atchison, Ms. Nancy Crispy, Ms. Rhonda Partridge, Dr. Zhuanzhuan (Shirley) Xie, Dr. Meng Li, Ms. Qing Pan, Mr. Steve Tang, Mr. Dupeng Liu, Mr. Xiang Xu, Mr. Pengjun Gu for their kind help during my Ph.D life in the University of Kansas. It would not have been such a wonderful experience without them.

I also want to thank Mr. Alan Walker for his help in manufacturing PTFE materials for my experiments, Dr. Prem Thapa for his timely help with catalyst characterization, Ms. Carol Miner, Dr. Karen Nordheden and Dr. Marylee Southard for their nice suggestions during my Ph.D program.

I would like to thank my parents for their unconditional love for my higher level education. Thanks to my wife Wenjuan’s patience and faith throughout my PhD and my son Kevin’s entry in my life.

Table of Contents

List of Figures

Chapter 1

Chapter 2

Chapter 3

Chapter 4

Chapter 5

List of Schemes

Chapter 1

Chapter 2

Chapter 3

Chapter 4

Chapter 5

List of Tables

Chapter 1

Chapter 2

Chapter 3

Chapter 4

Chapter 5

Chapter 1 Catalytic Conversion of Biomass-Derived Polyols to High Value Chemicals: Challenges and Opportunities

1. Biomass as a renewable resource for fuels and chemicals

Although the world oil production is expected to increase[1] continuously, according to recent reports, the percentage increase in production rates of crude oil (CO in Figure 1) and natural gas liquid (NGL in Figure 1) has passed the peak (4.97% in 2004[2]) and predicted to decrease in the follow decades. Three important issues are associated with the large-scale utilization of fossil fuels: availability, global warming and uneven geographical distribution of reserves.[3]

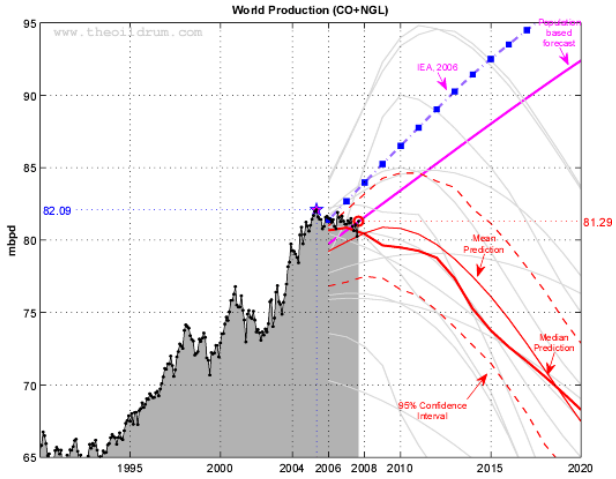

Figure 1. World production of crude oil (CO) and natural gas liquid (NGL)[2]

In order to solve the issues brought by the depletion of the fossil fuels resources, people are trying to find alternative energy resources. Potential alternatives should have the following properties: (a) sufficient volumes to replace

petroleum/coals in current energy production system, (b) well distributed or widely available around the world, (c) renewable and not contributing to the accumulation of greenhouse gases in the atmosphere.[4] In this respect, biomass is the only feedstock that meets the requirements for local/worldwide demands for fuels and chemicals. Therefore, conversion of biomass based feedstocks to value-added products will undoubtedly alleviate our dependence on conventional fossil sources.

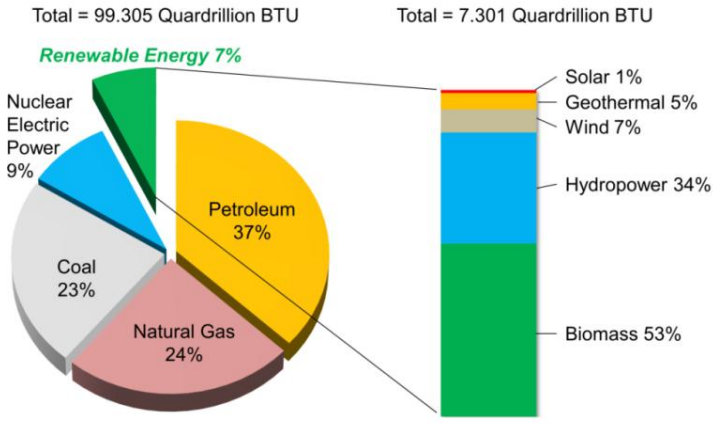

Figure 2. U.S. Energy composition in 2008

Biomass represents an important section in energy security for the United States,[5] as seen from Figure 2. Biomass such as lignocellulosic materials consist of large fraction of cellulose and hemicellulose (75~90w%) and lignin (10~25w%).[6] Considering the fact that large amounts of cellulosic biomass are available for saccharification to fermentable sugars, there is a strong motivation to develop commercial processes that generate various products with high volumes and low prices. Currently, the only successful way of using cellulosic biomass is enzymatic hydrolysis to make the feedstock more compatible with

enzymatic catalysts, which could produce bio-based ethanol (EtOH), for example.[7] The estimated cost is shown in Figure 3 [from National Renewable Energy Laboratory (NERL)].[8] The major cost for the conversion of cellulosic biomass is the use of enzyme catalysts, which consist of almost 40% of the costs and result in complex downstream separation processes.

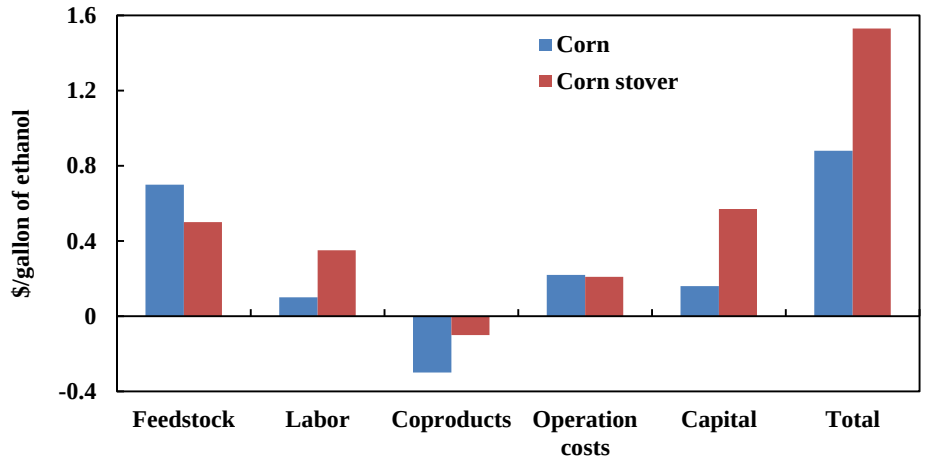

Figure 3. Cost components in production of fuel EtOH from corn and corn stover[8]

At present, approximately 17% of high volume products derived from petroleum are classified as chemicals, which provide basic raw materials for the need of almost the whole human society, such as food additives, containers, detergents and various other everyday products.[6] If these chemicals can be produced from renewable carbon sources, it would significantly reduce the dependence on petroleum and also have a positive environmental impact. The biocatalysts have been extensively used for chemical production. However, similar to the case of fuel production, these routes for biomass conversion encounter issues such as low productivity, high sensitivity to process

parameters (*e.g.* temperature, pH values), expensive feedstock treatment and compatibility with various biomass resources. Typical examples such as sugars-to-1,3-PDO,[9-11] sugars-to-lactic acid,[12] and inulin-to-difructose anhydride have been discussed in previous reports.[6]

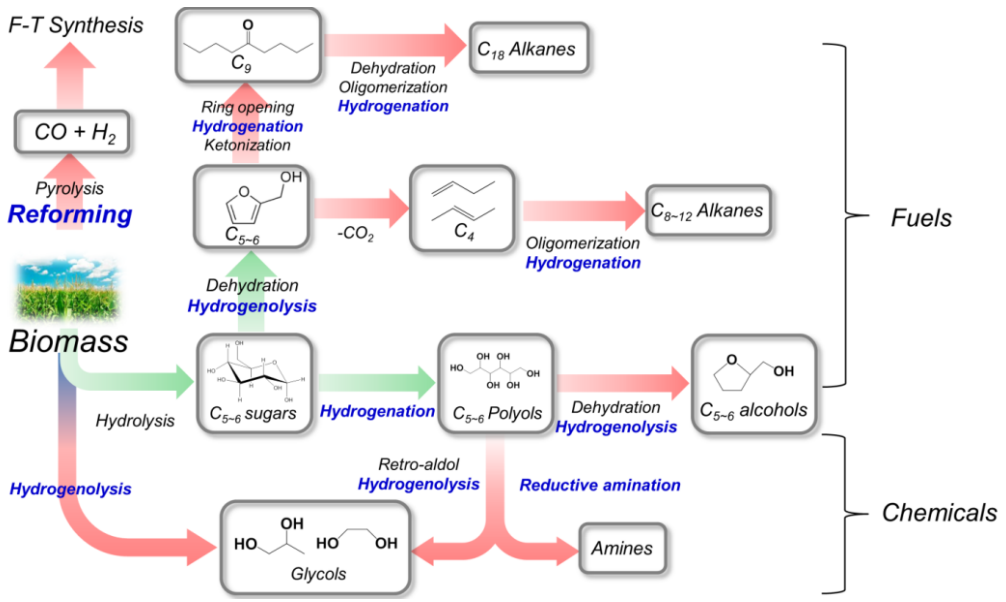

Figure 4. Catalytic conversion of biomass to fuels and chemicals

Obviously, catalytic conversion of non-food cellulosic and hemi-cellulosic biomass feedstocks to high value chemicals attracts attention due to their wide availability in farmlands and non-competitiveness with human food demands. However, designing active, selective and cost effective catalysts for converting the biomass feedstocks is challenging. While conventional technologies for converting crude oils focus on functionalization of hydrocarbons, which have high C/H ratios, biomass already consists of functionalized molecules with high oxygen contents.[13-15] In other words, petroleum refining is focused on C-H

bond activation while biomass upgrading technologies involve hydrodeoxygenation reactions, or the activation of both C-C and C-O bonds are critical. Therefore, the conventional catalysts (*e.g.* zeolites, metal-based catalysts) may not be directly applicable for biomass feedstocks.

Figure 4 illustrates the importance of the activation of C-C and C-O bonding during the biomass upgrading processes for chemical production.[3,4,16] It is clear that conversion of cellulose to sugars involves hydrolysis (C-O activation), dehydration (DHD) of sugars and subsequent hydrogenolysis (HDO) demanding C-O activation on catalyst surfaces. Production of gasoline ($C_{8\sim12}$) and diesel (C_{18}) range compounds further require C-C bond coupling in the presence of hydrogen. Similarly, synthesis of high value/volume chemicals such as glycols, alcohols and amines also demand good C-O activation catalysts during hydrotreatment processes. Therefore, development of active catalysts for C-C and C-O activation is of great importance in biomass conversion. It is clearly seen in Figure 4 that HDO of biomass feedstocks (highlighted in blue) is the key reaction for the production of both renewable fuels and chemicals. Up to date, extensive research efforts were focused on the catalytic HDO of biomass feedstocks to fuel range compounds. Although only a relatively small fraction of crude biomass will be converted to chemicals, production of renewable chemicals would make significant profits, compared with what is derived from fuels. This will compensate a large percentage of the cost in bio-refinery and enhance the economic sustainability of biomass conversion

technologies. However, unlike fuels production from petroleum and biomass, which convert feed "oil" to a preferred range of compounds (*e.g.* high octane number $C_{8\sim12}$ molecules) rather than to a specific product, conversion of the crude feedstocks to chemicals demands high selectivity to specific products in order to meet the environmental and economical requirements. Due to the complex structure of cellulosic molecules and simultaneous parallel and consecutive reactions involved in biomass conversion, selective activation of preferred C-C and C-O bonding is a major challenge for chemical production.

Bio-derived polyols, such as glycerol (C_3), xylitol (C_5), mannitol (C_6) and sorbitol (C_6) are part of the list of top twelve platform chemicals from biomass feedstocks by Department of Energy (DOE).[17] These polyols have similar chemical structures as each carbon is attached with one hydroxyl group (-OH), which can be easily derived from abundantly available sugar feedstocks (see Figure 4). Catalytic HDO of these polyols to high value chemicals, including glycols, carboxylic acids and alcohols provides alternative routes to conventional petrochemical based pathways.

2. Catalytic conversion of bio-derived polyols to chemicals

2.1 HDO of glycerol in the presence of external hydrogen

Glycerol, or 1,2,3-propanetriol, is an important by-product from bio-diesel production (10w%).[18] Glycerol is also the smallest polyol readily available from biomass feedstocks. It has been widely used as food additives, cosmetic

chemicals and various other industrial intermediates. As the demand of biodiesel continues to increase, corresponding amounts of glycerol will be available in the market as a byproduct. European total glycerol production was 860,000 million tons in 2011.[19] For United States, almost 371,000 million tons of glycerol was produced in 2011. A projection estimates by Procter & Gamble shows that glycerol production expands at a rate of 5% per year globally over an annual production of 1,900,000 million tons.[18,20]

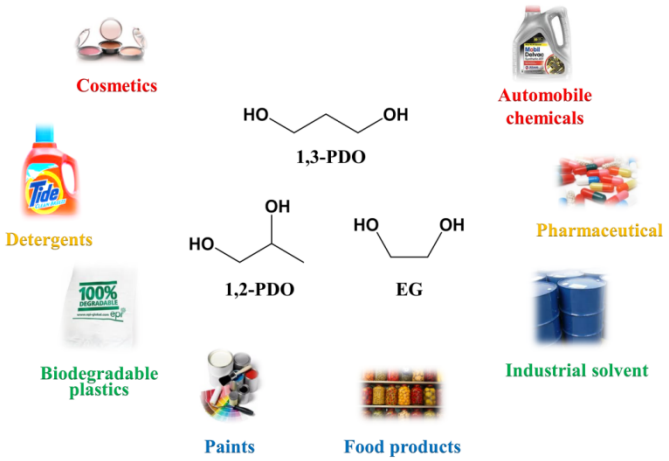

Figure 5. Applications of 1,2-PDO, 1,3-PDO and EG

Researchers previously found that HDO of glycerol, in which one -OH group is knocked off, produce 1,2-propanediol (1,2-PDO), 1,3-propanediol (1,3-PDO), propanols (PrOH) or ethylene glycol (EG) in a single step.[21-25] These chemicals have wide ranging applications as anti-freeze chemicals and drug materials (shown in Figure 5). 1,2-PDO is conventionally produced *via* propylene epoxidation-hydration route, which demands multiple energy intensive steps.[26-28] 1,3-PDO is mainly used as a key raw material in the production of

polytrimethylene terephthalate, a new class of polyester. Direct HDO of glycerol to 1,2-PDO and 1,3-PDO has great potential as an alternative technology to replace the bio-catalytic route and fossil fuel based feedstocks.

2.1.1 Catalyst & processes

Table 1. Catalysts for HDO of glycerol to 1,2-PDO (leading results in literature)

#	Catalyst	Promoter	TOF (h^{-1})	T (^oC)	P (MPa)	X (%)	$S_{1,2\text{-PDO}}$ (%)	Key points	Ref
1	Ru/C	Amberlyst	804	180	8.0	50	70.2	DHD	21,29-31
2	Ru/Al_2O_3	Re	21.5	160	8.0	53.4	50	DHD	32
3	$RuRe/SiO_2$	Re	20.5	160	8.0	52	45	Bimetal RuRe DHD	33
4	$RuRe/ZrO_2$	Re	23.7	160	8.0	57	47	Bimetal RuRe DHD	34
5	CuO/ZnO	Zn^{2+}	~0.9	200	5.0	75	94	DHD	35-38
6	Cu/MgO	Mg^{2+}	1.0	180	3.0	72	98	DH and DHD	39
7	Cu/MgAlO	Mg^{2+}	2.7	180	3.0	80	98	DH	40-42
8	Cu/SiO_2	-	2.6	200	9.0	73	94	Precipitation	43,44
9	Cu/Al_2O_3	-	9.2	200	1.5	42	93	-	23,45-48

Several types of supported metal catalysts have been investigated for HDO of glycerol and some important developments have been reviewed recently. The general order of catalyst activity for glycerol conversion is Pt > Ru > Rh > Ir > Ni > Co > Cu, while the selectivity for 1,2-PDO is Cu >> Ni > Ru, Rh, Ir >> Pt.[49] Archer Daniel Midland (ADM) announced their glycerol processing plant for the production of glycols (1,2-PDO and EG).[50] But the overall selectivity towards 1,2-PDO and EG reported is very low (S < 43%).[51] Ru catalysts are known for high HDO activity, as described in several patents.[52] The major

problem with Ru catalysts is the low selectivity for 1,2-PDO and EG but high selectivity for methane formation (S > 40%).

Extensive research efforts have been made to enhance the overall selectivity of 1,2-PDO on Ru catalysts at lower temperatures (130~180 ^{o}C).[21,53] Ru/C catalyst displayed turnover frequency (TOF) in the range of 17~46 h^{-1} with selectivity of 1,2-PDO from 16~40% in the presence of acidic promoters (*e.g.* Amberlyst).[21,29,30] Various solid acid promoters were also tested by researchers but the maximum selectivity to 1,2-PDO was below 71% (see Table 1).[54] Since solid acids display strong promotional effects on the glycerol conversion, one would expect supporting Ru nanoparticles (NPs) on solid acid supports would combine the advantages of both DHD and HDO functions. However, the experimental evidence showed that performance of Ru catalysts on TiO_2, Al_2O_3 and ZrO_2 (S < 58%) supports were not as good as Ru/C+solid acids admixtures.[21,29,32-34,53,55]

Further efforts focused on adding a second metal, such as Pt and Re, to monometallic Ru catalysts with the goal of promoting the selectivity.[53] The presence of Re in Ru system was found to promote the dispersion of Ru element on the solid supports, which partly explains the overall activity increase of Ru catalysts in the presence of Re.[33,34,53,55] Methane selectivity was also reduced from almost 50% to 35%.[56] Bimetallic RuPt/C catalysts and compared the performance with monometallic Ru/C catalysts.[57] However, methane formation (S ~20%) was still the major side reaction on Ru catalysts.[57]

Table 2. Effects of metal-support interaction on HDO of glycerol to 1,2-PDO

#	Catalyst	Promoter	T (^oC)	P (MPa)	X (%)	$S_{1,2\text{-PDO}}$ (%)	Active form	Key points	Ref
1	Cu/Al_2O_3	Al^{3+}	220	5.0	92	93	$CuAl_2O_4$	Cu^{2+}(934.2eV)[a]	58
2	Cu/Al_2O_3	Al^{3+}	220	2.4	13	80	Cu^0	Cu^0 (86%) Cu^+ (14%)	23
3	Cu/Al_2O_3	Na^+	220	5.2	63	88	Cu^+	Strong acidic sites (>30%)[b]	59
4	Cu/MgAlO	OH^-	200	4.0	70	92	N.R.	MgAlO reconstructed	60,61
5	Cu/MgO	Mg^{2+}	200	4.0	49	92	Cu^{2+}	Cu^{2+}(934.4eV)[a]	39
6	Cu-ZnO-$ZnAl_2O_4$	$ZnAl_2O_4$	180	4.0	86	92	$Cu^0/ZnAl_2O_4$	Zn donate electrons to Cu	62
7	Cu/ZnMgAlO	ZnO	180	2.0	78	99	Cu^0	Strong Cu^0-ZnO interaction[a,b]	63
8	$CuCr_2O_4$	Cr^{3+}	130	2.0	52	99	$CuCr_2O_4$	DHD	64-66
9	$CuFe_2O_4$	Fe_2O_3	190	4.1	43	83	$CuFe_2O_4$	Strong Cu^{2+}-Fe_2O_3 interaction	67
10	CuB/SiO_2	B_2O_3	200	5.0	100	98	Cu^0	B promotes Cu dispersion[b]	68
11	CuRh/MgAlO	Rh^{3+}	180	2.0	95	99	RhCu	Hydrogen spillover on Rh	69
12	CuRu/CNT	Cu	200	4.0	100	86	RuCu	Ru(shell)Cu(core)[a]	70
13	Ru-$CaZnMg/Al_2O_3$	CaZnMg	180	2.5	58	86	RuO_2	-	71

a. characterized by X-ray photoelectron spectroscopy (XPS); b. characterized by temperature programmed reduction/desorption/oxidation (TPR, TPD and TPO).

Despite of good activity on noble metal catalysts, the relatively high costs motivate researchers to explore more inexpensive catalysts, such as Cu, for glycerol conversion. Overall, Cu catalysts exhibited much lower activity for HDO of glycerol (TOF = 0.9~18 h^{-1} at 200 ^oC) but the selectivity to 1,2-PDO (S = 84~98%) is much higher than Ru based catalysts.[49] Acidic supports and promoters such as ZnO promoted DHD of glycerol to acetol, which is then converted to 1,2-PDO in the presence of hydrogen.[37,38,62] As seen from Table 1, basic supports (promoters) such as hydrotalcite ($Mg_xAl_yO_z$)[40-42] and MgO[39,72] were found to outperform acidic promoters in terms of selectivity to 1,2-PDO (>

90%). In addition, Cu/SiO_2 catalysts prepared *via* precipitation method showed much higher activity and stability (200 h) for HDO of glycerol, in comparison catalysts prepared by impregnation approach.[24,43,68,73-76] Major research efforts were focused primarily on the effects of supports on reaction pathways. Increasing experimental studies (from year 2011~2014) were focused on improving the performances of Cu catalysts, particularly on understanding Cu-support interaction (Table 2). Various bi-functional materials, including hybrid structures such as $CuAl_2O_4$, $CuCr_2O_4$ and $CuFe_2O_4$, and oxides such as B_2O_3 and $ZnAl_2O_4$ showed significant enhancement on Cu catalyst performances.

2.1.2 Reaction pathways and mechanisms

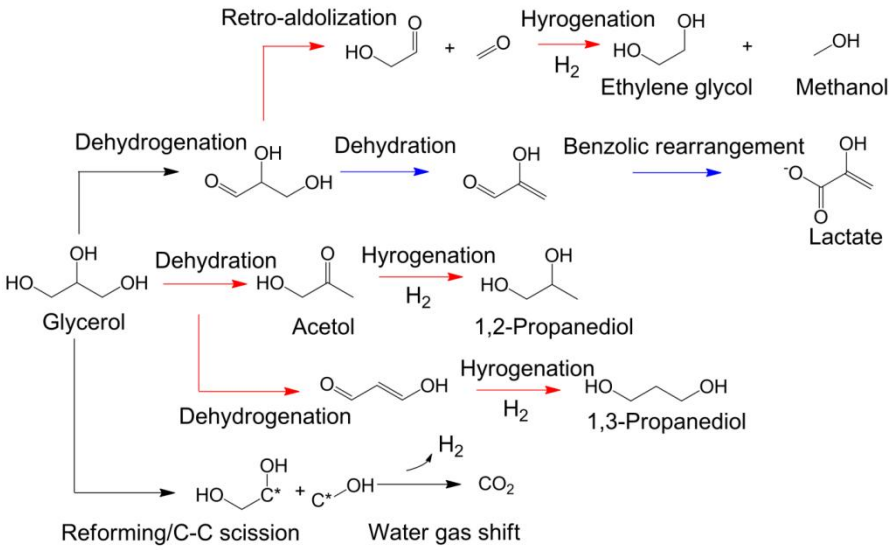

Scheme 1. General reaction pathways for HDO of glycerol

Several reports described possible reaction pathways of HDO of glycerol, the overall scheme for which is summarized in Scheme 1.[30,37,56,60,77] It is generally

believed that glycerol conversion is initiated with DH or DHD on catalyst surfaces. The two possible pathways give glyceraldehyde (GLA) and acetol (DHD) as the key intermediates, respectively, which are transformed instantaneously to alcoholic products in the presence of external hydrogen.

Specifically, acetol can be hydrogenated to 1,2-PDO over metal catalysts, while 1,3-PDO can be generated if DHD occurs associated with middle carbon in glycerol molecule.[25] GLA could undergo either retro-aldol (C-C cleavage) or further DHD under reaction conditions. Retro-aldol leads to the formation of EG and methanol (MeOH) while pyruvaldehyde (PAD) formed during DHD will be converted to lactate *via* benzilic rearrangement.[78,79] MeOH can be easily further hydrogenated to methane in the presence of metal catalysts. Direct C-C cleavage (not retro-aldol) will take place under relatively harsh reaction conditions, giving CO_2 *via* reforming coupled with WGS reactions.[13,15] Possible reaction mechanism based on previous literature is summarized in Scheme 2.[30,37,60] As discussed in the previous section, acidic and basic promoters are found to facilitate the formation of 1,2-PDO. As seen in routes II and III, glycerol conversion follows E_1 mechanism if acidic promoters are present with metal catalysts,[31,54,55] followed by two possible paths, one yielding 1,2-PDO (III, easy) another 1,3-PDO (II, difficult).[25] E_1 mechanism involves protonation of a -OH group, which releases water (DHD). The resulting carbo-cation is neutralized in polar protic solvents and then hydrogenated to 1,2-PDO or 1,3-PDO. E_2 mechanism (IV) is believed to be the main source for 1,2-PDO

formation in the presence of basic promoters.[80] As seen from the catalyst performances, experimental evidence demonstrated that E_2 steps are more favorable for the formation of 1,2-PDO compared with E_1 mechanism.

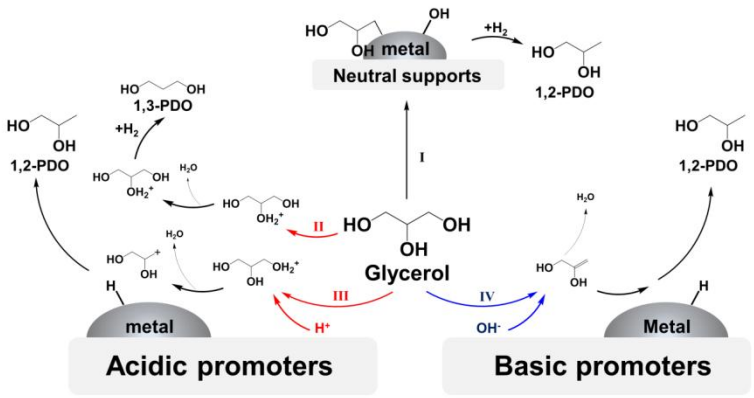

Scheme 2. Reaction mechanism of HDO of glycerol in the presence of metal catalysts

Density functional theory (DFT) calculations confirm the reaction steps (routes II and III in Scheme 2) experimental findings for acid-base catalyzed glycerol conversion on supported Ni, Rh and Pd catalysts.[81] The most stable forms of intermediates on various catalysts are however different, in which C=C and C=O could be present in the intermediates. Despite of detailed mechanistic description of 1,2-PDO formation in glycerol conversion, one major question on how to improve catalyst activity while avoiding excessive C-C cleavage is still an unsolved issue for design of metal catalysts.

2.1.3 Kinetic modeling

Kinetic models on HDO of glycerol are summarized in Table 3. Shanks' group[82] proposed the reaction network for the formation of glycols (1,2-PDO and EG) and degradation products in HDO of glycerol over Ru/C catalysts in

the presence of CaO and $CaCO_3$. In this model, degradation products (methane) came from direct HDO of glycerol and decomposition of EG and 1,2-PDO on Ru/C catalysts. GLA from DH of glycerol contributed significantly to the formation of degradation products. Therefore, the overall formation rates of EG and 1,2-PDO were the combination of HDO and decomposition reactions. The total carbon balance in their system was however poor (< 63%), the global reaction network was thus not clear. Updated kinetic models in the same system reveal that the presence of sulfur actually influenced the rates of decomposition reactions.[83] With sulfur/Ru ratios increasing from 0 to 0.4, the activation energy for glycerol decomposition was enhanced from 44 to 88 kJ/mol. Torres *et al.*[56] proposed a similar reaction network based on comprehensive characterization of both liquid and gas phase products, finding the activation energies of degradation reactions on RuRe/C catalysts approximately around 84 kJ/mol.

A different reaction mechanism was proposed by Zhou and co-workers based on experimental data in a continuous reactor.[77] It was believed that hydrogen is dissociatively adsorbed on one type of active site while the substrate and products on another site. The activation energies for DHD and HDO were reported as 86 kJ/mol and 58 kJ/mol respectively. A simplified model describing the adsorption of glycerol, GLA and acetol on the same site was proposed by Xi and co-workers.[84] With negligible adsorption of a base promoter (NaOH) and 1,2-PDO, this model fitted the experimental data quite well in the range of 180~200 ^{o}C. An empirical kinetic model was discussed for

Pd-$CuCr_2O_4$ catalyst.[85] The addition of Pd to $CuCr_2O_4$ facilitated the conversion of glycerol. Pd was believed to accelerate hydrogen spillover on Cu catalyst surface thus HDO rates were increased by almost two folds. A similar reaction model was also discussed by Vasiliadou[24] for on Cu/SiO_2 catalysts.

Table 3. Kinetic Models for HDO of Glycerol

Catalyst	Reactor type	Glycerol Reaction Rate Law	Mechanism
Ru/C	Batch	$-r_{gly} = \frac{k_{gly} \cdot C_{gly}}{1 + K_{gly} \cdot C_{gly} + K_{EG} \cdot C_{EG} + K_{1,2-PDO} \cdot C_{1,2-PDO}}$	Single-site DH-HDO Degradation
RuRe/C	Batch	$-r_{gly} = w \cdot C_{gly} \frac{\left(C_{H_2}\right)_g}{H_{H_2}} \left[k_1 + k_2 + \frac{H_{H_2}}{\left(C_{H_2}\right)_g} \right]$	Single-site DH-HDO DH-degradation
Cu-ZnO-Al_2O_3	Fixed Bed	$-r_{gly} = \frac{k_{gly} \cdot C_{gly}}{1 + K_{gly} \cdot C_{gly} + K_{Ace} \cdot C_{Ace} + K_{1,2-PDO} \cdot C_{1,2-PDO}}$	Two-site DHD-HDO
CoPdRe/C	Fixed Bed	$-r_{gly} = \frac{k C_{gly} C_{OH^-} C_{H_2}^2}{C_{gly} C_{OH^-} + K_{H_2} C_{H_2}^3}$	Single-site DHD-HDO
$PdCuCr_2O_4$	Batch	$-r_{gly} = k_{gly} C_{gly}^{2.28} C_{H_2}^{1.09}$	-
Cu/SiO_2	Batch	$-r_{gly} = k_{gly} C_{gly}^{0.27} C_{H_2}^{0.96}$ $+ r_{1,2-PDO} = k_1 C_{gly}^{0.17} C_{H_2}^{1.06}$	DHD-HDO
Ru/ZrO_2	Batch	$-r_{gly} = \frac{k_{DH} K_{gly} K_{alkoxide}}{K_{H_2}^{0.5}} \frac{C_{gly}}{P_{H_2}^{0.5}} \theta_*^2$	DH-DHD

See appendix III for notation

An alternative model was derived and discussed by Liu's group.[86] Several elementary steps, including DH, DHD, HDO and decarbonylation (C-C cleavage) were taken into account to explain the formation of methane, EG on Ru/ZrO_2 surface. The apparent activation energy on Ru catalyst was about 72 kJ/mol, lower than the results obtained by other researchers. It was found that, reaction rates of C-O cleavage (DH, DHD and HDO reactions) was more

significant than C-C cleavage reactions as temperature increases, while further increase in temperature resulted in dramatic enhancement in C-C cleavage.

2.2 Conversion of sugar polyols in the presence of external hydrogen

Xylitol, sorbitol and mannitol are polyols obtained from hydrogenation of sugars.[87] Xylitol, the primary product of xylose hydrogenation, is one of the best artificial sweeteners because it is able to reduce side effects and has low cariogenicity compared to sucrose. Sorbitol is the product from glucose hydrogenation having wide ranging applications in sweeteners, laxatives and medical treatment. Mannitol is obtained from the reduction of fructose, which also has extensive applications in food and medicines.[88-91]

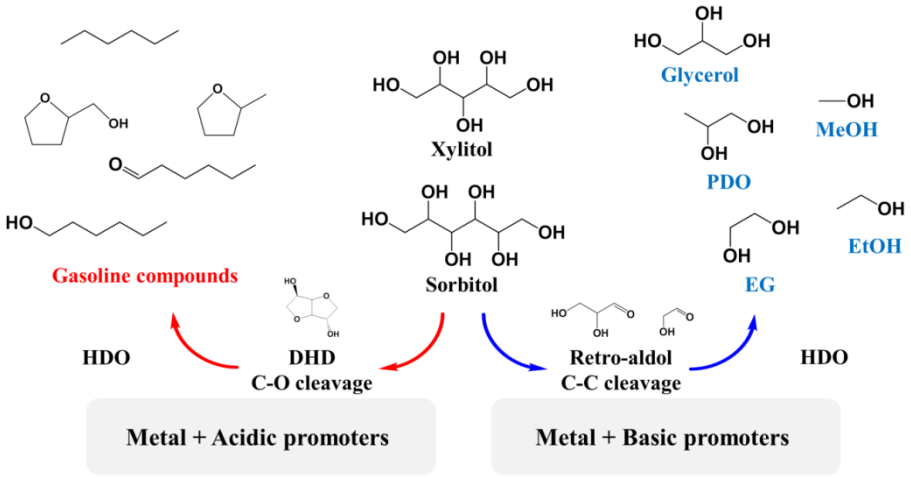

Scheme 3. Catalytic conversion of sorbitol to fuels and chemicals

Catalytic conversion of xylitol, sorbitol and mannitol is of increasing interest because these can be converted to various products such as furfurals, furans, alcohols and hydrocarbons as fuel compounds,[92,93] as well as other high value chemicals such as 1,2-PDO, EG and glycerol (Scheme 3).[88,90,94] Up to date,

extensive research efforts were focused on fuel range products from xylitol and sorbitol. Pt-based catalysts on acidic silica-alumina (SiAl) and zirconium phosphate (ZrP) supports were evaluated for catalytic upgrading of these $C_{5\sim6}$ polyols at 230 ^{o}C and 3.0 MPa hydrogen pressure.[93,95] Pt/SiAl catalysts displayed only about 10% selectivity to liquid hydrocarbons, contributing to ~90% selectivity to gas phase products.[96] Tetrahydrofurfuryl alcohol was observed as the major product from gasoline range compounds on ZrP support, with the overall yield of gasoline of about 66% (research octane number, RON = 80).[97] In comparison, PtRe/C catalysts displayed much lower yield of gasoline products (Y = 40%) but improved RON = 89 under similar reaction conditions.[95] Recently Ni/ZSM-5+MCM-41 showed good C_6 alkane selectivity (S = 90%).[98]

2.2.1 Catalyst & performance

There existed limited research results on the conversion of sugar polyols to valuable chemicals such as 1,2-PDO and EG. Only a few Ru, Ni and Cu catalysts have been reported in the past two decades. A summary of literature is presented in Table 4. Sohounloue and co-workers reported Ru/SiO_2 catalyst for HDO of sorbitol with a combined EG and 1,2-PDO selectivity of 46% (Entry#1).[94] But, SiO_2 supports were found to leach in the presence of $Ca(OH)_2$ used as a base promoter. Tronconi's group found that Ru/C+NaOH catalyst led to the formation of both glycols (S = 54.3%) and LA (S = 6.9%) in conversion of sorbitol in a continuous reactor (Entry#2).[99] Zhao and co-workers (Entry#3)

carried out sorbitol conversion over supported Ru catalysts on carbon nanofiber (CNF) and graphite-based composite materials and reported 68% conversion with ~51.3% selectivity of glycols (EG and PDO) at 220 ^{o}C and 8 MPa (P_{H2}).

Table 4. Aqueous phase HDO of sorbitol over metal based catalysts

#	Catalyst	Promoter	P_{H2} (MPa)	T (^{o}C)	TOF[a] (h^{-1})	Selectivity (%)				Ref
						Glycols[b]	LA	Alcs[c]	Gas[d]	
1	Ru/SiO_2	$Ca(OH)_2$	8.0	210	78.3	46	N.R.[f]	N.R.	N.R.	94
2	Ru/C	NaOH	13.0	250	16.6	54.3	6.9	N.R.	N.R.	99
3	Ru/CNF	NaOH	8.0	220	183.1	51.3	N.R.	N.R.	N.R.	88
4	$NiCe/Al_2O_3$	$Ca(OH)_2$	7.0	240	46.7	55.3	N.R.	11.1	11.1	100
5	Ni/C	$NaOCH_3$	14.0	215	46.7	33	N.R.	N.R.	N.R.	101
6	NiPt/NaY	$Ca(OH)_2$	6.0	220	N.A.[e]	76	N.R.	N.R.	N.R.	89
7	CuO-ZnO	ZnO	13.0	240	0.8	< 10[f]	N.R.	N.R.	N.R.	102

a. defined as mol/mol/h or h^{-1} in literature; b. Glycols: 1,2-PDO and EG; c. Alcs: $C_{1\sim3}$ linear alcohols; d. Gas: CH_4 and CO_2; d. N.A.: TOF cannot be calculated due to lack of experimental details; e. deoxyhexitols are the major products (S =35~67%); f. N.R.: not reported in the manuscripts.

Clark and co-workers reported that HDO of sorbitol over kieselguhr supported Ni catalysts and $NaOCH_3$ as a liquid phase promoter with yields of EG, 1,2-PDO and glycerol as 16%, 17% and 40%, respectively at 215 ^{o}C and 14 MPa (hydrogen pressure, P_{H2}).[103] Ye *et al.*[100] found that when adding trace amount of Ce^{4+} to Ni/Al_2O_3+CaO catalytic system, the activity of Ni catalysts was enhanced by almost three folds with 55.3% selectivity to glycols (Entry#4) at 240 ^{o}C and 7 MPa (P_{H2}). But side reactions including methanation and water gas shift reaction (WGS) were also significant (methane and CO_2 selectivity = 10~22%) at the same time. Banu *et al.*[89] found that the activity of Ni/NaY catalyst was enhanced in the presence of CaO as a basic promoter with a

combined selectivity to EG and 1,2-PDO of 76% at 220 ^{o}C and 6 MPa (P_{H2}), the use of alkalis and zeolites, however led to the catalyst sintering (Entry#6).

Sun *et al.*[90] tested different carbon supported catalysts (Pt, Pd, Ru, Rh, *etc*) for xylitol hydrogenolysis and found that with Ru/C+$Ca(OH)_2$ (Entry#1 in Table 5), catalyst, EG, 1,2-PDO and lactic acid (LA) were the main products with 32%, 25% and 17% selectivity respectively at relatively mild conditions (200 ^{o}C and 7 MPa). Isomerization of xylitol (to threitol and arabitol) and methanation were the major side reactions on Ru/C catalysts. Ru showed superior performance compared to other noble metal catalysts.

Table 5. Aqueous phase HDO of xylitol with $Ca(OH)_2$ as the base promoter

#	Catalysts	P_{H2} (MPa)	T (^{o}C)	TOF (h^{-1})	Selectivity (%)				Ref
					EG	1,2-PDO	LA	Others[c]	
1	Ru/C	7.0	200	184.4	32.4	24.9	16.8	14.2	[90]
2	$Ru/Mg_xAl_yO_z$	7.0	200	145.2	19.5	7.9	36.5	17.3	[90]
3	Pd/C	7.0	200	63.0	30.0	29.0	28.4	5.3	[90]
4	Rh/C	7.0	200	61.2	26.4	30.0	23.3	11.8	[90]
5	Pt/C	7.0	200	754.5	25.0	23.3	15.5	20.8	[90]
6	NiRe/C[a]	8.0	200	N.A.[b]	37	28	10	21	[101]

a. KOH [not $Ca(OH)_2$] as the base promoter; b. N.A.: TOF cannot be calculated due to lack of experimental details; c. Others including small amounts of glycerol, $C_{1\sim2}$ carboxylic acids and linear alcohols.

2.2.2 Reaction pathways and mechanisms

Conversion of xylitol and sorbitol to EG and 1,2-PDO involves simultaneous C-C and C-O cleavage as the key intermediate steps though the detailed mechanism of these steps is still debated. Sohounloue and co-workers proposed

retro-aldol (C-C cleavage) mechanism for HDO of xylitol and sorbitol in the presence of Ru/SiO_2 and Raney Ni catalysts, the activity of which can be enhanced in strong basic medium (pH>12).[94] Montassier *et al.*[104] conducted detailed work in the activity of Ru/C and proposed that the main reaction causing C-C bond cleavage in sorbitol conversion was a retro-Michael rather than retro-aldol reaction. [105, 106]

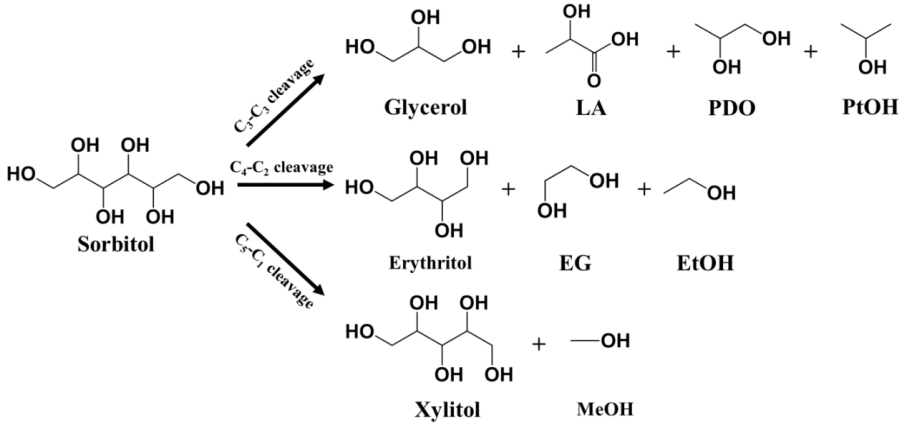

Scheme 4. Possible products from sorbitol conversion

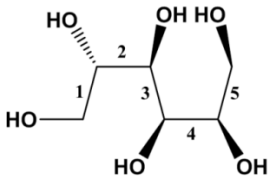

Bond (B)	Length (Å)	ΔB_{Pt} (%)	ΔB_{Ni} (%)	ΔB_{Ru} (%)
1	1.520	+1.09	+1.18	+1.13
2	1.525	+1.78	+1.73	+1.77
3	1.522	+2.07	+2.13	+2.10
4	1.522	+2.11	+2.12	+2.16
5	1.521	+1.37	+1.39	+1.37

Figure 6. Activation of sorbitol molecule on metal catalyst surface[107]

The possible products from sorbitol conversion are shown in Scheme 4. With regard to the primary product of C-C cleavage, experimental results showed that glycerol might be the key intermediate for secondary products such as EG

and 1,2-PDO, as known from HDO of glycerol. However, the comprehensive understanding of reaction pathways is still challenging, because, as seen from previous reports (as shown in Tables 4 and 5), there was lack of complete material balance (65~82%) in current reaction systems.[88,94,100,101] More importantly, the molecular structure of xylitol and sorbitol is much more complex compared with glycerol. DFT calculation for xylitol and sorbitol, C-C cleavage at any position (shown in Figure 6) was all possible.[88,94,100]

2.2.3 Kinetic modeling

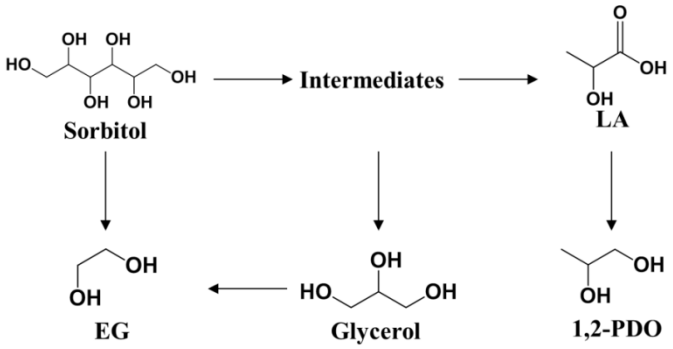

Scheme 5. Reaction network of sorbitol conversion on Ru/C catalyst

Tronconi's group proposed a Langmuir-Hinshelwood rate model to describe the sorbitol conversion on Ru/C catalyst in the presence of NaOH.[99] A tentative reaction network for glycerol, EG, 1,2-PDO and LA was proposed and experimental data were fitted to determine rate parameters (as shown in Scheme 5). However, the major co-products such as MeOH (C_1), EtOH (C_2) and possibly gas phase products were not reported. The lack of complete material balance (< 78%) brought significant challenges to the fundamental

understanding of the C-C cleavage on Ru catalysts. Further, the reaction steps proposed for LA-to-1,2-PDO are not possible as LA cannot be further converted to 1,2-PDO in alkaline medium.[57] Further, the underlying mechanism for C-C and C-O cleavage of sorbitol and xylitol on metal catalysts is still not clear.

2.3 Conversion of polyols in the presence of hydrogen formed *in situ*

2.3.1 Glycerol to 1,2-PDO: catalysts and surface reactions

At present, hydrogen required for industrial hydrogenation processes comes from fossil fuel-based sources (*e.g.* petroleum, coal, *etc*). The cost of hydrogen is an important aspect in developing competitive processes, particularly, in the manufacture of low value/high volume commodity products or those cases where hydrogen is consumed for unwanted side reactions. Hydrogen cost is even more important in biomass conversion processes such as HDO of oxygen rich feedstocks (polyols, polyhydroxy carboxylic acids, *etc*) as a large amount is consumed in deoxygenation to undesired products. The development of alternative HDO processes without the need of external hydrogen or using *in situ* formed hydrogen may therefore have a significant economic and environmental impact.

It is well known that aqueous phase reforming of polyols leads to the formation of hydrogen in the presence of various metal-based catalysts, such as Pt,[108,109] Ru,[110] Ni,[111] Cu.[112] These metal catalysts are also known as potentially good

candidates for HDO of polyols to 1,2-PDO and EG.[88,89,100,113-120] One would expect that hydrogen generation and HDO could occur simultaneously on the catalyst surface or in a one pot process. Scheme 6 shows the stoichiometry of tandem reforming/HDO of glycerol, where the maximum theoretical selectivity of 1,2-PDO can be 87.5%. This value is even higher than most of the existing experimental results of glycerol conversion in the presence of external hydrogen, which indicates the strong economical and environmental favorability of the *in situ* process. Summary of leading experimental results on glycerol conversion using hydrogen formed *in situ* is presented in Table 6.

(a) Reforming: $C_3H_8O_3 + 3H_2O \rightarrow 3CO_2 + 7H_2$

(b) DHD: $7C_3H_8O_3 \rightarrow 7C_3H_6O_2 + 7H_2O$

(c) HDO: $7C_3H_6O_2 + 7H_2 \rightarrow 7C_3H_8O_2$

Overall: $8C_3H_8O_3 \rightarrow 7C_3H_8O_2 + 3CO_2 + 4H_2O$

Scheme 6. Stoichiometry of tandem reforming/HDO of glycerol

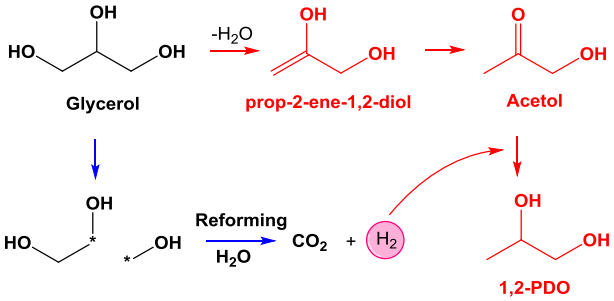

Scheme 7. Glycerol to 1,2-PDO *via* reforming/DHD/HDO route[121]

D'Hondt and co-workers[121] first reported tandem reforming/DHD/HDO of glycerol in the presence of Pt/NaY catalysts with 64% selectivity to 1,2-PDO at 85% conversion. Roy *et al.*[122] later investigated the feasibility of using an admixture of two supported metal catalysts for the tandem reforming/HDO of

glycerol. They reported that Pt/Al_2O_3+Ru/Al_2O_3 admixture displayed significantly higher conversion (X = 50.1%) and selectivity to 1,2-PDO (S = 47.2%) than the two catalysts (X < 20%) when tested individually. But methane selectivity was about 20% under the experimental conditions (T = 180~240 ^oC).

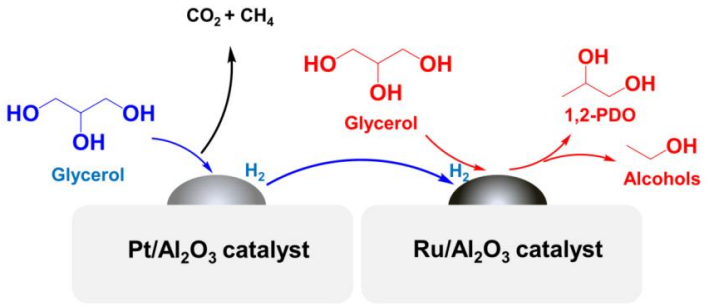

Scheme 8. Glycerol to 1,2-PDO on Pt and Ru catalyst admixtures[122]

Further efforts by were carried out on modifying Pt/TiO_2 catalysts by adding a second component such as Sn[123] or Ni[14] as promoters aiming at minimizing the significance of methanation reactions. Barbelli & Nichio[123] found that the reaction rate of glycerol was enhanced significantly from 15 to 907 h^{-1} at 200 ^oC by adding Sn as the promoter, leading to a higher 1,2-PDO selectivity (S = 32%, X = 54%) on Pt/TiO_2 catalysts. Martin[14] later found that the addition of Ni to Pt/Al_2O_3 catalysts seemed to increase the overall activity of Pt catalysts, but selectivity to 1,2-PDO (S = 47~52%) was still poor. Inexpensive Cu/Al_2O_3 catalysts were also investigated by Mane & Rode for glycerol conversion,[124] because Cu catalysts usually exhibit low methanation activities. It was found that $CuAl_2O_4$ species in Cu/Al_2O_3 catalysts promoted DHD, thus acetol was formed as the major component (S = 32~100%). But as conversion of glycerol

increased from 59% to 90%, the maximum selectivity towards 1,2-PDO was only 55% with significant amounts of CO_2 (S > 20%) generated at 220 ^oC. This is possibly due to the WGS reaction occurring dominantly on Cu/Al_2O_3 compared with *in situ* HDO of glycerol.

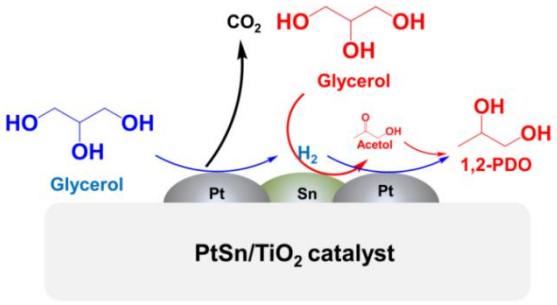

Scheme 9. The role of Sn in tandem reforming/HDO on Pt/TiO_2 catalyst[123]

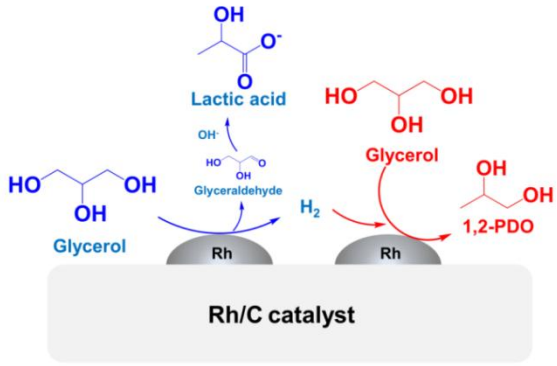

Scheme 10. DH/HDO on Rh/C catalyst[125]

Although the presence of acidic sites promote DHD of glycerol to acetol, reforming of glycerol and formed alcoholic products (*e.g.* 1,2-PDO, EG, MeOH)[126] is also enhanced on acidic surfaces.[80] The selectivity to liquid products is thus relatively low. Experimental studies showed that alkaline medium restrained the unwanted methanation reaction to a large extent.[41,57,127]

Thus further efforts were carried out to understand the role of base (promoters) during *in situ* HDO of glycerol. King and co-wokers[80] observed that the addition of trace amounts of KOH to Pt/C catalysts led to significant enhancement in hydrogen production rate, while the selectivity to glycols and alcohols was enhanced from 45% to approximately 70% at 225 ^{o}C. Meanwhile, the formation methane and ethane was almost reduced (S < 5%). This implied that the presence of basic species prevented the methanation of intermediates and favors the *in situ* HDO reactions.

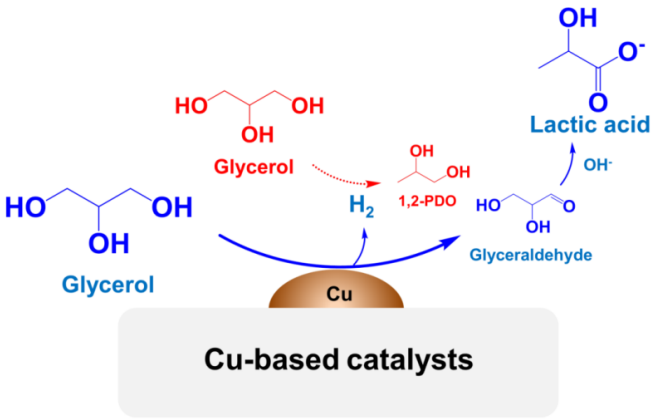

Scheme 11. Glycerol conversion to LA on Cu-based catalysts

A recent study combing DFT with experimental results on Rh/C and Ir/C catalysts revealed that both DHD and DH route are possible for glycerol conversion in the presence of NaOH.[125,128,129] LA was detected as one of the main products (S = 30~55%). 1,2-PDO selectivity was also enhanced with the addition of NaOH (S > 40% in most cases). Another study showed that LA was the major products on Cu catalysts in alkaline medium (Scheme 11),[79] implying that DH reaction was the dominant reactions. A recent DFT study of glycerol

DH proposed that it was possibly initiated with C-H rather than O-H rupture on metal surface.[130] Two metallic sites, according DFT calculations,[123,124] should be available for stable dehydrogenated species (Scheme 12), indicating that the extraction of second hydrogen atom from adjacent C or O atoms is actually the "difficult step" during DH.[131,132] This study provides insightful information about reaction mechanism of DH.[121,122,125]

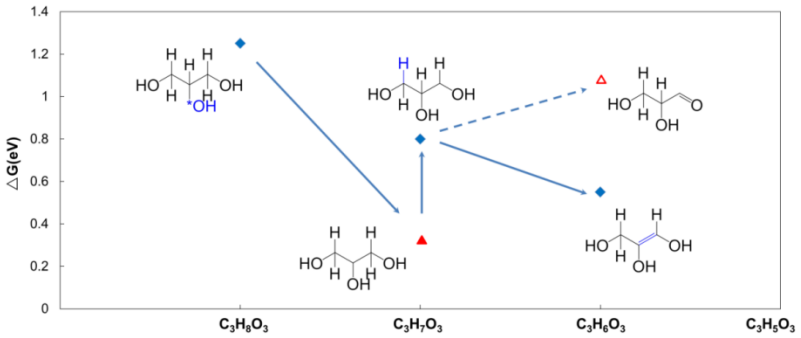

Scheme 12. Proposed glycerol conversion route on Pt [111] surface

Catalytic transfer hydrogenation (CTH) reaction was also investigated by various researchers. CTH can be of industrial importance because the storage of hydrogen generators (donors) such as EtOH, 2-PrOH and formic acid is relatively cheaper than those for molecular hydrogen.[14] Musolino & Pietropaolo proposed an *in situ* HDO of glycerol to 1,2-PDO by using the hydrogen generated from 2-PrOH on Pd/Fe_2O_3 catalysts.[14] The selectivity to 1,2-PDO was 94%. However, the selectivity of corresponding ketones or aldehydes during DH of H-donors as well as the overall liquid/gas products ratio was not mentioned in these reports. Therefore the overall efficiency of the proposed CTH process is still unknown.

Table 6. HDO of glycerol using hydrogen formed *in situ* (leading results in literature)

#	Catalysts	Solvent[a]	Promoter	T (^oC)	P[b] (MPa)	TOF (h^{-1})	X (%)	S[d] (%)	Ref
1	Pt/NaY	H_2O	Na^+	230	4.2	71.2	85.4	64.0	112
2	Pd/Fe_2O_3	EtOH 2-PrOH	Fe_2O_3	180	0.5	-	100	94	133
3	Ru/Al_2O_3, Pt/Al_2O_3 (admixture)	H_2O	-	220	1.4	34.0[c]	50	47	122
4	$PtSn/TiO_2$	H_2O	Sn	200	0.4	907	54	59	123
5	Cu/Al_2O_3	H_2O	-	220	2.0	-	90	22	124
6	Pt/hydrotalcite	H_2O	Mg^{2+}	250	1.0	-	94.5	29	14
7	PtNi/hydrotalcite	H_2O	Mg^{2+}	250	1.0	-	89.8	35.2	14
8	Pt/C	H_2O	KOH	225	2.9	612	90	22	80
9	Rh/C	H_2O	NaOH	180	3.0	20.8	55	6	125
10	Ir/C, $Ir/CaCO_3$	H_2O	NaOH	200	3.0	1086	76	~40	128
11	Cu_2O	H_2O	NaOH	220	1.4	2.4	90	5	79

a. solvent is an important hydrogen source; b. N_2 or He atmosphere; c. calculated based on Ru content; d. Selectivity to 1,2-PDO

2.3.2 Glycerol to LA: Catalysis and reaction mechanism

LA is a naturally occurring organic acid.[134] Owing to its unique structure with both carboxylic and hydroxyl groups, LA has been widely used in food, pharmaceutical and chemical industries. The main demand for LA is due to the use of polylactic acid as a biodegradable material to replace petroleum-based products (*e.g.* polyethylene, polypropylene).[135] The sustainable market growth of LA is strongly expected because it has a significantly low carbon impact on the environment.[136] Presently, LA is mainly synthesized *via* fermentation of

sugars.[135] The main disadvantages of biological route include limited space-time yield, tough needs for the control of reaction conditions and complex post-separation processes (as shown in Scheme 13).

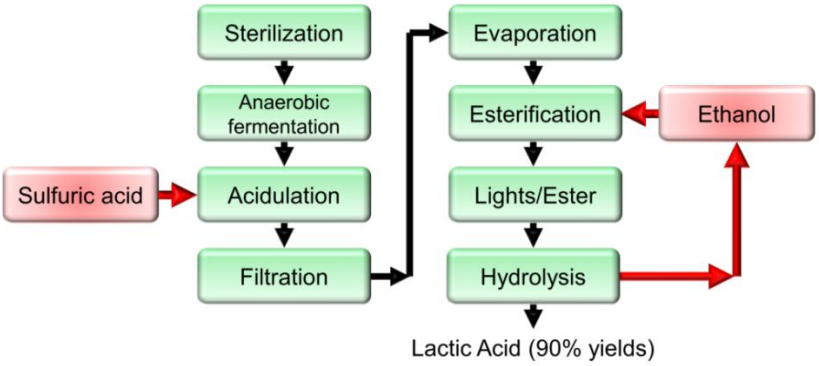

Scheme 13. Flow chart of fermentation of starch sugars for LA production[135]

Experimental results on the synthesis of LA *via* chemical routes, including hydrothermal, HDO, oxidation and DH, have been summarized in Table 7.[16] Possible reaction mechanism involved will be discussed in the following sections.

(1) Hydrothermal route. Hydrothermal conversion is one such technology that can instantaneously transform glycerol to LA under relatively harsh reaction conditions (T > 300 ^{o}C). Hydrothermal technologies may directly convert crude glycerol to various value-added products without a dewatering pretreatment.[78,137] At such high temperatures, alkaline-induced DH of glycerol occurs (Scheme 14), accompanied with consecutive DHD to generate pyruvaldehye and form LA as the major product *via* benzilic rearrangement (Scheme 14).[78]

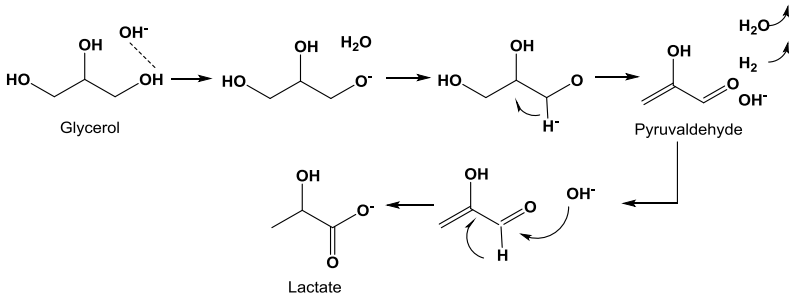

Scheme 14. Conversion of glycerol to LA under hydrothermal conditions

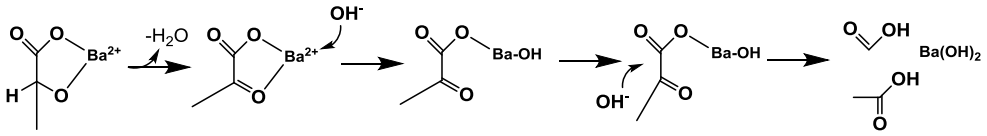

Scheme 15. Formation of pyruvate with Ba^{2+} and formation of formic and acetic acids

Side reactions of LA to formic and acetic acid (C-C cleavage) can also proceed under this reaction conditions.[137] Hydrothermal treatment of glycerol provides an efficient approach for LA synthesis, corrosion of reactor materials is however the major problem plaguing such technology.

(2) HDO route. HDO of glycerol (T = 160~240 ^{o}C, P_{H2} = 2~8 MPa) to 1,2-PDO in the presence of metal catalysts (*e.g.* Ru, Cu, Co, Ni, Pt, Rh, *etc*) has been extensively studied in the past decades.[49] LA is often found as a co-product to 1,2-PDO during glycerol HDO when using bases as catalytic promoters.[57] It raises extensive interests because LA actually has oxidized carbon but it can be formed during reductive environment. For HDO of glycerol, metal (*e.g.* Ru/C, Pt/C and Cu/hydrotalcites) catalyzed DH is believed to be the first step, which seems to be strange. If there is any alkaline species presence in the reaction media (aqueous phase), the dehydrogenated intermediate, GLA can

undergo DHD easily under reaction conditions (T > 60 ^{o}C).[138] The as formed PAD goes through benzilic rearrangement (oxidized by OH^-) to form LA (as mentioned in previous sections). It is clear to us that the formation of LA does not require externally added hydrogen, however, molecular hydrogen is often needed for C-O activation on metal catalysts surface.

(3) Oxidation route. The synthesis of LA from glycerol can occur at 90 ^{o}C in the presence of Pt/TiO_2 catalysts with atmospheric oxygen flow through a glass reactor.[139] Oxygen and OH^- are two key components for LA formation.[139,140] GLA is an important intermediate for LA formation, which is observed to be generated by partial oxidation of glycerol (First step in Scheme 16). The computational study shows that OH^- is critical for the deprotonation of glycerol[140] and DHD of GLA therefore high LA selectivity is obtained. Another effort focusing on oxidation of glucose to LA was also reported by Onda and co-workers.[141,142] The selectivity to LA depended slightly on the types of metal catalysts, implying that the conversion of glucose to LA is an OH^- catalyzed homogeneous reaction.

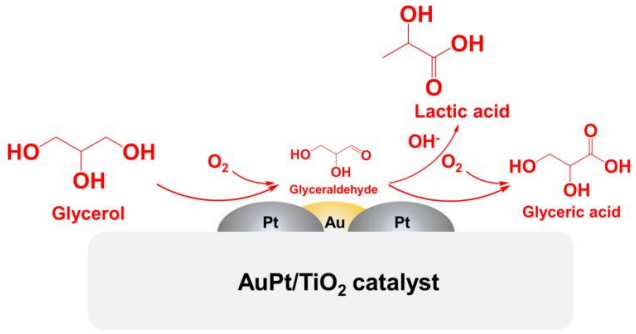

Scheme 16. Plausible pathways for oxidation of glycerol to LA and glyceric acid

(4) DH route. Oxidation of sugar polyols to GLA usually leads to form significant amounts of humic substances due to high NaOH/substrate ratios (4~20 in molar ratio). The DH chemistry is somewhat similar to hydrothermal synthesis but it occurs under milder reaction conditions (T < 250 ^{o}C) and is a metal catalyzed heterogeneous reactions[79] rather than homogeneous reactions of alkali catalysis.[78] Roy and co-workers[79] found that DH of glycerol was dominant on Cu catalysts in alkaline medium. Both DH and HDO reactions were observed on Rh/C and Ir/C catalysts.[125,128,129] DFT calculation found that DHD *via* E_2 route[129] is equally possible as DH on Rh surface. But DHD reaction will not release hydrogen during glycerol conversion. Experimental results confirmed that both DH[79] and HDO[57,125] rates would increase with more alkali addition. The role of alkalis in metal catalyzed DH of polyols is still not clear. More experimental evidence is thus needed to support this hypothesis.

Table 7. Synthesis of LA from glycerol and glucose

#	Cat.	Substrate	OH^-/substrate molar ratio	P (MPa)	T (^oC)	TOF (h^{-1})	X (%)	S_{LA} (%)	Key Points	Ref
1	N.A.[a]	Glycerol	4	8.6[b]	300	-	100	~90	OH^- induces hydride transfer and DHD	78
2	N.A.[a]	Glycerol	4	8.6[b]	300	-	100	90	Ba^{2+} facilitates LA to formic and acetic acid	137
3	Rh/C	Glycerol	2	3.0[c]	180	20.8	90	44	Both DH and DHD are significant	125,143
4	Ir/C	Glycerol	2	3.0[c]	180	1086	76	48	Both DH and DHD are significant	128
5	Cu_2O	Glycerol	1.1	1.4[d]	200	2.2	70	80	Cu catalysts are selective for DH reaction; Cu catalysts show low activity	79
6	$AuPt/TiO_2$	Glycerol	4	0.1[e]	90	517.1[f]	-	85	Bimetallic AuPt improves the stability	139
7	N.A.[a]	Glucose	12	5.5[b]	300	-	100	25	Acids and cyclo-C_6 are major by products	144
8	Pt/C	Glucose	20	0.1[e]	80	-	100	55	Lower temperature favors oxidation reactions	141

a. N.A.: no catalysts; b. vapor pressure; c. inert He atmosphere; d. inert nitrogen atmosphere; e. oxygen bubbling; f. based on Pt content.

3. Challenges and opportunities

3.1 Challenges

As discussed in this chapter, polyols with wide availability from cellulosic biomass attract extensive interests because they can be catalytically converted to various high volume industrial products. If chemicals which are conventionally derived from petroleum can be synthesis from biomass, it will significantly reduce the carbon footprint of bio-refinery. However, several problems still remain, which pose significant challenges for the sustainable development of biomass conversion technologies:

(1) Fundamental difference between petrochemical refining and biomass upgrading. Although extensive research has been focused on converting petroleum-based feedstocks, due to the fundamental difference in molecular structures between petroleum hydrocarbons and oxygen-rich biomass carbohydrates, the reaction mechanism of several industrial important reactions such as DH, DHD, HDO and oxidation is still not clear in biomass conversion. For example, DH of hydrocarbons only involves carbon and hydrogen while that of polyols includes the breakage of C-H and O-H bonds possibly at the same time. **(2) Low activity and selectivity to targeted products.** Conventional catalysts such as zeolites and meta-based catalysts, which show good performances in petroleum refining, are not displaying low activity and selectivity for biomass conversion. More importantly, unlike fuel production,

which demands high selectivity towards a range of compounds with good ignition properties, synthesis of value-added chemicals demands both high activity and good selectivity. But several parallel and consecutive reactions such as reforming, WGS, DH, HDO and DHD occur at the same time, thus CO, CO_2, hydrogen and methane would be produced on catalyst surfaces. Therefore, selectivity towards targeted products such as 1,2-PDO, EG and alcohols is poor in existing catalytic systems. **(3) Lack of rational design of cost-effective catalytic systems.** High performance catalysts with (a) low energy input, (b) high activity/selectivity and (c) low costs are essential for breakthrough in biomass conversion technologies. Although we are able to improve industrial catalysts mostly *via* tuning element compositions, synthesizing novel supports, or optimizing preparation methods, those efforts still cannot lead us to an innovative catalysts with uniform compositions and fundamental understanding of structure-performance correlation. Advances in nanoscience enable us to fabricate nanoparticles with controlled sizes in 1~10 nm regime, and various shapes such as tetrahedral, octahedral and cubes, *etc*. Fundamental understanding on structure-activity relations on the atomic levels (*e.g.* surface facets and C-O/C-H bond activation) are needed, but to date limited progress has been made in biomass area possibly due to the complicated reaction behaviors involved in biomass conversions. **(4) Kinetic modeling of multiphase reactions.** Biomass conversion often involves gas-liquid-solid multiphase reactions. Current research efforts are however, primarily focused on evaluating catalyst and revealing reaction pathways. Detailed multiphase

kinetic modeling will undoubtedly provide insightful information about optimizing design of catalysts and process development.

3.2 Opportunities

The goal of this work is to understand the possible reaction pathways of various sugar polyols including sorbitol, mannitol, xylitol, erythritol and glycerol and rational design of active, selective and stable metal based catalysts for the synthesis of high value chemicals. In order to achieve this goal, four major tasks have been carried out and discussed in this dissertation.

(1) Product distribution and possible reaction pathways of polyols conversion on metal-based catalysts. Investigate the activity and selectivity of metal-based catalysts, for HDO of $C_{3\sim6}$ polyols. Based on the concentration~time profiles, experimental work aiming at revealing reaction mechanism including C-C and C-O cleavage, corresponding reaction pathways and product distribution will be conducted and relevant reactions will be modeled quantitatively.

(2) Reaction mechanism of HDO of polyols on multifunctional DH/DHD/HDO catalysts. On the basis of reaction pathways and product distribution, a rational design of cost-effective Cu-based catalytic system will be carried our systematically and experimental parameters including metal/promoter ratio, temperature, pressure and substrate concentration are studied in details. More importantly, various catalysts characterization

technique will be used to reveal the surface chemistry of Cu sites and to establish the structure-performance correlations.

(3) Tandem DH/HDO of polyols under very mild conditions. Combining hydrogen generation with HDO on one metal catalyst including Ni, Co, Rh, Pd, Ru and Pt supported on carbon will be evaluated for one pot conversion of polyols under very mild reaction conditions (T = 130~160 ^{o}C, P_{N2} = 0.3~1.4 MPa). Detailed kinetic modeling aiming at revealing the possible surface reaction mechanism will be carried out on Pt/C catalysts.

(4) Rational design of nanocatalysts for converting polyols to high value chemicals. The synthesis of super active Cu nanocatalysts with controlled structures is systematically carried out. The DH, HDO and WGS reactions will be correlated with various Cu surface planes. The well-defined Cu-based catalysts display five-fold enhancement in activity compared with conventional Cu catalysts.

Chapter 2 Hydrogenolysis of Sugar Polyols to Value-Added Chemicals on Supported Ru Catalysts: Reaction Pathways and Kinetic Studies

1. Introduction

Sugar polyols such as sorbitol, mannitol and xylitol produced from $C_{5\sim6}$ sugars are recognized as important renewable feedstocks for conversion to value-added chemicals, such as 1,2-propanediol (1,2-PDO) and ethylene glycol (EG), which were conventionally derived from petroleum-based feed stocks. The relevant literature on the type of catalysts used, reaction pathways and kinetics has been reviewed in Chapter 1. It is clearly seen that there is lack of complete understanding on the possible reaction products, as well as the plausible reaction mechanism involved in the conversion of sugar polyols. Therefore, in this chapter, experimental study on hydrogenolysis (HDO) of polyols (sorbitol and xylitol) using supported mono and bimetallic catalysts in aqueous medium is presented. The goal of this chapter is to obtain a comprehensive characterization of the possible reaction products and investigate the possible reaction pathways and mechanism of sugar polyols on metal based catalysts. The performance of different catalysts, role of supports, and solid acid and base promoters on catalytic activity and selectivity was studied in a batch slurry reactor. Based on the evaluation of different catalysts, studies with intermediate

products as substrates and kinetic modeling, a reaction pathway and possible mechanism of sorbitol and xylitol conversion are discussed.

2. Experimental section

2.1 Catalyst preparation

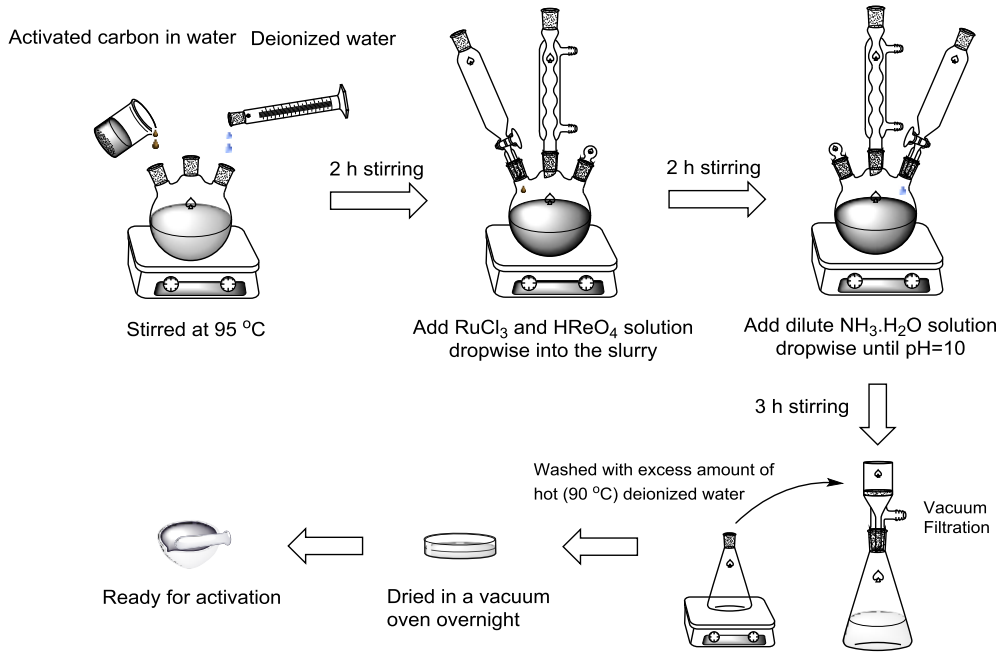

Figure 1. Outline of preparation of supported Ru and RuRe catalysts by co-precipitation method

Mono and bimetallic catalysts were prepared using a co-precipitation method shown in Figure 1. For Ru-based mono (Ru) and bimetallic (RuRe) catalysts, the detailed synthetic procedures of catalyst preparation is described as follows: 5.0 g of activated carbon (100 mesh, Sigma) was charged to 700 mL of deionized water and the slurry was heated to 95 ^{o}C in a round-bottom flask with magnetic stirring for 2 h to make sure carbon particles were well dispersed in

the aqueous medium. Then, required amounts of the noble metal salts [*e.g.*, $RuCl_3.xH_2O$ (99.98% trace metal basis, Sigma) and perrhenic acid (65w% in water, Sigma)] solution were first mixed with about 20 mL of deionized water in a beaker, and added to the slurry dropwise. The beaker was then washed at least three times using deionized water and the resultant slurry stirred for another 3 hours. A dilute $NH_3.H_2O$ solution (Fisher, about 10 mL/ 5 g catalysts) was added dropwise to the slurry obtained from previous step until a pH value of 10, and suspension stirred for another 3 hours. The mixture was then filtered and the solids pre-catalyst washed with 2000 mL of deionized water at 90 ^oC to remove chloride ions. The solid sample was then dried overnight in a vacuum oven at 120 ^oC.

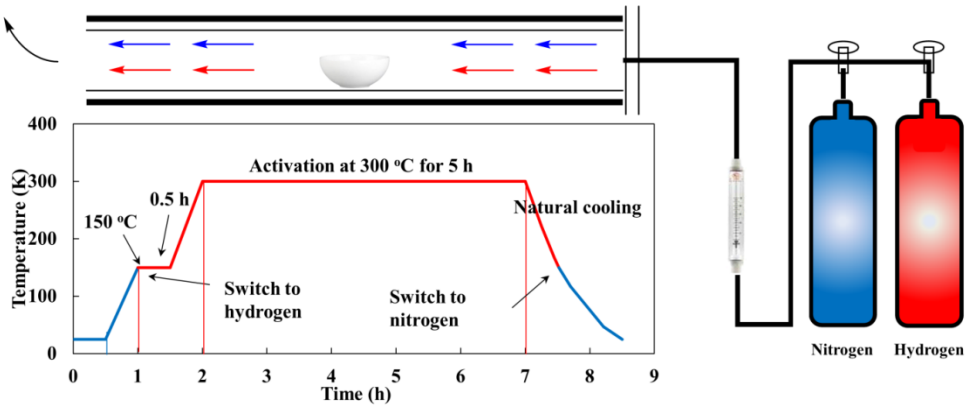

Figure 2. The temperature profile during catalyst activation and schematic of activation apparatus

The as-prepared catalysts were activated at 300 ^oC for 5 h in a tube furnace under the flow of hydrogen (99.95%, Linweld, flow rate: 20 cm^3/min/g catalyst) before testing for catalytic hydrogenolysis (HDO) in a slurry reactor. In the

activation procedure, the catalyst sample was placed in the tube, followed by purging with nitrogen (99.995%, Linweld, flow rate: 20 cm^3/min/g catalyst) at room temperature for 30 min, and heated at a rate of 5 ^oC/min to 150 ^oC. Then, the nitrogen flow was switched off and hydrogen was introduced to the tube. Next, the sample was heated at a rate of 5 ^oC/min to 300 ^oC and activated for 5 h under the flow of hydrogen. Finally, the system was cooled to 150 ^oC and then flushed with nitrogen gas again. This process is shown schematically in Figure 2. The samples were taken out of the tube furnace at room temperature and stored in a brown container. Several catalyst samples containing 0.25w%, 0.5w%, 1w%, 2w% Ru on carbon and Ru(1w%)-Re(1w%)/C were prepared following the above procedure.

The same preparation procedure was followed for the synthesis of other metallic catalysts consisting of Rh(1w%)/C, Pt(1w%)/C, and Ir(1w%)/C. $RhCl_3.xH_2O$ (99.9%, trace metal basis, Sigma), $H_2PtCl_6.xH_2O$ (99.9%, trace metal basis, Sigma) and $IrCl_3.xH_2O$ (99.9%, trace metal basis, Sigma) were used as metal precursors.

2.2 Catalyst performance evaluation

2.2.1 Evaluation of metal catalysts

Evaluation of metal catalysts for HDO of polyols was carried out in a high-pressure, high-temperature 300 mL reactor supplied by Parr Instrument Co. About 3.0 g of polyol substrate [*e.g.* sorbitol (98%, sigma), xylitol (99%,

sigma), glycerol (99.5%, sigma), ethylene glycol (99.8%, sigma)] were charged into a 100 mL graduated cylinder. Then deionized water was added to the cylinder under vigorous stirring at 800 rpm until the solution was homogeneous. The final volume of the aqueous solution was 91 mL. A sample of the prepared solution (about 1 mL) was taken out and injected into high performance liquid chromatograph (HPLC) to determine the initial concentration of the polyol substrate. 0.4 g of solid catalyst [*e.g.* Ru(1w%)/C] was introduced to the reactor. For studies on promoter effect, 0.4 g of solid promoters [*e.g.* MgO (99% trace metals basis, 325 mesh, Sigma), CeO_2 (99.9%, Fisher) or Hβ zeolite (CP811C-300, Zeolyst)] were then charged in the reactor before introducing the substrate solution. Then the prepared 90 mL aqueous solution was slowly added to the reactor.

Figure 3. Experimental setup of 300 mL Parr reactor setup (left) and monitoring system (right)

Next the reactor head was then connected with the body. The pressure transducer, temperature sensor, gas inlet was connected in order before the reactor was heated. The reactor was purged thrice each with nitrogen at 1.0

MPa. Then hydrogen was charged to the reactor to purge nitrogen for three times at 2.0 MPa. Then hydrogen was released and the reactor was set at normal pressure. The reactor was then heated up to desired temperature. During the reactor heating process, the stirring rate was set at <50 rpm to ensure negligible reactions during the heating period. When the reactor reached the desired temperature, the stirring speed was increased to > 1000 rpm to avoid external mass transfer limitations, which signified as the start of HDO experiment. The temperature and pressure profiles were recorded every 2 seconds by a monitoring system (as shown in Figure 3).

2.2.2 Experiments for kinetic study

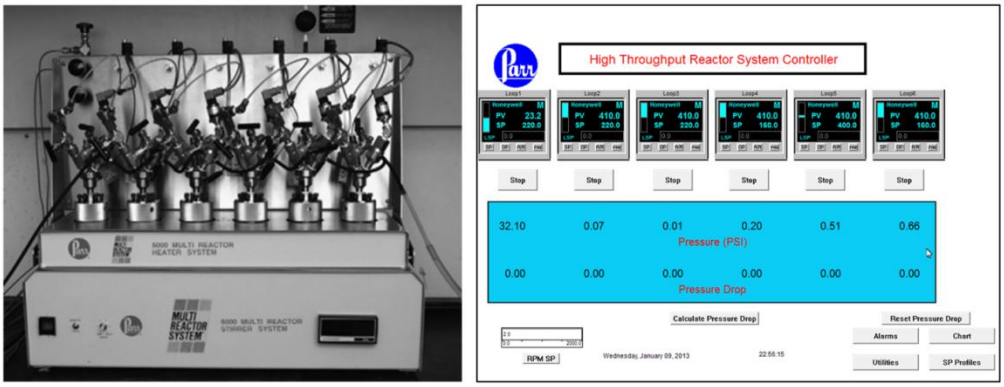

Figure 4. The multiple-slurry-reactor system (left) with control system (right)

Experiments for kinetic modeling of HDO of sorbitol were carried out in a high-pressure, high-temperature multiple-slurry-reactors system supplied by Parr Instrument Co (shown in Figure 4). PTFE liners were used in each reactor in order to avoid the catalytic effect of reactor wall materials at elevated temperatures (> 140 ^{o}C) in the presence of base promoters. For a typical test,

about 1.5 g of sorbitol was dissolved in 15 mL of water in a graduated cylinder, by stirring at 200 rpm until a homogeneous solution A was formed. If NaOH, KOH and $Ba(OH)_2$ were used as the base promoter, sorbitol and base promoter were mixed together to obtain a 15 mL aqueous solution. Known amounts of solid catalyst sample (0.1 g), such as Ru/C catalyst, were charged into the PTFE liner along with MgO or $Ca(OH)_2$ as the base promoter. Solution A was then added to PTFE liner already containing solid catalyst and promoter and the suspension stirred at 200 rpm at room temperature for 2 min. The PTFE linear was placed into the slurry reactor, which was then sealed and purged three times with nitrogen. The stirring speed was set at 100 rpm in order to flush the air in the reactor void space and any dissolved air from the solution. Then the reactor was purged with hydrogen at 2.0 MPa, the gas phase released to normal pressure and the heating process was started. Once the desired reaction temperature was reached, hydrogen pressure was increased to a required value. Agitation speed was set at 800 rpm to start the reaction.

2.3 Analytical methods

After a certain period of time, the reaction was stopped by switching off the agitation and heating duty. Then the reactor contents were cooled to room temperature and the final pressure of the reactor was noted. Then, the reactor was depressurized by releasing the gas-phase products to fill two external sampling loops for offline gas chromatographic (GC) analysis (Shimadzu, Model GC-2014). The sample in one loop was used for analysis of C_2~C_5

alkanes which were separated in RT-QPLOT column (15 m long, inner diameter of ID = 0.53 mm) and analyzed using flame ionization detector (FID). The sample in a second loop was used for analysis of methane, ethane, CO, and CO_2 which were separated using a 60/80 Carboxen 1000 packed column (4.57 m long, ID = 3.175 mm) and analyzed using a thermal conductivity detector (TCD) device. Detailed operation procedures for GC analysis are described in Appendix I.

Figure 5. Instruments of gas chromatography (left) and liquid chromatography (right)

Table 1. HPLC conditions

Parameter	Value	
	Method 1	Method 2
Oven temperature (^oC)	60.0	60.0
Mobile phase (N)	0.005	0.005
Total mobile phase flow rate (mL/min)	0.50	0.20
Detector	RID	RID
Cell temperature (^oC)	40.0	40.0

The liquid samples were analyzed using an HPLC (a Rezex ROA-Organic Acid H^+ column, 0.005 N aqueous H_2SO_4 as mobile phase and an RI detector). These

analytical results were combined to obtain a quantitative assessment of each product in the gas and liquid phase, and for calculation of conversion and selectivity. An example of HPLC result is shown in Scheme 1.

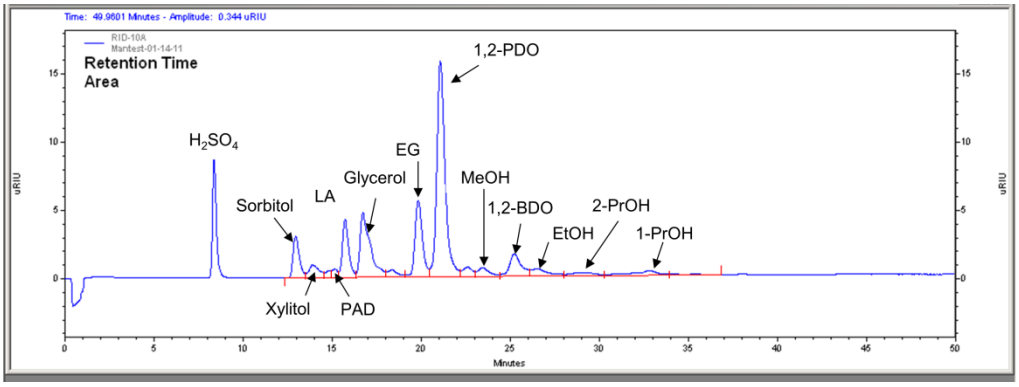

Scheme 1. A typical liquid chromatography result from sorbitol conversion

Definitions. *Conversion rate* (CR) is defined as the amount of substrate converted (mol) in the presence of certain amount of bulk metal (*e.g.* g atom Ru) after a fixed reaction time (h), expressed as mol/g atom/h. *Turnover frequency* (TOF) is defined as amount of substrate converted (mol) in the presence of certain amounts of surface metal atoms (mol) during reaction (h), expressed as mol/mol/h. Both CR and TOF are calculated for conditions such that the conversion level is in the range of 5~27%. *Conversion* is defined as the ratio of moles of substrate converted to the moles of substrate charged initially. *Selectivity* is defined as the ratio of the moles of carbon in specific product to the moles of carbon equivalent to converted substrate. *Yield* of a specific product is defined as conversion multiplied by selectivity of a specific product.

Error analysis. Experimental error includes the uncertainty from repeated experimental data under identical reaction conditions as well as the error in HPLC analysis. Some of the key experiments, including substrate/product concentration of sorbitol hydrogenolysis at relatively low conversion levels (X < 35%) and that at relatively higher conversion levels (X = 55~87%). The (experimental) error (from repeated experiments) for low conversion level is in the range of 3.5~14.2%, while this value is approximately 4.2~10.2% at X = 55~87% (see Figures 15~17). The relatively error from HPLC analysis (repeated injection of one sample) is as low as < 0.08% in all cases. The concentration data measured from repeated experiments were input to software when parameter estimation was conducted. Therefore the uncertainty value for estimated parameters such as reaction rate constants already takes into account the all types of experimental error. The detailed procedures for error analysis are shown in Appendix I.

2.4 Catalyst characterization

2.4.1 Transmission electron microscopy (TEM)

Figure 6. TEM instrument and work station

Samples were prepared by suspending the solid catalyst in ethanol (EtOH) and agitating in an ultrasonic bath for 15 minutes. 10 μL of catalyst sample was placed onto a copper mesh grid with lacey carbon film (purchased from Ted Pella Inc.). The wet grid was allowed to air-dry for several minutes prior to being examined under TEM. The catalyst particle size and morphology were examined by bright-field and dark-field TEM using an FEI Technai G_2 transmission electron microscope at an electron acceleration voltage of 200 kV (shown in Figure 6). The equipment is located in Microscopy and Analytical Imaging Laboratory (www.mai.ku.edu) on the campus of University of Kansas. High resolution images were captured using a standardized, normative electron dose and a constant defocus value from the carbon-coated surfaces. Energy dispersive X-ray spectroscopy (EDX) was carried out using an EDAX detector.

2.4.2 Inductively coupled plasma (ICP)

The supported metal catalysts were characterized by ICP for bulk metal content. The procedure is briefly described here: 0.1 g of solid catalyst was digested using a mixture containing 2.0 g of hydrofluoric acid (47~51%, Fisher), 1 g of sulfuric acid (98%, Sigma) and 7.0 g of H_2O. The slurry was sealed in a steel autoclave and kept in a drying oven at 120 ^oC for 10 h. The resultant sample was then diluted further and stored for two days. The same procedure was repeated in order to extract all metal components on solid supports before ICP measurement. Then the extractant solution was then diluted to a certain volume. The ICP measurement was conducted in JY-2000 ICP instrument (HORIBA,

Jobin Yvon Inc., flow rates of plasma gas: 12 L/min, aux: 0 L/min and gainage: 0.2 L/min). The measured value of metal content (ppm) in the solution was divided by dilution ratio to calculate the actual metal content on carbon supports. The specific metal content for Ru(0.25w%)/C, Ru(0.5w%)/C, Ru(1w%)/C and Ru(2.5w%)/C catalysts are 0.21w%, 0.49w%, 0.98w% and 2.42w%, respectively. The metal content for Ru(1w%)Re(1w%)/C catalyst is Ru(0.97w%) and Re(1.08w%). A typical example of ICP calibration is shown in Appendix I.

3. Catalyst performances and reaction pathways

3.1 Catalyst performance evaluation

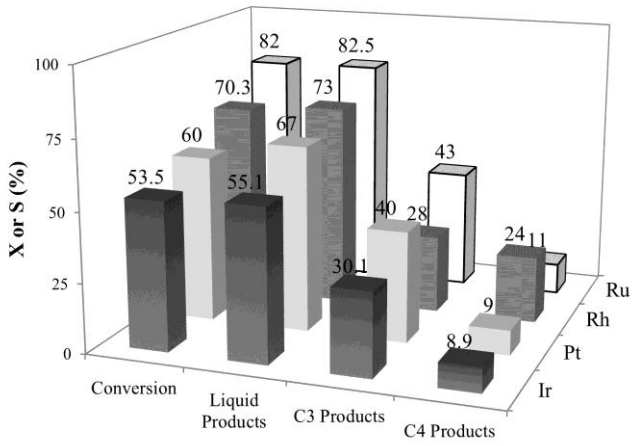

Figure 7. Conversion and liquid product carbon selectivities for sorbitol HDO
Experimental conditions: metal/carbon+MgO admixture: 3 g of sorbitol in 90 mL of aqueous solution, 0.4 g of solid catalysts, 0.4 g of MgO, 230 ^{o}C, 7.6 MPa (P_{H2}), 10 h. Liquid Products: methanol (MeOH), ethanol (EtOH), ethylene glycol (EG), C_3, and C_4 products. C_3 products: propanediol, glycerol, lactic acid; C_4 products: meso-erythritol, 1,2-butanediol (1,2-BDO).

A variety of monometallic catalysts consisting of Ru, Rh, Pt, and Ir were prepared and tested for HDO of sorbitol in the presence of MgO as a solid basic promoter. In all the experiments, the carbon balance closure was found to be within a range of 85~95% for the catalysts tested. It is clearly seen from Figure 7 that Ru showed higher activity and selectivity for sorbitol HDO compared to other metals. After 6 h of reaction, approximately 82% of sorbitol was converted with a total liquid products selectivity of about 82%. Furthermore, the Ru/C catalyst displayed slightly higher selectivity to C_3 products including 1,2-PDO, glycerol and lactic acid (LA) compared to the Pt/C catalyst, whereas the Rh/C showed relatively higher selectivity for meso-erythritol and 1,2-butanediol (1,2-BDO). Therefore Ru/C catalyst was chosen for further evaluation.

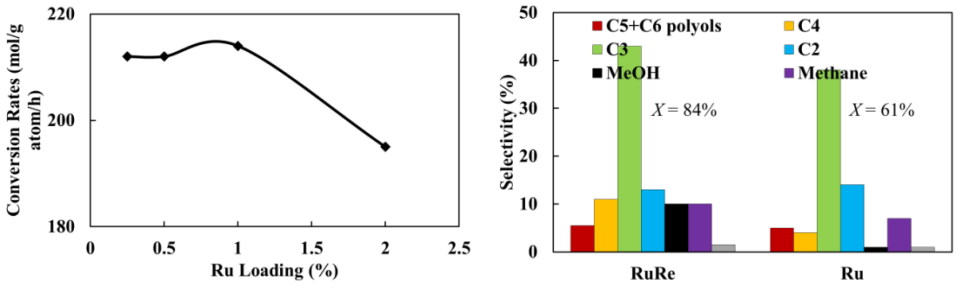

(a) (b)

Figure 8. Conversion and selectivity of sorbitol conversion, (a) effect of Ru loading (3 g of sorbitol in 90 mL of aqueous solution, Ru/C catalyst: 0.4 g, MgO: 0.4 g, T: 230 ^{o}C, hydrogen pressure: 7.6 MPa, 0.5~1.0 h, sorbitol conversion ~20%) and (b) comparison of Ru/C and RuRe/C catalysts (X: conversion, T: 230 ^{o}C, hydrogen pressure: 7.6 MPa, 6 h, other conditions same as (a). C_2: EG and EtOH, C_3: 1,2-PDO, glycerol, LA; C_4: meso-erythritol, 1,2-BDO; C_5+C_6 polyols: xylitol, 1,2,3-hexanetriol).

Effect of metal loading on sorbitol conversion was studied over monometallic Ru/C catalysts. As seen in Figure 8 (a), a CR of 214 mol/g atom/h is observed for Ru loadings up to 1w%, which decreases by 10% at a higher Ru loading (2w%). The maximum CR observed is greater than that reported (182 mol/g atom/h) with a liquid base at the same temperature.[88]

Bimetallic Ru(1w%)-Re(1w%)/C was further prepared and compared with mono Ru(1w%)/C catalyst. It is found that, the addition of Re increases the sorbitol conversion rate (256 mol/g atom/h) over the monometallic Ru catalyst [shown in Figure 8 (b) for sorbitol]. The presence of Re is also found to increase the selectivity of C_3 and C_4 diols. Thus, it is clear that bimetallic RuRe catalyst displays relatively better performance compared with monometallic Pt, Rh, Ir and Ru catalysts. RuRe/C catalyst was thus chosen for further studies as its performance was better than other catalysts.

3.2 Characterization

TEM Characterization of Ru/C and RuRe/C is shown in Figure 9. It is found that monometallic Ru particles display a size distribution of 9.6~12.4 nm on carbon support as seen in Figure 9 (a) and 9 (b). In sharp contrast, bimetallic RuRe particles show slightly smaller size and narrow distribution (in the range of 7.2~10.1 nm). From Figures 9 (d) and 9 (e), the average particle size of Ru in bimetallic RuRe particles is ~8.5 nm. Surface mapping of Ru and Re elements [Figure 7(f)] further confirmed the existence of bimetallic nanoparticles on the

surface of carbon supported catalysts. It is clear that Ru shows better dispersion in the presence of Re than monometallic Ru particles [Figure 9 (c)].

In addition, lattice parameters measured from high resolution TEM images [Figure 9 (b) and 9 (e)] show that RuRe particles have 0.22 and 0.34 nm distance between lattices, which is the characteristic value for Ru [101] surface plane. These results agree well with the previous findings by X-ray diffraction (XRD) analysis.[91] Therefore, it is clearly shown that the addition of Re to Ru enhances the dispersion of Ru on carbon surface, which is believed to promote the overall activity of Ru catalysts for sorbitol conversion.

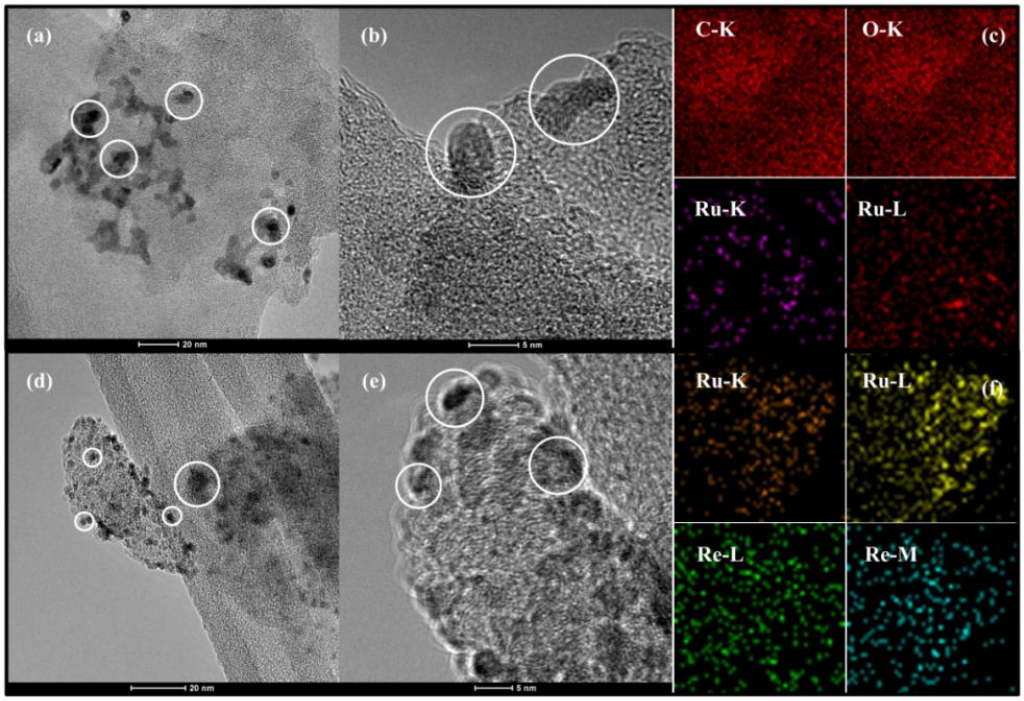

Figure 9. TEM data of monometallic Ru/C (a~c) and bimetallic RuRe/C catalysts (d~f) and EDX mapping of Ru and Re element

3.3 Role of acidic/basic promoters

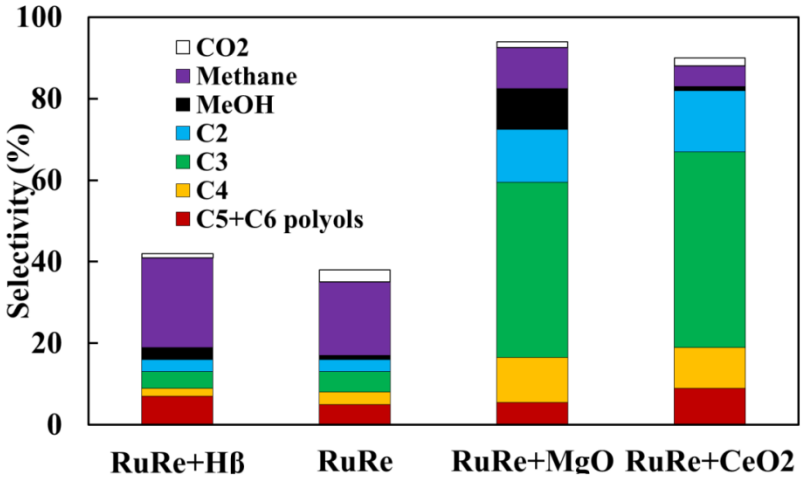

Figure 10. Effects of acid and solid base promoters in sorbitol conversion (experimental conditions same as Figure 7, except that reaction time is 12 h, sorbitol conversion is 100% for this figure)

The effects of acid and base promoters on the HDO of sorbitol were also investigated. It is clear from the results in Figure 10 that acid and base promoters have a strong influence on product distribution. The results are shown in Figure 10 for conditions where complete sorbitol conversion is obtained. It was observed that significant amounts of gas phase alkanes (mainly methane) were formed with the addition of Hβ zeolite as a solid acid promoter, while the addition of a solid base (MgO or CeO_2) reduced the gas phase products selectivity from 25 to 11%.

The product distribution during sorbitol conversion on acidic promoters agrees well with previous findings. Kusserow[145] and Montassier[104] reported that unsaturated polyols (with similar structures as sugars) underwent dehydration

(DHD) in acidic medium (*e.g.* Ru/C+a sulfate promoter) and resulted in the formation of furfurals (such as 5-hydroxymethylfurfural), which might undergo facile HDO reactions to form hydrocarbons, instead of products from C_3-C_3 cleavage. Further, Huber and Dumesic found that sorbitol underwent HDO at a higher temperature (250 ^{o}C) over an acidic support with random C-C bond cleavage resulting in the formation of significant amounts of methane, ethane, and propane (combined selectivity > 54%).[92]

Although the preliminary results shown in Figure 10 indicate that lower $C_{2\sim4}$ products in liquid phase are dominant during sorbitol conversion in the presence of basic MgO and CeO_2 promoters. However, the possible positions of C-C cleavage and HDO reaction pathways in the presence of solid base promoters were not yet clearly understood. The promoting effect of a base on C-O cleavage was not reported previously for HDO of glycerol and EG as well.[57,82] Therefore, several possible intermediate products (glycerol and EG) were therefore tested as starting substrates to understand the effect of solid base promoters on the catalyst activity and product distribution (Figure 11). Specifically, a better understanding of the role of solid base in (a) C-O and C-C breakage and (b) methanation reactions, over bimetallic catalysts was sought.

It was noted that a liquid base such as NaOH enhanced the conversion of polyols over Ru or Ni monometallic catalysts.[88,94] In contrast, it was found that the addition of MgO as a solid base promoter did not enhance the activity of the RuRe bimetallic catalyst (Figure 11).

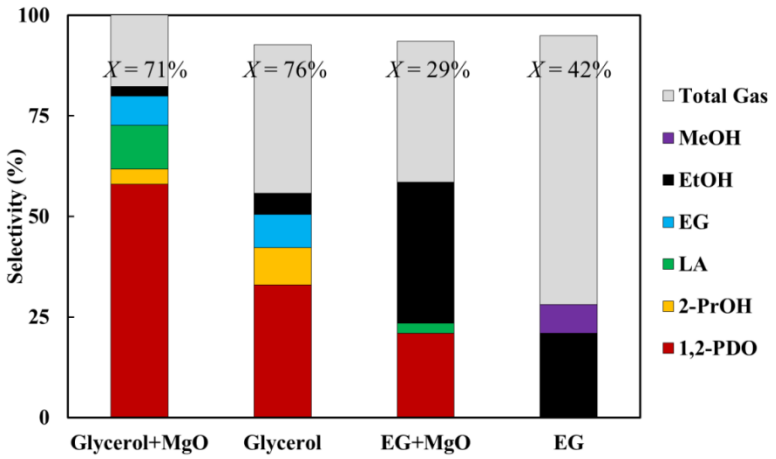

Figure 11. Product distribution of glycerol and ethylene glycol conversion with/without MgO (3 g of glycerol/EG in 90 mL of aqueous solution, other conditions same as Figure 7. X: conversion; Total gas: methane, ethane; 2-PrOH: 2-propanol)

Also seen from Figure 11, the selectivity of C_2~C_3 alcohols increased significantly in the presence of a base promoter (from 60% to 82% and from 30% to 60% for glycerol and EG conversion, respectively). In contrast, the methanation selectivity was restrained when a base promoter (MgO) was added, from almost 40% to 18% and 70% to 50% during glycerol and EG conversion, respectively. These results are different from Davda's report, where they found that during aqueous phase reforming of polyols on Pt catalysts, the selectivity to hydrogen decreased with increasing carbon number (from glycerol to sorbitol), but the selectivity to gaseous alkanes (methane, ethane, *etc*.) increased as carbon chain increases.[146] In sharp contrast, our results clearly show that the reforming potential of EG is more restrained than for glycerol in the presence of a base, producing EtOH as the major liquid product. Our experiments support two important conclusions: (a) C-C cleavage trend over Ru is different from

that in the presence of OH^-; (b) C-C cleavage is restrained for lower carbon number polyols in the presence of MgO.

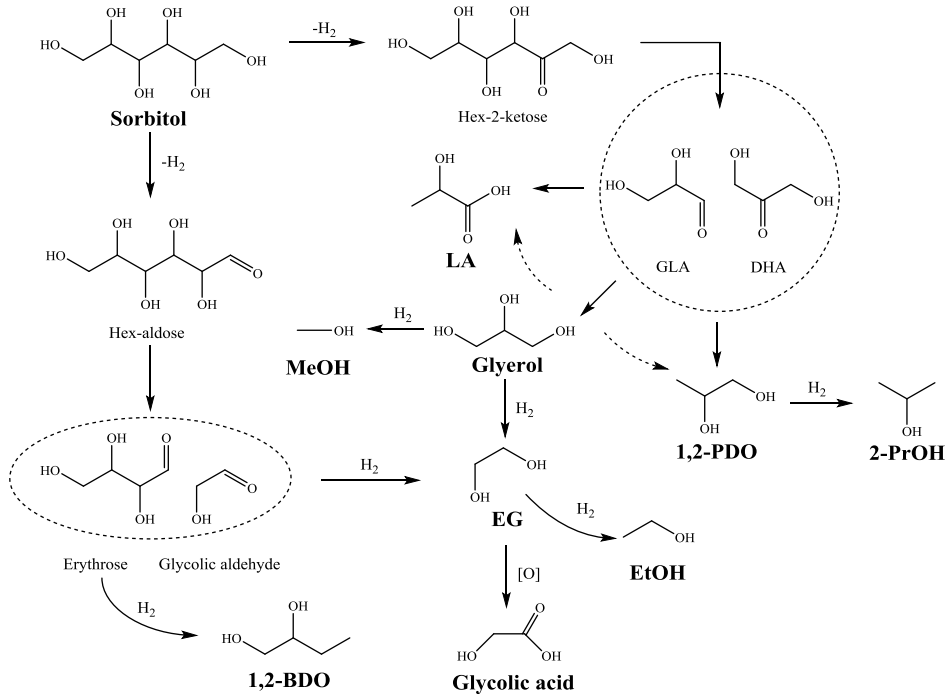

Scheme 2. Proposed reaction network for HDO of sorbitol

Based on the product distribution obtained in our experimental findings on sorbitol conversion as well as the preliminary results from previous reports,[88,89,94,104] a detailed reaction pathway is proposed as shown in Scheme 2. According to the proposed scheme, the conversion of sorbitol initiates with the base promoted dehydrogenation (DH) and C=O bond formation. Then, the unsaturated intermediate undergoes C-C cleavage *via* retro-aldolization. The possible C-C cleavage positions include C_1-C_5 (then C_2-C_3), C_2-C_4, and C_3-C_3. Prediction of thermodynamic properties on reaction energies of C_2-C_4 and C_3-C_3 cleavage reveals that both reaction pathways are highly possible during

sorbitol conversion.[147] The resulting small molecules undergo further hydrogenation, thus leading to glycerol, xylitol, and traces of erythritol in the final products. These intermediate polyols are further hydrodeoxygenated to 1,2-BDO, 1,2-PDO, EG, and EtOH as the major products. Glycerol can also undergo DH and benzilic rearrangement to form LA under our reaction conditions.[79] In our system, it is also found that DHD is also important in facilitating C-O bond cleavage followed by hydrogenation. The observation of 1,2-BDO (approximately 10% in selectivity) in the product mixture, not mentioned in the previous reports, seems to support our hypothesis.

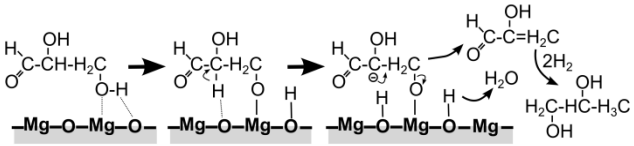

Scheme 3. Possible reaction pathway for DHD of glyceraldehyde (GLA) over MgO

Furthermore, a number of publications previously assumed that glycerol undergoes retro-aldol reaction leading to the formation of MeOH and C_2 alcohols,[56,57,82] but in our work it is found that the majority of the liquid products consist of 1,2-PDO and LA, with only less than 10% of C_1~C_2 alcohols, even in the presence of a base. This indicates that the solid base provides a favorable environment for the formation of aldehydes/ketones and hydrogenation of these unsaturated compounds, rather than C-C cleavage and generating gases products. King and coworkers found that alkali promoters with PtRe/C catalysts enhanced glycerol conversion and also the fraction of carbon in liquid (C_2~C_3 alcohols) suggesting the suppression of reforming activity.[80]

The observed increases in the selectivities of liquid products from glycerol conversion indicate that hydrogen is more efficiently utilized in a basic medium (as suggested from Scheme 3) for the formation of alcoholic products (*e.g.* 1,2-PDO) than in neutral and acidic environments. In summary, the role of the solid base promoter can be summarized as follows: (a) the base promoter activates polyols in retro-aldol condensation; (b) the base promoter affects the relative activities of the following three steps in the order: hydrogenation ≈ DHD > retro-aldol condensation >> methanation.

3.4 Effects of reaction temperature

As shown in Scheme 2, conversion of sorbitol initiates with DH and results in C_1-C_5, C_2-C_4, and C_3-C_3 products as intermediates. In order to understand the temperature effects on the C-C bond cleavage in xylitol and sorbitol conversion, and resulting product distributions, several experiments were carried out at low conversion levels (~25%). As shown in Figure 12, low temperatures favor C_3 products compared to other products. At 210 ^{o}C, the C_3 selectivity from xylitol and sorbitol was about 15% higher than the results at 230 ^{o}C and 245 ^{o}C, while the C_1 and C_2 selectivity increased with increasing reaction temperatures. Therefore, it is plausible that at relatively low temperatures, C_3-C_3 cleavage is favored, whereas C_1-C_5 and subsequent C_2-C_3 cleavage dominate at high temperatures. It is important to recognize that C_3-C_3 bond breaking will result in glyceraldehyde (GLA) formation as intermediate products, which can be hydrogenated to glycerol[89] over the RuRe catalyst in the presence of hydrogen,

while C_1-C_5 breakage [confirmed by the formation of traces of CO (<1%) in selectivity] probably leads to the formation of MeOH and xylitol. Xylitol is found to easily undergo further C_2-C_3 cleavage under similar reaction conditions (Figure 12). Once C_3 or C_2 compounds are formed, the presence of Re enhances the C-O cleavage reactions, consistent with the reaction pathways in glycerol and EG conversion (shown in Figure 11).

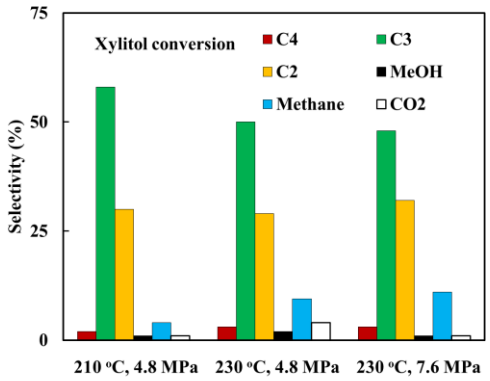

(a)

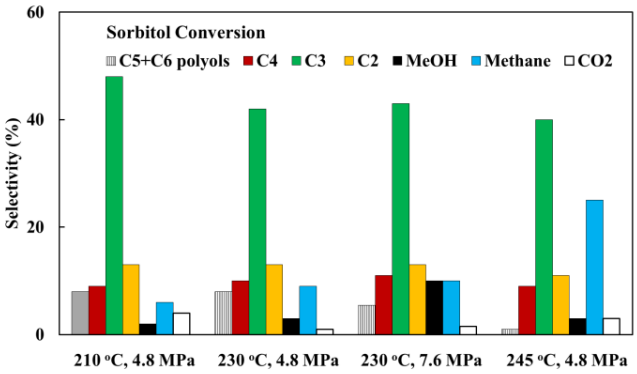

(b)

Figure 12. Temperature effect on (a) xylitol and (b) sorbitol conversion on RuRe/C catalyst (reaction time: 0.5~1.5 h, sorbitol conversion ~25%, other reaction conditions same as Figure 7)

The recyclability of the catalysts was also studied (at 210 ^{o}C, hydrogen pressure 7.6 MPa, and 1 h). The CR of the fresh RuRe/C catalyst was found as 256 mol/g atom/h, whereas those of the 1st and 2nd recycle were 213 and 210 mol/g atom/h, respectively. The selectivity of C_3 products was 47.2%, 46%, and 46%, respectively. These results show that RuRe/C catalysts are stable and recyclable under the reaction conditions.

4. Kinetic modeling of HDO of sorbitol on RuRe/C catalyst

4.1 Comparison with previous work

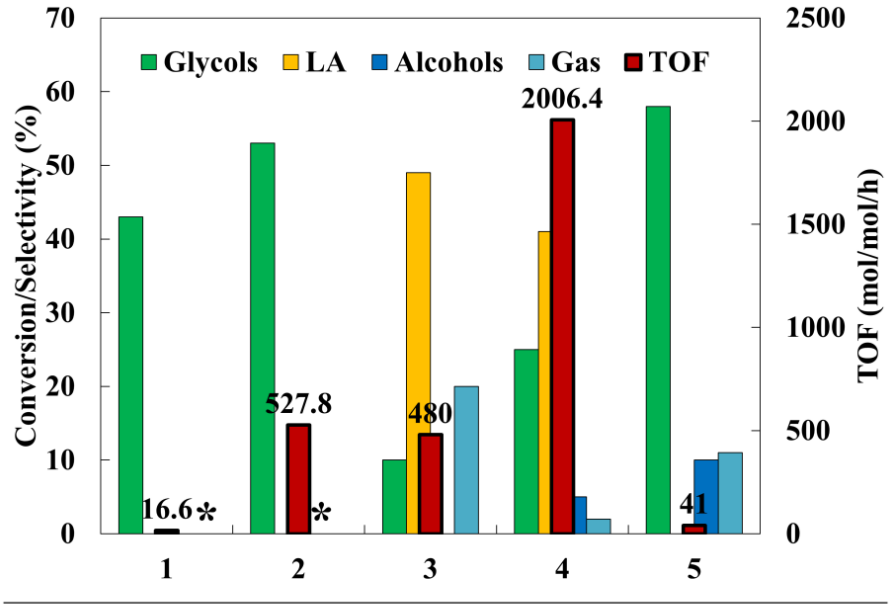

No.	1	2	3	4	5
Catalyst	Ru/C	Ru/CNF	RuRe/C	RuRe/C	$NiCe/Al_2O_3$
Promoter	NaOH	$Ca(OH)_2$	MgO	$Ca(OH)_2$	Ce^{4+}

Figure 13. Comparison of various metal catalysts for sorbitol conversion (*: not reported by authors)

A further comparison with previous reports was also carried out at 230 ^{o}C. As shown in Figure 13, the TOFs for Ru/C (NaOH as the promoter), Ru/CNF [$Ca(OH)_2$], RuRe/C (MgO) and RuRe/C [$Ca(OH)_2$] are 16.6, 527.8, 480.0 and 2006.4 mol/mol/h, respectively. Obviously, our RuRe/C catalysts show superior performances compared with previously reported catalysts in terms of conversion and selectivity under the same reaction conditions. RuRe/C+$Ca(OH)_2$ system (Entry#4 in Figure 13) exhibits best performance in both activity and selectivity, thus been chosen for kinetic study of HDO of sorbitol.

4.2 Reaction profiles

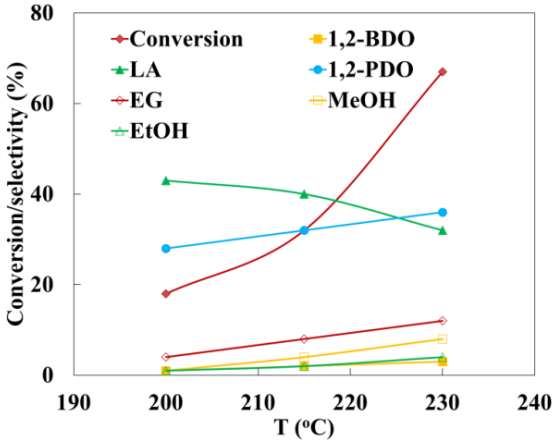

Figure 14. Temperature effect on sorbitol conversion and selectivity to major products at P_{H2} = 3.5 MPa. Reaction conditions: sorbitol concentration: 0.272 kmol/m^3; solvent, H_2O; catalyst loading, 6.7 kg/m^3; $Ca(OH)_2$ loading, 10.0 kg/m^3; initial liquid volume, 15 mL; reaction time, 1 h.

Temperature effects on the conversion as well as selectivity of sorbitol were also investigated. As seen from Figure 14, conversion increased from <20% to

almost 70% when temperature increased from 200 ^{o}C to 230 ^{o}C. An increase in temperature resulted in decreasing selectivity to LA (from 42% to 35%), while that to 1,2-PDO, EG and alcohols increased marginally with increasing temperature. This implies that higher reaction temperatures favor hydrodeoxygenation reactions and lead to further conversion of 1,2-PDO and EG to 2-PrOH and EtOH, which also agrees well with the previous work.[91]

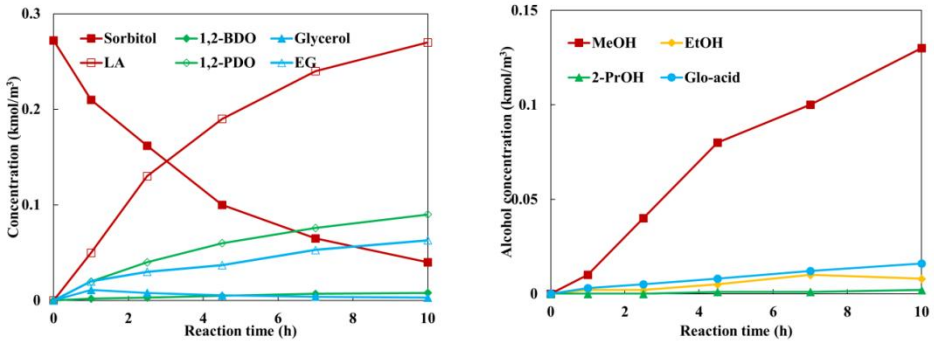

Figure 15. Concentration~time profiles at 200 ^{o}C and P_{H2}: 2.0 MPa. [Reaction conditions: sorbitol concentration: 0.272 kmol/m^3; solvent: H_2O; catalyst loading: 6.7 kg/m^3; $Ca(OH)_2$ loading: 10.0 kg/m^3; initial liquid volume, 15 mL. Experiments at 1 h and 7 h were repeated, the maximum error is 3.5% and 4.2% respectively.]

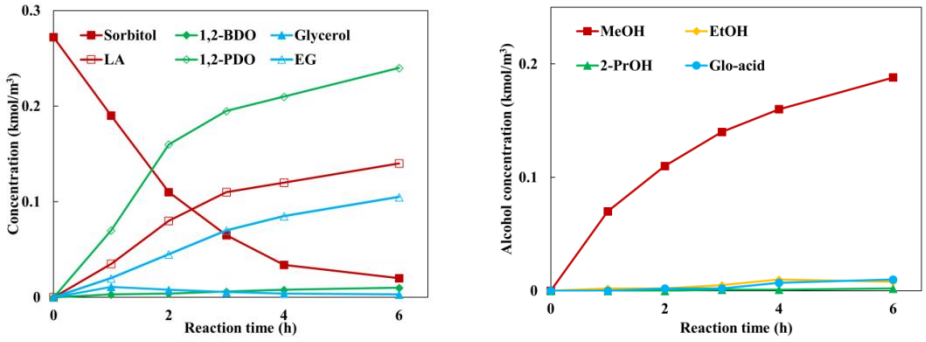

Figure 16. Concentration~time profiles at 200 ^{o}C and P_{H2}: 5.0 MPa

(Reaction conditions same as Figure 15. Experiments at 1 h and 2 h were repeated, the maximum error is 10.9% and 8.2% respectively.)

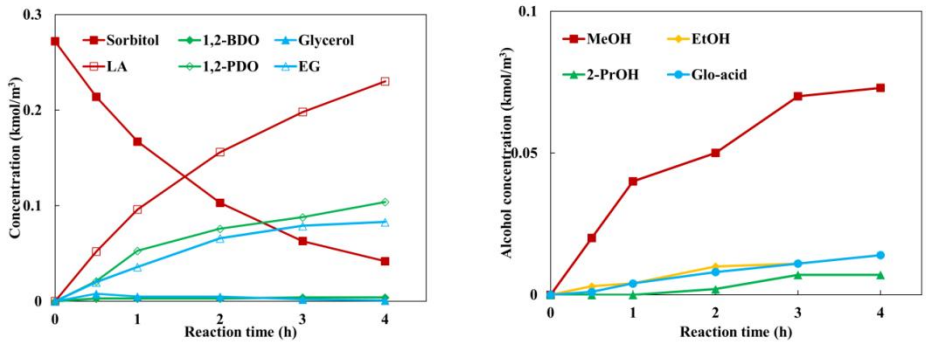

Figure 17. Concentration~time profiles at 215 ^{o}C and P_{H2}: 2.0 MPa

(Reaction conditions same as Figure 15. Experiments at 0.5, 1 h and 2 h were repeated, the maximum error is 14.2%, 8.8% and 10.2% respectively.)

Typical concentration~time profiles of sorbitol conversion in the presence of RuRe/C catalyst are shown in Figures 15~17. It is seen that in sorbitol conversion, the concentration of LA, 1,2-PDO, EG increased with increasing conversion of sorbitol. As reaction temperature increased (from 200 ^{o}C to 215 ^{o}C), the hydrodeoxygenation rate increased significantly, evident from the increase in glycerol, 1,2-PDO and EG concentration in the final product (from 0.20 kmol/m^3 to 0.25 kmol/m^3 at the conversion level of 65~75%). It is also found that the concentration of 2-PrOH and EtOH increased (from 0.002 kmol/m^3 to 0.01 kmol/m^3) as hydrogen pressure increased, a clear evidence of further conversion of 1,2-PDO and EG under relatively higher hydrogen pressure, which is shown in Figures 15 and 16. Furthermore, it is seen that increasing hydrogen pressure (from 2.0 MPa to 5.0 MPa) resulted in the increase in the overall hydrogenation rate (Figure 18).

Effect of RuRe/C catalyst loading was also investigated (Figure 19). It is found that selectivity to LA decreased (from 46% to 40%) with increasing amounts of RuRe/C loading, while the combined selectivity to 1,2-PDO, EG and alcohols obviously increased by approximately 8% with increasing amount of RuRe/C catalyst.

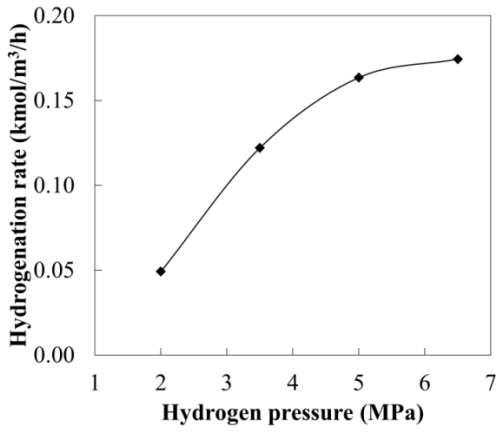

Figure 18. Hydrogen pressure effect on hydrogenation rate at 200 °C

(Reaction conditions same as Figure 15, conversion < 20%)

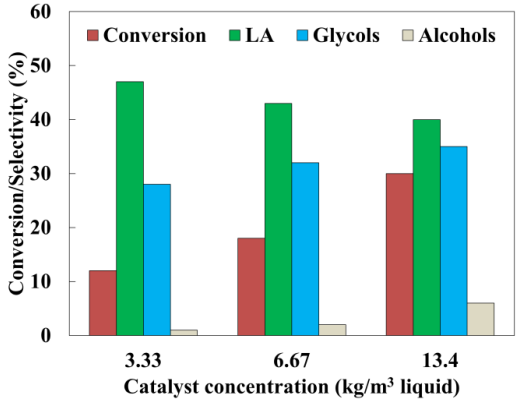

Figure 19. Catalyst concentration effect on hydrogenation rate at 200 °C

(Reaction conditions same as Figure 15, conversion < 20%)

The reaction models are proposed in Scheme 4 based on the qualitative description of reaction pathways in Scheme 2. Clearly, several reaction pathways can lead to the formation of C_2 and C_3 products. With regard to the fact that C_3 (1,2-PDO, LA and glycerol) are the major liquid products detected in the liquid phase, another reaction route, C_3-C_3 cleavage, seems to be dominant in sorbitol conversion. The formation of another unsaturated C_6, hex-2-ketose will lead to C_3-C_3 cleavage according to retro-aldolization mechanism. GLA and dihydroxyacetone (DHA) will form as a result. As observed previously, GLA and DHA are not stable at all under our reaction conditions and can be quickly converted to LA *via* DHD route, or 1,2-PDO *via* HDO pathway.[91] It is necessary to point out that glycerol is also detected (S < 10%) in final product mixture. Another possible route of sorbitol conversion is starting from hex-3-ketose, which lead to C_1-C_5 cleavage or decarboxylation of sorbitol. But it hardly happens according to our preliminary observation in product distribution (shown in Table 4-2-1 of Appendix IV), thus not added in the proposed reaction model (Scheme 4). Additionally, it is observed that the activity of methanation is almost completely restrained in RuRe/C+$Ca(OH)_2$ system thus will not be taken into account for kinetic modeling.[91]

The initial rates of HDO of sorbitol were calculated for a wide range of experimental conditions (as seen in Table 2) from the production rates of various hydrodeoxygenated products in order to ensure that the batch data were obtained in the kinetic regime. Those data were used to evaluate the

significance of mass transfer effect, including gas-liquid, liquid-solid and intraparticle resistance, based on the criteria proposed by Ramachandran and Chaudhari.[148] The mass transfer coefficient, diffusion properties and hydrogen solubility data were used as obtained previously. It is found that the external and internal mass transfer effect was negligible in our experiments (detailed calculation shown in Appendix I).

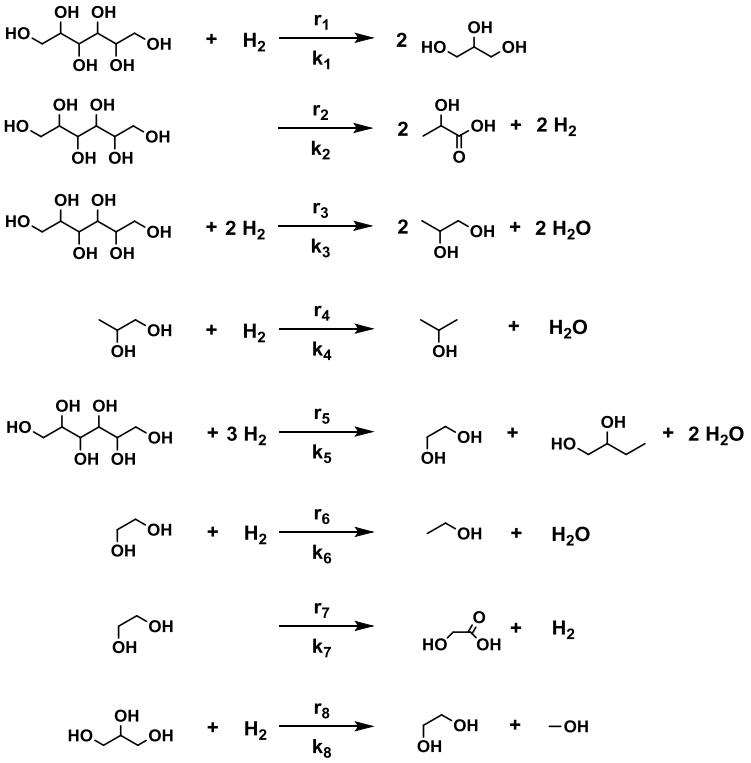

Scheme 4. Proposed reactions for sorbitol conversion

4.3 Proposed reaction models

Table 2. Experimental parameters in kinetic modeling of sorbitol conversion

Sorbitol concentration (kmol/m^3)	0.272
Catalyst concentration (kg/m^3)	3.33~13.3

T (^{o}C)	200~230
Hydrogen pressure (MPa)	2.0~6.5
Solvent	Water
Volume of initial liquid mixture (m^3)	15×10^{-6}
Reaction time (h)	0.25~6.0

Table 3. Reaction rate terms presented in Scheme 4

$r_1 = w \cdot k_1 \cdot C_{H_2} \cdot C_{Sor}$	$r_2 = w \cdot k_2 \cdot C_{Sor}$
$r_3 = w \cdot k_3 \cdot C_{H_2} \cdot C_{Sor}$	$r_4 = w \cdot k_4 \cdot C_{H_2} \cdot C_{1,2-PDO}$
$r_5 = w \cdot k_5 \cdot C_{H_2} \cdot C_{Sor}$	$r_6 = w \cdot k_6 \cdot C_{H_2} \cdot C_{EG}$
$r_7 = w \cdot k_7 \cdot C_{EG}$	$r_8 = w \cdot k_8 \cdot C_{H_2} \cdot C_{gly}$

w is catalyst charged (kg/m^3)

Table 4. Material balance in a batch slurry reactor

$\frac{dC_{Sor}}{dt} = -r_1 - r_2 - r_3 - r_5$	$\frac{dC_{1,2-BDO}}{dt} = r_5$
$\frac{dC_{gly}}{dt} = 2 \cdot r_1 - r_8$	$\frac{dC_{LA}}{dt} = 2 \cdot r_1$
$\frac{dC_{1,2-PDO}}{dt} = 2 \cdot r_3 - r_4$	$\frac{dC_{EG}}{dt} = r_5 - r_6 - r_7 + r_8$
$\frac{dC_{EG}}{dt} = r_8$	$\frac{dC_{EtOH}}{dt} = r_6$
$\frac{dC_{2-\mathrm{Pr}OH}}{dt} = r_4$	$\frac{dC_{Glo-acid}}{dt} = r_7$

Initially C_{sor} is 0.272 kmol/m^3 at time=0

Sorbitol conversion experiments were carried out at different catalyst loadings, hydrogen pressure and temperatures (Table 2), in which all liquid products were analyzed and concentration profiles were plotted as a function of time. In these batch experimental studies, the reaction rate of each component (Table 3) in the isothermal and constant-volume reactors are described by the material balance presented in Table 4. The hydrogen pressure was nearly constant during an experiment as the amount of hydrogen charged was in large stoichiometric excess compared to the sorbitol substrate used.

Table 5. Henry's constant for hydrogen in water[56]

Henry's constant, H [atm/(kmol/m^3)]		
200 ^{o}C	215 ^{o}C	230 ^{o}C
0.577	0.502	0.429

ATHENA Visual Studio (www.athenavisual.com) was used for parameter estimation and optimization of reaction rate constants. Results from ATHENA software were plotted to simulate concentration~time profiles. Hydrogen solubility data, presented as Henry's constants, are shown in Table 5 after appropriate correlation of relevant data from previous literature.[149]

4.4 Parameter estimation

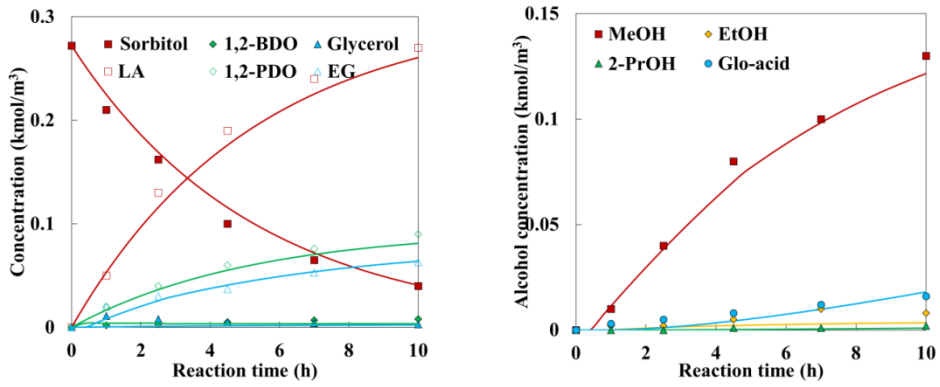

Figure 20. Concentration~time profiles and fitted values at 200 ^{o}C and P_{H2}: 2.0 MPa.

(Other reaction conditions same as Figure 15)

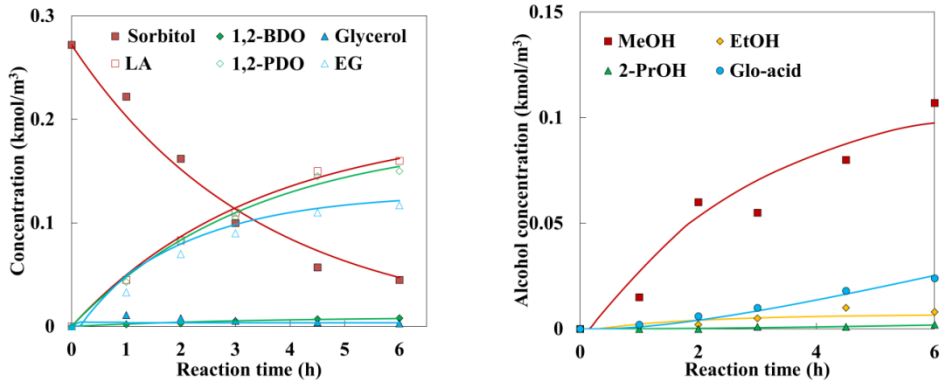

Figure 21. Concentration~time profiles and fitted values at 200 ^{o}C and P_{H2}: 3.5 MPa.

(Other reaction conditions same as Figure 15)

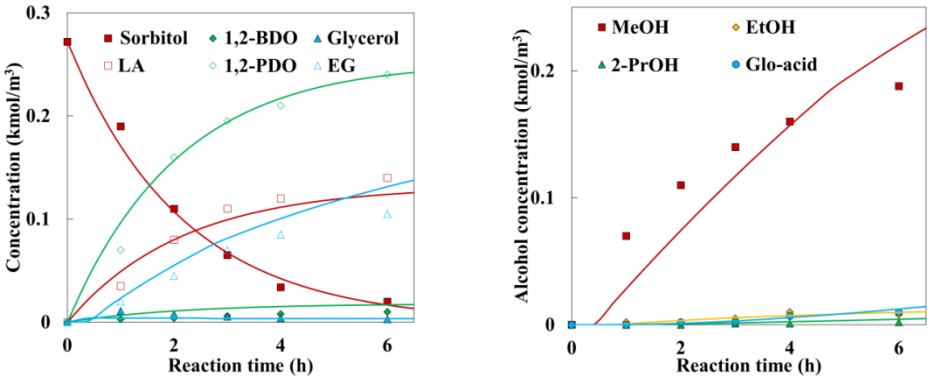

Figure 22. Concentration~time profiles and fitted values at 200 ^{o}C and P_{H2}: 5.0 MPa.

(Other reaction conditions same as Figure 15)

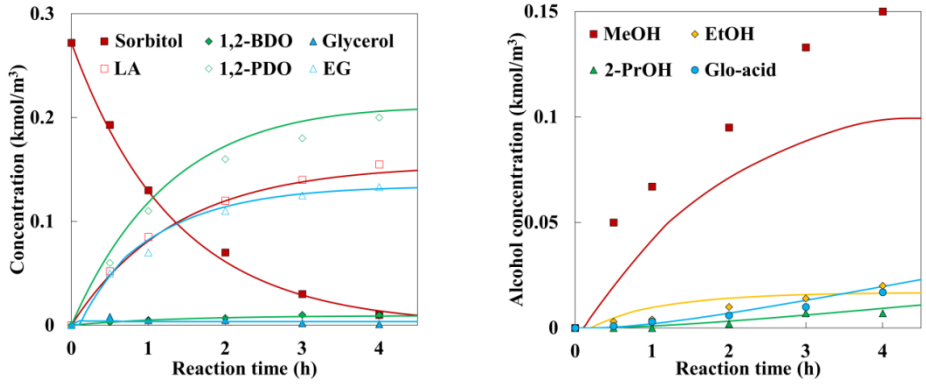

Figure 23. Concentration~time profiles and fitted values at 215 ^{o}C and P_{H2}: 3.5 MPa.

(Other reaction conditions same as Figure 15)

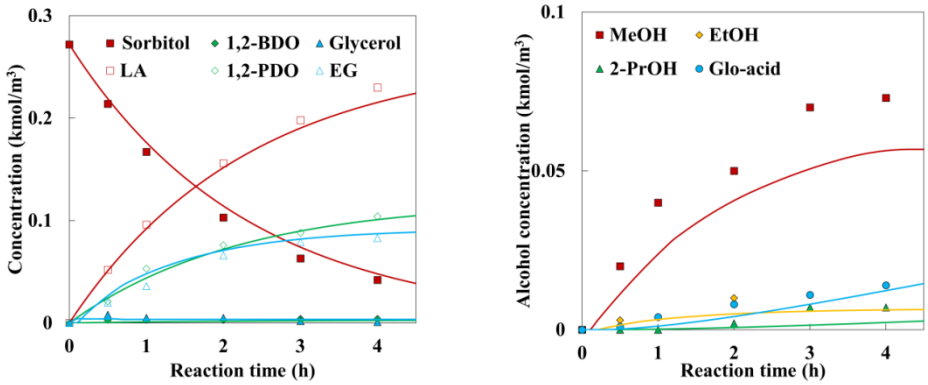

Figure 24. Concentration~time profiles and fitted values at 215 ^{o}C and P_{H2}: 2.0 MPa.

(Other reaction conditions same as Figure 15)

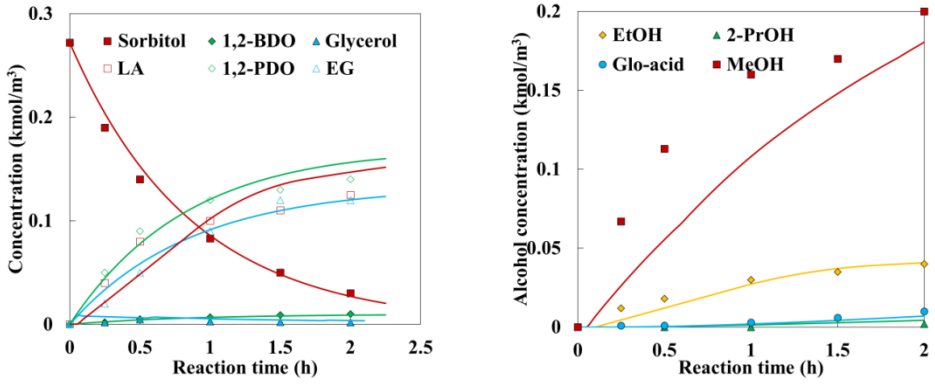

Figure 25. Concentration~time profiles and fitted values at 230 ^{o}C and P_{H2}: 3.5 MPa. (Reaction conditions same as Figure 15)

4.5 Results and discussion

Table 6. Reaction constants and activation energies

k_i	Temperature (^{o}C)			E_a (kJ/mol)
	200	215	230	
$k_1(\times 10^4)$	3.22±0.22	4.60±0.40	5.75±0.22	38.33±0.33
$k_2(\times 10^4)$	2.53±0.02	5.02±0.25	10.5±1.63	93.39±2.34
$k_3(\times 10^4)$	2.44±0.18	4.92±0.16	9.72±0.38	75.98±0.68
$k_4(\times 10^5)$	0.77±0.12	2.56±0.36	5.12±0.57	125.98±1.33
$k_5(\times 10^5)$	2.37±0.16	5.16±0.28	9.98±0.49	94.78±0.73
$k_6(\times 10^4)$	0.51±0.04	1.55±0.39	10.10±3.11	195.81±6.28
$k_7(\times 10^4)$	0.74±0.21	1.24±0.08	3.54±2.62	103.26±13.32
$k_8(\times 10^2)$	0.87±0.09	1.25±0.44	2.71±0.49	74.64±1.99

Typical experimental and simulated results for concentration~time profiles under different temperatures and hydrogen partial pressures are shown in Figures 20~25. The corresponding optimized reaction rate constants as well as activation energies are presented in Table 6. It is found that the activation energy for sorbitol reaction is in the range of 38~93 kJ/mol, which agrees well with value predicted by Tronconi.[99] Besides, an Arrhenius plot is also shown in Figure 26. The parity plot in Figure 27 clearly shows the goodness of fit for our experimental data under different reaction conditions. It is found that predicted values fit very well with our experimental results except for MeOH concentration at relatively high temperatures (see Figures 23~25). It is highly

possible that the presence of certain amount of MeOH in gaseous phase under the reaction conditions will affect the prediction of its reaction rates.

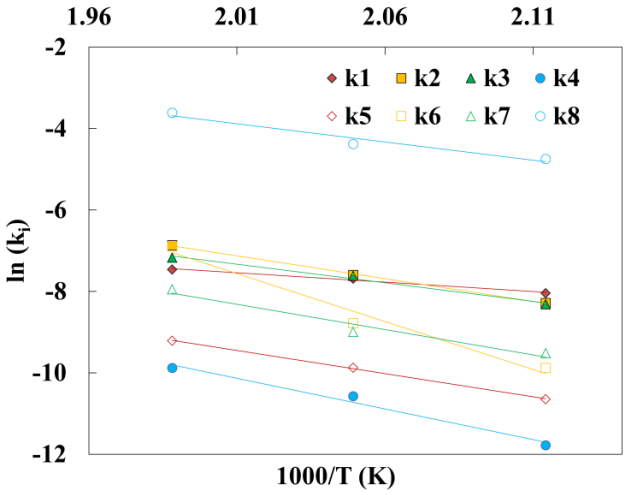

Figure 26. Arrhenius plots of reaction rate constants

Important findings:

(1) C-C cleavage of sorbitol at different positions. It is found that the reaction barrier for r_1 is only 38.33 kJ/mol in the catalytic system, while that for r_5 is 94.78 kJ/mol, indicating that C_3-C_3 cleavage reactions occur relatively more easily compared with C_2-C_4 on RuRe/C catalyst surface. As discussed in the reaction Scheme 2, C_3-C_3 cleavage is initiated with the formation of hex-2-ketose on catalyst surface while C_2-C_4 cleavage is initiated with the formation of hex-aldose. This means that the formation of ketose is more favorable than aldose, which seems to be unlikely because DH of primary carbon is obviously much easier than secondary position. Therefore it is highly possible that fast

isomerization of aldose to ketose occurs in our catalytic system, after which C_3-C_3 cleavage occurs.

(2) Formation of EtOH and 2-PrOH. A very interesting finding is the activation energy of r_4 and r_6 (Scheme 4). The value of corresponding activation energy for these two reactions is 126 kJ/mol and 196 kJ/mol respectively on RuRe/C catalyst. The reaction barrier for 1,2-PDO hydrogenation is slightly higher than EG conversion. But it is important to mention that these two values are much higher compared with predicted results from glycerol conversion (as shown in Table 7).[56] It was found that 1,2-PDO and EG are easily hydrogenated to 2-PrOH and EtOH on RuRe/C catalyst, which are further converted to gaseous alkanes such as propane, ethane and methane *via* hydrogenation and C-C cleavage. Therefore the gas phase selectivity was about 36% under relatively harsh reaction conditions. It is however not true in our case with $Ca(OH)_2$ as the base promoter. First of all the gas phase product selectivity is negligible in our system. The high values of the activation energy for these two reactions indicate that HDO of 1,2-PDO and EG to alcohols is not favored in the presence of $Ca(OH)_2$. Therefore consecutive methanation and C-C cleavage to form gaseous products are also restrained on RuRe/C catalyst. This experimental finding confirms the role of $Ca(OH)_2$ in selective HDO of sorbitol to valuable liquid products rather than less valuable gaseous products. The addition of solid base promoters improves the overall performances of RuRe/C in sorbitol conversion.

Table 7. Comparison of RuRe/C and RuRe/C+Ca(OH)$_2$ in HDO of 1,2-PDO and EG

		RuRe/C	RuRe/C+Ca(OH)$_2$
1,2-PDO to 2-PrOH	k (200 °C)	3.17×10^{-2}	7.67×10^{-6}
	E_a (kJ/mol)	25.11	125.98
		RuRe/C	RuRe/C+Ca(OH)$_2$
EG to EtOH	k (200 °C)	0.103	5.14×10^{-5}
	E_a (kJ/mol)	34.78	159.8

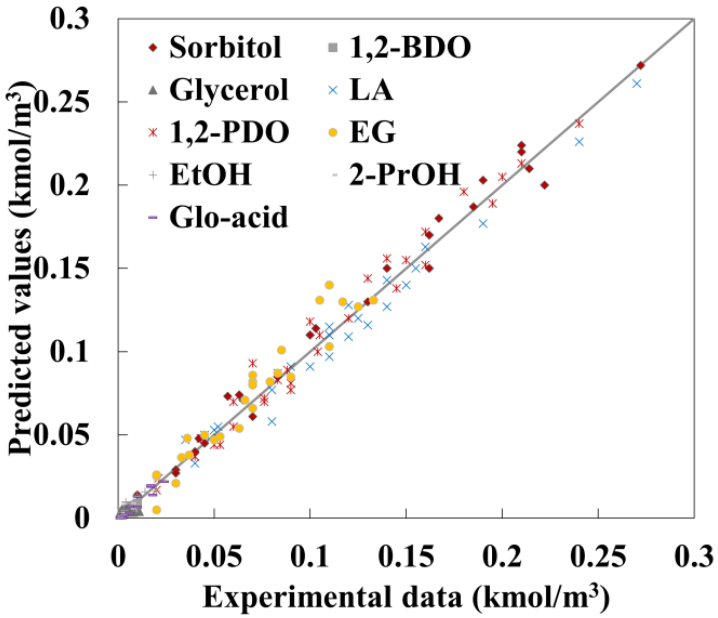

Figure 27. Parity plots of experimental *vs* fitted values

(3) C-C cleavage of glycerol. It has already been demonstrated that the presence of a solid base [*e.g.* MgO, Ca(OH)$_2$] restrains the C-C cleavage of glycerol to some extent compared with the case without a solid base. And HDO rate of glycerol is enhanced thus the selectivity towards 1,2-PDO is higher in the presence of a solid base. It is found that activation energy for C-C cleavage

of glycerol is actually not lowered by the addition of $Ca(OH)_2$. But considering the fact that the activation energy for the formation of glycerol is very low, it is highly possible that the high reactivity of glycerol precursor (*e.g.* GLA) and its formation at significant rates on catalyst surface contribute to the overall reaction rate of C-C cleavage ($k_8 / k_1 \approx 50$) on RuRe/C catalyst.

5. Conclusion

The HDO of xylitol and sorbitol in aqueous phase was studied on admixtures of carbon supported Ru, Rh, Pt, and Ir catalysts. All catalysts were active for the formation of liquid products (MeOH, EtOH, EG, 1,2-PDO, glycerol, LA, erythritol, and 1,2-BDO) following an increasing order of activity of Ir/C < Pt/C < Rh/C < Ru/C. Furthermore, the addition of a second metal (Re) not only increases the activity of Ru catalysts but also enhances the selectivity of C_2 and C_3 polyols.

A detailed kinetic modeling of sorbitol HDO using RuRe/C catalyst was studied in multiphase slurry reactors. It is found that RuRe/C+$Ca(OH)_2$ system shows the best performance in sorbitol HDO compared with the presence of other base promoters. It is also observed that sorbitol conversion occurs with complicated parallel and consecutive reactions, which leads to the formation of 1,2-BDO, 1,2-PDO, LA, EG, alcohols and other acids. Experimental data under different reaction conditions including temperatures, hydrogen pressures, catalyst concentrations were obtained and relevant kinetic parameters were estimated

and optimized. The reaction parameters of HDO were determined in kinetic regime and mass transfer effect was found to be insignificant according to our calculation. The proposed RuRe+$Ca(OH)_2$ system shows high selectivity to deoxygenated products and generate negligible gaseous products based on our experimental data. The kinetic data will be further used for the optimization of catalyst design and process development.

Chapter 3 Hydrogenolysis of Sugar-Derived Polyols to Renewable Glycols and Alcohols on Bi-functional Supported Cu Catalysts

1. Introduction

It has been demonstrated that noble metal-based catalysts such as Ru and Pt are active for catalytic conversion of sugar-derived polyols to glycols. The high cost and low selectivity to glycols still remain a major drawback of these catalysts. The sustainable development of biomass conversion technologies demands rational design of active, selective and cost-effective catalysts. Therefore, in this chapter, results on a new family of bi-functional Cu based catalysts supported on $CaO\text{-}Al_2O_3$ will be proposed. It is shown that the proposed Cu based catalysts are very selective in the hydrogenolysis (HDO) of xylitol, sorbitol and mannitol in aqueous phase. While conventional Cu catalysts only display limited activity for C-O cleavages even at harsh reaction conditions ($T > 200\ ^oC$, $P_{H2} > 4$ MPa), it is shown for the first time that the new Cu catalysts show high activity for both C-C and C-O bond cleavage of polyols. The surface morphology (lattice spacing, phase diagram), activity, selectivity and structure-performance correlations of the proposed catalysts will be discussed. Particularly, the following aspects will be addressed:

(1) Development of reliable synthetic procedures for Cu catalysts on MgO-Al_2O_3, ZnO-Al_2O_3 and CaO-Al_2O_3 supports;

(2) Evaluation of these Cu-based catalysts in HDO of xylitol, sorbitol and mannitol to 1,2-propanediol (1,2-PDO), ethylene glycol (EG) and $C_{1\sim3}$ alcohols;

(3) Understanding the interaction between the cations in solid supports (*i.e.* H^+, Mg^{2+}, Zn^{2+} and Ca^{2+}) and Cu species;

(4) Structure-activity correlation based on experimental catalyst performance studies and surface characterization using scanning electron microscope (SEM), transmission electron microscope (TEM) and temperature programmed reduction (TPR) techniques.

2. Experimental Section

2.1 Catalysts preparation

2.1.1 Supported Cu on metal oxides

Cu-based catalysts on various solid base supports were prepared using concurrent precipitation (CP) method according to the following procedure (as shown in Figure 1). Required amount of $Cu(NO_3)_2.2.5H_2O$ (purum, ≥ 98%, Sigma), $Ca(NO_3)_2.4H_2O$ (≥ 99.0%, Sigma) and $Al(NO_3)_3.9H_2O$ (purum, ≥ 98.0%, Sigma) were mixed with deionized water (DI water), denoted as solution A. The total concentration of Cu^{2+}, Ca^{2+} and Al^{3+} was about 0.2 kmol/m^3. Then calculated amount of NaOH (reagent grade, ≥98% pellets,

anhydrous, Sigma) and $Na_2CO_3.10H_2O$ (purum, ≥ 99.0%, Sigma) were mixed with DI water (denoted as solution B). The concentrations of NaOH and Na_2CO_3 were 0.25 kmol/m^3 and 0.8 kmol/m^3 respectively. In another 500 mL beaker (C), 50 mL of deionized water was introduced under vigorous stirring (>800 rpm) at 60 ^oC. In the next step, solutions A and B were added dropwise simultaneously (concurrently, as shown in Figure 1) to beaker C (approximately 2 drops every 3 seconds). Blue slurry mixture was then formed. The pH of the solution in the beaker C was kept at 10~11 throughout the preparation process. The resulting slurry was stirred at 60 ^oC for 16 h. Then, the mixture was filtered and the solids were washed with 2000 mL of DI water at 90 ^oC to remove Na^+ ions. The solid cake obtained was then dried overnight in a vacuum oven at 120 ^oC.

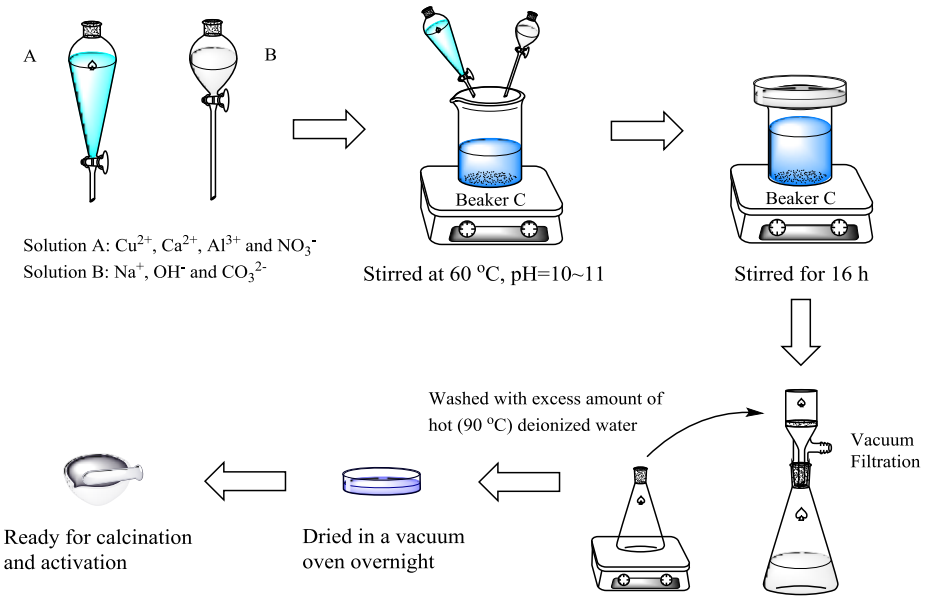

Figure 1. Synthetic procedure for Cu/CaO-Al_2O_3 catalyst *via* CP method

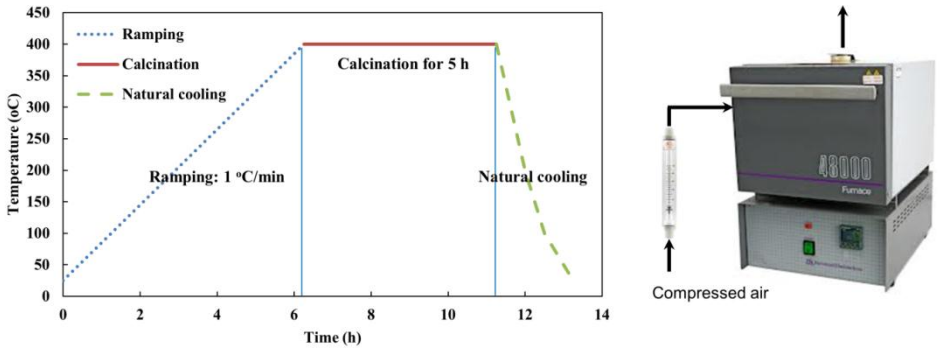

Figure 2. Calcination of solid catalyst samples in Barnstead/Thermolyne 48000 furnace (right) and a typical temperature curve during calcination (left)

The dried solid catalyst sample was charged to a porcelain bowl, which was then transferred to a calcination furnace (Barnstead/Thermolyne 48000) with flowing air (flow rate: 5 cm^3/min/g catalyst). The furnace was then heated at a rate of 1 ^oC/min to 400 ^oC, for 5 h of dwelling time. Then, the contents in the furnace were cooled naturally by flowing air (Figure 2). Calcined Cu catalysts as prepared were denoted as CuO/CaO-Al_2O_3-1 (Cu loading = 43w%), CuO/CaO-Al_2O_3-2 (Cu loading = 28w%), CuO/CaO-Al_2O_3-3 (Cu loading = 43w%, ramping rate = 5 ^oC/min instead of 1 ^oC/min). The catalysts were then activated by a procedure described in Chapter 2. The reduced Cu catalysts were denoted as Cu/CaO-Al_2O_3-1 (Cu loading = 43w%), Cu/CaO-Al_2O_3-2 (Cu loading = 28w%), Cu/CaO-Al_2O_3-3 (Cu loading = 43w%, ramping rate = 5 ^oC/min instead of 1 ^oC/min).

The same procedure was followed for the preparation of Cu/ZnO-Al_2O_3, and Cu/MgO-Al_2O_3catalysts. $Zn(NO_3)_2.6H_2O$ (reagent grade, 98%, Sigma) and $Mg(NO_3)_2.6H_2O$ (purum, ≥ 99.0%, Fluka) were used for preparation of solution

A to replace $Ca(NO_3)_2.3H_2O$ during preparation. These catalyst samples were denoted as $CuO/MgO\text{-}Al_2O_3$, $CuO/ZnO\text{-}Al_2O_3$ for calcined catalysts, while $Cu/MgO\text{-}Al_2O_3$, $Cu/ZnO\text{-}Al_2O_3$ represent the corresponding reduced Cu catalysts.

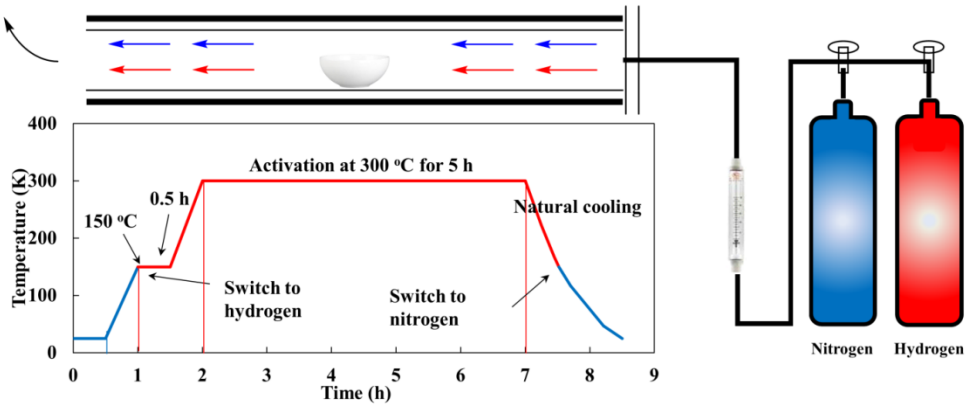

Figure 3. The temperature profile during catalyst activation and schematic of activation apparatus

2.1.2 Cu catalyst on H-ZSM5

Cu/H-ZSM5 samples were prepared *via* insipient wetness impregnation (IWI) method.[76] A typical synthetic procedure of IWI approach was described as follows: About 5 g of ZSM5 in ammonium form (NH_4-ZSM5) was pretreated under calcination conditions with a flow of air to remove NH_3, the conditions of which were identical to those in Figure 2. The ammonium ion was removed during calcination thus ZSM5 is now in the form of H-ZSM5. Calculated amounts of $Cu(NO_3)_2.2.5H_2O$ (purum, ≥ 98%, Sigma) was added to H-ZSM5 solid in a 50 mL of evaporating flask (Chemglass). Then small amounts of DI water were added. The resulting slurry was stirred at ~500 rpm for at least 4 h

at room temperature in order to obtain well dispersed solid-liquid slurry. The solvent (water) in the slurry was then removed using rotary evaporator at 55 ^{o}C (bath temperature) and 250~70 mmHg vacuum. The solid sample (blue color) was well dispersed on the inner wall of an evaporating flask. Next, the sample was dried at 120 ^{o}C in a vacuum oven overnight to further remove the remaining water in the sample. Calcination (ramping rate = 1 ^{o}C/min) and activation processes are identical to the procedures described in Figures 2 and 3. The sample was denoted as Cu/H-ZSM5.

2.2 Catalyst activity tests

Performance evaluation of Cu catalysts for HDO of sorbitol and xylitol was carried out in a 300 mL Parr reactor (Figure 3 of Chapter 2). The procedure was already briefly described in "2.2 Catalyst performance evaluation" in Chapter 2.

2.3 Analytical methods

The analytic procedure and definition of conversion, selectivity, yield, conversion rate (CR) are identical to those described in "2.3 Analytical methods" in Chapter 2.

2.4 Catalyst characterization

2.4.1 Temperature programmed reduction (TPR)

TPR was carried out in Autochem 2910 Instrument. The equipment flow sheet is shown in Figure 4. The TPR procedure is described below: Cu-based

catalysts in oxide form (*e.g.* $CuO/CaO\text{-}Al_2O_3$) were used for TPR studies. The size of Cu catalysts was in the range of 50~100 mesh. Certain amounts of Cu catalyst sample were introduced to the U-shape tube (see Appendix II for details). The U-shape tube was then connected with Autochem 2910 Instrument and finger-tighten carefully.

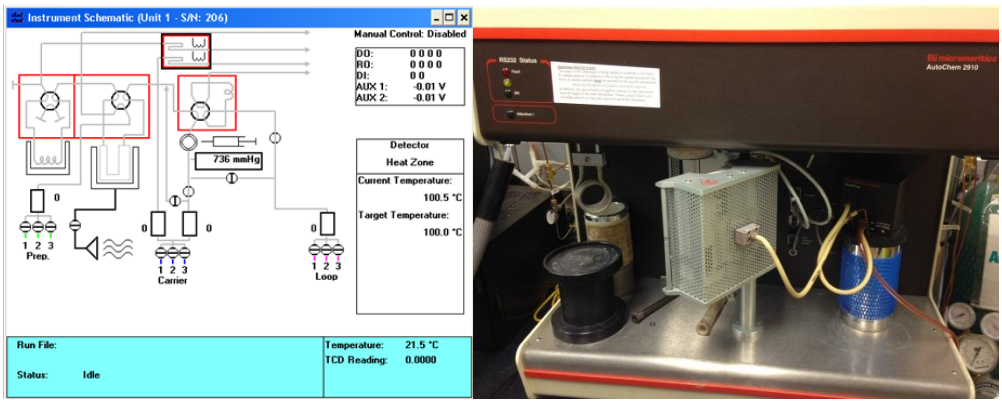

(a) (b)

Figure 4. Autochem instrument, (a) schematic flow sheet and (b) equipment

TPR programming: Small amounts of ice and *i*-propanol (2-PrOH) were placed on the cooler to condense the vapor content generated from the solid sample during heating. Then the sample temperature was increased from room temperature to 300 ^{o}C at a rate of 5 ^{o}C/min. The temperature was then maintained at 300 ^{o}C until the baseline of the instrument was stable. After the baseline stabilized, the instrument was cooled to room temperature at a rate of 20 ^{o}C/min. Carrier gas was then switched to hydrogen-argon (10.3% hydrogen in argon). Once the baseline was further stabilized at room temperature, data recording was started by thermal conductivity detector (TCD) at a frequency of

one second. And temperature was increased at a rate of 10 ^{o}C/min until 500 ^{o}C, at which the recording was stopped. The carrier gas was then switched to argon and the contents cooled to room temperature.

2.4.2 Transmission electron microscopy (TEM)

Experimental details and instruments for TEM were similar to Chapter 1.

2.4.3 Scanning electron microscopy (SEM)

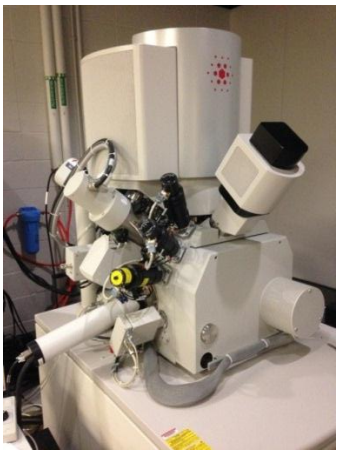

Figure 5. Dual beam SEM

SEM-EDX Measurement: A Versa 3D dual beam Scanning Electron Microscope/ Focused Ion Beam (FEI, Hillsboro, OR, USA) with a silicon drift EDX detector (Oxford Instruments, X-Max, UK) was used to measure the surface morphology, elemental composition and distribution of metals. All the SEM data reported were obtained at an acceleration voltage of 15kV, spot size 3.0 and the images were collected with an ET (Everhart Thornley) detector. The elemental mapping and energy spectrums were acquired with Aztec tools (Oxford Instruments, UK).

3. Results and Discussion

3.1 Catalyst evaluation

Table 1. HDO of sorbitol over different Cu catalysts

#	Catalysts	Time (h)	X[a] (%)	Selectivity (%)					
				1,2-PDO	LA	glycerol	EG	$C_{4\sim6}$[b]	Others[c]
1	$Cu/MgO-Al_2O_3$	6	54.1	29.1	19.0	4.9	12.8	3.2	7.7
2		12	80.6	31.6	11.5	5.7	10.2	5.5	12.9
3	$Cu/ZnO-Al_2O_3$	6	55.9	38.3	11.0	2.2	12.2	14.4	3.8
4		12	94.9	35.9	1.1	6.3	11.7	29.0	10.5
5	$Cu/CaO-Al_2O_3$-1	3	57.1	39.0	16.6	14.3	14.3	6.4	6.9
6		6	98.1	46.1	1.8	11.8	15.4	6.5	14.5
7	Cu/H-ZSM5[d]	6	85.7	Anhydroglucitol: ~30%			Isosorbide: 46%		

a. Conversion at 9.8 kg/m^3, Cu/Mg^{2+}, Zn^{2+}, Ca^{2+} molar ratio: 5.4, sorbitol: 0.18 kmol/m^3, T: 230 ^oC, P_{H2}: 7.6 MPa; b. $C_{4\sim6}$ tetrols, triols, diols, *etc*; c. Mainly MeOH and EtOH, trace 1-propanol (1-PrOH), 2-PrOH, methane and carbon dioxide, *etc*.

The performances of $Cu/MgO-Al_2O_3$, $Cu/ZnO-Al_2O_3$ and $Cu/CaO-Al_2O_3$-1 catalysts were first evaluated for sorbitol conversion, the results of which are shown in Table 1. Entry#1 shows that 54.1% of sorbitol was converted over $Cu/MgO-Al_2O_3$ catalyst at T = 230 ^oC and P_{H2} = 7.6 MPa in 6 h reaction, main products being 1,2-PDO (S = 29.1%), lactic acid (LA in Table 1, S = 19.0%), glycerol (S = 4.9%) and EG (S = 12.8%). After 12 h reaction (Entry#2), approximately 81% conversion of sorbitol was achieved under the same conditions. It was also observed that the selectivity of glycols (1,2-PDO and EG) was almost unchanged during the conversion. C_3 products (1,2-PDO, LA and

glycerol) selectivity was found to decrease slightly. The increasing selectivity to ethanol (EtOH) and methanol (MeOH) implies further conversion of C_3 products *via* C-C cleavage and HDO reaction to form C_{1-2} products. These initial results indicate that Cu catalysts show high potential for C-C bond cleavage of polyol molecules, which however was not reported in earlier work.[38,39,61,102]

Compared to Cu/MgO-Al_2O_3 catalyst, Cu/ZnO-Al_2O_3 displayed slightly higher conversion (55.9%) after 6 h reaction (Entry#3). It is worth noting that after 12 h (Entry#4), 95% conversion was achieved with more $C_{4\sim6}$ polyols (including tetrols, triols, diols, about 29% in selectivity) compared to Cu/MgO-Al_2O_3 catalyst (< 6% in selectivity). Selectivity to $C_{2\sim3}$ products was lower on Cu/ZnO-Al_2O_3 than Cu/MgO-Al_2O_3 catalyst. The difference in the product distribution implies that more C-O bond breakage of sorbitol molecules occurs over CuZnO-Al_2O_3 than Cu/MgO-Al_2O_3 under similar reaction conditions. Product distribution on Cu/ZnO-Al_2O_3 catalyst is consistent with the previous report by Blanc and co-workers.[102] They found that Cu catalyst favored the formation of $C_{4\sim6}$ tetrols, triols and diols (about 56% in selectivity) rather than C-C bond cleavage in sorbitol conversion when ZnO was used as a promoter, although complete material balance was not reported in their report.

The difference of the sorbitol conversion and product selectivity over ZnO-Al-$_2O_3$ and MgO-Al_2O_3 supports indicates that the activity and selectivity of Cu particles might be influenced by the types of cations (*e.g.* Zn^{2+}, Mg^{2+}, Ca^{2+} and

H^+) in catalyst supports. Therefore, other catalysts such as Cu/CaO-Al_2O_3-1 and Cu/H-ZSM5 were tested and compared. It is observed that Cu/CaO-Al_2O_3-1 catalyst shows significantly higher conversion compared with Cu/ZnO-Al_2O_3 than Cu/MgO-Al_2O_3 catalysts. As shown in Entry#5, sorbitol conversion reached 57.1% in only 3 h. The combined selectivity to 1,2-PDO, glycerol and EG was also higher than the first two catalysts. Furthermore, as the conversion increased (Entry#6, 98.1% in 6 h), the total selectivity towards glycerol, glycols and linear alcohols was found to increase from 68% to 84%.

It is also interesting to note that Cu/H-ZSM5 catalyst showed completely different product distribution compared to the other three catalysts. Clearly, major products formed were anhydroglucitol and isosorbide with approximately ~30% and 46% selectivity, respectively at a conversion of 85% under similar reaction conditions, instead of glycols with short carbon chains. It reflects that dehydration (DHD) is favored[96] but retro-aldolization and HDO are restrained over Cu catalysts on acidic support.

The results over different Cu catalysts show that the interaction with supports significantly affected activity of metallic Cu catalysts and reaction pathways during HDO of sorbitol. The order of the size (radius) of those cations is $Ca^{2+}>Mg^{2+}>Zn^{2+}>H^+$,[150] which is consistent with the results shown here in terms of the activity of C-C bond cleavage.

As mentioned above, Cu/CaO-Al_2O_3-1 catalyst, which was not reported in any previous literature, showed significantly high conversion and selectivity

compared to conventional Cu/MgO-Al_2O_3 and Cu/ZnO-Al_2O_3 catalysts during sorbitol conversion. The presence of Ca^{2+} in the structure of the basic support selectively facilitated C-C cleavage of one sorbitol molecule to two C_3 intermediates in the presence of external hydrogen. Those C_3 intermediates were found to be further converted into 1,2-PDO and EG under our reaction conditions. This phenomenon reflects that Cu/CaO-Al_2O_3-1 has a high C-O cleavage activity even without introducing any liquid base promoters. Furthermore, Ye *et al.* recently investigated HDO of sorbitol on Ni/Al_2O_3+CaO catalysts.[100] They found that the addition of Ce^{4+} to Ni/Al_2O_3+CaO catalytic system substantially enhanced the activity of Ni metals, which again supports our hypothesis that the presence of cations will tune the activity of metal catalysts. However, the selectivity of glycols at the same time dropped significantly (approximately 15%) and gaseous products (mainly methane and carbon dioxide) were increased by nearly 10% on NiCe/Al_2O_3+CaO catalysts. This suggests that methanation and water gas shift (WGS) reactions were enhanced at the same time in the presence of Ce^{4+} (CeO_2). In contrast, Cu/CaO-Al_2O_3-1 catalyst displayed not only high conversion of sorbitol but also significantly low selectivity of gaseous products (selectivity of methane and carbon dioxide <1% in all cases). Our results indicate that the presence of Ca^{2+} in the structure of the basic supports enhanced C-C and C-O cleavage activity of Cu metal catalyst rather than promote side reactions such as methanation and WGS.

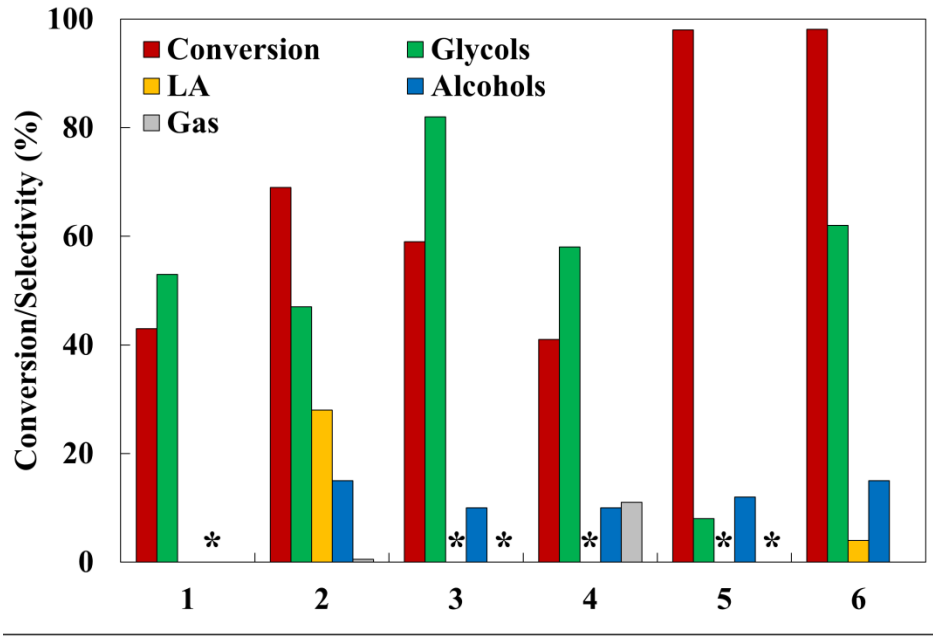

No.	1	2	3	4	5	6
Catalyst	Ru/C	RuRe/C	NiPt/NaY	$NiCe/Al_2O_3$	CuO/ZnO	$Cu/CaO-Al_2O_3$
Promoter	NaOH	$Ca(OH)_2$	$Ca(OH)_2$	Ce^{4+}	ZnO	Ca^{2+}
CR (mol/g atom.h)	16.6	233.3	*	46.7	0.8	1.2

Figure 6. Comparison of $Cu/CaO-Al_2O_3$ catalysts with previous work for sorbitol conversion[88,89,91,94,100,102,107] (Conditions: T: 230 ^oC, P_{H2}: 4~8 MPa; *: results not reported or cannot be calculated based on given details)

In addition, the catalytic performance comparison of the Cu catalysts in this work with other supported metal catalysts proposed by previous researchers was carried out (see Figure 6). Ru/C catalyst and bimetallic RuRe/C studied in Chapter 2 shows relatively high catalytic activity compared Ni and Cu based catalysts, while the selectivity to glycols is only in the range of 45~53% at 230 ^oC. In comparison, NiPt/NaY catalyst displays improved selectivity to glycols (S ~ 82%).[89] Although $NiCe/Al_2O_3$ catalyst exhibits enhanced activity for sorbitol conversion, the selectivity to gaseous products (methane and carbon

dioxide) is also high on the Ni catalysts (S > 10%).[100] CuO/ZnO catalyst displays poor activity for sorbitol conversion compared with Ru and Ni catalysts, with low selectivity to glycols and other lower products.[102] Our proposed Cu/CaO-Al_2O_3 catalyst shows improved catalytic activity compared with CuO/ZnO catalyst. More importantly, the overall yield of glycols and alcohols is much higher compared with other metal catalysts under similar reaction conditions (T = 230 ^oC, P_{H2} = 4~8 MPa). The interaction between cations and metal particles and its influence on catalysts activity and selectivity has also been investigated further. The detailed reaction mechanism will be also discussed in the following sections.

3.2 Cu loading effect

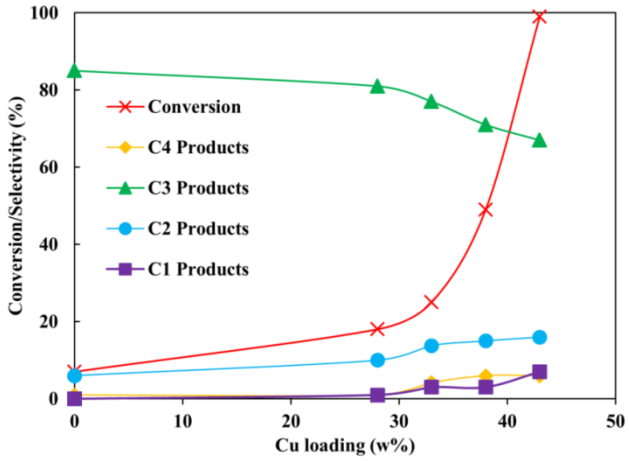

Figure 7. Effect of Cu loadings on sorbitol conversion

(Reaction time: 6 h, other conditions same as Table 1)

In order to understand the effect of Cu content on the activity and selectivity of Cu catalysts, several Cu/CaO-Al_2O_3-1 catalysts with various Cu loadings were

prepared and tested in sorbitol conversion (see Figure 7). Firstly, it is clear that $CaO\text{-}Al_2O_3$ support with no Cu addition achieved only 6% of sorbitol conversion in 6 h, as shown in Figure 7 (with LA as the major products, S > 76%). When Cu loading is 28w%, approximately 18% of substrate was converted under the same reaction conditions, with selectivity of C_3 products as high as 81%, which was the highest value ever observed compared with literature reports.[88-90,94,100,107,151,152]

Surprisingly the activity of Cu catalyst was increased by almost four fold for the catalyst with a Cu loading of 43w% (CR = 1.2 mol/g atom/h, Figure 7), in comparison with the one with 28w% loading (CR = 0.24 mol/g atom/h), although the selectivity of C_3 products decreased to about 64%. This observation is different from previous results since higher loading of metal content usually leads to a decrease in catalytic activity. These results imply that the formulation of Cu on the support and the interaction between Cu and Ca^{2+} have a strong influence on the activity and reaction pathways of solid base supported catalysts. Therefore, TPR, TEM and SEM characterization was carried out to provide further insights into the surface chemistry of Cu catalysts and understand the metal-support interaction.

3.3 Catalyst characterization

3.3.1 TPR

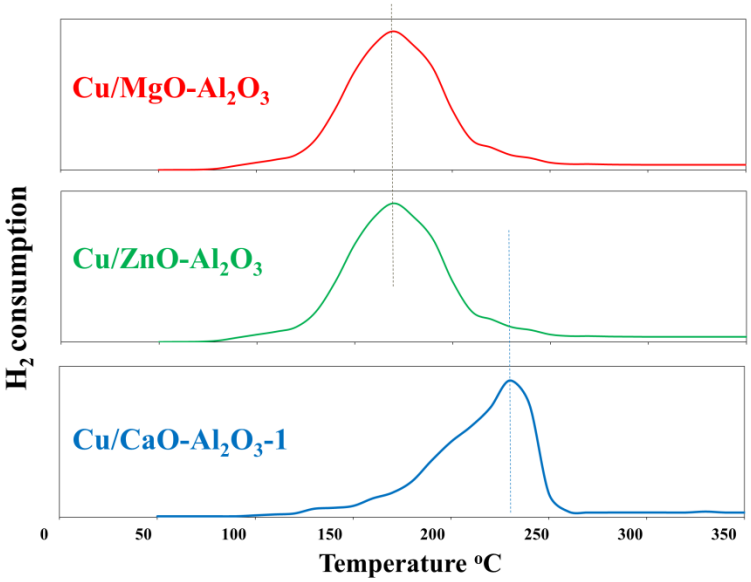

Figure 8. TPR of $CuO/MgO\text{-}Al_2O_3$, $CuO/ZnO\text{-}Al_2O_3$ and $CuO/CaO\text{-}Al_2O_3$-1 catalysts

$CuO/MgO\text{-}Al_2O_3$, $CuO/ZnO\text{-}Al_2O_3$ and $CuO/CaO\text{-}Al_2O_3$-1 catalysts were characterized by TPR. As shown in Figure 8, the hydrogen reduction peak of $Cu/MgO\text{-}Al_2O_3$ catalyst showed at 180 ^{o}C position, which is the normal reduction temperature for $Cu^{II}O$ species to Cu^{0}. $Cu/ZnO\text{-}Al_2O_3$ sample showed similar reduction behavior with $Cu/MgO\text{-}Al_2O_3$ catalyst. This phenomenon implies that interaction between $Cu^{II}O$ species and $MgO\text{-}Al_2O_3$ and $ZnO\text{-}Al_2O_3$ supports is not strong.[153] TPR profile for $CuO/CaO\text{-}Al_2O_3$-1 sample exhibited a different reduction behavior. The reduction peak of $Cu^{II}O$ species shifted from 180 ^{o}C to 225~230 ^{o}C position. The difference indicates that the interaction between Cu species and $CaO\text{-}Al_2O_3$ is very strong compared with other two Cu catalysts. Considering the fact that $CuO/CaO\text{-}Al_2O_3$-1 displayed higher C-C

cleavage activity than CuO/MgO-Al_2O_3, CuO/ZnO-Al_2O_3 catalysts, the support interaction is the key to activate metal sites during sorbitol conversion.

3.3.2 TEM

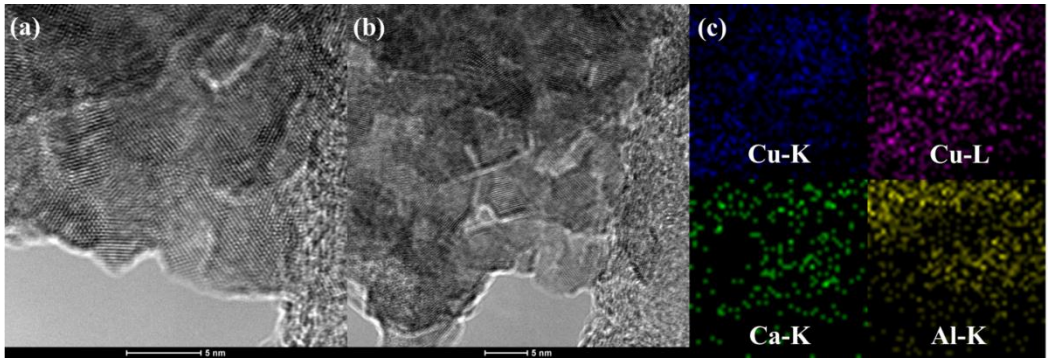

Figure 9. TEM data of Cu/CaO-Al_2O_3-1 catalyst

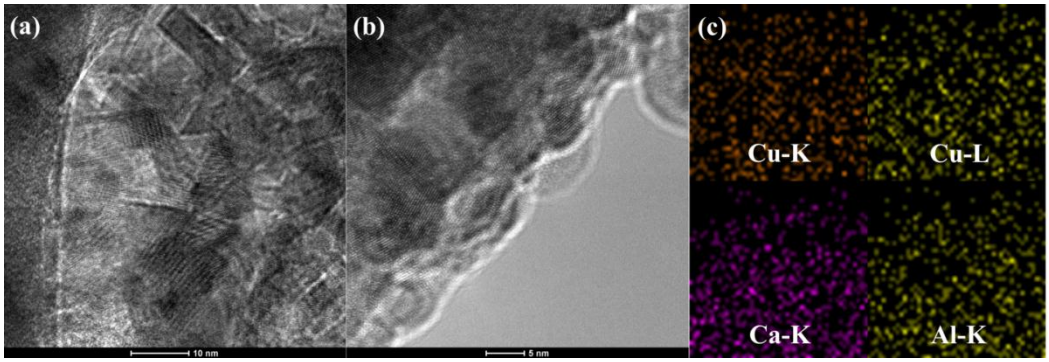

Figure 10. TEM data of Cu/CaO-Al_2O_3-2 catalyst

The surface morphologies of Cu/CaO-Al_2O_3-1, CuO/CaO-Al_2O_3-2 and CuO/CaO-Al_2O_3-3 were investigated by TEM characterization. As shown in Figure 9 (a) and (b), Cu/CaO-Al_2O_3-1 displays highly crystallized structure, unlike the conventional CuO/MgO-Al_2O_3 and CuO/ZnO-Al_2O_3 catalysts, which exhibit Cu particles of 50~200 nm in size.[35,61,63,127] The Cu/CaO-Al_2O_3-1 catalyst on the other hand does not show any Cu particles with detectable sizes.

In other words, Cu element is well dispersed and forms hybrid species with $CaO\text{-}Al_2O_3$ support. TEM figure of $Cu/CaO\text{-}Al_2O_3$-1 is consistent with the shift of reduction peak of $Cu^{II}O$ species shifts from 180 ^oC to 225~230 ^oC position shown in Figure 8, indicating a strong interaction between Cu species and $CaO\text{-}Al_2O_3$ support.

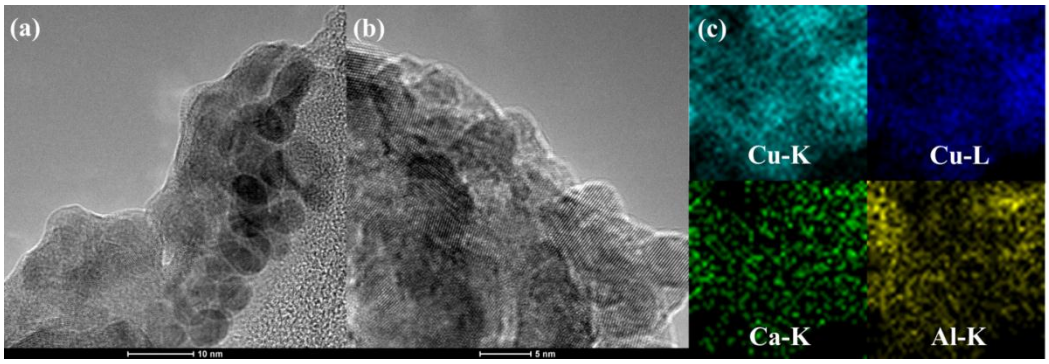

Figure 11. TEM data of $Cu/CaO\text{-}Al_2O_3$-3 catalyst

EDX analysis of bulk composition of $CuO/CaO\text{-}Al_2O_3$-1 [Figure 9 (c)] confirms that Cu, Ca and Al elements are well distributed in the catalyst sample. Similarly, highly crystalline structures were also observed on $Cu/CaO\text{-}Al_2O_3$-2 (Figure 10) sample. Besides, $Cu/CaO\text{-}Al_2O_3$-3 (Figure 11) exhibits ordered structured lattices as well, but there seems to exist a phase separation, which is slightly different from $Cu/CaO\text{-}Al_2O_3$-1 sample.

3.3.3 SEM

SEM characterization confirms the well distributed Cu, Ca and Al in Cu catalysts. Figure 12 presents the distribution of Cu, Ca, Al and O elements on

Cu/CaO-Al_2O_3-1 catalyst surface. Element analysis on the selected catalyst particle shows that all four elements are well dispersed.

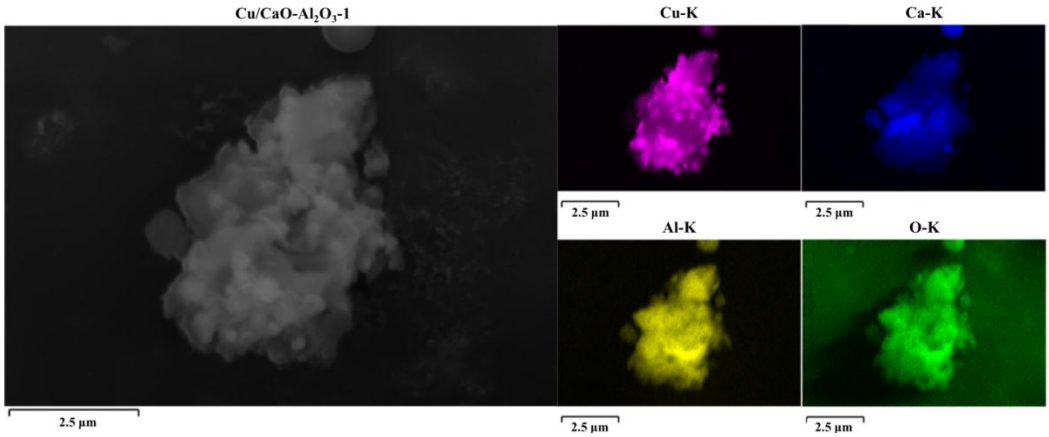

Figure 12. SEM images of Cu/CaO-Al_2O_3-1 sample

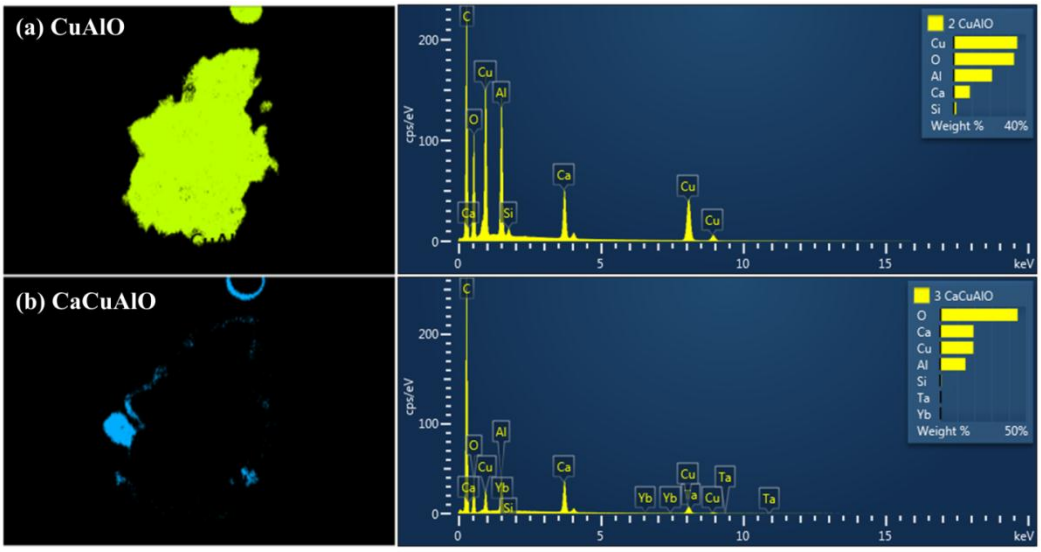

Figure 13. Phase diagram of Cu/CaO-Al_2O_3-1 sample

As shown in TEM images (Figure 9), Cu, Ca, Al and O in Cu/CaO-Al_2O_3-1 form hybrid structures and hence the size of Cu particles is not detectable. The hybrid composition is however not known from the elements analysis. Phase analysis was therefore further conducted in order to reveal the chemical

composition of Cu catalysts. Figure 12 shows that CuAlO is the major phase, while Ca is concentrated on surface thus CaCuAlO is dominant at surface of Cu/CaO-Al_2O_3-1 sample. It was counted for 693 thousand points in the region shown Figure 13. The molar ratio of the two phases is about 18/1. Therefore it is clear that the highly crystalline structure mainly represents CuAlO and CaCuAlO phases. The existence of CuAlO and CaCuAlO phases confirm the strong interaction between Cu and metal oxide supports, which is consistent with TPR and TEM images.

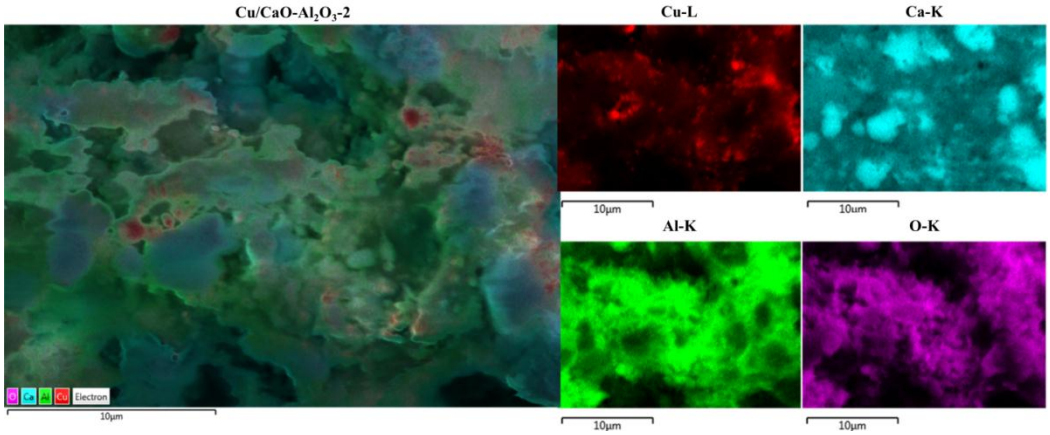

Figure 14. SEM images of Cu/CaO-Al_2O_3-2 sample

It is known that CuAlO easily forms a $CuAl_2O_4$ spinel structure, which is believed to be the major active phase for HDO reactions.[23,48,58] Based on the EDX analysis for CuAlO phase, the chemical content for Cu/Al/O molar ratio is roughly 0.6/1.1/2.5 (or 1.8/3.3/7.5), which is consistent with the composition of spinel $CuAl_2O_4$ or its dimer (dicopper aluminum oxide, $Cu_2Al_4O_7$) structure. The chemical composition for CaCuAlO phase is about $Ca_5Cu_3Al_6O_{17}$. Cu species in both phases suggest strong interactions with other elements, therefore

reduction of Cu^{II} was shifted to 225~230 ^{o}C from 180 ^{o}C, as already shown in Figure 8.

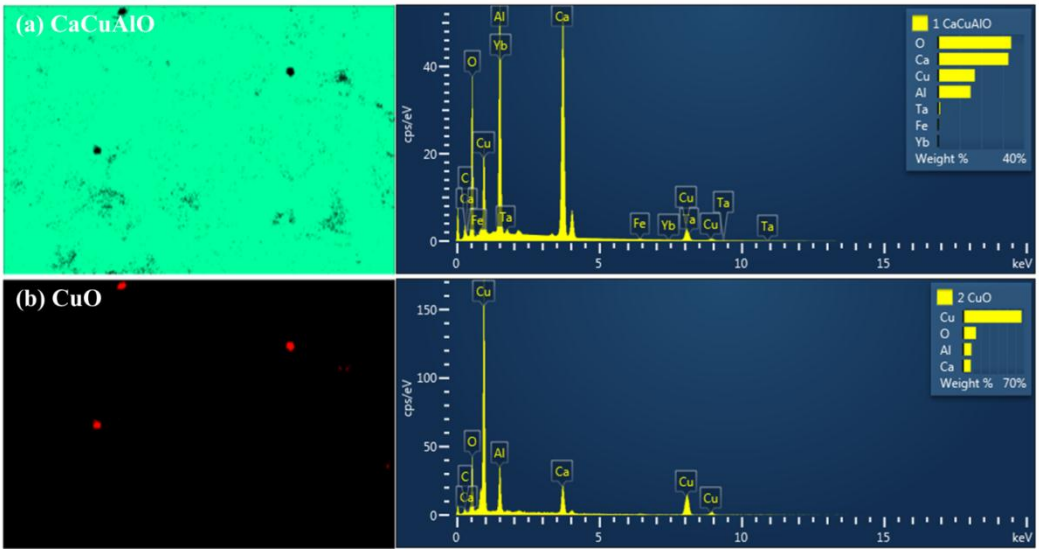

Figure 15. Phase diagram of Cu/CaO-Al_2O_3-2 sample

SEM images of Cu/CaO-Al_2O_3-2 sample are shown in Figure 14. It is found that Ca, Al and O are well distributed throughout the sample region, while Cu species displays only a slight phase separation. Compared with Cu/CaO-Al_2O_3-1 sample (Figure 12, Cu loading = 43w%), Cu content in this one is much lower (Cu loading = 28w%). The red color region (Figure 14) is not as sharp as in Figure 12. The difference in SEM images clearly indicates that the active phases in the two samples are distinct from each other. Phase diagram of Cu/CaO-Al_2O_3-2 sample was thus carried out. As shown in Figure 15, it has been counted for more than 708 thousand points for the region shown and found that major phases for Cu/CaO-Al_2O_3-2 sample are CuO/Cu and CaCuAlO. In sharp contrast, CaCuAlO is the dominant phase (98.1%) in this

sample compared with Cu/CaO-Al_2O_3-1 (CaCuAlO ≈ 6%). CuO/Cu is only < 2% in this sample.

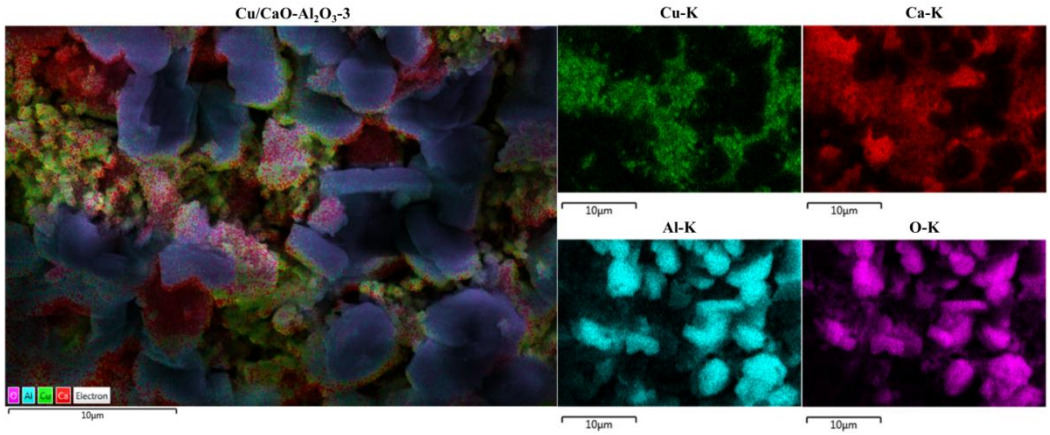

Figure 16. SEM images of Cu/CaO-Al_2O_3-3 sample

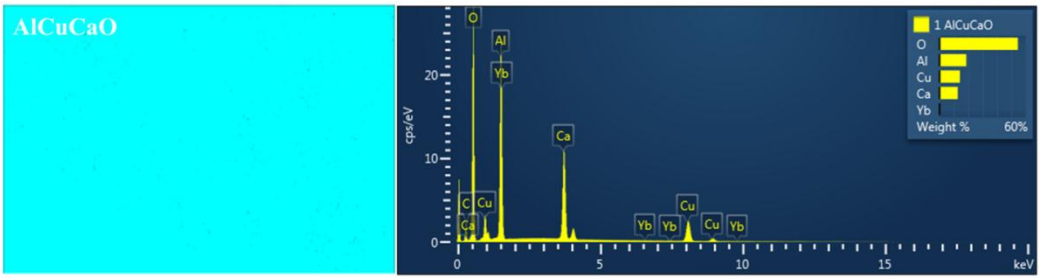

Figure 17. Phase diagram of Cu/CaO-Al_2O_3-3 sample

Figure 16 presents the distribution of Cu, Ca, Al and O elements on Cu/CaO-Al_2O_3-3 catalyst surface. Element analysis on a selected catalyst particle shows that all four elements are not well dispersed. It shows a trend of elements segregation on the catalyst surface. It is important to point out that the composition of Cu/CaO-Al_2O_3-3 catalyst is almost identical with Cu/CaO-Al-$_2O_3$-1 catalyst. The pretreatment conditions are however different from each other. As mentioned in the experimental section, Cu/CaO-Al_2O_3-1 sample

underwent a 1 ^{o}C/min ramping rate during calcination (under flowing air), while Cu/CaO-Al_2O_3-3 experienced a 5 ^{o}C/min ramping rate. The uniformity and crystallinity of Cu/CaO-Al_2O_3-3 is not as good as Cu/CaO-Al_2O_3-1 sample. Figure 16 shows that Al_2O_3 is a dominate phase. Therefore it is highly possible that fast heating rate results in the phase separation. Phase diagram of Cu/CaO-Al_2O_3-3 sample further confirms our hypothesis.

3.4 Structure-activity correlation

Table 2. Product distribution of Cu catalysts in sorbitol conversion

#	Catalysts	X(%)	Selectivity (%)				
			1,2-PDO	LA+PAD	glycerol	EG	Others
1	Cu/CaO-Al_2O_3-1	98.1	46.1	1.8	11.8	15.4	21
2	Cu/CaO-Al_2O_3-2	17.9	12.9	64.3	4.3	9.5	-
3	Cu/CaO-Al_2O_3-3	12.1	8.4	75.2	15.1	1.1	-

Catalyst charge: 9.8 kg/m^3, sorbitol: 0.18 kmol/m^3, T: 230 ^{o}C, P_{H2}: 7 MPa, reaction time: 6 h. PAD: pyruvaldehyde.

The conversion of sorbitol on the three Cu catalysts, Cu/CaO-Al_2O_3-1, Cu/CaO-Al_2O_3-2 and Cu/CaO-Al_2O_3-3 was investigated in the 300 mL Parr reactor. As shown in Table 2, Cu/CaO-Al_2O_3-1 catalyst displayed almost 100% conversion of sorbitol in 6 h, while Cu/CaO-Al_2O_3-2 and Cu/CaO-Al_2O_3-3 only showed < 20% conversion under the same reaction conditions. The selectivity towards 1,2-PDO, LA+PAD and EG is completely different on the three catalysts. It is found that the combined selectivity to 1,2-PDO, glycerol and EG was about 73% on Cu/CaO-Al_2O_3-1 catalyst, but this value was only 20~32%

on other two catalysts. In contrast, the selectivity of LA+PAD was only < 2% on the active Cu/CaO-Al_2O_3-1 catalyst, the number on the other two catalysts was as high as 64~76%. It is believed that C_3-C_3 cleavage occurs after dehydrogenation (DH) of sorbitol leads to the formation glyceraldehyde (GLA) and dihydroxyacetone (DHA), which undergoes rearrangement to form LA or HDO reactions to generate 1,2-PDO as shown in Scheme 1. Therefore, it can be seen that Cu/CaO-Al_2O_3-1 are active for DH and HDO reactions while only DH occurs on Cu/CaO-Al_2O_3-2 and Cu/CaO-Al_2O_3-3 catalysts.

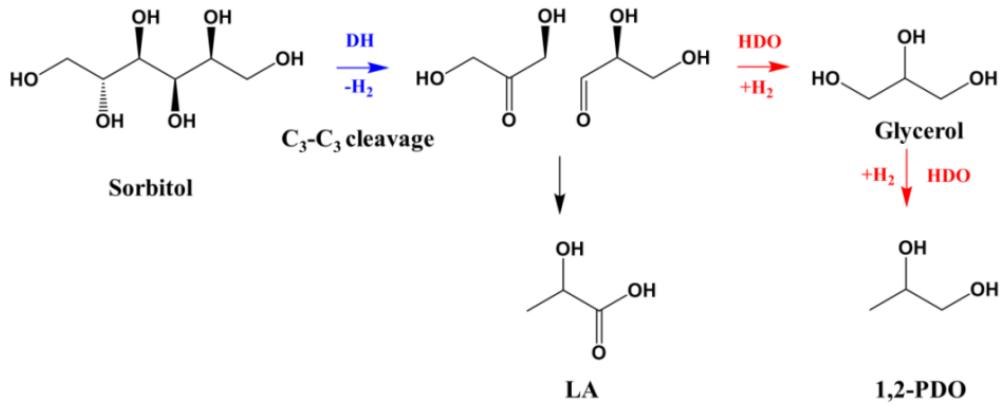

Scheme 1. Formation of 1,2-PDO, glycerol and LA from C_3 intermediates

Further, the selectivity towards C_3 products (1,2-PDO, LA and glycerol) is 83~98%, which implies that C_3-C_3 cleavage is dominant on Cu/CaO-Al_2O_3-2 and Cu/CaO-Al_2O_3-3 catalysts. It is already found that Cu/CaO-Al_2O_3-2 sample has almost one phase, CaCuAlO, while Cu/CaO-Al_2O_3-1 shows CaCuAlO and CuAlO phases. So it is highly possible that CaCuAlO is the active site for DH reactions of sorbitol, while CuAlO (spinel $CuAl_2O_4$) species are active for HDO

reactions thus 1,2-PDO, glycerol and EG are dominant on Cu/CaO-Al_2O_3-1 catalyst.

HDO reactions consume C_3 intermediates species formed from DH of sorbitol on Cu catalysts, which in turn favors the chemical equilibrium towards DH reactions. Therefore Cu/CaO-Al_2O_3-1 catalyst shows a much higher conversion level. But Cu/CaO-Al_2O_3-2 and Cu/CaO-Al_2O_3-3 catalysts do not have active sites for HDO reactions, thus the conversion levels on these catalysts are poor, since DH reactions are obviously not favored at higher hydrogen pressure.

Another important finding is about C-C cleavage of C_3 species. As found in Table 2, the selectivity to EG (S > 15%) is much higher on Cu/CaO-Al_2O_3-1 catalyst compared with Cu/CaO-Al_2O_3-2 (S < 2%). This implies that C-C cleavage of C_3 species to C_2 is also significant on Cu/CaO-Al_2O_3-1 catalyst. This is because of the existence of spinel structure of $CuAl_2O_4$, which is known to be active for C-C cleavages at relatively high reaction temperatures.[58]

From the discussion above, it can be seen that for an optimum activity and selectivity of Cu/CaO-Al_2O_3 catalyst, it should have both DH (CaCuAlO phase) and HDO (spinel $CuAl_2O_4$ phase) sites. This is a possible reason that Cu/CaO-Al_2O_3-1 catalyst displayed higher activities for both C-C and C-O cleavage for catalytic conversion of sorbitol compared to other catalysts.

3.5 Reaction profiles

Since, Cu/CaO-Al_2O_3-1 showed superior performance compared with other catalysts, a detailed concentration-time profile was also investigated. Figure 18 shows a typical plot of the substrate and different products [including 1,2-PDO, EG, glycerol, butylene glycol (1,2-butanediol, 1,2-BDO), *etc*] concentration *vs* reaction time. Complete conversion of sorbitol was achieved in 6 h at 230 ^oC and 4.9 MPa of hydrogen pressure [Figure 18 (a)]. Concentration of 1,2-PDO, EG and glycerol increased linearly with reaction time, while that of LA+PAD (pyruvaldehyde) first increased and then decreased at prolonged times. It is known that LA and PAD can be further hydrogenated to 1,2-PDO in the presence of hydrogen,[57] which explains increase in 1,2-PDO with reaction time.

The concentration of linear alcohols (others in Figure 18) increased sharply with reaction time, which is clearly a result of significant consecutive HDO of 1,2-PDO and EG to propanols (PrOH) and EtOH. A linear dependence of conversion of sorbitol with time and in some cases even until almost 100% conversion [Figure 18 (b)] showed a weak dependence of the HDO rates on sorbitol concentration. The concentration of glycerol and 1,2-PDO also increased linearly with reaction time while that of LA+PAD initially increased but then decreases sharply at prolonged reaction time. The trend of the C_3 products concentration profile also indicates a parallel conversion of these intermediates to MeOH and EtOH.

Results at lower temperature [210 ^{o}C, Figure 18 (c)] showed that the concentration of sorbitol decreased nearly linearly when reaction time was prolonged from 5 h to 20 h. Different trends of concentration profile of different products were obtained. The declining concentration of C_3 products over reaction time was not obviously observed when conversion was higher than 33%, which is different from the trend at 230 ^{o}C. It is also found that the concentration of EtOH and MeOH in liquid products was much lower at 210 ^{o}C at similar conversion. The altered concentration profile implies that the consecutive C-C bond cleavage of C_3 products was restrained at lower temperature (210 ^{o}C).

In addition, the selectivity for secondary (*e.g.* 1,2-PDO, 1,2-BDO and alcohols) rather than primary (*e.g.* glycerol and EG) C-O reactions (combined selectivity for HDO products) was 67%, while this value was only in the range of 30~82% on much more expensive Ru and Ni catalysts under similar reaction conditions.[88-90,94,100,107,154,155] Again, the trace detection of gaseous products (mainly methane and CO_2, S ~0.3% even at 230 ^{o}C) indicates the methanation and WGS are negligible over Cu catalysts. Considering the fact that the proposed Cu/CaO-Al_2O_3-1 catalyst shows high activity and selectivity for both C-C and C-O cleavage, an excellent selectivity of liquid products above 98% has been achieved for sorbitol conversion.

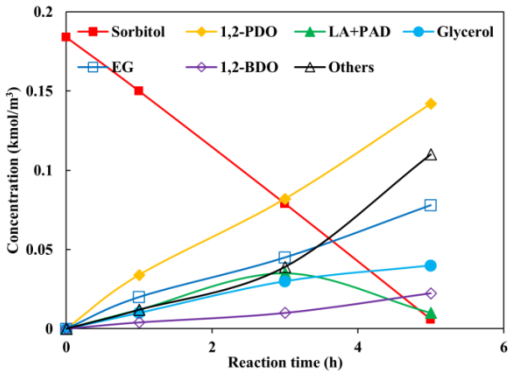

(a)

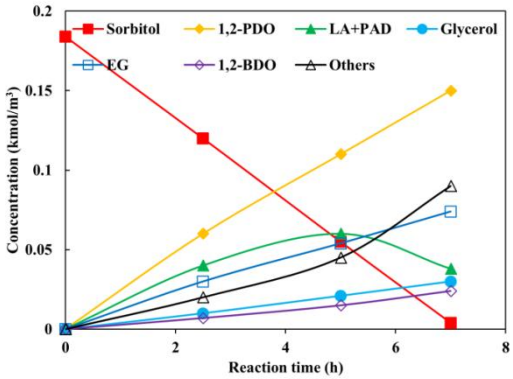

(b)

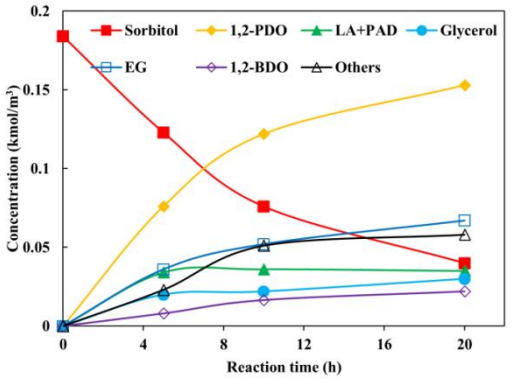

(c)

Figure 18. Concentration-time profiles of sorbitol conversion on Cu/CaO-Al_2O_3-1 catalyst (a) T: 230 ^oC, P_{H2}: 7.6 MPa; (b) T: 230 ^oC, P_{H2}: 4.9 MPa; (c) T: 210 ^oC, P_{H2}: 4.9 MPa

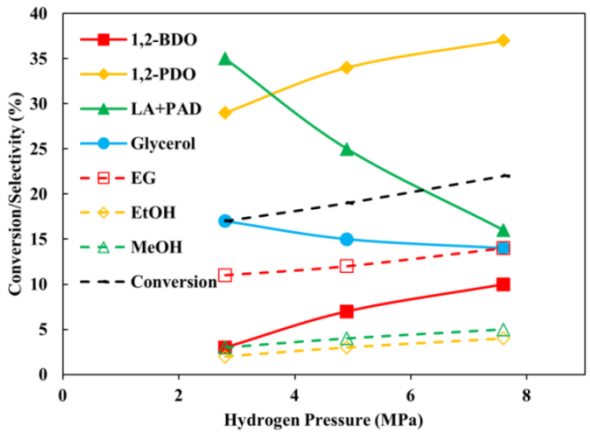

Figure 19. Effect of hydrogen pressure on product selectivity at 230 ^{o}C (X < 25%)

The availability of hydrogen on catalysts surface is found to affect the reaction pathways and product selectivity. As shown in Figure 19, the effect of hydrogen pressure on the selectivity of C_3 and other products was investigated for sorbitol conversion less than 25% at 230 ^{o}C. The reason why the study should be carried out under low substrate conversion is that the intermediate products (from C_1-C_5, C_2-C_4 and C_3-C_3 cleavage) formed initially might instantaneously undergo further C-C breakage under the reaction conditions.[94,154] Therefore it is necessary to investigate initial product selectivity in order to understand the effect of reaction conditions on product distribution. In Figure 19, it is obvious that more LA was formed, with relatively low selectivity compared to 1,2-PDO at low pressure (2.8 MPa). With increasing hydrogen pressure, the combined selectivity of glycerol and LA decreased by about 22% while the initial selectivity of 1,2-PDO increased by only 10%. In contrast, the total selectivity of C_1, C_2 and C_4 products increased by approximately 11%, although C_3 products still dominate. This indicates C_3-

C_3 cleavage is more favored under lower hydrogen pressure. With regard to the temperature effect on the behavior of C-C cleavage, no obvious variation of product selectivity was observed.

3.6 Reaction pathways

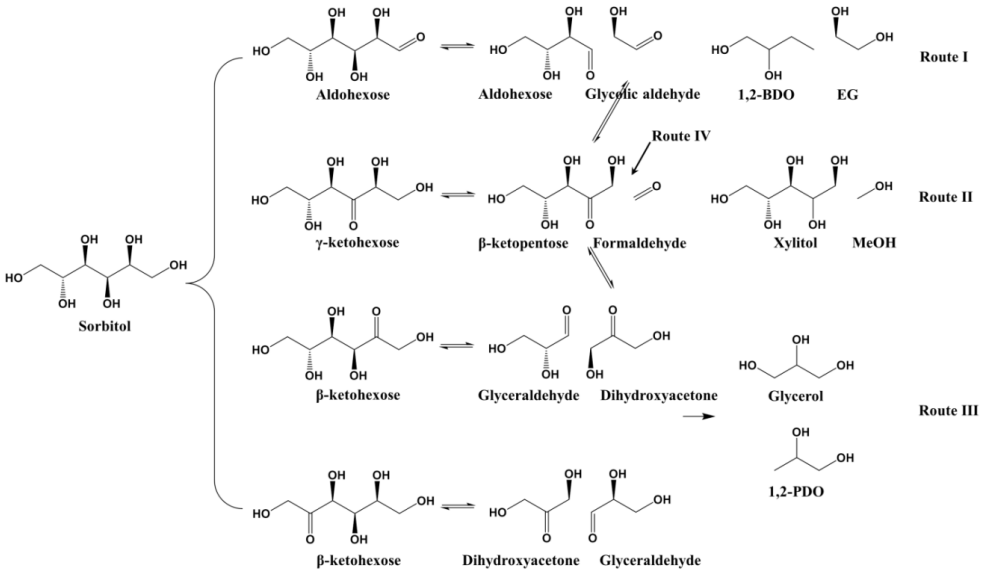

Scheme 2. Possible reaction pathways of sorbitol on Cu/CaO-Al_2O_3 catalyst

The positions where C-C cleavage occurs initially determine the major products selectivity. Therefore, it is first necessary to study the possible reaction pathways to understand the mechanism of C-C and C-O cleavage over the Cu/CaO-Al_2O_3 catalysts. As found in Scheme 2, the formation of aldohexose (primary C_6 aldehyde) initially will generate C_2 and C_4 (Route I) products, while β-ketohexose leads to C_3-C_3 cleavage (Route III).

γ-Ketohexose formed initially results in C_1-C_5 breakage (Route II) and C_5 may further convert to β-ketopentose or aldopentose to generate C_2 and C_3 products

(Route IV). The likelihood of the formation of β-ketohexose is high under low hydrogen pressure on Cu catalysts, because combined selectivity of C_3 products is much higher than other products, as shown in Figure 19. But it should also be noted that selectivity of C_2 (mainly EG) is higher than C_4 (mainly 1,2-BDO). This phenomenon reflects that C_1-C_5 cleavage also occurs over Cu catalysts, as also confirmed by the existence of C_1 (MeOH) in products, although it is formed in minor quantities compared to C_3-C_3 cleavage. Such an observation implies that DH over Cu catalysts tends to generate β-ketohexose rather than γ-ketohexose and aldohexose. Therefore, it can be seen that at a higher pressure aldehyde-like intermediate compounds are likely to be formed (still minor compared with β-ketohexose) while at lower hydrogen pressure the formation of β-ketone like intermediate is favored which lead to the formation of 1,2-PDO and EG in HDO of sorbitol.

Table 3. HDO of xylitol, erythritol and glycerol on Cu/CaO-Al_2O_3-1 catalyst

#	Substrate	X(%)	Selectivity (%)						
			1,2-BDO	1,2-PDO	LA+PAD	glycerol	EG	EtOH	MeOH
1	Mannitol	100	trace	51.5	4.1	9.5	11.4	3.6	6.6
2	Xylitol	98.9	trace	44.4	6.7	5.6	26.0	5.6	1.5
3	Erythritol	85.4	38.6	15.7	3.9	1.0	10.9	trace	7.7
4	Glycerol	67.5	-	81.1	5.7	-	8.1	-	3.8

Cu/CaO-Al_2O_3-1 catalyst: 9.8 kg/m^3, sorbitol: 0.18 kmol/m^3, T: 230 ^oC, P_{H2}: 2.8 MPa, reaction time: 10 h.

Sun & Liu's work implies that in xylitol conversion, the formation of aldopentose (primary C_5 aldehyde) was favored rather than ketopentose because C_1 and C_4 products were found to be in trace amounts.[90] In fact only γ-ketopentose leads the formation of C_1 and C_4 products. From the mechanism shown above it is obvious that β-ketopentose will also facilitate C_2-C_3 cleavage. In order to further justify the validation of our hypothesis, xylitol (C_5 polyol), erythritol (C_4 polyol) and glycerol (C_3 polyol) were also studied as substrates.

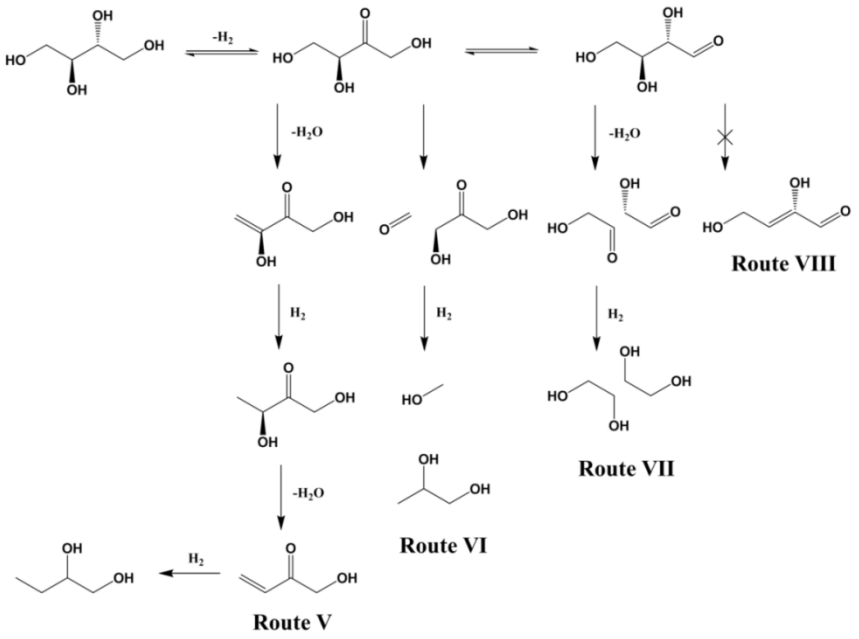

Scheme 3. Possible reaction pathways of erythritol on Cu/CaO-Al_2O_3 catalyst

Results on catalytic HDO of mannitol, xylitol, erythritol and glycerol on Cu/CaO-Al_2O_3-1 catalyst are summarized in Table 3. Mannitol conversion was > 65% in C_3 selectivity (Entry#1), while the combining selectivity to EG and EtOH (C_2 products) was only 15%. The conversion of xylitol showed mainly C_2

and C_3 products (Entry#2), possibly following retro-aldolization mechanism.[105] It is obvious that the theoretical selectivity of C_3 and C_2 should be 60% and 40% respectively. Here it is found that the total selectivity of 1,2-PDO, LA, PAD and glycerol were approximately 56.7% over Cu/CaO-Al_2O_3-1 catalyst and combined selectivity toward EG and EtOH was about 31%. The ratio of C_3/C_2 was almost equal to the theoretical value (60/40). The limited selectivity of MeOH and 1,2-BDO implies that xylitol conversion follows primarily C_2-C_3 cleavage. These results agree well with Sun & Liu's observations on Ru/C catalyst.[90]

HDO of meso-erythritol showed that the dominant product was 1,2-BDO (S ≈ 39%). This suggests that, as carbon number decreases from 6 (sorbitol, mannitol) and 5 (xylitol) to 4 (erythritol), the tendency of C-C cleavage becomes less significant, while the activity of C-O cleavage is enhanced. This is consistent with the observation that erythritol follows sequential dehydration (DHD) and HDO reactions to form 1,2-BDO (Route V in Scheme 3). $C_{1\sim3}$ products are also detected in HPLC, including glycerol, LA, 1,2-PDO, EG and MeOH. The ratio of C_3/C_1 was found to be almost 3/1. Besides, the combined selectivity of C_1+C_3 was much higher than C_2, as shown in Table 3. This observation clearly indicates that C_1-C_3 bond breakage (Route VI in Scheme 3) rather than C_2-C_2 cleavage (Route VII) prevails over Cu/CaO-Al_2O_3 catalyst. The observed facts support our hypothesis that the formation of β-ketose (*e.g.*

β-ketohexose, ketopentose and ketoerythrose) is favored over Cu/CaO-Al_2O_3 catalysts.

The argument on whether 1,2,3-butanetriol (1,2,3-BTO, Route V) or 1,2,4-butanetriol (1,2,4-BTO, Route VIII) is the precursor for 1,2-BDO can be answered by the detected species in GC-MS. Trace 1,2,4-BTO (S < 2%) was found at the beginning of sorbitol conversion (X < 10%), which indicates that generation of 1,2-BDO is instantaneous on Cu/CaO-Al_2O_3-1 catalyst. Moreover, this observation confirms that active basic species tend to attack terminal carbon and promote DHD at primary and secondary carbons. The formation of 1,2-PDO can also be explained by this tendency and confirmed by various previous studies. However, the reason that sequential DHD and hydrogenation occur to form 1,2-BDO is still not clear. Here a representative mechanism is proposed to verify the formation of 1,2-BDO. Unlike sorbitol and xylitol, the β-ketose intermediate from erythritol might undergo either retro-aldolization (Route VI) or secondary DHD (Route V in Scheme 3) because the stable conjugated structure might also be favored. Detailed description of reaction mechanism over Cu/CaO-Al_2O_3-1 catalyst will be presented in next section.

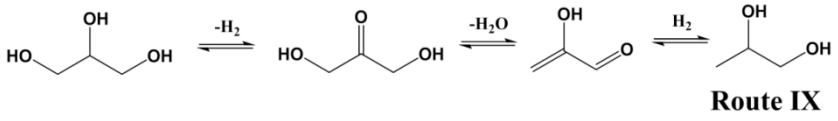

Scheme 4. Possible reaction pathways of glycerol on Cu/CaO-Al_2O_3 catalyst

Different from the reaction results over Ru catalysts shown in Chapter 1, sorbitol and xylitol conversion over Cu/CaO-Al_2O_3-1 catalyst imply that the potential of C-C breakage of C_3 molecules is likely to be restrained. These observed facts were further confirmed by our study on HDO of glycerol. It showed a conversion of 67.5% with a major product as 1,2-PDO (S = 81%). It is interesting to notice that, compared with sorbitol (C_6), xylitol (C_5) and erythritol(C_4), the potential of C-C cleavage of glycerol (C_3) molecules was significantly restrained with regard to the low selectivity of $C_{1\sim2}$. Maris found that the addition of base (NaOH and CaO) increased the conversion of glycerol to both EG (S ≈ 20%) and 1,2-PDO (S ≈ 27%) because the retro-aldol and HDO reactions are enhanced by adsorbed hydroxyls even under much milder conditions. Again, such difference can be explained by our alternate representative pathways, the formation of DHA, which is a type of β-ketose in Scheme 4 (Route IX) over Cu/CaO-Al_2O_3 catalyst rather than GLA, which can lead to C-C cleavage in glycerol conversion. DHA is formed then undergo further DHD to generate a conjugated unsaturated alcohol, which hydrogenates to form 1,2-PDO.

3.7 Reaction mechanism

As indicated above, product distribution from HDO of sorbitol, xylitol and erythritol suggests that C-C cleavage is likely to be initiated by β-ketone and thus displays a C_x-C_3 like cleavage in the presence of divalent Ca^{2+}. Therefore a representative C-C cleavage mechanism over the Cu/CaO-Al_2O_3-1 catalyst is

proposed for the first time. It is known that DH of α-alcohols easily takes place on Cu catalysts while DH of secondary and tertiary alcohols demands extremely harsh conditions.[156,157] Therefore, as shown in Scheme 5, sorbitol most likely undergoes DH reaction to form aldohexose catalyzed by Cu sites. Thus an adsorbed aldehyde polyol is formed on the Cu catalyst. As supported by TPR (reduction peak position) and SEM (phase diagram) characterization, Ca^{2+} sitting as a neighbor with Cu species has strong influence on Cu sites and tends to isomerize the aldohexose intermediates thus forming β-ketohexose (or γ-ketohexose). This is on the basis of retro-aldol mechanism, which describes that the formation of β-ketohexose results in C_3-C_3 cleavage. In the case of xylitol, this mechanism also applies and similar equilibrium structures (aldopentose, β-ketopentose and γ-ketopentose) are formed. And it is clear that aldopentose and β-ketopentose both result in C_2-C_3 scission, although in a different way.

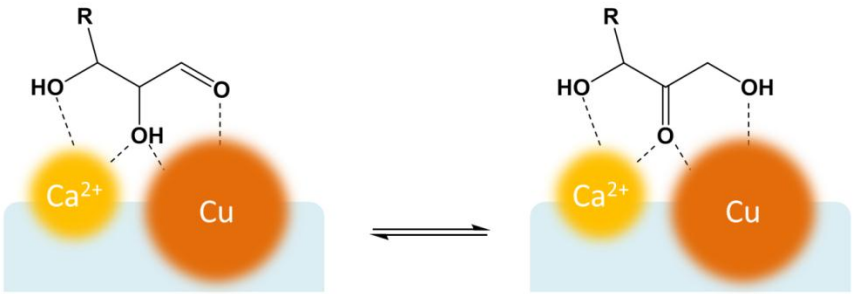

Scheme 5. Reaction mechanism of bio-derived polyols in CaCuAlO phase

Peng and coworkers proposed that Cr^{3+} could isomerize aldohexose (glucose) molecules *via* bonding with α and β carbon chain to form glucose-fructose

equilibrium structures, the latter of which easily goes through DHD in the presence of an acidic promoter (pH < 5 in the solution containing Cr^{3+}).[158] Davis' group also found similar effects over lewis acid, Sn-containing zeolites and depicted the same mechanism for the formation of hydroxymethylfurfural in glucose and fructose conversion.[159] Differently, Yan and coworkers found that the LA (C_3) yield from glucose (C_6) was facilitated by $Ca(OH)_2$ to a greater extent compared with NaOH (at the same initial OH^- concentration) in hydrothermal conversion (270~400 ^oC).[144] These observations confirm that Ca^{2+} is the key to determine C_3-C_3 scission is initiated over Cu catalysts during HDO of sorbitol and xylitol (as shown in Scheme 5).

For xylitol, dominant C_2-C_3 cleavage occurs because of the formation of the β-ketose. Analogously, formation of C_1 and C_3 *via* asymmetrical C_1-C_3 cleavage can also occur *via* forming a β-ketose from a C_4 polyol and is confirmed by our experimental results from the conversion of erythritol, although the potential of C-C scission is much lower than sorbitol and xylitol. The asymmetrical cleavage seems not to be favored for sorbitol (C_1-C_5) and xylitol (C_1-C_4) over Cu/CaO-Al_2O_3 catalyst. These unsaturated intermediates generated from DH and C-C cleavage are then be hydrogenated to alcoholic products in the presence of hydrogen. Besides, it is clear from our experimental results that HDO reactions are also metal catalyzed reactions. The existence of spinel $CuAl_2O_4$ is the key for hydrogenation of polyols to glycols and alcohols.

4. Conclusion

In this chapter, novel Cu-based bi-functional catalysts are proposed for selective HDO of various bio-derived polyols such as sorbitol, mannitol, xylitol, erythritol and glycerol. It is found that, in comparison with Mg^{2+} and Zn^{2+}, Ca^{2+} displays significant promotional effects on the activity as well as the selectivity of Cu catalysts for C-C cleavage of these polyols. TPR characterization shows that Cu species have strong interaction with $CaO\text{-}Al_2O_3$ supports, which is believed to be the key factor that governs the performance of Cu catalysts. Detailed surface characterization confirms the existence of binary phases, CaCuAlO and CuAlO in Cu catalysts, which is responsible for DH and HDO respectively during the conversion of polyols. Results with different polyols further show that Ca^{2+} also promotes the isomerization of aldoses, and that $C_3\text{-}C_x$ cleavage is significant. A possible reaction mechanism involving DH and isomerization on catalyst surface is proposed for the first time for Cu-based catalysts and correlation of the trends with catalyst characterization discussed. Our proposed Cu catalysts display much better activity for C-C and C-O cleavages for polyols compared with literature reports.

Chapter 4 Atom Economical Conversion of Polyols to Lactic Acid and Glycols

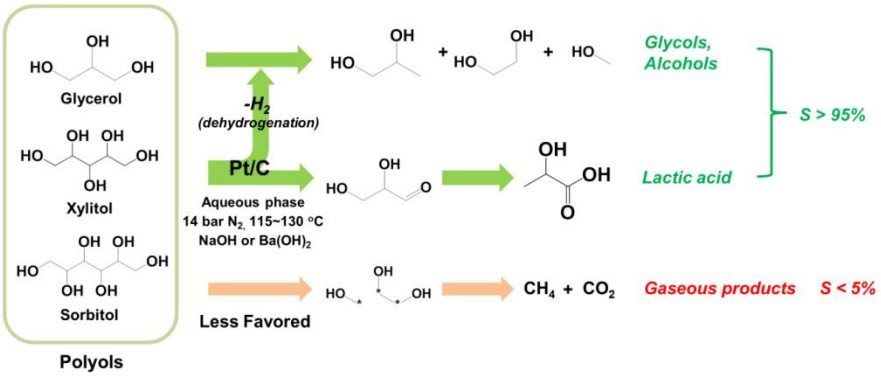

Tandem dehydrogenation/hydrogenolysis can achieve higher carbon utilization under significantly milder reaction conditions in the conversion of biopolyols to valuable chemicals compared to conventional oxidation and hydrogenolysis processes.

1. Introduction

As discussed in the previous chapters, catalytic upgrading of polyols, for example hydrogenolysis (HDO) processes, usually involves consumption of large excess of expensive hydrogen. At present, industrial hydrogen mainly comes from steam reforming of non-renewable natural gas, which imposes significant economic and environmental challenges for the sustainable development of biomass conversion technologies. More importantly, the presence of excess hydrogen under severe conditions (T = 200~300 ^{o}C, hydrogen pressure = 4.0~8.0 MPa) facilitates unwanted side reactions such as random C-C cleavage and methanation. The *carbon selectivity* (selectivity to valuable liquid products) is thus low for economic viability.

From the results presented in Chapters 2 and 3, it was found that dehydrogenation (DH) is one of the most important steps in catalytic conversion of polyols, which often generates lactic acid (LA), an emerging renewable chemical, as the direct product. It is important to note that DH actually does not require externally added hydrogen but releases hydrogen to the reaction system instead. Other reactions such as reforming will also provide *in situ* formed hydrogen to the reaction system. Therefore, combining the hydrogen generation with HDO reactions in one single pot, or tandem approach will potentially lead to environmental and economical advantages over the conventional biomass upgrading processes.

Previous researchers have evaluated several metal based catalysts for tandem conversion of polyols showing its feasibility but the overall liquid selectivity to useful products was very low (S < 56%).[14,122] This is because several side reactions particularly methanation and water gas shift (WGS) were so significant on the proposed metal catalysts at elevated temperatures (T > 200 ^{o}C), that significant amounts of carbon values were converted to less valuable gaseous products such as methane and CO_2.

In this chapter, experimental results on a novel approach for converting bio-derived polyols, including glycerol, xylitol, sorbitol and mannitol at very mild reaction conditions are presented. Particularly, the following issues have been addressed: (a) The chemistry of tandem DH/HDO reactions for glycerol, xylitol, sorbitol and mannitol conversion on heterogeneous catalysts consisting of

supported metals; (b) Key factors governing the activity and selectivity of the catalysts; (c) Detailed kinetic modeling of the multi-step reactions, possible reaction pathways and mechanism.

The proposed process route has several advantages over the conventional biomass conversion technologies. (1) No externally added hydrogen is needed. HDO occurs in the presence of hydrogen formed *in situ* from only a small fraction of bio-polyol substrate under mild conditions eliminating the use of high hydrogen pressure (4.0~8.0 MPa); (2) the reaction occurs under significantly lower temperatures (T = 115~160 ^{o}C) compared with conventional HDO processes (T = 200~300 ^{o}C); (3) the overall atom efficiency in the proposed route is as high as 96%.

2. Experimental Section

2.1 Catalyst preparation

Chemicals including glycerol (>99.5%), D-sorbitol (99+%), D-glucose (99.5%), D-fructose (99+%), glyceraldehyde (95%), pyruvaldehyde (40w% in H_2O), 1,2-propanediol (1,2-PDO, 99.5+%), ethylene glycol (EG, 99.8+%), ethanol (EtOH, 99.5%), methanol (MeOH, 99.8%), $Ca(OH)_2$, KOH and NaOH were identical to those described in Chapters 2 and 3. Precious metal catalysts such as Pt, Pd, Ru, Rh, all supported on activated carbon with 5wt% metal loading and unsupported Cu_2O catalysts, were purchased in powder form from Sigma-Aldrich. Raney Ni and Raney Co were purchased from Grace Davison and

Sigma-Aldrich, respectively. Raney Ni and Raney Co catalysts were freshly reduced at 240 ^{o}C and 10 MPa hydrogen pressure for 6 h prior to batch reaction tests. Hydrogen (> 99.5%) and nitrogen (> 99%) were procured from Air Gas Inc. and Linweld, respectively and used without further purification.

A few supported Pt catalysts on activated carbon support were prepared by precipitation method. In brief, known amount of activated carbon (100 mesh, Sigma) was charged to 700 mL of deionized water and the slurry was heated to 95 ^{o}C in a round-bottom flask with magnetic stirring for 2 h. Then, required amount of H_2PtCl_6 (Sigma) was added to the slurry dropwise. The resultant slurry was stirred for another 3 h. A dilute $NH_3 \cdot H_2O$ solution (Fisher) was added to the system dropwise until a pH value of 10 was achieved to reduce the Pt salts to metallic Pt. After stirring for 3 h, the mixture was filtered and the solid catalyst was washed with 2000 mL of deionized water at 90 ^{o}C to remove chloride ions. The solid sample was then dried overnight in a vacuum oven at 120 ^{o}C. Prepared Pt/C catalyst sample was denoted as Pt/C-P. Commercial Pt/C catalysts were purchased from Acros, denoted as Pt/C.

The catalysts were activated at 300 ^{o}C for 5 h in a tube furnace under the flow of hydrogen (20 cm^3/min/g-catalyst) before testing in a slurry reactor, the temperature profile of which was identical to that shown in Figure 2 of Chapter 2 thus will not be described in details here.

2.2 Catalytic activity tests

Catalytic performance tests for the tandem conversion of polyols were carried out in a magnetically stirred multiple batch slurry reactor setup described in Chapter 2 at high temperature, high pressure conditions. The experimental procedures were however slightly different from that in Chapter 2. Particularly, polyol substrate (*e.g.* glycerol, xylitol) was mixed with alkali (*e.g.* NaOH, KOH) in aqueous solution with a total volume of 30 mL at room temperature before introducing into the reactor with PTFE liner. Then the reactor was sealed and flushed with nitrogen thrice before heating was started.

2.3 Analytic methods

After a batch reaction experiment, the contents in the reactor were cooled to room temperature, and the gas phase products were analyzed using GC shown in Figure 5 of Chapter 2. Then, the reactor was opened and 20 mL of sulfuric acid solution in water was added to acidify the liquid products. The pH value was adjusted to a pH = 5~6 and final volume of the liquid sample made up to 50 mL for analysis using HPLC. The analytical procedures for GC and HPLC as well as basic definitions (*e.g.* conversion, TOF, *etc*) were similar to that described previously in "2.3 Analytical methods" of Chapter 2 in details. A typical liquid chromatography of the products is shown in Scheme 1.

Error analysis for glycerol conversion on Pt/C was conducted, the experimental error of which is shown in Figures 8 and 9. The detailed error analysis for kinetic modeling on Pt/C catalyst is presented in Appendix IV.

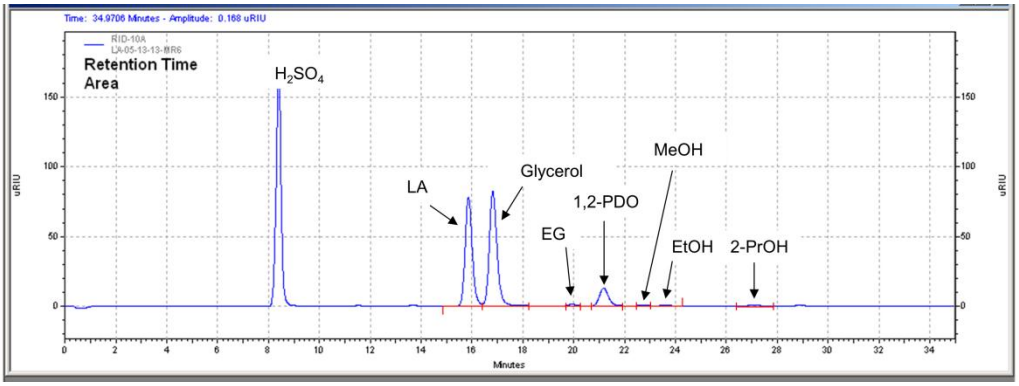

Scheme 1. A typical liquid chromatograph of products from aqueous phase conversion of glycerol to LA and co-products

2.4 Catalyst characterization

The procedures for Transmission electron microscopy (TEM), Brunauer-Emmett-Teller (BET) and Inductively Coupled Plasma (ICP) followed have already been discussed in "2.4 Catalyst characterization" of Chapter 2.

3. Tandem DH/HDO of glycerol at low temperature

3.1 Catalyst performance

Conversion and selectivity of carbon-supported Pt, Pd, Ru, Rh, Raney Ni and Raney Co catalysts were evaluated for glycerol conversion in aqueous phase under alkaline conditions without adding external hydrogen. The experimental results at 220 ^{o}C are presented in Table 1 as conversion and selectivity. High

glycerol conversions were achieved in 6 h over almost all the catalysts tested even though no external hydrogen was used. However, the LA selectivity was different in each case. It was observed that Raney Ni displayed poor selectivity towards LA (S = 7%, Entry#1 in Table 3) with significant methane formation. Raney Co and Ru catalysts (Entries#2 and #3 in Table 1) showed relatively higher LA selectivity and lower methane selectivity (S = 65%) compared to Raney Ni.

Table 1. Comparison of different catalysts in aqueous phase glycerol conversion

#	Catalysts	X[a] (%)	Selectivity (%)						
			LA	1,2-PDO	G+P[d]	EG	Alcs[e]	CH_4	C_{2+} alkanes
1	R-Ni[b]	99.3	7.4	0.3	0.3	-	0.6	64.6	3.0
2	R-Co[b]	99.0	37.6	1.1	0.3	-	1.8	34.3	2.2
3	Ru/C[c]	97.7	39.6	4.8	0.5	-	13.2	15.8	8.7
4	Pt/C[c]	97.1	37.2	9.6	0.4	0.9	15.9	1.9	1.3
5	Pd/C[c]	91.1	40.1	6.9	0.5	1.4	14.5	3.7	0.5
6	Rh/C[c]	87.0	37.9	10.9	0.5	1.0	15.0	7.9	2.9

a. Conversion at 220 ^{o}C, reaction time: 6 h, P_{N2}: 1.4 MPa; glycerol: 1.1 kmol/m^3, solvent: H_2O; NaOH/glycerol molar ratio: 1.1;
b. Raney Ni and Raney Co catalysts, charge: 100.0 kg/m^3;
c. Noble metal catalyst supported on carbon, charge: 6.7 kg/m^3;
d. G+P: Glyceraldehyde (GLA) and pyruvaldehyde (PAD);
e. Alcs: Alcohols including MeOH and EtOH, traces of propanols.

Supported Pt, Pd and Rh catalysts on carbon (Entries#4~6 in Table 1) also showed high glycerol conversion with LA selectivity between 37~40% and significantly lower methane formation. A carbon balance deficiency (15~24%) in the final products was obvious for the supported metal catalysts (in Table 1)

at 220 ^{o}C due to significant gas phase products. Most notably, GC analysis of the gas phase showed no detectable CO_2. This does not seem possible given the preponderance of evidence that CO_2 is formed by aqueous phase reforming on such catalyst systems at the temperatures under investigation.[8,17,29] Hence, this C deficit is partly attributed to the absorption of gas phase CO_2 at 220 °C and reaction with alkali to form carbonates (which could not be reliably measured). In previous work[8] and this work, it is observed the release of gas bubbles from the liquid phase when dilute H_2SO_4 was added during the liquid products workup for analysis. The CO_2 formed in the gas phase during reaction most likely reacts with the base in the liquid phase to form carbonate or bicarbonate which is released upon H_2SO_4 addition. The fact that the pH of the product mixture remained > 11 (prior to product workup) confirms that the conditions are favorable for CO_2 to react with alkali to form bicarbonate but that the CO_2 amount was not significant enough to lower the pH value. Under similar conditions, Cu_2O catalyst was reported to give high LA selectivity (S = 74%) at 70% conversion of glycerol.[79] The intermediate products such as glyceraldehyde (GLA) and pyruvaldehyde (PAD) observed with Cu_2O catalysts were also observed with other catalysts, albeit in small quantities, indicating that the reaction pathway for LA formation is similar on different catalysts. It must be noted that a reaction with NaOH but without the metal component gave negligible conversion of glycerol (< 1%) in a PTFE lined reactor in a temperature range of 130~220 ^{o}C. A similar result was also obtained previously when the reaction was performed with a Cu catalyst but without a base.[79]

Further, a comparison of the foregoing results with previous studies with Ru/C and Pt/C catalysts under neutral conditions (*i.e.*, without adding bases or acids)[160] indicates that the selectivity for methane on noble metals is significantly reduced in the presence of alkali (see Table 1, Entries #3, #4 and #6) while increasing the total yield of liquid products.

Table 2. Glycerol conversion over metal catalysts at low temperatures (150~160 ^{o}C)

#	Catalysts	Time (h)	X[a] (%)	Selectivity (%)					
				LA	1,2-PDO	G+P[d]	EG	Alcs[e]	Gas[f]
1	R-Ni[b]	6	87.0	20.3	41.0	5.0	3.8	3.9	5.2
2	R-Co[b]	6	94.4	44.5	37.5	5.1	1.0	0.7	2.7
3	Pt/C[c]	2	44.9	54.1	20.9	1.0	1.6	17.7	0.4
4		6	78.7	36.5	25.8	0.6	1.9	21.6	2.0
5	Ru/C[c]	2	51.8	30.4	35.9	0.9	2.8	10.5	4.0
6		6	83.9	32.5	35.9	0.5	2.1	18.0	4.4
7	Rh/C[c]	2	33.0	46.3	27.3	0.5	0.9	16.9	4.7
8		6	57.1	46.9	31.2	0.2	1.2	14.8	4.4

a. Conversion at P_{N2}: 1.4 MPa, glycerol: 1.1 kmol/m^3, solvent: H_2O, NaOH/glycerol molar ratio:1.1;
b. Raney Ni and Raney Co catalysts, T: 150 ^{o}C, charge: 33.3 kg/m^3;
c. Noble metal catalyst supported on carbon, T: 160 ^{o}C, charge: 6.7 kg/m^3.
d. G+P: Glyceraldehyde (GLA) and pyruvaldehyde (PAD);
e. Alcs: Alcohols including MeOH and EtOH, traces of propanols
f. Mainly methane, traces of C_{2+} alkanes.

In order to understand the temperature effect, additional tests were carried out on the various catalysts at milder conditions (T = 150~160 ^{o}C) with varied batch times, the results of which are shown in Table 2. To our surprise, significant glycerol conversion was observed with all the catalysts even at

lower temperatures. Compared with the results at 220 ^{o}C, combined LA and 1,2-PDO selectivity increased on Raney Ni and Co catalysts at 160 ^{o}C with significantly lower gaseous products (S < 10%). The initial LA selectivity was relatively higher on Pt/C than Raney Ni, Ru/C and Rh/C, but decreased with reaction time (compare Entries#3, #5 and #7 with #4, #6 and #8). The selectivities to LA and 1,2-PDO remained almost unchanged with time on Ru/C and Rh/C catalysts. For Pt and Ru catalysts, the combined selectivity to LA and 1,2-PDO was approximately 70~78% initially but declined with batch time while the formation of linear alcohols increased at longer reaction times.

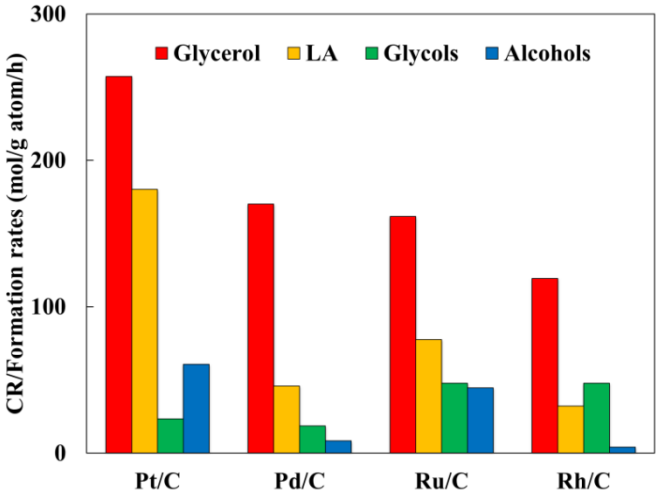

Figure 1. Activity of supported metal catalysts for aqueous phase glycerol conversion (T: 160 ^{o}C, P_{N2}: 1.4 MPa, glycerol: 1.1 kmol/m^3, solvent: H_2O, NaOH/glycerol molar ratio: 1.1, catalyst charge: 6.7 kg/m^3; glycols: 1,2-PDO and EG, alcohols: MeOH, EtOH and propanols). Note: CR values were calculated based on polyol conversion of ~20%)[161]

The activities of the noble metal catalysts were also compared with the Cu catalyst reported previously.[79,162] As shown in Figure 1, Pt/C, Pd/C, Ru/C and

Rh/C catalysts exhibited CRs of 257.4, 170.2, 161.7 and 119.4 mol/g atom/h, respectively at 160 ^{o}C. In contrast, the CR observed on Cu catalyst (0.26 mol/g atom/h) was significantly lower. The formation rates (also in terms of CR) for LA and linear alcohols on Pt/C were 180.2 and 60.7 mol/g atom/h respectively, while Ru/C and Rh/C showed slightly higher formation rates for glycols compared to other products. In addition, Ru/C and Rh/C also displayed higher CRs for linear alcohols (mainly MeOH). From these results, it is clear that Pt/C catalyst outperformed other noble metal catalysts during low temperature conversion of glycerol to LA and glycols.

Table 3. Comparison of various catalytic systems for glycerol conversion

#	Catalyst	Glycerol (w%)[b]	NaOH ratio[c]	T (^{o}C)	P[d] (MPa)	TOF (mol/mol.h)	S_{LA} (%)	$S_{glycols}$ (%)	ref
1	N.A.[a]	3.3	4.0	300	H_2O, 9	N.R.[e]	95	N.R.[e]	[78]
2	Ru/C	1.0	8.0	200	H_2, 4	72	47	36	[57]
3	PtRu/C	1.0	8.0	200	H_2, 4	1080	41	37	[57]
4	Cu_2O	10	1.1	240	N_2, 1.4	2.1	78.1	6.3	[79]
5	Cu/rGO	10	1.1	200	N_2, 1.4	33.0	87	4.2	[162]
6	CuPd/rGO	10	1.1	200	N_2, 1.4	114.2	84.5	5.6	[162]
7	Rh/C	5	2.0	180	He, 3.0	122.6	43	6.5	[125]
8	Ir/C	5	2.0	180	He, 3.0	1086	51	22	[128]
9	Pt/C	10	1.1	160	N_2, 1.4	1132.2	69.8	13.3	This work

a. Hydrothermal conversion, no metal catalyst added; b. glycerol concentration in aqueous solution; c. NaOH/glycerol molar ratio; d. Gas atmosphere and pressure; g. N.R. or not formed.

Further, a comparison between catalysts proposed by previous researchers and the Pt/C investigated in this work was also made. As shown in Table 3, it was

observed that hydrothermal conversion of glycerol in water shows high selectivity (95%) to LA under very severe reaction conditions (P_{total} = 9 MPa, T = 300 ^{o}C). In contrast, Ru/C (Entry#2) and PtRu/C (Entry#3) catalysts displayed a selectivity towards LA in the range of 41~47% at 200 ^{o}C in the presence of external hydrogen (P_{H2} = 4 MPa). Cu-based catalysts (Entries#4~6) reported recently in our laboratory showed relatively higher selectivity to LA (S > 78%) compared with Ru/C and PtRu/C catalysts in the presence of inert nitrogen (P_{N2} = 1.4 MPa) rather than hydrogen atmosphere, though the overall activity was very low. Other metal-based catalysts such as Rh/C and Ir/C (Entries#7~8) also exhibit very good activity in helium environment but the combined selectivity to LA and glycols are poor compared with other catalysts. Among all the catalysts investigated, it was observed that Pt/C catalyst showed superior performance under mild reaction conditions with: (a) high glycerol concentration, (b) low NaOH/glycerol ratio, (c) low reaction temperature and pressure but with highest activity and selectivity. Therefore detailed kinetic modeling of DH/HDO of glycerol was carried out using Pt/C catalyst.

3.2 Structure-activity correlation

Figure 2 shows the TEM data for fresh [(3a) and (3b)] and used [(3c) and (3d)] Pt/C catalysts. Fresh Pt/C catalyst displays a size distribution of approximately 5~10 nm. The dominant plane manifested in fresh C-supported Pt nanoparticles (NPs) is the [111] surface plane. Further, the lattice structure of Pt NPs appears to remain stable after the experimental runs [Figure 3 (c) and (d)].

The activity and selectivity of commercial Pt/C catalysts with various Pt loadings (from 1~5w%) were compared at 160 ^{o}C (Figure 3). It is found that commercial Pt(1w%)/C, Pt(3w%)/C and Pt(5w%)/C catalysts displayed similar conversion rates (CRs) for glycerol conversion. Similar trend is also observed for selectivity to LA and glycols. These results indicate that the conversion of glycerol and corresponding product distribution is not dependent on Pt loadings.

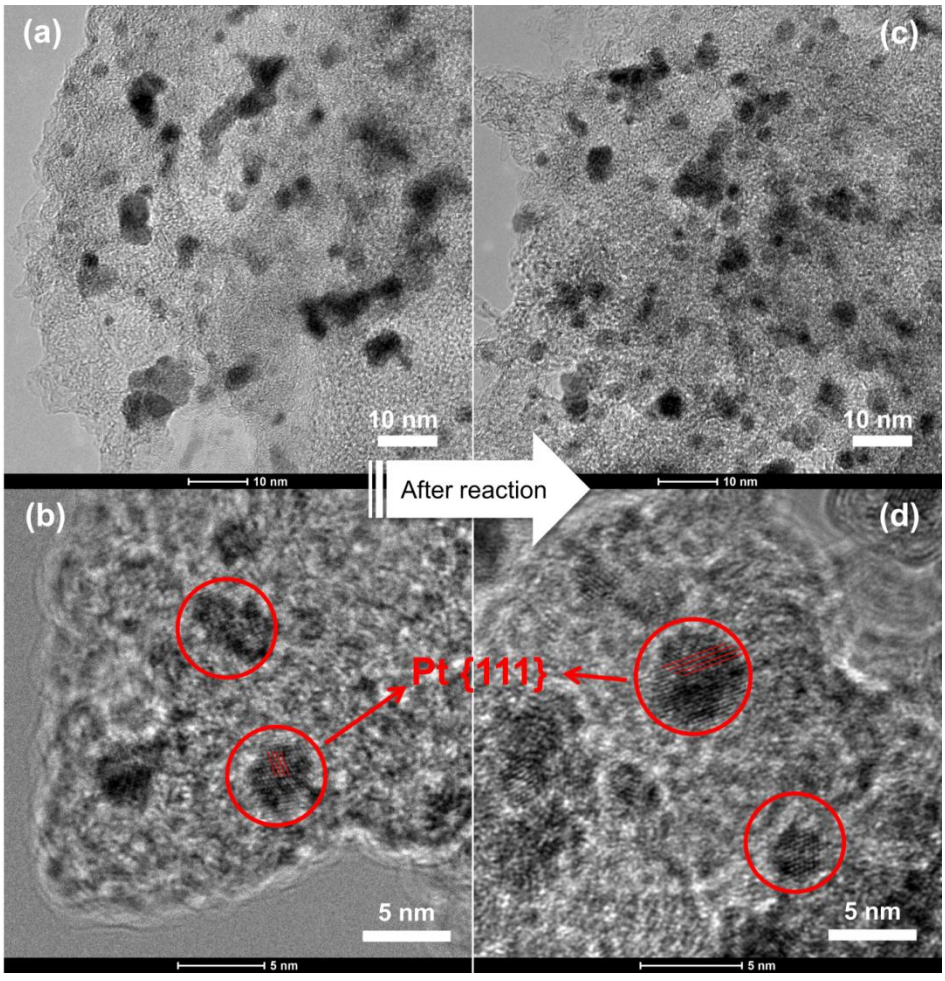

Figure 2. TEM data for fresh [(a), (b)] and used [(c), (d)] Pt/C catalysts

In order to understand the influence of surface morphologies of Pt nanoparticles on glycerol conversion and product distribution, two more catalysts samples, Pt(2w%)/C-P and Pt(5w%)/C-P were prepared and tested. The activity and selectivity results are shown in Figure 4. It is found that the observed activity for Pt(2w%)/C-P (CR = 483.5 mol/g atom Pt/h) and Pt(5w%)/C-P (CR = 349.9 mol/g atom Pt/h) catalysts are higher than the commercial Pt(5wt%)/C sample. The initial selectivity to LA follows the order: commercial Pt(5w%)/C > Pt(5w%)/C-P > Pt(2w%)/C-P. The combined selectivity to glycols and alcohols exhibits a reverse order of Pt(2w%)/C-P > Pt(5w%)/C-P > commercial Pt(5w%)/C. The difference in CR and product selectivity implies that DH rates are higher on Pt/C-P catalysts compared with the commercial samples.

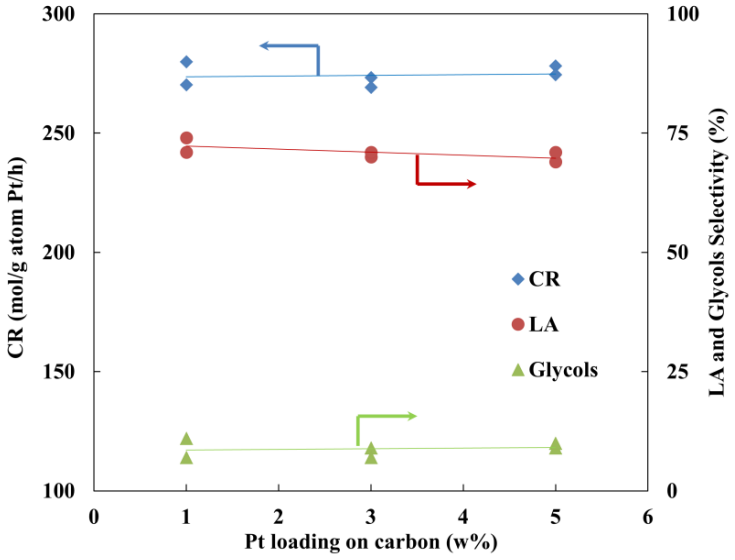

Figure 3. Activity of commercial Pt/C catalysts with various loadings for aqueous phase glycerol conversion (T: 160 ^{o}C, P_{N2}: 1.4 MPa, glycerol: 1.1 kmol/m^3, solvent: H_2O, NaOH/glycerol molar ratio: 1.1, Pt/C catalyst charge: 6.7 kg/m^3, conversion ~20%; glycols: 1,2-PDO and EG)

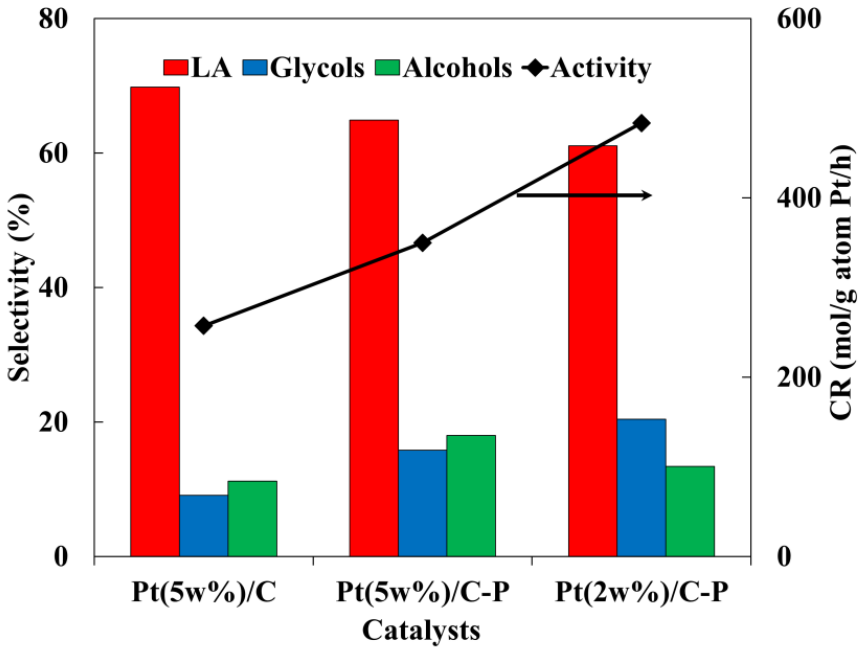

Figure 4. Activity of commercial and prepared Pt/C catalysts for aqueous phase glycerol conversion (T: 160 ^{o}C, P_{N2}: 1.4 MPa, glycerol: 1.1 kmol/m^3, solvent: H_2O, NaOH/glycerol molar ratio: 1.1, Pt/C catalyst charge: 6.7 kg/m^3, conversion 5~20%; glycols: 1,2-PDO and EG; alcohols: MeOH, EtOH and propanols)

TEM data of the three catalysts show that the particle sizes and shapes for prepared and commercial samples are different. As shown in Figure 5, the particle sizes for commercial Pt(5w%)/C, Pt(5w%)/C-P and Pt(2w%)/C-P are 4 nm, 1.2 nm and ~1nm. Furthermore, detailed inspection of these three samples reveals that commercial catalyst sample displays mostly Pt [111] lattice structure on carbon support, while Pt(5w%)/C-P and Pt(2w%)/C-P samples exhibit amorphous structures. Although the values of CR reflect the efficiency of bulk metal involved in catalytic reactions, the surface activity, which is the conversion rates based on surface metals, is still not clear. Therefore, it is

necessary to compare the reaction rates on the basis of amounts of surface (Pt) metal.

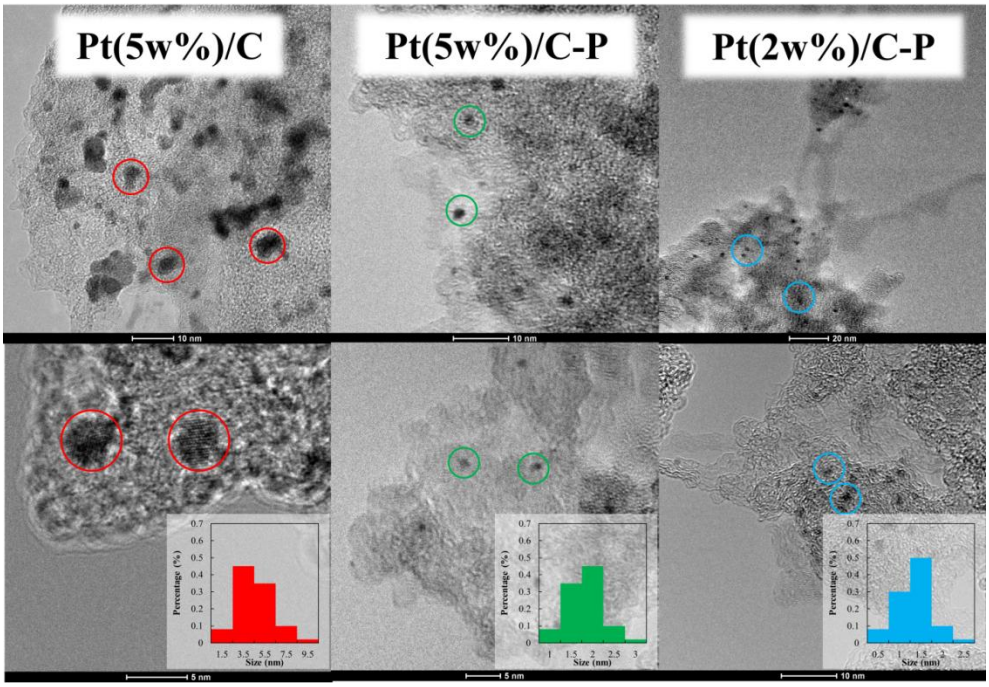

Figure 5. TEM images of commercial Pt(5w%)/C, Pt(5w%)/C-P and Pt(2w%)/C-P samples

The surface Pt atoms can be calculated based on the reverse ratio of particle sizes measured from TEM data. Table 4 compares CR, TOF, product selectivity and HE on Pt/C-P and Pt/C catalysts. It was observed that the conversion of glycerol was slightly higher on Pt/C-P (Entry#1, X = 26%) compared with Pt/C catalyst (Entry#3, X = 21.6%) after 0.5 h. The selectivity to LA was approximately 65~70%, while the combined selectivities of glycols (1,2-PDO and EG) and alcohols [MeOH, EtOH and 2-propanol (2-PrOH) in Table 4] were almost identical (30~32%), in the presence of both catalysts. This result agrees

well with our previous observation that HDO can occur effectively on bi-functional Pt catalysts even without externally added hydrogen and milder reaction conditions (P_{N2} = 1.4 MPa, T = 160 ^{o}C) compared with conventional HDO catalysts with external hydrogen addition (P_{H2} > 4 MPa, T > 200 ^{o}C), due to DH reaction that occurs simultaneously.[163]

Table 4. Performance comparison of Pt/C and Pt/C-P catalysts

Entry #	1	2	3	4	5
Catalysts	Pt/C-P		Pt/C		Pt/C
CR (mol/g-atom-Pt.h)	349.5		257.4		117.7
TOF(mol/mol/h)	384.9		1132.2		470.8
P (MPa)	N_2, 1.4		N_2, 1.4		H_2, 4.1
Reaction time (h)	0.5	4	0.5	4	6
Conversion (%)	26.0	73.0	21.6	64.7	64.8
Product Selectivity (%)					
LA	64.9	62.9	69.8	45.1	28.5
1,2-PDO	14.8	17.1	13.3	20.2	57.4
EG	0.05	0.7	0.1	1.1	2.2
MeOH	9.0	9.0	4.6	10.3	0.9
EtOH	5.9	5.9	4.7	7.1	2.64
2-PrOH	3.0	3.2	2.1	4.3	-

T: 160 ^{o}C, P_{N2}: 1.4 MPa, glycerol: 1.1 kmol/m^3, solvent: H_2O, NaOH/glycerol molar ratio: 1.1, Pt catalyst charge: 6.7 kg/m^3; MeOH: methanol, EtOH: ethanol, 2-PrOH: 2-propanol

Further, after 4 h of reaction time, the selectivity to glycols increased from 13% to 20% and that of alcohols from 10% to 22% on Pt/C catalyst (Entry#4). In comparison, product distribution during glycerol conversion on Pt/C-P was almost unchanged from 0.5 h to 4 h reaction time, where the ratio of HDO

(glycols and alcohols) to DH products (LA) changed by 1/2. The fact that glycol and alcohol selectivity increased significantly with conversion implies that HDO and C-C cleavage are dominant on Pt/C catalyst.

In order to understand the effect of surface properties of Pt NPs on the catalytic behavior of Pt NPs and establish structure-activity relations, the values of CR and TOF were further compared. The CRs on Pt/C and Pt/C-P catalysts are 257.4 and 349.5 mol/g atom Pt/h respectively. Obviously Pt/C-P catalyst displayed better efficiency than Pt/C because the particle sizes on former are lower. Surprisingly, further inspection of structural properties of Pt NPs in the two samples shows that the surface activity is completely different for the two Pt catalysts. Pt NPs with low crystallinity (Pt/C-P, d = 1.2 nm) displayed a TOF about 384.9 mol/mol/h, while Pt NPs with dominant [111] facet (Pt/C, d = 4 nm) exhibited a significantly higher TOF of 1132.2 mol/mol/h. Calculation of hydrogen utilization ratio (HE, see definition) values on both Pt NPs further confirms the unique performance of Pt/C catalyst. As shown in Table 3, Pt/C catalyst showed a 95.5% HE ratio at high conversion level (X = 65%), while the value on Pt/C-P was only 57.1%, a much lower value.

Additionally, the conversion and selectivity for HDO of glycerol in the presence of externally added hydrogen on Pt/C catalyst were also compared with DH/HDO process. As found in Entry#5 (Table 4) the selectivity of 1,2-PDO was higher than Entries#1~4. This is because conventional HDO usually demands excess hydrogen, the majority fraction of which is not used during

reactions and remains in gas phase. Although Pt NPs in Pt/C sample have larger particle size compared with Pt/C-P catalyst, the comparison of TOF indicates that highly crystalline Pt [111] NPs are unique catalytic sites that show high catalytic activity for DH and HDO reactions compared with Pt NPs with low crystallinity. Therefore, detailed kinetic modeling of DH/HDO of glycerol was carried out using Pt/C catalyst.

3.3 Effect of reaction parameters

3.3.1 Effect of temperature

Table 5. Glycerol conversion on Pt/C catalyst at 130 ^{o}C and 160 ^{o}C

#	Temperature (^{o}C)	Time (h)	X (%)	Selectivity (%)		
				LA	Glycols	Alcohols
1	130	2.5	20.1	63.6	27.9	-
2	130	4.5	30.0	64.0	24.3	6.2
3	130	8.0	45.6	62.8	26.7	5.7
4	160	0.5	21.6	69.8	9.1	11.2
5	160	1.0	30.2	62.0	16.5	19.9
6	160	2.0	44.9	54.1	22.4	17.7

P_{N2}: 1.4 MPa, glycerol: 1.1 kmol/m^3, solvent: H_2O, NaOH/glycerol molar ratio: 1.1, Pt/C catalyst charge: 6.7 kg/m^3

Table 5 shows results at even lower temperature (130 ^{o}C). It is found that glycerol conversion to LA and 1,2-PDO is also significant at even lower temperature compared to previous reports.[57,122] Particularly, the reactions results at 220 ^{o}C (Table 1), 160 ^{o}C and 130 ^{o}C (Tables 2 and 5) were compared. It was observed that initial selectivity to LA was almost identical at 130 ^{o}C and 160 ^{o}C (compare Entries#1 and #4 in Table 5). As conversion increased

(Entries#3 and #6), selectivity to LA remained almost constant at 130 ^{o}C, while that at 160 ^{o}C declined. The selectivity to linear alcohols at 130 ^{o}C is < 6% at 45 % conversion (compared to 18% at the same conversion at 160 ^{o}C). Similarly, reaction results at 220 ^{o}C on Pt/C catalyst also showed > 14% selectivity to alcohols and carbon balance was low (C% < 70%). It is tempting to hypothesize that at 160 ^{o}C, the 1,2-PDO undergoes progressive reaction through C-C cleavage to form alcohols (MeOH and EtOH), while these alcohols tend to reform at even higher reaction temperature (T = 220 ^{o}C).

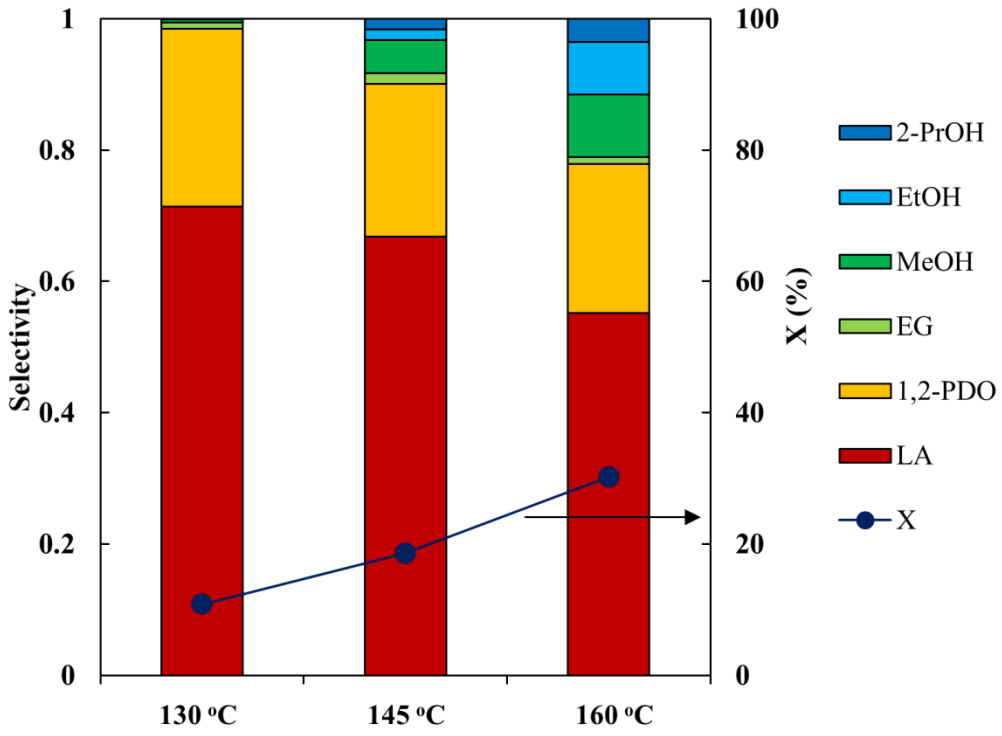

Figure 6. Effects of reaction temperatures on glycerol conversion and product distribution on Pt/C catalyst (reaction time: 1 h, other reaction conditions same as Table 5)

The effect of reaction temperature was further compared for identical reaction times in order to compare the activity and selectivity on Pt/C catalyst. As seen in Figure 6, conversion increased with temperature from 10% (130 ^{o}C) to 31% (160 ^{o}C) after 1 h reaction. LA selectivity decreased from 70% to 55%. The formation of glycols and alcohols was enhanced with increasing temperature. A total of MeOH, EtOH and 2-PrOH selectivity increased from almost < 2% to almost 20% at 160 ^{o}C, indicating high activity for HDO and C-C scission on Pt catalyst surface.

3.3.2 Effect of reaction atmosphere

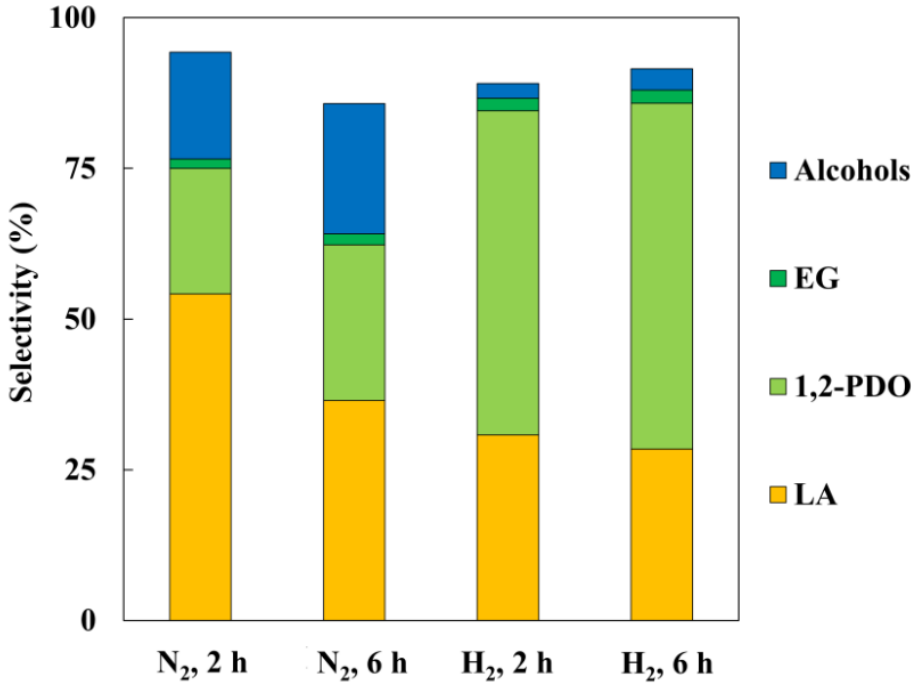

Figure 7. Product distribution over Pt/C catalyst at 160 ^{o}C under P_{N2}: 1.4 MPa and P_{H2}: 4.1 MPa. Conversion under P_{N2}: 44.9% in 2 h, 78.7% in 6 h; conversion under P_{H2}: 37.3% in 2 h and 64.8% in 6 h. Other conditions are same as in Table 4.

Comparison between nitrogen and hydrogen atmosphere was also investigated. At 160 ^{o}C, glycerol conversion (shown in the description of Figure 7) on Pt/C catalyst with externally added hydrogen (H_2, 2 h and H_2, 6 h in Figure 7) was lower than that observed when hydrogen was replaced with nitrogen at the same total pressure (N_2, 2 h and N_2, 6 h in Figure 7). Without external hydrogen addition (*i.e.*, with nitrogen only), the glycerol conversion increased from 45% in 2 h to 79% in 6 h. In contrast, the glycerol conversion was approximately 15% lower when external hydrogen was added, which is attributed to the fact that in the presence of excess hydrogen (comprised of externally added H_2 and H_2 formed *in situ*), GLA formation by DH step is likely to be hindered by equilibrium limitation.[122] It is to be noted from Figure 7 that after 2 h, LA selectivity was higher with *no* external H_2 addition compared to that with external hydrogen addition. In contrast, 1,2-PDO selectivity was higher under conditions with external H_2 addition. After 6 h, even without external hydrogen addition, 1,2-PDO selectivity increased significantly while the LA selectivity decreased from 54% in 2 h to 36% in 6 h. These trends indicate that under limited hydrogen availability (*i.e.*, with *in situ* generated H_2 alone), LA is favored while in the presence of excess hydrogen (*i.e.*, includes *in situ* hydrogen and externally added hydrogen), 1,2-PDO is more easily formed. Furthermore, the selectivity of linear alcohols was much higher without external hydrogen addition than with external hydrogen addition. The significant HDO activity without external hydrogen addition suggests that hydrogen formed *in situ via* DH is in a highly active form of adsorbed H_2 that

reacts rapidly on the catalyst surface. The experimental results confirm that the overall performance of low temperature conversion of glycerol is even better compared with conventional HDO processes.

Effect of nitrogen pressure was also investigated. Since no external hydrogen was added during the tests, nitrogen pressure was varied in order to understand the effect of inert atmosphere on conversion and selectivity. Glycerol conversion and product distribution were almost unchanged when nitrogen pressure changed from 0.3~3.5 MPa (see Table 6).

Table 6. Nitrogen pressure effects on glycerol conversion

#	1	2	3
P_{N2} (MPa)	0.3	1.4	3.5
Conversion (%)	47.1	44.9	46.9
LA	52.1	54.1	53.3
1,2-PDO	25.0	23.9	23.1
EG	1.1	1.6	2.1
MeOH	11.8	10.8	9.8
EtOH	7.5	8.0	9.2
2-PrOH	1.9	2.0	1.6

T: 160 ^{o}C, reaction time: 2 h, glycerol: 1.1 kmol/m^3, solvent: H_2O, NaOH/glycerol molar ratio: 1.1, Pt/C catalyst charge: 6.7 kg/m^3.

3.3.3 Effect of glycerol and NaOH concentration

Further studies were carried out to understand the effect of glycerol and NaOH concentration on the reaction rates. The influence of glycerol concentration on initial reaction rates is shown in Figure 8 (a). As glycerol concentration

increased from 0.25 to 3.3 kmol/m^3, the initial reaction rates on Pt/C catalyst increased from 53.9 to 451.2 mol/mol/h at 130 ^{o}C showing almost linear dependence, after which the rate became independent of glycerol concentration. Similar trend was also observed at 145 ^{o}C but the reaction rates displayed a slight decrease when concentration of glycerol was further increased. A similar plateau of reaction rates on Pt/C catalyst was found at 160 ^{o}C. It is seen in Figure 8 (a) that when glycerol concentration was higher than 1.63 kmol/m^3, reaction rate slowed down to almost independent of glycerol concentration. The effect of NaOH concentration was studied at 130 ^{o}C and 160 ^{o}C and similar trend of reaction rates was observed.

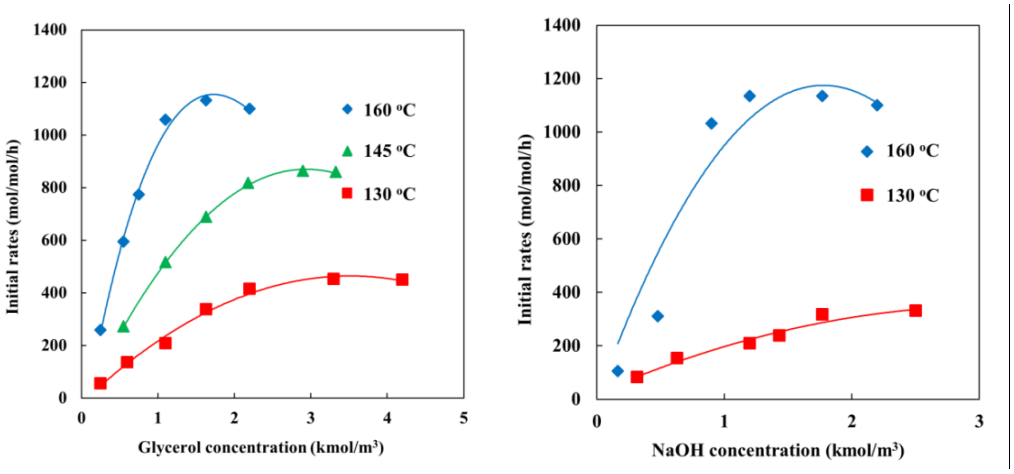

(a) (b)

Figure 8. Effects of (a) glycerol (NaOH: 1.22 kmol/m^3) and (b) NaOH concentration [glycerol: 1.1 kmol/m^3) on initial reaction rates (reaction conditions same as Table 4; initial rates were measured at the conversion level of 5~28%. Experiments in (a) were repeated for glycerol concentration > 2.2 kmol/m^3, the maximum error% < 15%; experiments in (b) were repeated for NaOH concentration > 1.4 kmol/m^3, the maximum error% < 18%)

Experiments with various initial alkali concentrations (Table 7) were also carried out. Results reveal that the initial rates were increased by several folds with increasing initial NaOH concentration and reached a plateau. The optimal alkali/glycerol ratio is approximately ~0.9. It is important to point out that, this ratio is significantly lower compared with literature reports (2.0~10.0 molar ratio).[57,78,125,137,141]

Table 7. Influence of NaOH concentrations on observed reaction rates on Pt/C catalyst

#	Alkali ratio[a]	Reaction/Formation rates[b] (mol/g atom Pt/h)			
		Glycerol	LA	Glycols	Alcohols
1	0.15	25.4	12.2	0.5	0.8
2	0.44	52.5	30.6	6.0	8.8
3	0.90	103.3	52.7	15.5	43.5
4	1.10	103.2	45.5	21.7	46.5

a. NaOH/glycerol molar ratio; Reaction time: 4 h, T: 160 ^{o}C, P_{N2}: 1.4 MPa, glycerol: 1.1 kmol/m^3, solvent: H_2O, Pt/C catalyst charge: 6.7 kg/m^3;
b. Global reaction rates of glycerol, or formation rates of specific products.

3.4 Reaction profiles and product distribution

Figure 9 shows the temporal concentration profiles of each reactant/product as a function of batch time during glycerol conversion at 130~160 ^{o}C on Pt/C catalyst under nitrogen pressure and *without* external hydrogen addition. Clearly, LA is the major product with its concentration increasing with time and remains constant after 4 h at 160 ^{o}C. The concentration of the alkali decreased continuously (due to its consumption in benzilic rearrangement to form its sodium salt). The concentrations of the other liquid products, 1,2-PDO and

linear alcohols, increased continuously even after 4 h, resulting in not only higher glycerol conversion (almost 80% in only 6 h) but remarkably high selectivity to liquid products (95%) in alkaline medium at 160 ^{o}C.[161]

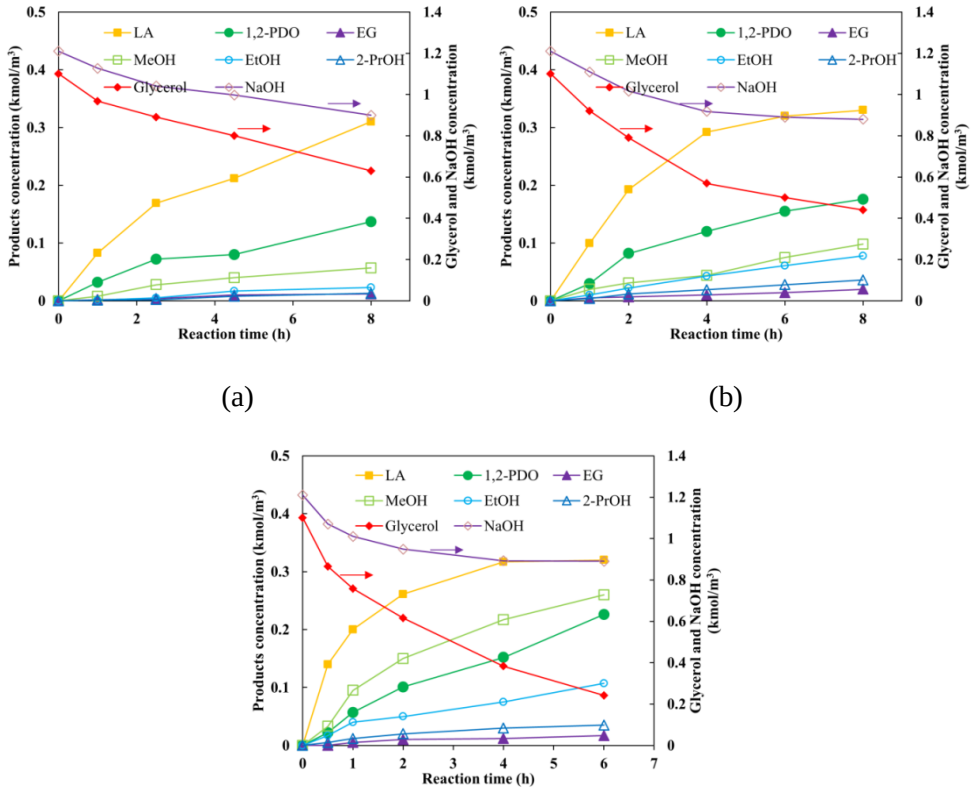

Figure 9. Concentration-time profiles of glycerol conversion on Pt/C catalyst at (a) 130 ^{o}C (experiments for 1.0 h and 4.5 h were repeated, error% = 1.9~14.2%), (b) 145 ^{o}C (experiments for 1.0 h and 4.0 h were repeated, error% = 2.1~14.9%), (c) 160 ^{o}C (experiments for 0.5 h and 4.0 h were repeated, error% = 2.2~12.1%) and selectivity to LA, 1,2-PDO and MeOH with conversion at 130~160 ^{o}C (other reaction conditions same as Table 2)

At 130 ^{o}C, glycerol concentration decreased from 1.1 to 0.6 kmol/m^3 in 8 h of reaction time. Concentration of LA and 1,2-PDO increased gradually with reaction time, while that of alcohols was at low levels. At 145 ^{o}C and 160 ^{o}C,

however, the overall concentration of alcohols increased rapidly. Specifically, the concentration of MeOH was enhanced by almost nine times when reaction temperature increased from 130 ^{o}C to 160 ^{o}C. The concentration of other alcohols, including EtOH and 2-PrOH, also increased at 160 ^{o}C, indicating that HDO of 1,2-PDO and EG to secondary products is facilitated at high temperature.[122]

3.5 Possible reaction pathways of glycerol conversion

Based on the conversion/selectivity data on Pt/C catalyst, a detailed reaction scheme for tandem DH/HDO of glycerol to LA and glycols at low temperatures is proposed. As depicted in Scheme 2, glycerol generates hydrogen *via* DH. Following DH, glycerol can form lactate in the alkaline medium *via* multiple sequential steps.[164] Thus, the LA selectivity at low temperatures is high (S = 64~69%, Table 5). The significant 1,2-PDO formation (S = 20~30%, Table 6 and Figure 7) without the addition of external hydrogen implies that the hydrogen formed (*via* DH) is very active resulting in facile glycerol HDO to form 1,2-PDO (rather than gaseous products) on Pt/C. The tandem DH/HDO pathways explain why the yields of liquid products including LA and 1,2-PDO are enhanced even at lower temperatures compared with previous reports.[22,122]

Further, MeOH is produced possibly from C-O* species adsorbed on Pt-surface and formed *via* C-C scission followed by *in situ* HDO.[165] With regard to EtOH formation, previous reports[56,57] proposed that HDO of EG is the main

source. It has been postulated that EtOH can form at elevated temperature (> 220 ^{o}C) by either C-O cleavage of *O-C-C-O* species or DHD and subsequent HDO of EG molecules.[165] However, this finding is not supported by control experiments with EG as the starting substrate (without external hydrogen addition) that showed no conversion at 130~160 ^{o}C. Therefore, it is likely that EtOH detected in our reaction system results from the direct C-O cleavage of the C_2 intermediate (shown in Scheme 2) from C-C scission before being hydrogenated to EG on the catalyst surface.

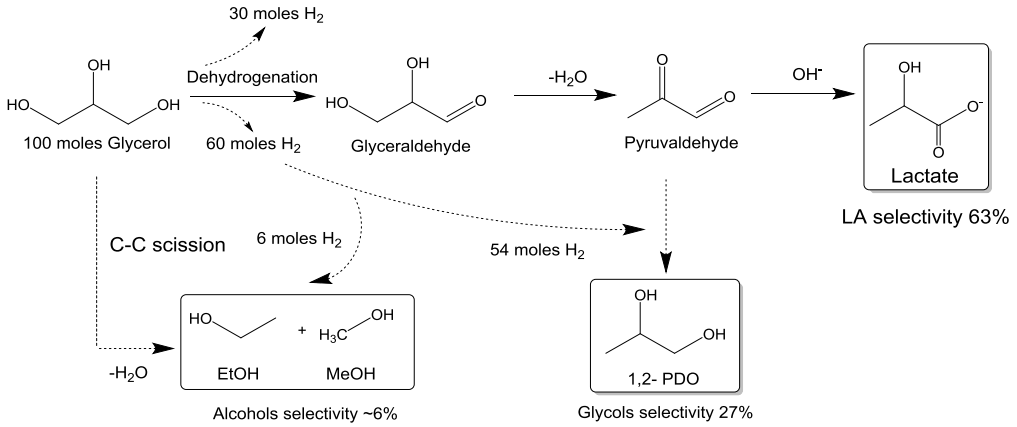

Scheme 2. Atom efficient aqueous phase conversion of glycerol to LA, 1,2-PDO and alcohols with hydrogen formed *in situ via* DH (no CO_2 formation)

A distinct and desirable characteristic for tandem DH/HDO of glycerol to LA and 1,2-PDO using hydrogen generated *in situ* on Pt/C catalyst is the atom economical nature of the conversion process towards valuable liquid products. As known previously, the conversion of polyhydroxy alcohols (like glycerol) to acids (*e.g.* LA) can be also realized *via* the oxidation of hydroxyl groups by externally added molecular oxygen.[140] The experimental results show that

similar products can form on Pt/C *via* DH of glycerol to GLA and benzilic rearrangement[164] in the presence of OH^- species to finally form the LA. Clearly, oxidation converts two hydrogen atoms in the substrate to one water molecule (not a useful product) and might also promote undesired side reactions.[141] In contrast, the glycerol DH pathway on Pt/C produces very active hydrogen that can be efficiently utilized for *in situ* HDO of the substrate itself. Entries#1~3 in Table 5 support this hypothesis quantitatively. The estimated carbon selectivity based on glycerol conversion to these liquid products is approximately 96%. Thus, there is almost no carbon loss (through WGS to form CO_2) to gaseous products and humic substances[141] during reactions.

Based on these observations, the proposed pathways in Scheme 2 may be justified as follows. Approximately 90 out of 100 moles of starting glycerol undergoes dehydrogenation to from GLA which upon dehydration (DHD) forms PAD. Thus, 90 moles of hydrogen are formed *in situ* on the Pt/C catalyst. Based on our experimental results, 63 moles of the intermediates react with OH^- to form LA (based on 63% selectivity to LA) while the remaining 27 moles are hydrogenated to glycols (based on 27% selectivity to 1,2-PDO and EG) utilizing 54 out of the 90 moles of hydrogen formed *in situ*. Approximately, 6~18 moles of hydrogen react with intermediates forming C-C scission of glycerol to produce the C_1 and C_2 alcohols (based on the combined 6% selectivity towards C_1 and C_2 alcohols). Clearly, the product selectivity in our proposed tandem aqueous phase conversion process provides higher carbon

utilization in the substrate towards liquid products compared to conventional oxidation and HDO processes.

4. Tandem DH/HDO of sugar polyols at low temperature

4.1 Catalyst activity and reaction profiles

The activity and selectivity of Pt/C catalyst were also investigated for conversion of C_5 and C_6 polyols (sorbitol, xylitol and mannitol) at 160 ^oC and 1.5 MPa nitrogen and the results are presented in Table 9. **To the best of our knowledge, this is the first report on the low temperature conversion of C_5 and C_6 polyols to LA, glycols and linear alcohols without external hydrogen addition.**

Table 8. Reactivity of different polyols on Pt/C catalyst

#	Substrate[a]	CR[b]	Formation rate (mol/g atom Pt/h)			
			LA[c]	Glycols[d]	Alcohols[e]	Other acids[f]
1	Glycerol	257.4	180.2	23.4	60.7	-
2	Xylitol	258.9	295.1	54.6	208.4	104.1
3	Sorbitol	308.9	321.3	34.0	157.5	201.1
4	Mannitol	360.4	497.4	58.4	206.5	246.5

a. T: 160 ^oC, P_{N2}: 1.4 MPa, substrate: 1.1 kmol/m^3, solvent: H_2O, NaOH/substrate molar ratio:1.1, Pt/C catalyst charge: 6.7 kg/m^3, Note: CR values were calculated based on polyol conversion of ~20%;
b. Reaction rate of substrates, mol/g atom Pt/h;
c. Formation rate of LA, mol/g atom Pt/h;
d. Formation rate of 1,2-PDO and EG, mol/g atom Pt/h;
e. Formation rate of MeOH, EtOH and propanols, mol/g atom Pt/h;
f. Formation rate of formic acid, acetic acid and glycolic acid, mol/g atom Pt/h.

Interestingly, like glycerol, the higher polyols can also be quantitatively converted to LA and useful hydrodeoxygenated products with hydrogen produced *in situ*. As shown in Table 8, the CRs over Pt/C catalyst are 257.4, 258.9, 308.9 and 360.4 (mol/g atom Pt/h) for glycerol, xylitol, sorbitol and mannitol substrates, respectively, increasing with the carbon number of the polyols. This trend indicates that sugar-derived polyols are converted to LA more efficiently compared to glycerol. Interestingly, the formation of linear alcohols (MeOH, EtOH and propanols) on Pt/C catalyst is significantly higher from C_5 and C_6 polyols than with glycerol.

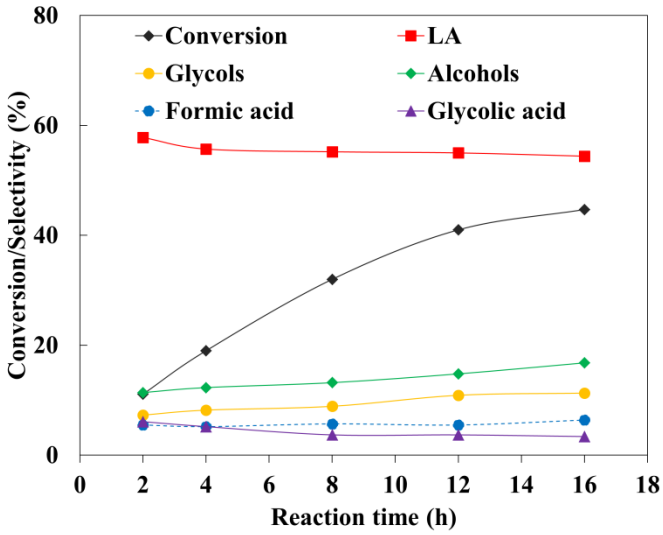

Figure 10. Reaction profiles for aqueous phase xylitol conversion on Pt/C catalyst (T: 115 ^{o}C, P_{N2}: 1.4 MPa, xylitol: 100 kg/m^3, solvent: H_2O, NaOH: 1.2 kmol/m^3, Pt/C catalyst charge: 6.7 kg/m^3)

High conversions of xylitol and sorbitol to LA and alcoholic chemicals can be achieved even at as low temperature as 115 ^{o}C. The reaction profiles for xylitol and sorbitol conversion in the presence of Pt/C and NaOH are presented in

Figures 10 and 11, respectively. It is found that xylitol conversion increased almost linearly with reaction time and the LA selectivity decreased slightly (from 60% to 55%, Figure 10) while the combined selectivity towards glycols and alcohols was found to increase (from 15% to 22%) with conversion. Similar product distribution was also observed during sorbitol conversion (Figure 11). The combined selectivity to formic and glycolic acid is about 13% in both cases. These results demonstrate that tandem DH/HDO of sugar polyols can occur under significantly milder reaction conditions (P_{N2} = 1.4 MPa, T = 115 ^{o}C) with much higher yields to liquid products compared with catalytic HDO processes (P_{H2} = 2~8 MPa, T > 180~220 ^{o}C).[88-90,100]

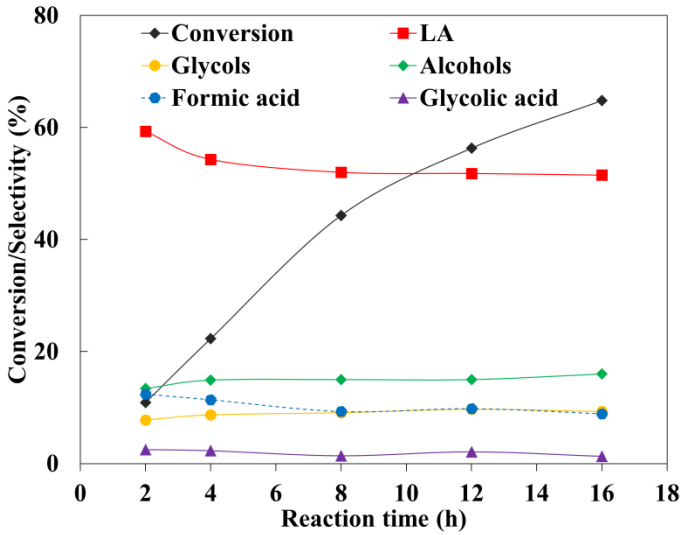

Figure 11. Reaction profiles of aqueous phase sorbitol conversion on Pt/C catalyst (T: 115 ^{o}C, P_{N2}: 1.4 MPa, sorbitol: 100 kg/m^3, solvent: H_2O, NaOH: 1.2 kmol/m^3, Pt/C catalyst charge: 6.7 kg/m^3)

Similar to glycerol, the selectivity towards glycols is not high for xylitol and sorbitol. However, the selectivities to linear alcohols (MeOH, EtOH and 2-

PrOH) and acids (glycolic acid and formic acid) in xylitol and sorbitol conversion are markedly different. As shown in Table 8, formic acid and glycolic acid are observed in significant amounts during xylitol and sorbitol conversion. Further, while the selectivity towards C_3 products (LA, 1,2-PDO and propanol) from xylitol are close to the theoretical value (60%), the selectivity towards C_2 products (EG, EtOH and glycolic acid) is much lower (< 15%) than the theoretical value (40%). This suggests facile C_1-C_1-C_3 retro-aldol cleavage is favored on Pt/C catalyst.

4.2 Role of alkali in activity and selectivity of Pt/C catalyst

Since it is known that alkali promotes C-C cleavage of aldehydes and ketones *via* retro-aldol condensation,[105] a direct comparison of the promotional effects of different liquid bases was performed to further understand the role of alkali in polyols conversion. The promotional effect of various cations including Na^+, K^+, Ba^{2+} and Ca^{2+} for sorbitol conversion is presented in Table 9 in terms of CR and selectivity for Pt/C catalyst at 115 ^oC. The Pt/C+NaOH system (Entry#1) displayed a CR of 17.7 mol/g atom Pt/h and approximately 95% selectivity to liquid products. The Pt/C+KOH system (Entry#2) showed a higher CR than Pt/C+NaOH but a slightly lower formation of liquid products. Compared with K^+ and Na^+, a lower CR of 10.7 mol/g atom Pt/h was observed with Ca^{2+} promoter (Entry#3) although selectivity towards LA is much higher. The lower CR with Ca^{2+} could be attributed to lower solubility of $Ca(OH)_2$ under reaction

conditions (only 0.165 g/100 g water at 25 ^{o}C and 0.077 g/100 g water at 100 ^{o}C).[166]

Table 9. Activity of Pt/C catalyst for aqueous phase sorbitol conversion

#	Alkali[a]	CR[b]	Selectivity (%)			
			LA	Glycols[c]	Alcohols[d]	Acids[e]
1	NaOH	17.7	54.5	8.6	15.0	17.2
2	KOH	42.8	35.1	5.8	5.0	2.3
3	$Ca(OH)_2$	10.7	78.1	1.2	0.9	4.3
4	$Ba(OH)_2$	214.2	57.0	11.7	9.7	14.7

a. T: 115 ^{o}C, P_{N2}: 1.4 MPa, sorbitol: 100 kg/m^3, solvent: H_2O, OH^-/sorbitol molar ratio: 2.2, Pt/C catalyst charge: 6.7 kg/m^3, conversion: ~20%, Note: CR values were calculated based on polyol conversion of ~20%.;
b. Reaction rate of sorbitol, mol/g atom Pt/h;
c. Selectivity of 1,2-PDO and EG;
e. Selectivity of MeOH, EtOH and propanols;
f. Selectivity of formic acid, acetic acid and glycolic acid.

In the presence of $Ba(OH)_2$ (Entry#4), a 12-fold higher activity is observed although the selectivity towards LA and glycols is similar to NaOH promoter. Zhao and coworkers[88] also found distinct differences in the performances of different alkali promoters during sorbitol HDO with external hydrogen addition. At similar OH^- concentration, a metal catalyst (supported Ru on carbon nanofiber) showed higher sorbitol conversion but lower selectivity towards glycols (1,2-PDO and EG) with Na^+ compared to Ca^{2+} promoter. King and co-workers[80] proposed that cations (*e.g.* K^+) might influence the electron density of Pt and thus alter its catalytic activity and reaction pathways. Yan and coworkers[144] observed that Ca^{2+} as a bication works more efficiently than Na^+

at the same concentration as it affects the position where C-C cleavage (preferentially C_3-C_3 cleavage) occurs. However, this conclusion is not consistent with our observation. Unlike $Ca(OH)_2$ that has limited solubility in the aqueous phase, $Ba(OH)_2$ is completely soluble in the aqueous phase under our reaction conditions and provides higher overall yield of LA, glycols and other liquid products than $Ca(OH)_2$. The lower activity of Ca^{2+} may be due to limited solubility of $Ca(OH)_2$.

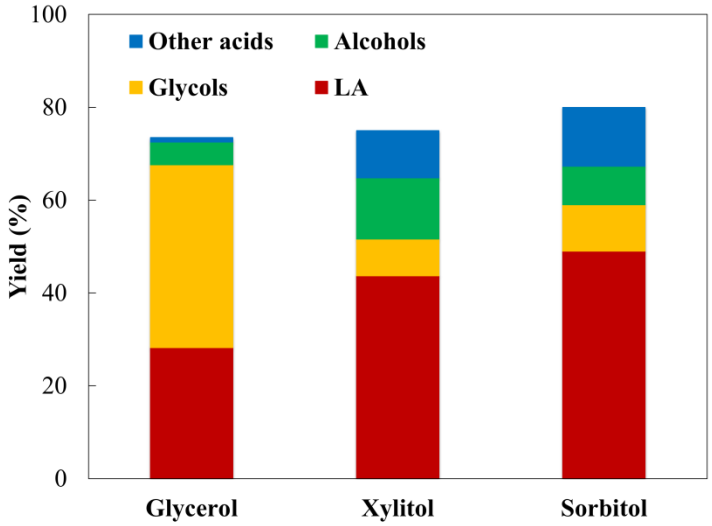

Figure 12. Conversion of various polyols on Pt/C in the presence of $Ba(OH)_2$ (P_{N2}: 1.4 MPa, substrates: 100 kg/m^3, solvent: H_2O, OH^-: 1.2 kmol/m^3, Pt/C catalyst charge: 6.7 kg/m^3. For glycerol, T: 160 ^oC, reaction time: 1.5 h; for sorbitol, T: 115 ^oC, reaction time: 1.5 h)

The presence of Ba^{2+} was found to not only facilitate pyruvate formation *via* cationic effect and OH^- attack at electron deficient parts[167] in the carbon chain but also convert the pyruvate and LA to formic acid, acetic acid and CO_2 at higher temperatures ($T \geq 250$ ^oC).[168] However, the byproducts (aliphatic acids

and CO_2) are not significant under our mild reaction conditions (115~160 ^oC). This result also reveals that $Ba(OH)_2$ facilitates GLA DHD (to form pyruvate) at higher rates than alkali-metal hydroxides possibly due to the extra positive charge of the bications.[137,144] Additional tests conducted for glycerol and xylitol conversion (see Figure 12) also confirm that $Ba(OH)_2$ is an effective promoter for conversion of various polyols to LA and co-products. After only 1.5 h, the overall yield of LA, glycols, alcohols and other products from xylitol and sorbitol was observed to be approximately 80% at 115 ^oC in the presence of Pt/C+$Ba(OH)_2$.

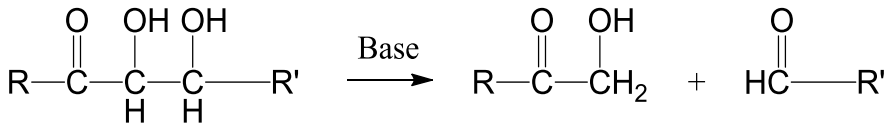

Scheme 3. Retro-aldol reaction of dehydrogenated polyols in alkaline medium

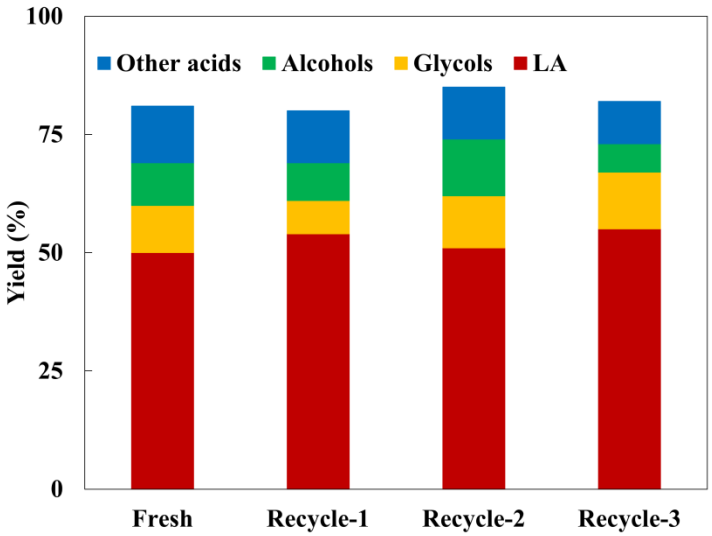

Figure 13. Recycle of Pt/C+$Ba(OH)_2$ catalyst for aqueous phase conversion of sorbitol (T: 115 ^oC, P_{N2}: 1.4 MPa, sorbitol: 100 kg/m^3, solvent: H_2O, OH^-: 1.2 kmol/m^3, reaction time: 1.5 h, Pt/C catalyst charge: 6.7 kg/m^3).

Similar to the observations with NaOH promoter, the polyols with higher carbon number display higher activity than lower polyols in the presence of $Ba(OH)_2$ as well (see results in Figure 12). With regard to the nature of C-C cleavage of polyols, Aguilera and coworkers[169] observed that the rate of (retro-) aldol condensation increased with higher electron density in the R and R' groups (Scheme 3) because they more easily form carbonium ions with base promoters. Our results are consistent with this explanation since xylitol and sorbitol have more -OH groups (compared to glycerol) that share electrons with a carbonium ion structure.

Table 10. Pt leaching measurement from inductively coupled plasma analysis

Substrate	T	Pt leaching ratio
Glycerol+NaOH[a]	160	n.d.[e]
Glycerol+NaOH[b]	160	n.d.[e]
Glycerol+$Ba(OH)_2$[c]	160	n.d.[e]
Sorbitol+$Ba(OH)_2$[d]	115	n.d.[e]

a. catalyst and liquid samples from Figure 7 (N_2, 6 h)
b. catalyst and liquid samples from Figure 7 (H_2, 6 h)
c. catalyst and liquid samples from Figure 12 (Glycerol)
d. catalyst and liquid samples from Figure 13 (after Recycle-3)
e. not detected

As shown in Figure 13, recycle studies of Pt/C catalyst for sorbitol conversion in the presence of $Ba(OH)_2$ showed excellent recyclability for conversion of sorbitol to LA, glycols, linear alcohols and other renewable acids. Further, elemental analysis for Pt *via* ICP revealed that there was negligible Pt leaching during our experiments (Table 10). This confirms that Pt/C is an active,

selective and stable catalyst for conversion of polyols to value added products at significantly lower temperatures (115~160 ^{o}C). These observations also confirm that the conversion of polyols to LA and other co-products is strongly dependent on the types of promoter cation and their concentrations in the aqueous phase.

4.3 Possible reaction pathways

The first step in the transformation of sorbitol and xylitol to various liquid phase products involves sorbitol DH over supported metal catalysts to produce hex-aldose (Scheme 4). Given that acids often result from the reaction between aldehydes/ketones and OH^- species, it seems plausible that the intermediate hex-aldose species undergoes retro-aldol reaction to form aldehydes and ketones of small molecules (formaldehyde, glycolic aldehyde and dihydroxyacetone/GLA) that react rapidly to form acids in alkaline medium. Due to these complex parallel reactions, the LA selectivity in sorbitol conversion is lower compared to glycerol as a substrate.

Table 11. Conversion of various C_3 intermediates under milder conditions

#	Substrate[a]	Promoter	X[b] (%)	Selectivity (%)				
				LA	Glucose	Fructose	$C_{1\sim2}$-acid	Unknown
1	GLA	NaOH	77.5	76.5	7.1	10.1	3.4	2.9
2	PAD	NaOH	100	99.6	-	-	-	0.4
3	GLA	$NaNO_3$	-	-	-	-	-	-

a. Substrates: 1.1 kmol/m^3, NaOH/substrate: 2.2 molar ratio, solvent: H_2O;
b. Conversion at T: 65 ^{o}C, P: 0.1 MPa, time: 30 min

Previous results have shown that the hex-aldose species undergoes reorganization to form hex-2-ketose, which further dehydrates in the presence of lewis acids (Sn^{2+} ion[170] and Cr^{3+} ion[158]). In contrast, alkaline earth metal ions (such as Ca^{2+} in Scheme 4) promote C_3-C_3 breakage (based on product distribution of Entry #3 in Table 9) with the product distribution depending on the cations. Consequently, two C_3 intermediates are likely to be formed. Furthermore, the formation of 1,2-PDO and EG indicates that C_3 intermediates can undergo consecutive HDO on Pt catalyst with the hydrogen generated *in situ*.

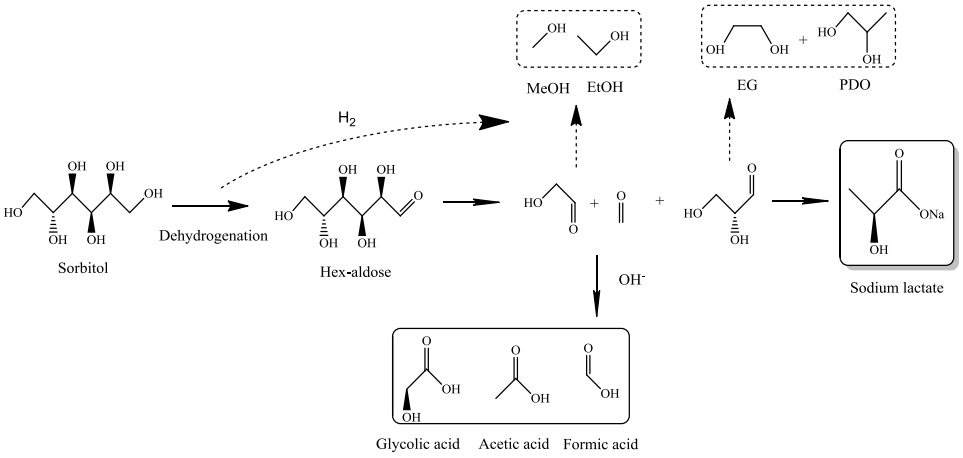

Scheme 4. Reaction pathway of sorbitol at low temperatures on Pt catalyst

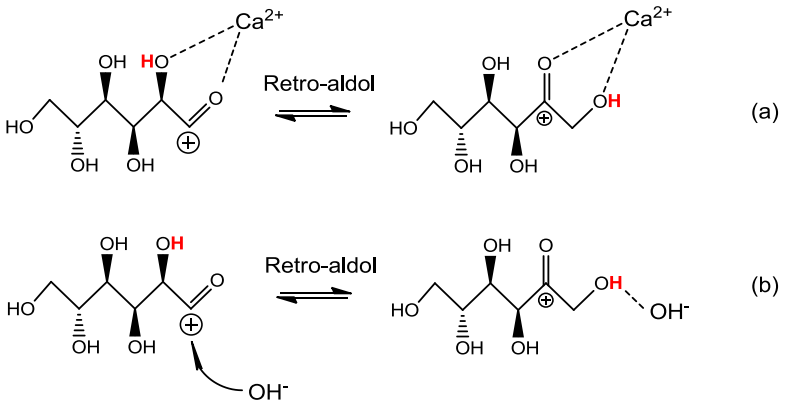

Scheme 5. Cation (a) and base-catalyzed (b) hydride transfer in sugar molecules[171,172]

As discussed in Scheme 3, C-C cleavage leads to the formation of GLA, which further converts to PAD in alkaline media. In order to understand the behavior of these intermediates as well as the mechanism involved in the formation of LA and other acids, additional experiments were carried out at milder conditions (T = 65 ^{o}C) in the absence of a catalyst. Entries#1 and #2 in Table 12 support our proposed mechanism that GLA and PAD are important intermediates[79] during LA formation. GLA undergoes DHD to form PAD, before forming LA *via* benzilic acid rearrangement.[78] Presumably, this step occurs instantaneously at 65 ^{o}C, since only PAD was detected in experiments in small amounts. At this temperature, aldolization of GLA also occurs because the formation of small amounts of hex-aldose and hex-2-ketose, while no reaction (Entry#3) is detected in the absence of OH^-. PAD was previously found in equilibrium with GLA at room temperature,[164] while it is observed here at 65 ^{o}C that PAD reacts easily and forms LA with a significant selectivity. The presence of Ba^{2+} enhances the conversion of polyols significantly possibly

via facilitating DHD of GLA to form PAD under our reaction conditions. However, no increase in the reaction rate of GLA was observed in the presence of $Ba(OH)_2$ (GLA conversion = 70.1% under the same reaction conditions as Table 12). It is possible that solubility of $Ba(OH)_2$ becomes a limiting factor at 65 ^oC.

5. Kinetics of DH/HDO of polyols on Pt/C catalyst

Development of reliable kinetic models for multiphase reactions is difficult as several parallel and consecutive reactions would occur simultaneously with such a catalytic system. The absence of external hydrogen but instantaneous HDO reactions on catalyst surface poses significant challenges to model the kinetics and validate experiments. In this section, key factors that influence DH and HDO reactions are studied on Pt/C catalysts using glycerol as the model compound. The information derived from this work will enable comprehensive understanding of the possible reaction mechanism on catalyst surface as well as optimizing catalyst design, and provide intrinsic kinetic data for multiphase reactor modeling.

5.1 Apparent activation energy

Before the actual reaction model was proposed, apparent activation energy for glycerol conversion was determined. Figure 14 (a) shows the glycerol concentration~time profiles for various temperatures. Glycerol conversion on Pt/C surface displays an apparent 1^{st} order reaction at lower conversion levels

(X < 30%) as indicated by the line plots in Figure 14 (b). The rate constants determined at 130 ^{o}C, 145 ^{o}C and 160 ^{o}C are 0.0858, 0.1754 and 0.394 h^{-1}, were plotted vs 1/T to determine the apparent activation energy. From the slope and intercept of the Arrhenius plot in Figure 15, apparent activation energy (E_a) and pre-exponential factor (k_o) were calculated: E_a = 80.4 kJ/mol, $k_o = 1.97\times10^{9}$ h^{-1}.

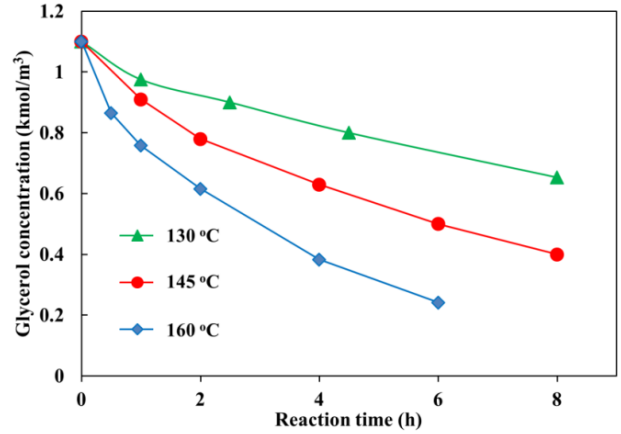

(a)

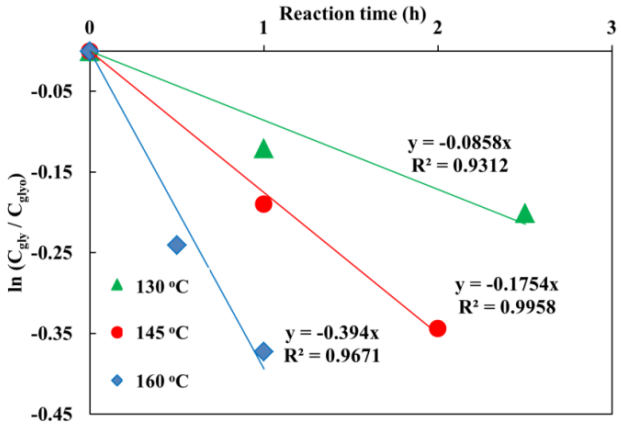

(b)

Figure 14. Effects of reaction temperature on concentration~time plots for glycerol conversion (see Table 2 for reaction conditions)

Interestingly, the apparent activation energy of 80.4 kJ/mol on Pt/C catalyst is much lower than reported for HDO reactions in previous experimental studies for glycerol conversion (158.6 kJ/mol),[173] indicating a possibility of a different reaction pathway in tandem conversion of glycerol. A detailed kinetic modeling is thus needed in order to understand the underlying reaction mechanism and pathways of DH/HDO of glycerol on Pt/C catalyst.

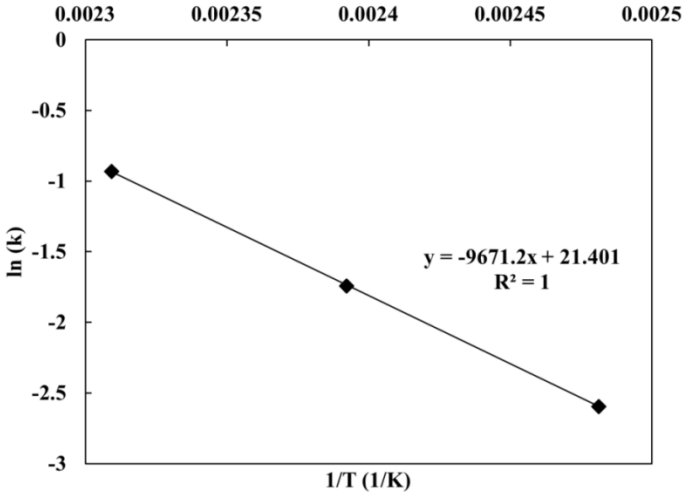

Figure 15. Apparent activation energy of glycerol conversion on Pt/C catalyst

5.2 Proposed reaction mechanism

For detailed kinetic modeling on DH/HDO of glycerol, six mechanisms in total were considered to fit the experimental data. Three models (Models *i*~*iii*) assume "dual-site" involving in the surface reactions, and the rest (Models *iv*~*vi*) take into account the "two different types of site" mechanism. Each model was derived based on our experimental observation as well as the prediction of previous DFT studies.[131,132,174,175] The basis of each reaction step for Model *i*

(shown in Scheme 6) will be described as an example and justified in details in the following section, after which the differences among all models are only briefly discussed. The rate equations of other five models are summarized in Appendix IV.

5.2.1 Description of Model *i*

Reaction r_1: The activation of C-H or O-H bonds. DH is described as step (A) in Scheme 6. DH reaction could lead to activation of C-H[132] and O-H bond[131,132] on Pt catalyst surface. DHD could also occur on metal catalyst surface but it will not provide *in situ* hydrogen,[174,175] thus will not be taken into account. In Model *i*, the role alkaline is believed to promote rather than participate in DH reaction of glycerol,[15,22,80,110] from the fact that the presence of metal catalysts[79,162] significantly decrease the required temperature at which DH of polyols would occur.

Liu and coworkers discussed possible reaction pathways of glycerol on Pt [111] surface.[132] It was found in gas phase simulation that DH was possibly initiated at α position *via* C-H activation (cleavage) and then O-H activation on the same carbon.[176] For mechanism Model *i*, as described in step (A) of Scheme 6, DH of glycerol is facilitated by hydride extraction (by Pt) and nuclear attack of carbon (by OH^-). This route is highly possible (confirmed later in the parameter estimation) since platinic hydride species are known to be formed favorably on noble metal surface. The extraction of the second hydrogen (-2H) will occur instantaneously as -2H species is more stable than its -H precursor.[176] (This is a

different chemical path compared with hydrothermal reactions,[78] in which OH^- is the reactant for DH not a promoter.) Once GLA (dehydrogenated species from glycerol) is formed on catalyst surface, DHD reaction occurs instantaneously in the presence of NaOH, after which benzilic rearrangement will convert PAD to lactate [steps (B, D) in Scheme 6].[78,79]

Reaction r_2: HDO of glycerol. HDO of glycerol to 1,2-PDO occurs on Pt surface, as described in steps (C, E) of Scheme 6. Based on our experimental observation in Figures 8 and 9, the addition of NaOH enhanced HDO rate, which suggests that OH^- species tend to be absorbed on Pt functional sites thus the reaction pathways are altered.[79,125,162] Therefore the OH^- adsorption is considered in our proposed reaction equations for reaction r_2.

Reaction r_3: HDO of 1,2-PDO to 2-PrOH. Previous studies on DHD of 1,2-PDO found that 1-PrOH rather than 2-PrOH was the dominant product, where bronsted acid was believed to activate H at β-carbon thus DHD occurred at β and γ-carbon positions.[175] It is not true in alkaline medium. DHD of 1,2-PDO to olefin aldehyde at α and β-carbons is favorable compared with β and γ positions, as shown in Scheme 8. Thus the formation of 2-PrOH is preferably formed in our case [steps (F, G)].

Reactions r_4, r_5 and r_6: C-C cleavage. For C-C cleavage of glycerol, the adjacent Pt site will extract the hydrogen (C-H activation at β-carbon) on adsorbed species in steps (A) of Scheme 6, R-*COH-*CHOH is therefore

formed on Pt surface.[132] Once *COH is formed, hydrogen adsorbed on neighboring Pt atoms will react with it and form MeOH. EG [$\boldsymbol{r_4}$, steps (H, I)] and EtOH [$\boldsymbol{r_5}$, steps (L, M, N)] molecules will form stoichiometrically in the presence of hydrogen formed *in situ*. For further decomposition of EG on Pt surface [$\boldsymbol{r_6}$, steps (J, K)], it is believed that it follows similar reaction path with glycerol decomposition: activation of C-H on α-carbon and subsequent activation of β-carbon, because the binding energy (BE) prediction indicates that HO-CH-CH-OH is relatively stable among all other -2H intermediates and the energy barrier of this process is relatively lower than other paths.[176]

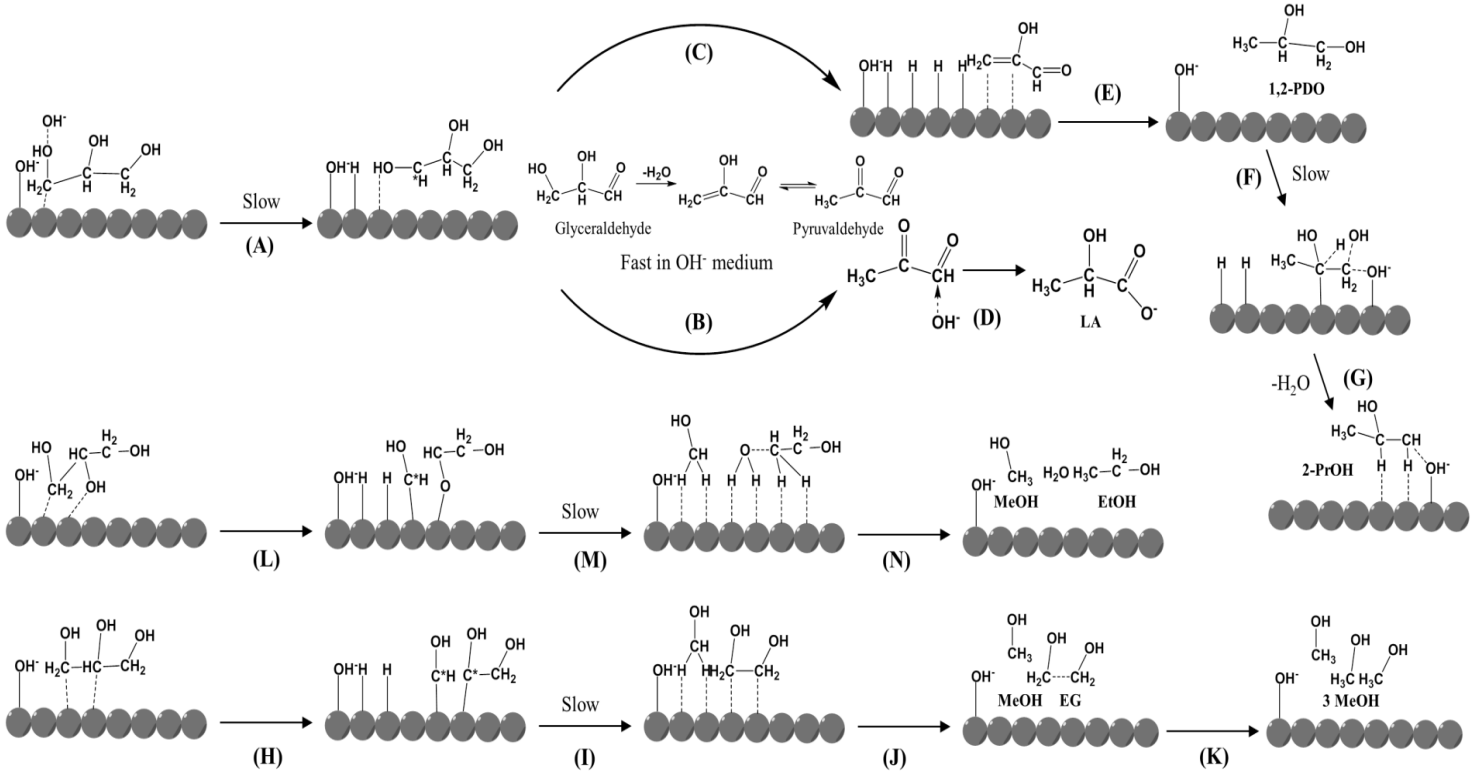

Scheme 6. Proposed reaction mechanism on Pt catalyst surface

5.2.2 Other models

Model *ii* also assumes that OH^- and glycerol are adsorbed on the same sites as Model *i*. Different from Model *i*, Model *ii* assumes that OH^- acts as a reactant for DH, HDO and C-C cleavage reactions rather than as a promoter. This model is proposed on the hypothesis and experimental findings in HDO of glycerol in the presence of external hydrogen and hydrothermal conversion of glycerol.[57,78]

It is hypothesized in Models *i* and *ii* that direct C-C cleavage of C_2 species occurs on EG, while in Model *iii* it is assumed that C_2 species undergo C-C cleavage (retro-aldol) before they are hydrogenated to EG. Thus EG is not a reactant but rather a final product in this system.

General chemistry between Models *i* and *iv*, Models *ii* and *v*, Models *iii* and *vi* are very similar to each other, but for Models *iv*~vi, it is assumed that alkalis are absorbed on the different types of Pt site, on the basis of the fact that the addition of alkalis often restrain the activity of methanation and WGS reactions for metal catalysts.

5.3 Lumped kinetic schemes and batch equations

Some surface reaction steps shown in Scheme 6 are rate limiting ones, while others like benzilic rearrangement occur instantaneously. Therefore, the reaction steps were lumped and proposed in Scheme 7. The reactions occurring on Pt/C catalysts include DH of glycerol to form LA [$\boldsymbol{r_1}$, lumping (A, B, D) of Scheme 6, the only reaction providing *in situ* hydrogen], HDO of glycerol to

1,2-PDO [r_2, lumping (A, C, E)], DHD-HDO of 1,2-PDO further to 2-PrOH [r_3, lumping (F, G)], C-C cleavage of glycerol *via* retro-aldol and subsequent hydrogenation to MeOH and EG [r_4, lumping (H, I)], C-C scission of EG and hydrogenation to MeOH [r_6, lumping (J, K)]and direct HDO of glycerol to MeOH and EtOH [r_5, lumping (L, M, N)]. Among these reactions, steps A, F, I, J and M are rate limiting steps.

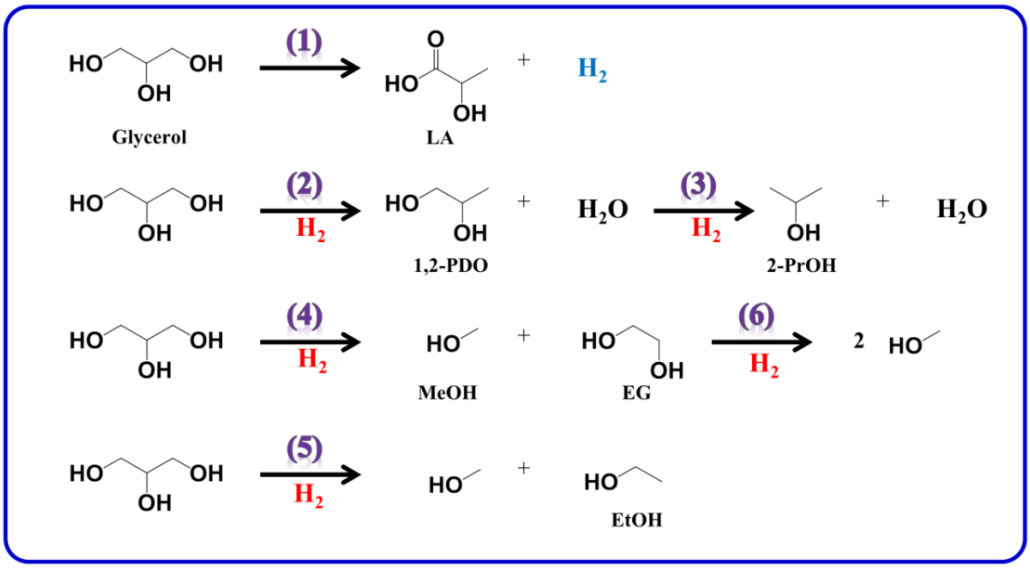

Scheme 7. Lumped kinetic models

Rate equations for each reaction (r_1 to r_6) of Model *i* are summarized in Table 12. Correspondingly, the experimental conditions for kinetic study are summarized in Table 13. For a typical experiment, for example, initial conditions were: glycerol concentration $C_{gly,\ i}$ = 1.1 kmol/m^3 and NaOH concentration, $C_{OH\text{-},\ i}$ = 1.2 kmol/m^3. The initial conditions for products are $C_{LA,\ i} = C_{1,2\text{-}PDO,\ i} = C_{2\text{-}PrOH,\ i} = C_{EG,\ i} = C_{EtOH,\ i} = C_{MeOH,\ i} = 0$.

Table 12. Rate equations for Model *i*

$$r_1 = \frac{k_{s1} \cdot K_{gly} \cdot C_{gly} \cdot C_{OH^-}}{\left(1 + K_{gly} \cdot C_{gly} + K_{EG} \cdot C_{EG} + K_{OH^-} \cdot C_{OH^-}\right)^2}$$

$$r_2 = \frac{k_{s2} \cdot K_{gly} \cdot C_{gly} \cdot C_{OH^-}}{\left(1 + K_{gly} \cdot C_{gly} + K_{EG} \cdot C_{EG} + K_{OH^-} \cdot C_{OH^-}\right)^2}$$

$$r_3 = \frac{k_{s3} \cdot K_{1,2-PDO} \cdot C_{1,2-PDO} \cdot C_{OH^-}}{\left(1 + K_{1,2-PDO} \cdot C_{1,2-PDO}\right)^2}$$

$$r_4 = \frac{k_{s4} \cdot K_{gly} \cdot C_{gly} \cdot C_{OH^-}}{\left(1 + K_{gly} \cdot C_{gly} + K_{EG} \cdot C_{EG} + K_{OH^-} \cdot C_{OH^-}\right)^2}$$

$$r_5 = \frac{k_{s5} \cdot K_{gly} \cdot C_{gly} \cdot C_{OH^-}}{\left(1 + K_{gly} \cdot C_{gly} + K_{EG} \cdot C_{EG} + K_{OH^-} \cdot C_{OH^-}\right)^2}$$

$$r_6 = \frac{k_{s1} \cdot K_{EG} \cdot C_{EG} \cdot C_{OH^-}}{\left(1 + K_{gly} \cdot C_{gly} + K_{EG} \cdot C_{EG} + K_{OH^-} \cdot C_{OH^-}\right)^2}$$

See Appendix III for notations

Table 13. Experimental conditions

Glycerol concentration (kmol/m^3)	0.2~4.2
Pt/C concentration (kmol/m^3)	3.3~9.9
NaOH concentration (kmol/m^3)	0.2~2.5
T (^{o}C)	130~160
P_{N2} (MPa)	1.4 MPa
Reaction time (h)	0.25~8.0
Solvent	H_2O

Further, the batch equations were summarized in Table 14. It is important to mention that all DH/HDO reactions of glycerol were carried out under isothermal conditions in batch slurry reactors, because the temperature of the reactor was maintained at ±1 ^{o}C during experiments.

Table 14. Batch reactor equations

$\frac{dC_{gly}}{dt} = -r_1 - r_2 - r_4 - r_5$	$\frac{dC_{MeOH}}{dt} = +r_4 + r_5 + 2 \times r_6$
$\frac{dC_{LA}}{dt} = +r_1$	$\frac{dC_{EG}}{dt} = +r_4 - r_6$
$\frac{dC_{1,2-PDO}}{dt} = +r_2 - r_3$	$\frac{dC_{EtOH}}{dt} = +r_5$
$\frac{dC_{2-\mathrm{Pr}OH}}{dt} = +r_3$	$\frac{dC_{OH^-}}{dt} = -r_1$

5.4 Parameter estimation and model discrimination

The experimental data and models were input to Athena Visual Studio (www.athenavisual.com). For parameter estimation, the convergence criteria are:

$$\left| \frac{S_j^{(k)} - S_j^{(k+1)}}{S_j^{(k)}} \right| \leq 10^{-3}$$

$$S_j = \sum_1^N (C_{j,E} - C_{j,P})^2$$

Where S_j is the sum of squares of (concentration) residuals of component *j* and (k) and (k+1) is the iteration number. $C_{j,E}$ and $C_{j,P}$ are the concentration observed during experiments (*E*) and predicted (*P*) by the programming, respectively. The following criteria will be used to evaluate proposed kinetic models:

- Least sum of squares of residuals

- Uncertainty (95% confidence limit) of reaction/adsorption constants should not increase/decrease significantly with changing reaction conditions (*e.g.* temperature, concentration)
- All reaction/adsorption constants should be positive
- Reaction rate constants should increase with temperature

Parameter estimation for Model *i* is summarized in Table 15. The reaction constants for each reaction at various temperatures, activation energy and adsorption enthalpy are calculated based on Arrhenius and van't Hoff equations.

Table 15. Rate constants and activation energy of surface reactions

Rate constants	130 °C	145 °C	160 °C	E_a
$k_{s1}\times10^{0}$	1.33±0.09	1.97±0.15	4.09±0.59	53.0±0.5
$k_{s2}\times10^{-1}$	6.09±0.51	10.8±0.50	22.8±3.04	63.7±1.9
$k_{s3}\times10^{-2}$	6.48±0.98	24.8±3.38	55.6±14.0	104.2±7.1
$k_{s4}\times10^{-2}$	5.95±0.53	12.9±1.48	39.3±4.23	104.2±5.2
$k_{s5}\times10^{-2}$	7.00±1.87	24.2±1.64	131.6±9.01	141.6±3.1
$k_{s6}\times10^{-1}$	1.12±0.48	2.85±0.39	9.32±2.02	102.3±2.8
Adsorption constants	130 °C	145 °C	160 °C	$-\Delta H$
$K_{gly}\times10^{-2}$	3.83±0.47	3.75±0.25	3.50±0.48	4.3±0.2
$K_{OH\text{-}}\times10^{-3}$	2.21±0.17	1.81±0.22	1.33±0.29	24.5±0.4
$K_{1,2\text{-}PDO}\times10^{-1}$	3.72±0.08	2.02±0.45	1.01±0.48	63.0±3.2
$K_{EG}\times10^{-3}$	4.00±0.37	2.50±0.48	1.13±0.12	60.9±0.9

Rate constants: h^{-1}; E_a and ΔH: kJ/mol

Table 16. Comparison of Models *i*~*vi*

#	Description of dual-site models	Sum of squares of residuals		
		130 °C	145 °C	160 °C
i	Alkalis act as the promoter for DH and HDO	0.010	0.029	0.058
	Best fitted with experimental data			
ii	Alkalis are the reactant in DH and HDO	0.091	0.028	0.177
	Negative reaction constants			
iii	Glycolic aldehyde undergoes C-C cleavage instead of C-C cleavage of EG on Pt [111] surface	0.059	0.287	0.564
	Error > 428% in MeOH prediction at 160 °C			
iv	Alkalis absorbed on different site; others same as *i*	0.009	0.029	0.058
	95% confidence level > 120% for some estimated values			
v	Alkalis absorbed on different site; others same as *ii*	0.010	0.013	-
	Rate constants decrease with increasing temperature Not converged at 160 °C			
vi	Glycolic aldehyde undergoes C-C cleavage instead of C-C cleavage of EG on Pt [111] surface; others same as *iii*	0.008	0.029	-
	Rate constants decrease with increasing temperature Not converged at 160 °C			

The estimated parameters of Models *ii*~*vi* are shown in Appendix IV. The fitting of Models *i*~*vi* are compared in Table 16. Particularly, the sum of squares of residuals is compared for the six models. The 95% confidence levels are also shown for each model (see Table 15 for Model *i* and Appendix IV for

Models *ii*~*vi*). Model *i* shows the best fit compared with other models. Parameter estimation for Model *ii* gives two negative values for adsorption constants (k_5, k_6), while Model *iii* exhibits good fit for the concentration of all other species expect MeOH.

It is necessary to point out that Model *iii* describes C-C cleavage of glycolic aldehyde (HO-CH_2-CHO) that occurs in the solution (retro-aldol) rather than on catalyst surface. The sum of squares of residuals however for Model *iii* increases significantly as temperature increases, indicating that this model does not well describe the behaviors of C-C cleavage on Pt/C catalyst. But Model *i* deals with a mechanism that EG reacts *via* direct C-C scission on Pt surface. In other words, it is likely a metal catalyzed process that generates two H_2C*-OH intermediates, which undergoes quick hydrogenation to form two MeOH molecules.

In addition, it is found that Model *iv* was also fitted very well for most parameters. The 95% confidence level for some of the reaction constants in Model *iv* is however above 120% of predicted values. Similar problems were also found with Models *v* and *vi*. These three models were not well fitted with experiment data overall thus not further discussed here. As mentioned above, these three models assume alkalis are absorbed on a different site to block side reactions. This observation implies that the reduction of methanation reaction on Pt/C catalyst in alkaline medium is not because of the block of certain

(different) active sites. The justification of this point will be discussed in the next section based on the calculated activation energy for each reaction.

5.5 Results and discussion

It is found in Table 15 that the E_a for r_1 (DH) is about 53.0 kJ/mol. Compared with the results in hydrothermal conversion of glycerol in alkaline medium (E_a = 128.2 kJ/mol),[78] activation barrier calculated here is significantly smaller. The difference indicates that the addition of Pt catalysts lowers the activation barrier for DH reaction of glycerol thus the reaction can occur at milder temperatures. It was previously demonstrated that OH^- species actively participate in the activation of glycerol molecules *via* oxidative insertion (DHD) and reorganization of 2-hydroxypropaenal to PAD.[78] But kinetic analysis shows that OH^- species are not reactant in this case. Therefore it is clear that DH on Pt catalysts is a metal catalyzed reaction with OH^- as the promoter, while hydrothermal is an alkali-catalyzed DH reaction at harsh conditions. Prediction on DH of glycerol suggests that it is almost thermodynamically neutral at 25 ^oC in aqueous phase,[147] while the formation of LA is highly exothermic but still found to be highly favorable even at 300 ^oC.[78]

HDO of DHD intermediates (refer to Scheme 6) to 1,2-PDO is found to overcome 63.7 kJ/mol of reaction barrier. This value is smaller compared with previous experimental findings in HDO of glycerol on Pt catalysts in the

presence of external hydrogen (158.6 kJ/mol),[173] implying that HDO in the presence of absorbed hydrogen demands lower activation barrier.

Further, it is known that the activation energy of 1,2-PDO to 2-PrOH and propane is usually lower than that of glycerol to 1,2-PDO, alcohols such as MeOH, EtOH and 2-PrOH are therefore easily hydrogenated to corresponding hydrocarbons (methane, ethane and propane).[177] This phenomenon was also predicted by DFT on the reaction behaviors of 2-PrOH on Pt [111] surface.[178] However, it is not found to be true in our reaction system. DHD followed by hydrogenation of 1,2-PDO to 2-PrOH (r_3, E_a = 104.2 kJ/mol) exhibit a higher reaction barrier compared with (r_2, E_a = 63.7 kJ/mol). This is probably the reason that the formation of gaseous hydrocarbons is significantly restrained in alkaline reaction medium.

As mentioned above, an alternative reaction mechanism is proposed for the tandem DH/HDO reactions, the hypothesis of which is supported by the calculated lower activation energy for reaction r_1 and r_2. The adsorption enthalpy calculated for glycerol and OH^- species is also consistent with the findings in this work. The adsorption of glycerol and OH^- is found here to be slightly exothermic on Pt surface, although the adsorption enthalpy is different for the two substrates. Gas-solid adsorption of glycerol on Pt surface is known to be a highly exothermic process. The change in the nature of glycerol adsorption on Pt surfaces indicates the alternative adsorption mode of biopolyols molecules on catalyst surface in the presence of alkali species. The

adsorption of alkali species was previously found to alter the electron configuration of solid surface[179] thus the reaction barriers of substrate molecules can be lowered compared with the case without alkali adsorption.[80]

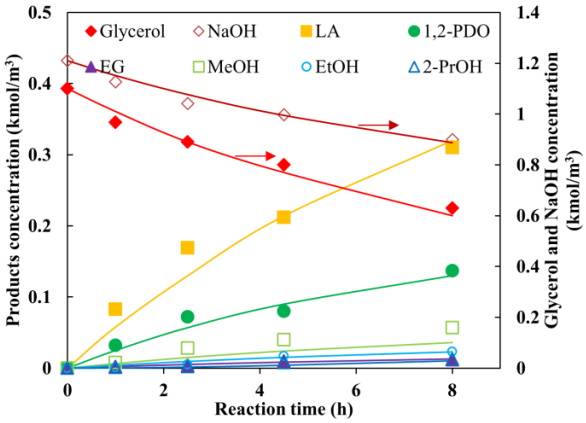

(a)

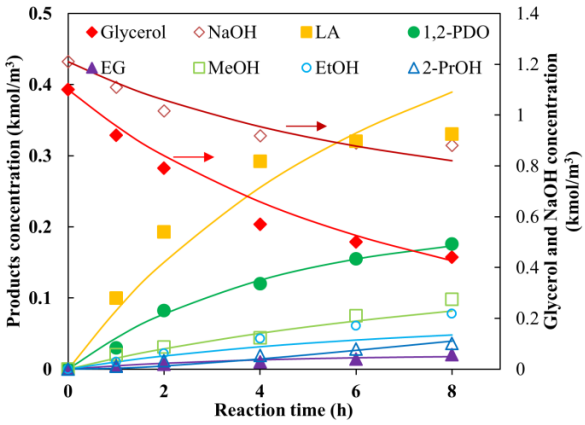

(b)

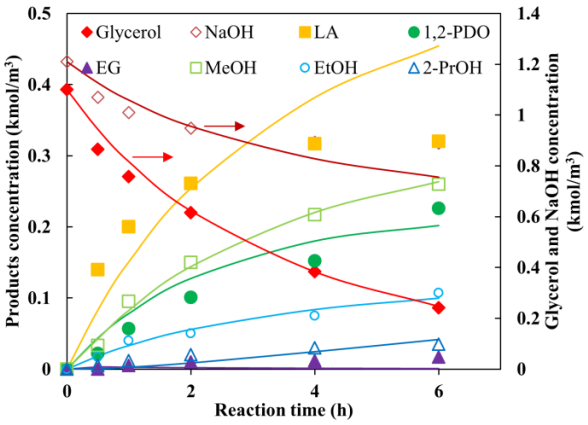

(c)

Figure 16. Experimental and fitted concentration-time profiles

Furthermore, as seen from fitted reaction data in Figure 16, the formation rates of MeOH, EG and EtOH are enhanced dramatically with increasing reaction temperature. This observation indicates that C-C cleavage is facilitated on Pt catalyst surface. The calculated E_a values (Table 15) for r_4, r_5 and r_6 precisely reflect the reaction behaviors. C-C cleavage of glycerol to MeOH and EG (E_a = 104.2 kJ/mol) or to MeOH and EtOH (E_a = 141.6 kJ/mol) displays high activation barriers on Pt/C surface. The formation of MeOH and EG is expected to undergo the activation of two adjacent carbons on two Pt sites (as seen in Scheme 6), which agrees well with DFT simulation on Pt surface.[176] It was demonstrated previously that the formation of EtOH follows C-O activation (cleavage) before C-C cleavage occurs, as an alternative route.[163] Simulation of glycerol decomposition implies that the two reaction routes are both highly possible, where activation barrier of both C-O and C-C activation are approximately 103.3 kJ/mol.[132]

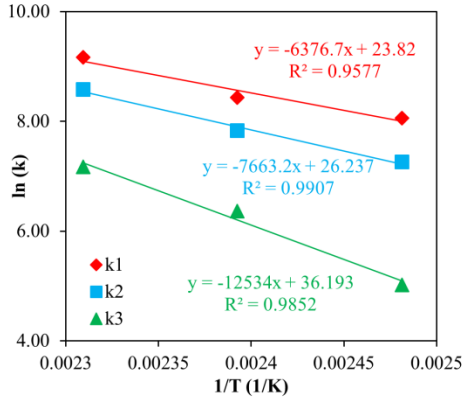

(a)

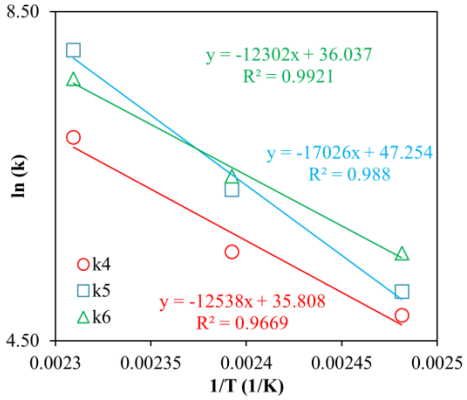

(b)

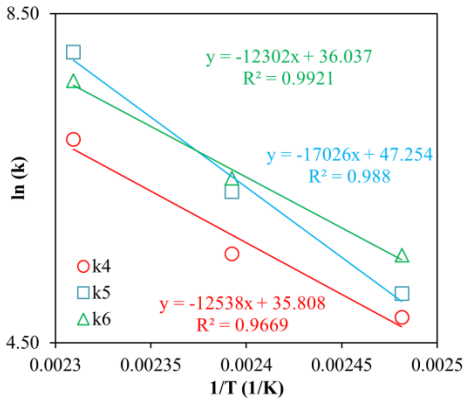

(c)

Figure 17. Arrhenius plots of rate and adsorption constants on Pt/C catalyst

Furthermore, the value of E_a for C-C cleavage of EG to MeOH is very high, 104.2 kJ/mol. This reaction is dominant as reaction temperature increases to 160 ^{o}C, as seen from concentration of MeOH in Figure 9. It implies that the decomposition of alcohols become dominant at relatively higher temperature. As it is observed in Tables 1 and 2 that if reaction temperature was further increased to 220 ^{o}C, significant amounts of CO_2 were formed thus the global carbon balance from HPLC analysis is poor (CO_2 adsorbed as carbonate in alkaline medium, which cannot be quantitatively analysis by HPLC).[163] MeOH could be the precursor for the formation of CO_2. These experimental facts indicate that DH is the major path for the decomposition of liquid substrates to CO_2, as it was known that DH of EG or MeOH on metal catalyst surfaces generate CO,[180] which was converted to CO_2 instantaneously under harsh reaction conditions. Interestingly, glycerol conversion in absence of alkalis leads to the formation of large quantities of methane rather than CO_2 on noble metal catalysts.[122] The difference in selectivity towards CO_2 and methane implies that the presence of OH^- enhances DH of polyol species to generate ketones or aldehydes, which undergo DHD and HDO at low temperatures (T < 160 ^{o}C) but may go through further DH to form CO and finally CO_2 at elevated reaction temperature (T > 200 ^{o}C). Complete DH of polyols finally forms CO_2 and significant amounts of hydrogen thus reforming is also enhanced in the presence of OH^-.[80] Therefore it is clear that low reaction temperature does not favor further decomposition or DH of alcoholic compounds (due to

significantly high activation barrier) thus the overall selectivity towards liquid products is much higher than harsh reaction conditions.

5.6 Effect of redox reactions on metal crystallinity

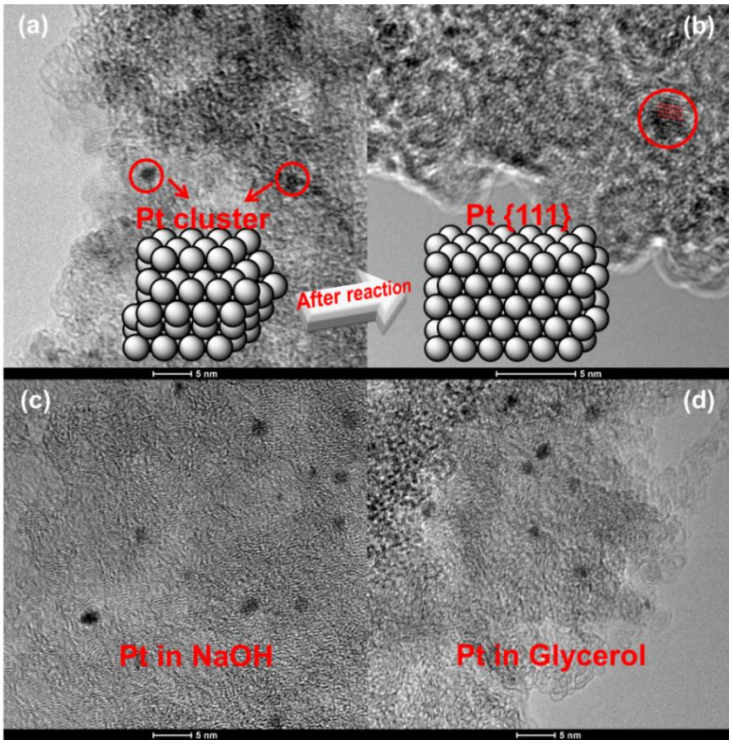

Figure 18. Evolution of Pt NPs in Pt(5w%)/C-P catalyst sample

Kinetic modeling of tandem DH/HDO of glycerol reveals the surface reaction mechanism on Pt surface. It is important to note that DH (oxidative) and HDO (reductive) are two reactions occurring simultaneously on catalyst surfaces, in other words, this process involves surface redox reactions. The impact fast surface redox reactions on the morphologies on Pt NPs was observed previously by other researchers, the underlying reason of which was however not well understood.[181] TEM characterization of fresh and used catalysts

provides insightful information of evolution of surface properties of Pt NPs during catalytic DH/HDO reactions.

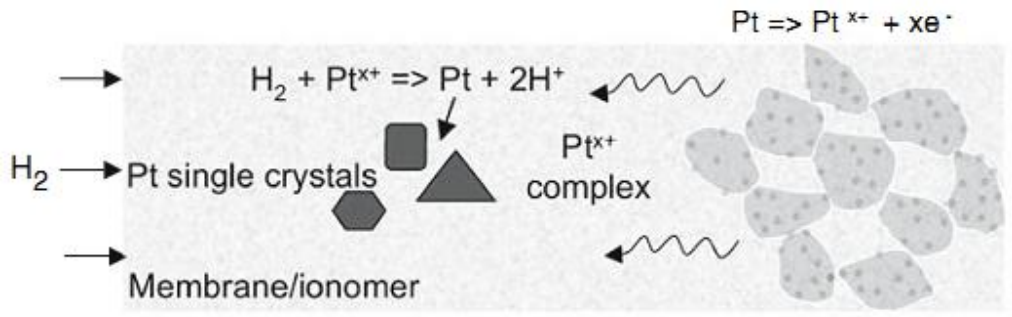

Figure 19. Evolution of Pt NPs during redox reactions

As shown in Figure 6, TEM data confirms that the fresh Pt NPs in Pt(5w%)/C-P sample are amorphous in structure and the clear lattice structure cannot be identified in this sample. A clear phase change on Pt(5w%)/C-P however occurred after reaction. It is found that the fraction of Pt [111] surface plane increases after 4 h of glycerol conversion at 160 ^{o}C, with detectable size growth of Pt nanoparticles still in the range of < 1.2 nm [see Figure 18 (a) and (b)]. This phenomenon indicates the amorphous Pt particles undergo reconstruction during the catalytic DH/HDO reactions of glycerol in the aqueous phase. In order to understand, whether NaOH, glycerol or surface reactions enable the phase evolution of Pt nanoparticles, two control experiments, one with only NaOH and another with only glycerol in aqueous solution were carried out under similar reaction conditions. As shown in Figure 18 (c) and (d), no detectable changes in morphologies are found on the two samples. The results

therefore mean surface reaction of glycerol and NaOH leads to the phase change of Pt particles.

With regard to the mechanisms of morphology changes, it is believed to be the outcome of competing effects of the minimizing surface tension of metal nanoparticles and hydraulic enforcement in the reaction medium.[182] For ideal face-centered-cubic (*fcc*) metals like Pt, the surface energy of atomic planes follow the order of [111] < [100] < [110], as calculated from surface atom density.[183,184] Therefore Pt [111] tends to be the favorable facet during the growth of NPs.[185] But this is not true in those most reactions catalyzed by Pt NPs, which were carried out in liquid phase, where the hydraulic effects induced by solvents and surface reactions usually enforce a phase change to spherical/amorphous shapes.[186,187] The dominant hydraulic enforcement thus often results in a shift of catalytic activity of Pt nanoparticles to a slightly lower level. In our case, a reverse process of formulating crystalline structures was instead found from amorphous Pt particles [observed on Pt(5w%)/C-P and commercial Pt(5w%)/C samples]. It indicates that an alternative reconstruction process was taking place on Pt particles during glycerol conversion. Conventionally, Ostwald ripening and crystal migration processes were found to apply the situation with significant changes in nanoparticles during surface reactions.[188] But those mechanisms can only explain the evolution in size due to the combined effects of surface free energy alteration and interaction with

carbon supports in reaction medium. As found in TEM figures (Figure 18), no obvious growth in particle size was observed after reactions.

Another piece of evidence that does not support the conventional mechanism is that no "necked" particles[182,189] were observed for any used Pt/C samples. And leached Pt is found absence in the reaction medium. An alternative mechanism of re-precipitation[190] (as shown in Figure 19, but still lack of sufficient experimental evidence[182]) is therefore proposed for redox reactions. Redox processes occurring on Pt surfaces favors a reconstruction of Pt particles towards increasing crystalline structures. It is similar to "re-growth" of Pt particles, or surface migration of Pt atoms on the surface of Pt particles in the reaction medium. As demonstrated by our experimental results, the proposed low temperature conversion of glycerol is a tandem DH/HDO catalytic process, which involved simultaneous reductive (HDO) and oxidative (DH) reactions on Pt particles. Therefore it is possible that the tandem catalysis enables an obvious phase change of Pt facets of Pt/C-P catalyst during surface reactions.

6. Conclusion

Aqueous phase conversion of polyols (glycerol, xylitol and sorbitol) is found to proceed remarkably well on Pt/C catalyst without external hydrogen addition at relatively low temperatures (115~160 ^{o}C). Our results show that tandem DH/HDO of biopolyols results in higher yields of LA and alcoholic co-products compared to conventional aqueous phase processes with external hydrogen

addition. High selectivity for LA formation with glycols and alcohols as useful co-products is achieved from polyols in the presence of Pt/C catalyst (and other noble metal catalysts). It is shown that Pt/C catalyst facilitates HDO with hydrogen formed *in situ* (*via* DH) to form useful liquid chemicals with high carbon utilization. The proposed low temperature conversion of various polyols in the absence of external redox agents displays significant potential as a sustainable alternative to conventional processes.

The developed kinetic model provides insights to two important questions:

(1) The mechanism of tandem DH/HDO conversion of glycerol. The presence of Pt catalysts alter the reaction paths of DH in alkaline medium thus facilitate the generation of hydrogen with large amounts of GLA being formed at much milder reaction temperatures compared with hydrothermal conditions. GLA undergoes quick DHD thus PAD is generated in alkaline medium. As a result, HDO of PAD can also occur even fast at significantly milder reaction conditions compared with HDO in the presence of externally added hydrogen. (2) The role of OH^- in polyols conversion. Adsorbed OH^- species activate Pt catalysts thus HDO and DHD reactions are facilitated compared with neutral conditions. But the activation barrier of further HDO of alcoholic products is much higher than the case without OH^- addition. Therefore the formation of less valuable gaseous alkanes such as methane, ethane and propane is restrained. This feature leads to high chemoselectivity of valuable liquid chemicals on Pt catalyst surfaces.

Chapter 5 Catalytic Conversion of Biopolyols on Nanostructured Catalysts

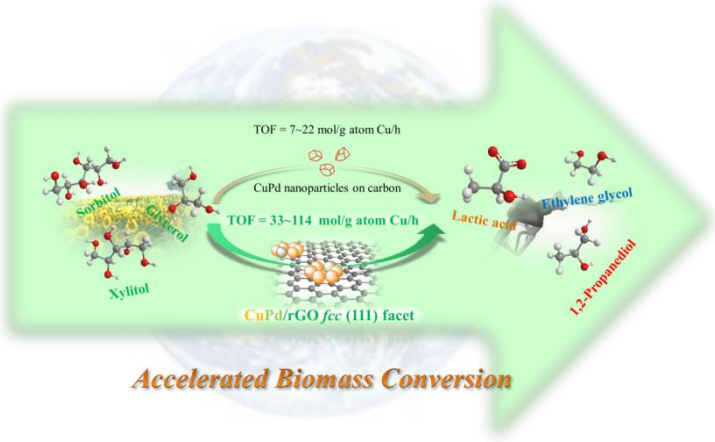

Cost effective Cu-based catalysts show high activity and selectivity for polyols conversion to lactic acid

1. Introduction

As discussed in previous chapters, dehydrogenation (DH) and hydrogenolysis (HDO) are the key reactions in the upgrading of biopolyols. Rational design of active and selective catalysts for these reactions is the key for the sustainable development of biomass conversion technologies. Conventional metal based catalysts have two major problems: (1) Noble metal catalysts show excellent catalytic activity (150~1200 mol/g atom/h) but significant side reactions at elevated reaction temperatures, such as excess C-C cleavage, methanation and water gas shift (WGS) reactions, thus the overall selectivity towards valuable liquid products is limited; (2) Inexpensive catalysts such as Cu, although selectively promoting DH and HDO reactions, exhibit poor overall activity

(0.1~6.8 mol/g atom/h).[39,43,47,70,73] For example, recently it was shown in our laboratory that Cu based catalysts offered good selectivity for DH reaction of glycerol to lactic acid (LA, S~80%) in alkaline medium. But low intrinsic activity (~2.2 mol/g atom/h), decreasing selectivity to liquid products at harsh reaction conditions (T > 220 ^{o}C) and low stability were the major drawbacks of the Cu catalysts.[79] In this chapter, designing nanostructured metal-based catalysts for polyols conversion to LA is reported. Particularly, the following aspects have been addressed: (a) key factors that govern the activity and selectivity of Cu-based nanocatalysts, (b) designing Cu based nanocatalysts with preferred active sites, (c) structure-performance correlation of Cu-based nanocatalysts and (d) possible reaction pathways on nanocatalysts. The proposed Cu nanocatalysts display a five-fold enhancement in catalytic activity compared to conventional catalysts.

2. Experimental Section

2.1 Catalyst preparation

Chemicals used in this work were similar to those described in Chapter 4. Unsupported Cu_2O, $CuCl_2$, Pd(*acac*)$_2$, acetonitrile and sodium borohydride ($NaBH_4$) were purchased from Sigma Aldrich and used as received without further purification. The preparation of nano-catalysts was carried out by researchers in Dr. Shenqiang Ren's group,[162,191] and the evaluation of the

catalytic performance for biopolyols conversion is part of this thesis. The basic methodology and preparation procedure are briefly summarized as follows.

2.1.1 Mono and bimetallic Cu catalysts

Several Cu based nano-catalysts were prepared on reduced graphene as a support. The crystal lattice engineering between the Cu and the graphene support [reduced graphene oxide: rGO, Figure 1(a)] was exploited to control the surface facet of mono and bimetallic Cu-based nanocatalysts. Since Cu [111] surface plane has the closest lattice parameter with the graphene support,[192] to minimize the lattice strain energy at the interface, the monometallic Cu or bimetallic CuPd nano-formulation tends to grow in the [111] direction onto the rGO support [Figure 1(b) and (c)]. The Cu catalysts with dominant [111] facet were prepared based on this methodology.

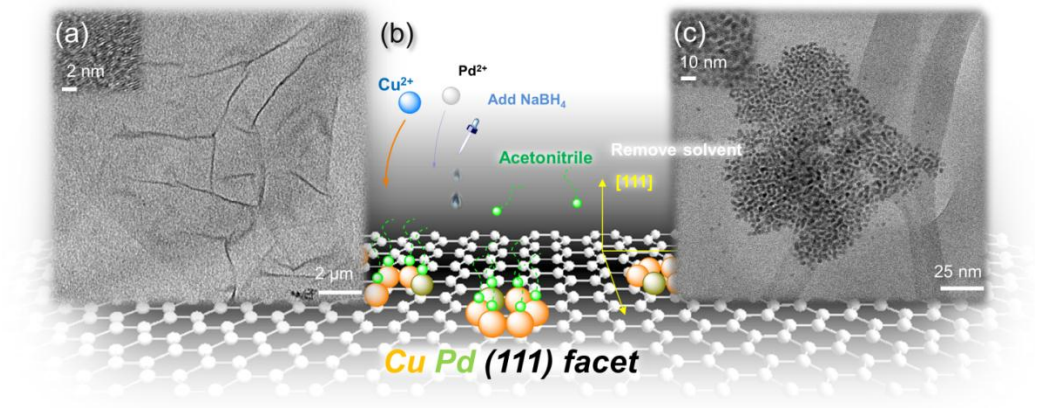

Figure 1. Preparation of Cu-based catalyst on rGO support

During preparation, GO was prepared in–house by a modified Hummers method starting from graphite powder (Bay Carbon, SP–1). For monometallic Cu/rGO and bimetallic CuPd/rGO samples, treatment of precursors-GO hybrids

with sodium borohydride ($NaBH_4$) resulted in precipitation of CuPd/rGO hybrids [Figure 1(c)]. Cu based graphene nanoparticles (NPs) were synthesized using $CuCl_2$ and $NaBH_4$ in the GO aqueous suspension and CH_3CN. Sodium borohydride ($NaBH_4$) solution was used as the reducing agent. The *in situ* reduction of Cu^{2+} and Pd^{2+} to Cu^0 and Pd^0 at room temperature is achieved with hydrogen slowly released from $NaBH_4$. Other bimetallic Cu catalysts, such as CuPt/rGO, CuRu/rGO, CuFe/rGO and CuNi/rGO, were prepared similarly using *in situ* reduction method.

Acetonitrile is used to control the growth of metal nanocrystals by sharing extra electron pairs in the nitrile functional group with metal nuclei and thereby passivate the nanocrystals from oxidation during the synthesis of Cu-based catalysts.[193] More importantly, the rGO support sheets are critical to protect NPs' oxidation during nanocatalyst testing.[194] Cu-based catalysts supported on conventional active carbon (AC), mesoporous carbon (MC) and single wall carbon nanotube (SWCNT) were also prepared.[35,72,127,195] The prepared nanocatalysts were sealed and stored at room temperature before catalytic activity tests.

2.1.2 Cu_2O catalysts protected by GO

Synthesis of GO protected Cu_2O were carried out in Dr. Shenqiang Ren's group by a different method.[191] Synthesis of cubic Cu_2O: cCu_2O or cCu_2O with GO, and rhombic Cu_2O: rCu_2O or rCu_2O with GO. By varying the ratios of DI water,

$NH_2OH \cdot HCl$, the nanocrystals were allowed to grow for 1 h, the cuprous oxide solutions were centrifuged before activity tests.

2.2 Catalytic activity tests

Catalytic tests were carried out in a high temperature, high pressure, magnetically stirred multiple batch slurry reactor setup described in Chapter 2. PTFE liners were used in each test in order to avoid the catalytic effect of reactor wall materials at elevated temperature (> 140 ^{o}C) in the presence of alkali. The experimental procedure is different from that described in other chapters.

For a typical test, about 3.0 g of polyols and 1.4 g of NaOH were dissolved in 15 mL of water in a graduated cylinder, under stirring at 200 rpm until homogeneous solution A was formed. The solvent (acetonitrile and water) in nanocatalyst slurry was first removed using rotatory evaporator at 55 ^{o}C (bath temperature) and 70~250 mmHg vacuum. Acetonitrile was evaporated quickly at the beginning when vacuum reached 250 mmHg. Then the vacuum level was slowly increased to remove water and avoid over boiling of solvent at 55 ^{o}C. When the vacuum level reached 70 mmHg, rotating was stopped and the vacuum was released to normal pressure. Approximately 20 mL of DI water was further added to the slurry, which was centrifuged at 1000 rpm for 2 min. Then the solvent were removed and fresh DI water was added. This procedure was repeated at least twice in order to remove the remaining organic solvent.

About 10 mL of slurry B was ready. Then catalyst slurry B was slowly added to solution A under vigorous stirring at about 600 rpm in order to minimizing temperature rise due to the heat generated from dissolution. The total volume of final solution was set at 25 mL, which was then transported to PTFE linear. Another 5 mL of DI water was added to rinse the cylinder and poured to the PTFE linear. Therefore 30 mL of reaction solution was further stirred in the PTFE liner for another 2 min, and then was ready for the activity test. A general procedure for this step is shown in Scheme 1. Other procedures are similar to the description in Chapter 4.

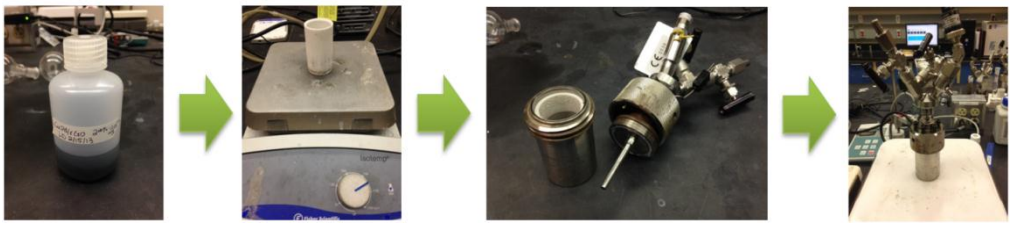

Scheme 1. Experimental procedures for mixing nanocatalysts with reaction mixtures

The weight of the catalysts for each batch test was approximately 0.2 g, which was predetermined during the preparation of GO and metal precursor slurry. For the first few experiments, the nanocatalyst samples were first dried and then the total weight (0.2 g) was confirmed by measurement before batch tests.

2.3 Analytic methods

After a batch reaction, the contents in the reactor were cooled to room temperature, the gas phase products analyzed using GC and liquid products by HPLC. The analytic procedures are identical to the description in Chapter 4.

2.4 Catalyst characterization

2.4.1Transmission electron microscopy (TEM)

Analytic procedures for TEM were already described in Chapter 2.

2.4.2 Ultraviolet–visible spectroscopy (UV-Vis)

Transmittance and absorbance spectra were measured with a Shimadzu UV-Vis-NIR dual-beam spectrophotometer. The measurement was carried out by Dr. Shenqiang Ren's group.[196]

2.4.3 Inductively coupled plasma (ICP)

For leaching tests, the procedure was presented as follows: about 2 mL of acidified reaction solution was measured and collected in a 20 mL vial. Acidified reaction solution from recycle tests were collected in the 20 mL vial. The resulting solution was diluted to 15 mL solution, which was ready for ICP analysis. The metal content in ICP report was further calculated to obtain the correct metal concentration in the reaction medium. The procedures are similar to the description in Chapter 2 and Appendix I.

3. Results and Discussion

3.1 Catalysts performances in glycerol conversion

The activity tests of the nanocatalysts were carried out for the conversion of glycerol, sorbitol and xylitol under inert atmosphere in order to evaluate their DH, and HDO activity using the *in situ* formed hydrogen. The major products

from these polyols are LA, 1,2-propanediol (1,2-PDO), ethylene glycol (EG) and some $C_{1\sim3}$ alcohols. In all catalyst samples in Figure 2, the Cu content was fixed at approximately 2 w%. With glycerol as substrate, it was found that rGO supported catalysts displayed superior performances compared with conventional AC, MC and SWCNT materials (Figure 2). The conversion of glycerol on Cu/rGO catalyst was almost 30% within 6 h of reaction, while Cu/MC, Cu/AC and Cu/SWCNT only exhibited 7~15% conversion. The selectivity to LA displayed similar trend, about 86% on Cu/rGO but only 40~70% on other Cu catalysts. Therefore it is clear that rGO supported Cu-based catalysts show superior performances in glycerol conversion.

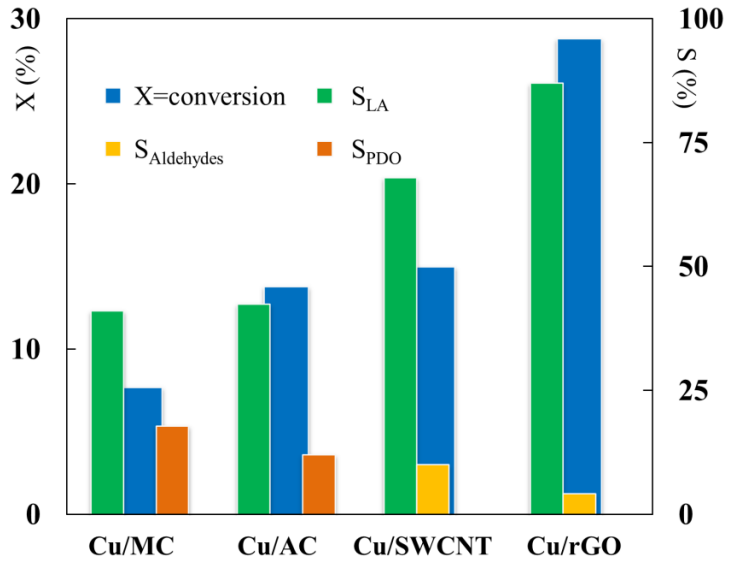

Figure 2. Comparison of Cu catalysts on MC, AC, SWCNT and rGO supports (glycerol: 100.0 kg/m^3; solvent: H_2O; Cu loading: 2 w%; catalyst charge: 6.7 kg/m^3; T: 200 ^oC; P_{N2}: 1.4 MPa; NaOH/glycerol molar ratio: 1.1; LA: lactic acid, PDO: 1,2-propanediol, Aldehydes: pyruvaldehyde and glyceraldehyde. For vertical y-axis, X: conversion, S: selectivity. Reaction time: 6 h)

Various Cu-based bimetallic catalysts, including supported CuNi, CuFe, CuCo, CuRu, CuRe, CuPt and CuPd catalysts on rGO were further prepared using the "same method as CuPd/rGO described in the “Experimental Section” and tested for glycerol conversion. The Cu loadings were all fixed at 2w% on rGO for all bimetallic catalyst samples. Among all bimetallic catalysts, the activity of CuNi(0.6w%), CuFe(0.6w%), CuRu(0.05w%) and CuRe(0.6w%) samples was even lower than monometallic Cu/rGO catalyst, while CuPt(0.05w%)/rGO and CuPd/rGO(0.05w%) displayed dramatic enhancement in glycerol conversion. The selectivity to glycols and alcohols on CuPt/rGO and CuPd/rGO samples was slightly higher than other bimetallic catalysts.

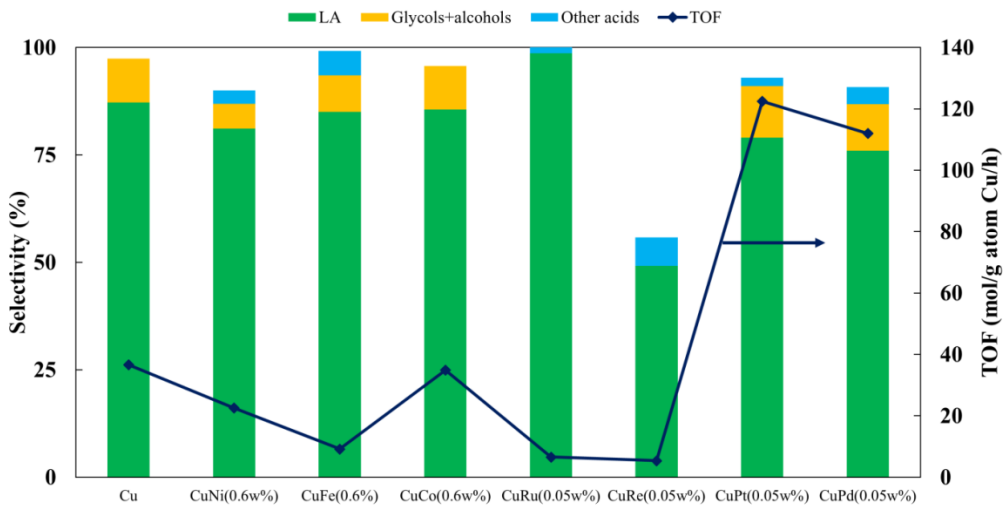

Figure 3. Comparison of different Cu-based bimetallic catalysts for glycerol conversion (Reaction time: 0.5~3 h, Cu loading: 2w%, other parameters same as Figure 2)

In order to understand the role of carbon supports on the activity of Cu catalysts, further comparison was carried out for monometallic Cu and bimetallic CuPd

catalysts. As seen in Figure 4, for the Cu/rGO nanocatalyst, remarkable activity (33 mol/g atom Cu/h) and LA yield (Y_{LA} = 25.2%) were observed, while Cu/AC catalyst displayed both low activity (13 mol/g atom Cu/h) and low LA yield (Y_{LA} = 6.2%). Further, the addition of Pd (0.05w%) to Cu/rGO nanocatalyst increased the TOF by approximately three folds (114 mol/g atom Cu/h) compared to the Cu/rGO catalyst. Supported CuPd on conventional carbon materials however only exhibited a negligible enhancement in activity and product yield. The activity of glycerol conversion and LA yield on CuPd/rGO catalyst was approximately five fold greater compared to CuPd/AC catalyst. These results indicate surface properties of carbon supports strongly affect the activity as well as product selectivity of Cu-based catalysts.

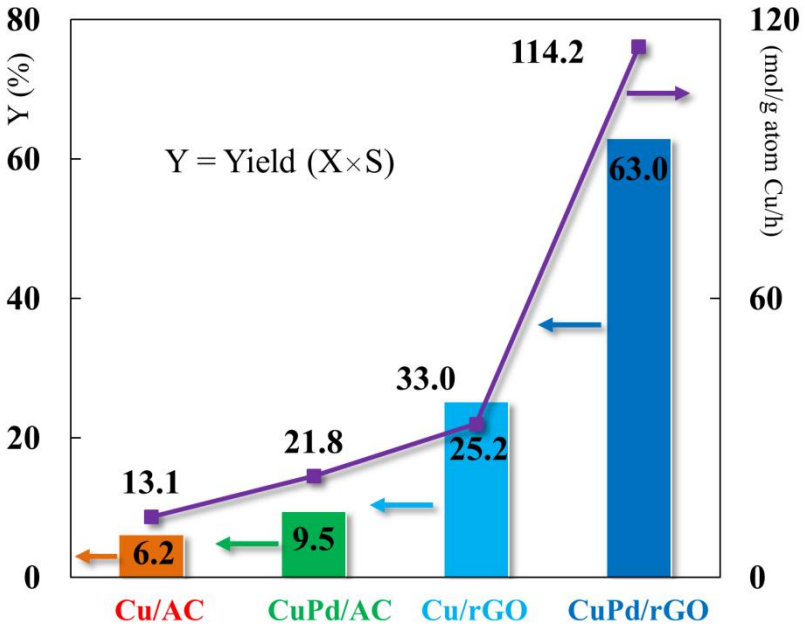

Figure 4. Comparison of Cu and CuPd catalysts on AC and rGO supports

3.2 Surface characterization of Cu-based catalysts

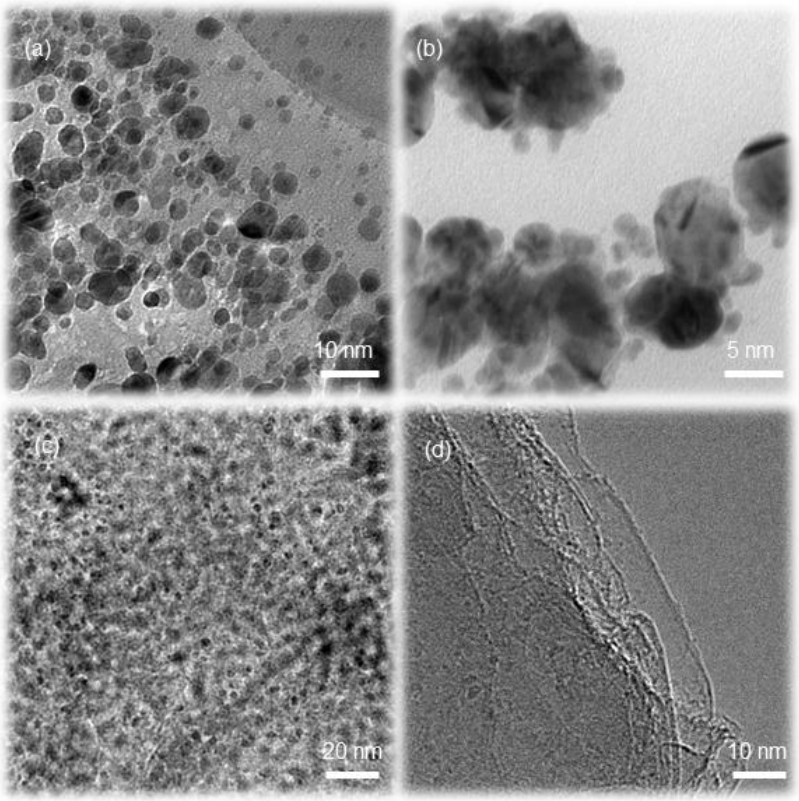

Figure 5. The TEM images of (a) Cu catalyst without the rGO support, (b) CuPd catalyst without the rGO support, (c) CuPd bimetallic catalyst on MC support, (d) CuPd bimetallic catalyst on SWCNT support. Synthesis of these nanoparticles was using the reducing procedure presented in Figure 1b (provided by Dr. Shenqiang Ren's group).

In order to understand the role of surface morphology of the carbon supports on the catalytic activity of Cu based catalysts, TEM and UV-Vis characterization were carried out. As seen in Figure 5, Cu and CuPd NPs without supports show large particle sizes with random shapes, while they (2~5 nm in size) display

mixed shapes with various surface planes on conventional MC and SWCNT supports.

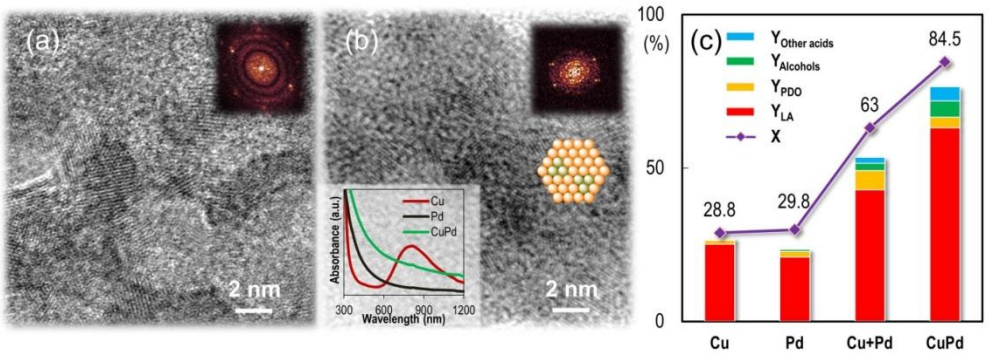

Figure 6. Structural characteristics and synergistic effect of CuPd/rGO catalyst. (a, b) The HRTEM image of monometallic Cu/rGO and bimetallic CuPd/rGO hybrid nanocatalysts, respectively. The inset shows the fast Fourier transform (FFT) spectra. (b) inset is the photoabsorption spectra of monometallic Cu/rGO, Pd/rGO and bimetallic CuPd/rGO hybrid nanocatalysts. (c) The catalytic performance of Cu/rGO, Pd/rGO, the admixture Cu/rGO and Pd/rGO, and bimetallic CuPd/rGO hybrid nanocatalyst. Alcohols: methanol, ethanol and propanols, Other acids: mainly acetic acid, traces of glycolic acid, reaction conditions same as Figure 2 [(a) and (b) provided by Dr. Shenqiang Ren's group].

Interestingly, the mean particle size of Cu NPs on rGO is also in the range of 2~5 nm, as seen from Figure 6, which however display completely different activity and selectivity in glycerol conversion. To better understand the observed catalytic enhancement on the rGO support, systematic studies on catalyst nanostructure and catalytic activity were performed. The HRTEM images of Cu/rGO [Figure 6 (a)] and CuPd/rGO hybrids [Figure 6 (b)], reveal homogeneous distribution of the metal nanocrystals[197] with [111] facet on rGO sheets (the average Cu and CuPd grain sizes are about 5 and 2 nm, respectively). The HRTEM images and FFT patterns exhibit the lattice spacing of Cu [111]

and CuPd [111] planes and rGO support as 2.58, 2.69 and 2.70 Å, accommodating the 4.4% and 0.3% mismatch between Cu [111], CuPd [111] and rGO. Considering the identical metal loadings on all catalyst samples, the distinct catalytic performances imply that the rGO support exposes the Cu atoms on dominant reactive [111] surface plane, while a thermodynamically stable state with random growth of Cu is preferred on other carbon supports. Therefore, the surface Cu atoms on the rGO support are more efficiently utilized than conventionally prepared Cu nanoparticles.

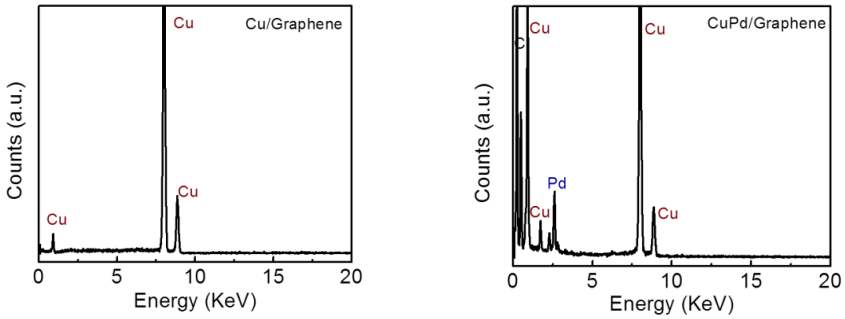

(a) (b)

Figure 7. The EDX Data for (a) Cu/rGO catalyst, (b) CuPd/rGO catalyst (provided by Dr. Shenqiang Ren's group).

UV-Vis absorption spectra [Figure 6 (b) inset] show that the plasmonic resonance of Cu nanocrystals[198] disappeared after the Pd loading, which can be attributed to the formation of bimetallic CuPd ultrasmall clusters on the rGO support. Similar absorption spectra have been noted for Cu *2p* and Pd *3d* interaction in a Cu-rich CuPd system.[199] Unlike the formulation in colloidal phase,[200] *tiny islands* of Pd tend to be present within Cu clusters ["cluster-in-

cluster" geometry, Figure 6 (b)]. The FFT pattern indicates the metal [111] growth direction and the existence of bimetallic CuPd nanoclusters by two different diffraction sets of Cu and Pd components [Figure 6 (b)]. The CuPd cluster formulation is however not observed with other carbon-based (AC, MC and SWCNT) supports. EDX spectra also confirm the existence of both Cu and Pd elements on rGO surfaces (Figure 7).

A comparison study was also performed on mono Cu/rGO, Pd/rGO, Cu/rGO+Pd/rGO admixture and bimetallic CuPd/rGO catalysts, in order to further confirm the observed synergistic coupling effect of bimetallic catalyst. Particularly, monometallic Pd/rGO catalyst [Figure 6 (c)] displayed approximately 30% conversion of glycerol but lower LA yield (Y_{LA} = 21%) compared to Cu/rGO nanocatalyst [Y_{LA} = 25%, Figure 6 (c)]. This is because Pd by itself promotes side reactions such as reforming and WGS.[127] Meanwhile, results from an admixture of Cu/rGO and Pd/rGO [Cu+Pd in Figure 6 (c)] showed that the glycerol conversion and LA yield increase to 63% and 43%, respectively, compared to individual Cu/rGO or Pd/rGO catalysts. With the (Cu+Pd) catalyst, noticeable HDO was undergoing (on the Pd metal) by *in situ* formed hydrogen to generate increased amounts of 1,2-propanediol (1,2-PDO) and $C_{1\sim2}$ alcohols.[122] The bimetallic CuPd/rGO catalyst displayed a strong synergistic effect resulting in approximately 85% glycerol conversion with a 73% total yield of products (Y_{LA} = 63%, $Y_{1,2\text{-PDO+Alcohols}}$ = 10%). Considering the fact that CuPd/AC catalyst does not show a synergistic effect for glycerol

conversion compared with CuPd/rGO catalyst sample (Figure 4), the unique "cluster-in-cluster" geometry is believed to be the main reason for the catalytic activity enhancement on rGO support.

3.3 Structure-performance correlations

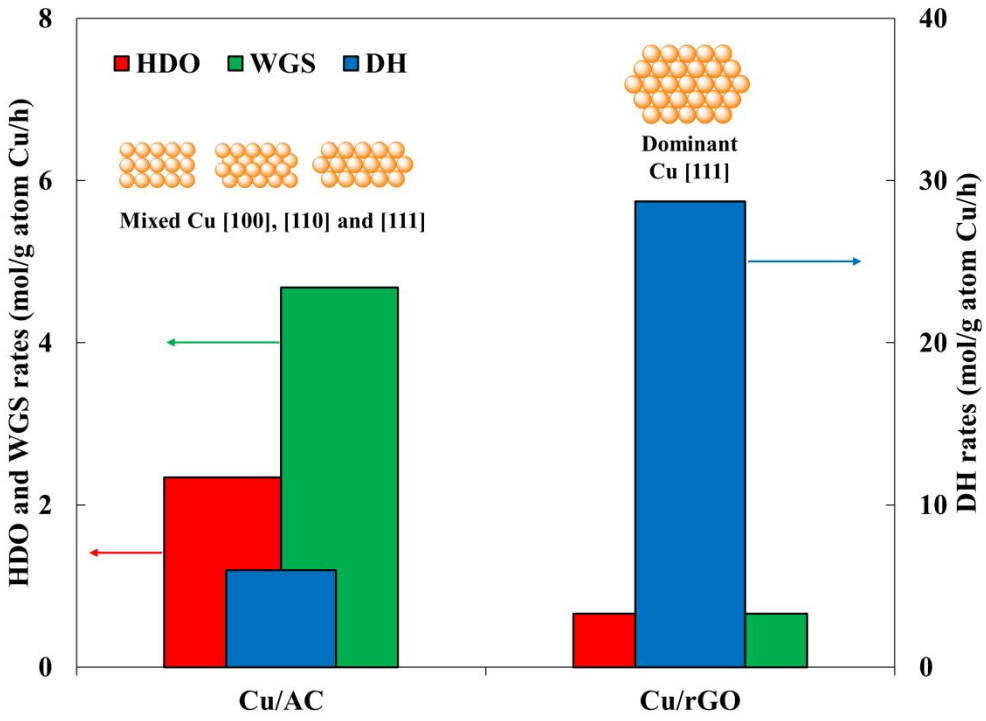

Figure 8. DH, HDO and WGS reaction rates on Cu/AC and Cu/rGO catalysts at 200 ^{o}C and nitrogen atmosphere

Based on the TEM characterization, it is clear that the catalytic performance of Cu nanocatalysts is strongly dependent on the surface morphology of NPs. The structure-performance correlations of DH, HDO and WGS reactions with various investigated Cu catalysts are established for the first time based on our experimental evidence in glycerol conversion.

It is known that LA is formed *via* DH-DHD-benzilic rearrangement route, in which DH is the key step. From our experimental results (Figures 2~4) it is clear that LA was actively and selectively formed on Cu [111] surface. In contrast, the deficit in carbon balance on other Cu catalysts (*e.g.* Cu/AC) implies that CO_2 was generated and absorbed by alkali species, which is the evidence of reforming and WGS reactions. As found in TEM characterization (Figure 5), Cu NPs on AC support show mixed shapes with different facets, including [100], [110] and [111]. Based on the reaction results and characterization, the structure-activity correlations are summarized in Figures 8 and 9 for mono and bimetallic Cu catalysts. The overall reaction rates for DH, HDO and WGS are compared on Cu/AC and Cu/rGO in Figure 8, according to the product distribution observed on the two catalysts (shown in Figures 2 and 3). Particularly, LA, glyceraldehyde (GLA), pyruvaldehyde (PAD) are the products from DH reaction, while glycols are generated from HDO and CO_2 (missing carbon balance) is formed in WGS reaction.

The overall DH rate on Cu/AC was only 6 mol/g atom Cu/h while this value is significantly higher on Cu/rGO (28.7 mol/g atom Cu/h) with dominant Cu [111] surface plane. Interestingly, HDO reaction rate on Cu/AC was approximately 2.3 mol/g atom Cu/h, which is about four times higher than the value on Cu/rGO catalyst. Similarly WGS reaction rate was about 4.7 mol/g atom Cu/h on Cu/AC, while it was only 0.7 mol/g atom Cu/h on Cu/rGO surface. The difference in measured reaction rates indicates that Cu [111] is selectively

promoting DH in alkaline medium. Cu [100] and [110] facets favor HDO and WGS (side reaction). Therefore LA can thus be selectively generated on Cu/rGO catalyst under our reaction conditions. The experimental observation clearly confirms that Cu [111] is active for DH but not a good platform for HDO and WGS reactions, while Cu [100] and [110] could be potentially better catalysts for HDO and WGS reactions of polyols.

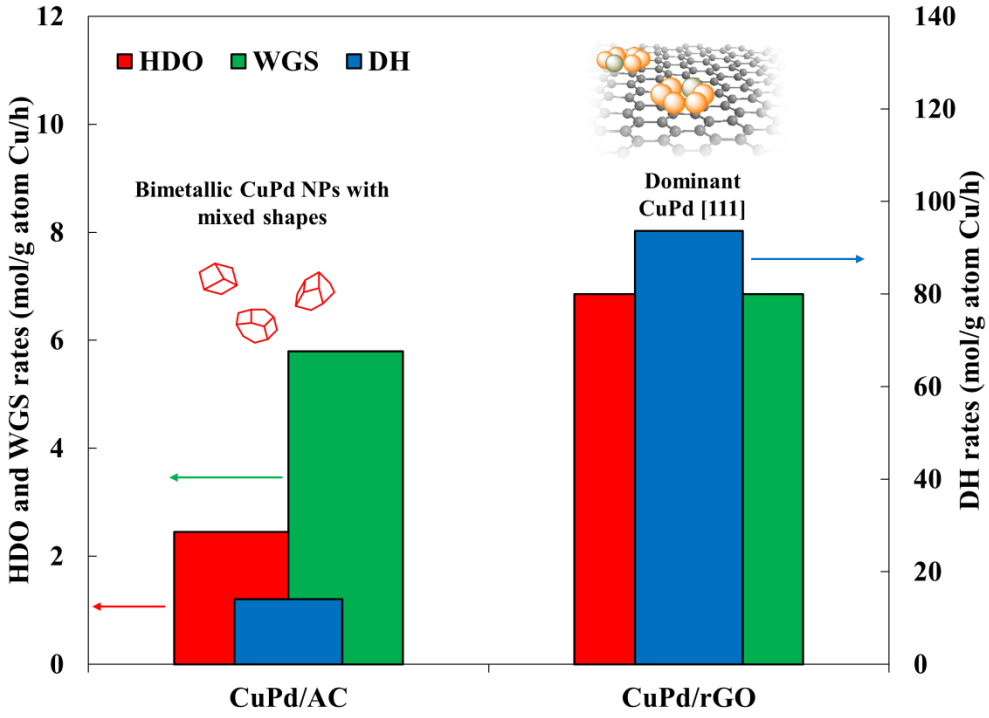

Figure 9. DH, HDO and WGS reaction rates on CuPd/AC and CuPd/rGO catalysts at 200 ^{o}C and nitrogen atmosphere

In order to understand the impact of bimetallic CuPd NPs for glycerol conversion, further comparison was made between CuPd/AC and CuPd/rGO catalysts, as shown in Figure 9. The reaction rates for DH, HDO and WGS were measured following the same criteria described in Figure 8. The overall rate of

DH on CuPd/AC was 14 mol/g atom Cu/h, which is about two folds compared with the value on Cu/AC catalyst. HDO and WGS reactions were also enhanced, 2.5 mol/g atom Cu/h and 5.8 mol/g atom Cu/h respectively, on bimetallic CuPd/AC catalyst.

A significant enhancement in reaction rates was observed on CuPd/rGO catalyst. First of all, DH rate was approximately 93.6 mol/g atom Cu/h on CuPd/rGO catalyst, which was about four-fold increase compared with Cu/rGO catalyst, while the enhancement on CuPd/AC was only two folds. HDO rate on CuPd/rGO was about 6.9 mol/g atom Cu/h compared with 2.3 mol/g atom Cu/h on Cu/rGO catalyst. WGS reaction rate was 6.9 mol/g atom Cu/h on CuPd/rGO surface.

Compared with bimetallic CuPd/AC sample, both DH and HDO rates on CuPd/rGO were much higher, while that of WGS was almost identical. The results imply that the presence of Pd in the form of hybrid CuPd clusters enhances DH of glycerol, HDO reactions were thus also facilitated. It is known that Cu displays much lower HDO activity compared with noble metals possible due to high Cu-H binding energy.[130] Although bimetallic CuPd on AC exhibited improved DH and HDO rates compared with monometallic Cu/AC catalyst, the experimental evidence clearly showed that bimetallic CuPd on rGO exhibited strong synergistic effects on glycerol conversion compared with on AC supports. Considering the fact that CuPd have dominant [111] surface plane on rGO, it is believed that rGO support alter the formulation of CuPd NPs and

significantly enhance the overall activity of CuPd catalysts. Therefore, CuPd/rGO could be a promising platform for conversion of glycerol to LA (from DH) with alcoholic compounds (from HDO) as valuable co-products. The establishment of structure-activity correlation is important for the rational design of metal based catalysts for polyols conversion.

A similar structure dependent effect on catalytic activity was also observed on Cu_2O NPs under the same reaction conditions. It was seen that cubic Cu_2O NPs displayed higher activity compared with rhombic Cu_2O NPs in DH of glycerol to LA. The reaction results are shown in Appendix IV.[191]

3.4 Effects of Pd loading

Since the addition of Pd shows synergistic effects with Cu/rGO catalyst for glycerol conversion, systematic work was carried out to understand the role of Pd on the activity and selectivity of Cu catalysts. More importantly, identifying an optimal Cu/Pd composition is the key to the high activity and selectivity of the proposed nanocatalysts. Table 1 summarizes the catalytic performances of mono Cu/rGO and Pd/rGO and bimetallic CuPd/rGO with various metal contents. As discussed earlier, Cu/rGO (Entry#1) displayed a 29% conversion and 87% selectivity towards LA. Pd/rGO catalysts (Entries#2~4) showed much higher activity (1728 mol/g atom Pd/h, calculated based on the conversion data, which is highest compared with the reported values in literature), but the selectivity to LA was lower than Cu/rGO catalyst. Bimetallic CuPd/rGO

obviously exhibited strong synergistic effects in catalytic activity within a wide range of Pd loadings (Entries#5~10) as compared with monometallic Cu and Pd catalysts on rGO supports. The selectivity towards LA decreased from 78% to 60% as Pd contents increased from 0.01w% to 0.1w%, while that of 1,2-PDO and alcohols increased from 5% to 14% at the same time. This observation implies that as more Pd is added to Cu/rGO catalysts, overall HDO reaction rates are enhanced.

Table 1. Activity and selectivity of Cu/rGO and CuPd/rGO catalysts

#	Catalysts on rGO	Time (h)	X (%)	Selectivity (%)			
				LA	1,2-PDO	Alcohols	Others
1	Cu(2w%)	6	28.8	87.0	4.2	-	-
2	Pd(0.01w%)	6	12.9	69.0	6.9	3.1	-
3	Pd(0.05w%)	6	29.8	70.0	6.2	2.4	-
4	Pd(0.1w%)	6	40.0	53.3	5.4	6.0	9.6
5	Cu(2w%)-Pd(0.01w%)	6	58.2	76.2	3.6	6.8	4.3
6	Cu(2w%)-Pd(0.03w%)	6	61.3	78.4	3.2	6.3	6.0
7	Cu(2w%)-Pd(0.05w%)	0.7	15.2	81.5	2.1	3.2	-
8	Cu(2w%)-Pd(0.05w%)	1.5	30.1	84.5	5.6	3.6	5.7
9	Cu(2w%)-Pd(0.05w%)	6	84.5	74.6	4.2	6.6	5.4
10	Cu(2w%)-Pd(0.1w%)	6	96.8	60.3	4.5	9.1	4.4
11	Cu(2w%)+Pd(0.05w%) admixture	6	63.0	68.0	10.1	3.6	3.2

Experimental conditions same as Figure 2.

3.5 Possible reaction pathways

Characterization of prepared Cu catalysts indicates that the Cu [111] surface dominates on rGO support and selectively catalyzes the DH reaction rather than WGS[79,201] at much higher rates than other Cu surfaces. Therefore Cu [111] displays higher activity and LA selectivity (S_{LA} = 74~84%) than previous observation.[79] But tandem DH/HDO was not obvious under our conditions possibly due to the low HDO activity of Cu in inert gas environment. The presence of Pd facilitates spillover of *in situ* formed hydrogen on carbon materials,[202] the hydrogen and some intermediates formed from DH undergo tandem HDO instead of forming waste methane and CO_2.

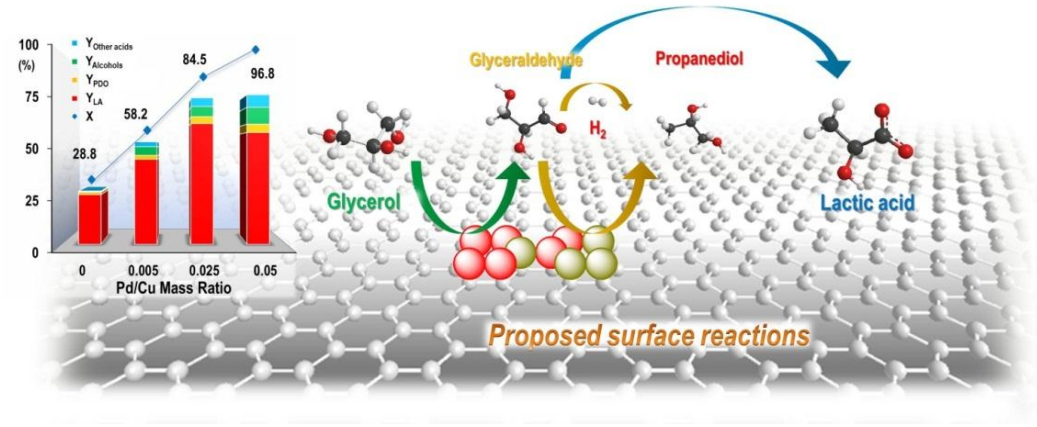

Figure 10. Proposed surface reactions on CuPd/rGO catalysts and the effects of Pd/Cu mass ratio on the yield of various products (inset) at 200 ^{o}C

This synergistic interaction between Cu and Pd sites and resulting tandem HDO are clearly much more remarkable on the CuPd/rGO than other catalysts, presumably due to the unique cluster-in-cluster alignment of the CuPd

nanostructures. Based on our experimental findings, the possible reaction pathways are shown schematically in Figure 10.

The glycerol conversion was enhanced to 96% at Pd/Cu mass ratio of 0.05, while the maximum LA yield was found to be 63% at 0.025 ratio (inset of Figure 10). With 1,2-PDO and linear alcohols as other co-products with a yield of 10%, the overall process shows high atom efficiency. At higher Pd/Cu ratios, Pd promotes side reactions decreasing the LA selectivity as well as other liquid products. Here, glycerol is believed to first react to form $R\text{-}CH_2\text{-}O^*$[140,146] as a primary intermediate species which rapidly forms GLA on surrounding Cu sites. Dehydrogenated species are instantaneously converted to LA[37,41] (with OH^-) or alcoholic chemicals[79,122] (by *in situ* formed hydrogen) in alkaline medium. This hypothesis is supported by the detection of increasing amounts of 1,2-PDO and linear alcohols [including methanol (MeOH), ethanol (EtOH) and propanols (PrOHs)] as Pd/Cu ratio increases (Figure 10). Therefore, it is concluded that the bimetallic CuPd clusters display a bifunctional nature for both the DH of glycerol to form LA and *in situ* HDO to other useful co-products without externally added hydrogen.

Further, CuPd/rGO with Cu (2w%) and Pd (0.05w%) loading was also evaluated for the catalytic conversion of sugar-derived polyols such as xylitol (C_5) and sorbitol (C_6) under the same reaction conditions. It is found that xylitol displayed 88.2% conversion after 6 h reaction at 200 ^oC. The major products were LA (S = 55%) and EG (24.4%) on CuPd/rGO catalyst. The major products

from sorbitol were LA (S = 70%) and alcohols (S = 7%) under the same conditions. Thus, it is clear that the CuPd/rGO catalysts effectively facilitate C-C and C-O cleavage, and convert bio-derived polyols to LA, glycols and linear alcohols under very mild reaction conditions.

Table 2. Catalytic conversion of xylitol and sorbitol on CuPd/rGO catalyst

#	Substrate	Conversion (%)	Selectivity (%)			
			LA	1,2-PDO	EG	Alcohols
1	Xylitol	88.2	55.4	1.2	24.4	4.3
2	Sorbitol	96.5	70.1	3.3	2.1	6.7

Substrate: 100.0 kg/m^3; solvent: H_2O; CuPd/rGO catalyst charge: 6.7 kg/m^3; T: 200 ^oC; reaction time: 6 h; P_{N2}: 1.4 MPa; NaOH concentration: same as Table 2.

3.6 Stability studies

Table 3. Stability studies on monometallic Cu/rGO and bimetallic CuPd/rGO catalysts

#	Catalyst	X (%)	Selectivity (%)			Percent of metal leached
			LA	1,2-PDO	Alcohols	
1	Cu/rGO-fresh	9.6	85.6	3.3	-	18.5w% After 1st run
2	Cu/rGO-spent	<1	41.1	-	-	
3	CuPd/rGO-fresh	56.2	88.1	4.1	2.4	2.2w% after three recycles
4	CuPd/rGO-1st recycle	53.1	84.2	4.6	5.2	
5	CuPd/rGO-2nd recycle	52.7	85.7	3.4	3.9	
6	CuPd/rGO-3rd recycle	48.9	82.0	0.8	2.0	

Glycerol: 100.0 kg/m^3; solvent: H_2O; catalysts charge: 13.2 kg/m^3; T: 140 ^oC; entries#1 and #2: reaction time, 6 h; entries#3~#6: reaction time, 16 h; P_{N2}: 1.4 MPa; NaOH/glycerol molar ratio: 1.1. LA: lactic acid, 1,2-PDO: 1,2-propanediol, EG: ethylene glycol, Alcohols: MeOH, EtOH and PrOHs. Metal content was determined by ICP measurement.

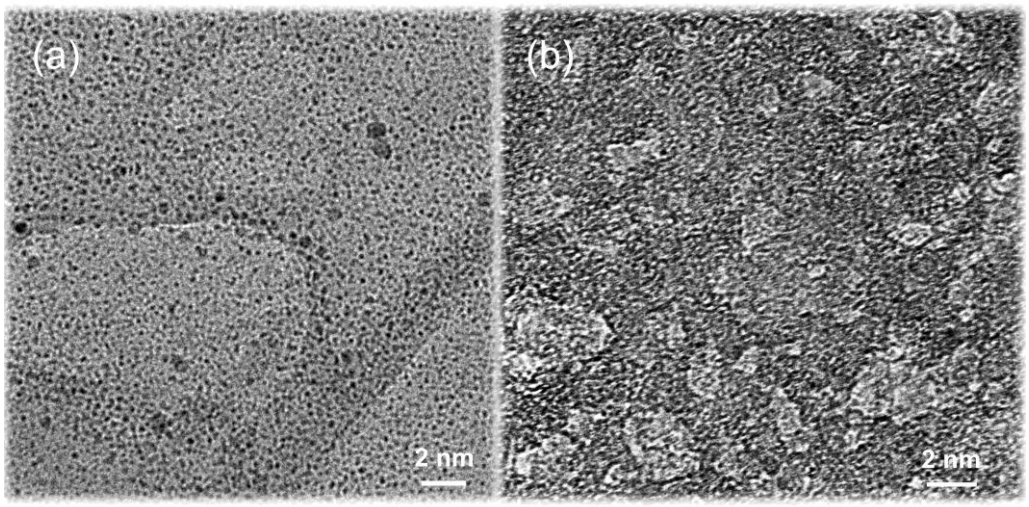

Figure 11. The TEM images of (a) spent Cu/rGO (after 1st run) and (b) CuPd/rGO (after 3rd recycle) catalysts. There exists obvious Cu metal leaching out on Cu/rGO during reaction, while no significant leaching is found on the CuPd/rGO sample.

The stability of nanocatalysts (Table 3) was also assessed by several recycle experiments. The results show that CuPd/rGO exhibited significant improvement in stability over Cu/rGO catalyst. For Cu/rGO catalyst, both ICP and TEM analysis revealed that deactivation due to metal leaching [Table 3 and Figure 11 (a)] was significant under the reaction conditions (Entries#1 and #2 in Table 3). However, for CuPd/rGO catalyst [Figure 11 (b), Entries#3~#6 in Table 3], it is clear that the glycerol conversion and LA selectivity remained almost constant during recycle experiments, indicating excellent stability and recyclability of the CuPd/rGO catalysts. The addition of Pd clearly increased the stability of Cu nanocatalysts. It is highly possible that the relatively stable cluster-in-cluster morphology and lattice match between metal clusters and rGO support enhances the interaction between CuPd and the graphene support. An important characteristic of Cu-based nanocatalysts is the high atom efficiency,

resulting from *in situ* hydrogen generation from the substrate itself to produce useful liquid products with significantly lower gaseous products compared to the supported noble metal catalysts.[57,125]

4. Conclusion

In summary, a new family of surface facet-controlled Cu-based nanocatalysts supported on the graphene derivative show exceptional catalytic activity and stability for aqueous phase biomass conversion. The novel features include the directed growth of dominant reactive surface facets of Cu nanocrystals using the graphene derivative (*e.g.* rGO) as a 2-D template, and the incorporation of Pd to achieve remarkable activity and stability enhancements. The bimetallic CuPd/rGO formulations can be potentially utilized in other applications such as DH/HDO of alcohols, fuel cells, catalytic CO oxidation as well as other green energy applications. The precise nature of Pd incorporation in the CuPd/rGO formulation and the role of the graphene support deserve further investigations in order to better understand and exploit the rGO supports for the rational design and synthesis of other families of multifunctional multimetallic nanocatalysts with enhanced activity, selectivity and stability.

Chapter 6 Conclusions and Recommendations

1. Conclusions

This thesis has been studying the catalysis and reaction engineering aspects of conversion of bio-derived polyols, including glycerol, xylitol, mannitol and sorbitol to various high value chemicals such as carboxylic acids [*e.g.* lactic acid (LA)] and glycols [*e.g.* 1,2-propandiol (1,2-PDO) and ethylene glycol (EG)] in gas-liquid-solid multiphase reaction systems. This work has contributed to the advances on (a) the fundamental aspects on the reaction behaviors of C-C, C-O and C-H bonding cleavage of these biomass molecules, (b) rational design of metal-based catalysts for effective conversion technologies and (c) kinetic modeling for the multiphase systems to understand and solve engineering issues involved in biomass conversion.

1.1 Catalytic conversion of sugar polyols: reaction pathways and kinetic modeling

Catalytic conversion of xylitol and sorbitol on Ru-based catalysts has shown that hydrogenolysis (HDO) of C_5 and C_6 polyols to lower chemicals is a series of metal-catalyzed simultaneous C-C and C-O cleavage reactions. Xylitol and sorbitol were found to undergo random C-C cleavage and significant methanation on Ru catalysts when acidic promoters (*e.g.* ZrO_2, H-β) were added to the system. In sharp contrast, xylitol tends to undergo C_2-C_3 cleavage

while C_1-C_2-C_3 cleavage easily occurs for sorbitol in the presence of base promoters (*e.g.* MgO, NaOH, CaO) following retro-aldolization mechanism.

Once C_2 and C_3 intermediates are formed after C-C cleavage, facile HDO reactions (mainly C-O cleavage) of these intermediates occurs instantaneously to form 1,2-PDO, EG and other alcohols in the presence of Ru-based catalysts, the chemistry of which is similar to glycerol HDO reported by previous researchers.

Reaction parameters such as temperature and pressure also impact the reaction behaviors of C-C and C-O cleavage. At relatively lower pressure (P_{H2} < 4MPa) and temperature (T < 215 ^{o}C), sorbitol tends to undergo C_3-C_3 cleavage. C_2-C_3 cleavage is dominant while C_1-C_4 cleavage is almost negligible for xylitol on RuRe/C catalysts in a wide range of reaction conditions.

The presence of base promoters significantly restrains the formation of methane on Ru catalysts. Kinetic modeling of sorbitol HDO on RuRe/C catalysts show that the presence of base significantly enhance the activation barrier for 1,2-PDO to propanol and EG to ethanol reactions (from 25~35 kJ/mol to 126~160 kJ/mol). Therefore the formation of gaseous alkanes is almost completely reduced on Ru catalysts.

1.2 Development of bi-functional Cu catalysts for upgrading of sugar polyols to glycols

On the basis of the fundamental understanding of C-C and C-O cleavage of xylitol and sorbitol molecules on Ru-based catalysts, a new family of bi-functional Cu catalysts supported on metal oxides was proposed for the first time for conversion of xylitol, erythritol, mannitol and sorbitol to glycols in the absence of corrosive alkali promoters. It is the first time to observe that Cu-based catalysts exhibit not just good activity for C-O cleavage, which has been extensively reported by previous researchers, but also high activity for C-C cleavage of polyols when immobilized on $MgO\text{-}Al_2O_3$, $ZnO\text{-}Al_2O_3$ and $CaO\text{-}Al_2O_3$ supports.

It is found that the promotional effects of Ca^{2+} in the catalyst supports significantly enhance the activity of C-C cleavages of Cu catalysts compared with other cations (*e.g.* Mg^{2+}, Zn^{2+}, H^{+}). Ca^{2+} has a stronger interaction with Cu species compared with other metal ions, which is characterized by temperature programmed reduction (TPR) as well as transmission electron microscopy (TEM) and scanning electron microscopy (SEM).

Moreover, $Cu/CaO\text{-}Al_2O_3$ catalysts prepared with different Cu loading and various synthetic conditions show that the activity for dehydrogenation (DH) and HDO on Cu sites is dependent on the highly crystallized phases formed in the solid catalysts. It is found that $Cu_xCa_yAl_zO_p$ phase shows high selectivity for DH and subsequent $C_3\text{-}C_3$ cleavage of sorbitol, while spinel $CuAl_2O_4$ structure

is responsible for HDO of intermediates to 1,2-PDO, EG, methanol and other alcoholic co-products. Therefore Cu/CaO-Al_2O_3 catalysts display excellent C-C and C-O cleavage for sorbitol conversion. The structure-activity relations are well established based on TEM, SEM and XRD characterization.

A further inspection on the possible reaction mechanism, along with experimental evidence of dominant C_3-C_x cleavage for xylitol, erythritol, mannitol and sorbitol, indicates that an instantaneous isomerization from aldehydes (*e.g.* hex-aldose in the case of sorbitol) to ketone (*e.g.* β-hex-ketose in the case of sorbitol), C-C cleavage thus occurs in the fashion of C_3-C_x for all investigated polyols.

In addition, reaction parameters such as temperature and pressure (of hydrogen) also influence the position where C-C cleavage occurs. It is observed that increasing reaction temperature and pressure tends to favor C_2-C_x cleavage, but breakage in C_3-C_x fashion is still the dominant way during the conversion of xylitol, erythritol, mannitol and sorbitol.

Experimental studies on Cu-based catalysts provide insights for the rational design of cost-effective catalysts for facile conversion of bio-polyols to various industrial important products.

1.3 Tandem dehydrogenation/hydrogenolysis of polyols to lactic acid and glycols

Given the fact that these bio-derived polyols are very promising feedstock for hydrogen generation on various metal-based catalysts, the possibility of combining the two rewarding reactions, "hydrogen generation" and "HDO" in one single pot was further investigated. In other words, carrying out HDO reactions using the hydrogen generated *in situ* from biomass itself, rather than adding external hydrogen, which is conventional produced *via* natural gas reforming, an energy intensive process.

It is found that at relatively high reaction temperature (T > 200 ^{o}C, P_{N2} = 1.4 MPa), glycerol tends to undergo both reforming and HDO on various metal catalysts such as Raney Ni, Raney Co, Ru/C, Pt/C, Pd/C and Rh/C. Water shift reaction is also significant thus a large amount of CO_2 is produced and absorbed by the alkalis (NaOH) in the reaction system. The overall selectivity towards valuable liquid products such as LA, 1,2-PDO is very poor (S < 60%). But these experimental results imply that the combination of hydrogen generation and HDO reactions in one single pot is achievable in the presence of metal catalysts.

A significant finding is that hydrogen generation reaction, DH of a small fraction of polyols can occur easily on Pt/C catalysts, HDO of the rest of polyols feedstocks take place at much faster rates but under significantly milder temperature (T = 115~160 ^{o}C, P_{N2} < 1.5 MPa) in comparison with

conventional HDO reactions (T > 220 ^{o}C, P_{H2} > 4.0 MPa). Reaction under mild conditions favors DH but restrain reforming and methanation on metal catalysts, thus hydrogen generated *in situ* selectively transform the rest of feedstocks to valuable liquid products such as LA, 1,2-PDO, EG and alcohols, with 96% atom efficiency.

At 130~160 ^{o}C, glycerol undergoes facile DH and HDO reactions and generate LA, 1,2-PDO, EG and alcohols as the major products with 95%+ selectivity. More importantly, xylitol and sorbitol is found to convert quickly on Pt/C catalysts even at 115 ^{o}C without the addition of external hydrogen. The selectivity to 1,2-PDO and EG is poor for xylitol and sorbitol. Methanol is the major products from C-C cleavage, indicating that C_1-C_x cleavage is significant for higher polyols.

The presence of alkalis significantly enhances the activity of Pt/C catalysts. The types of alkali are also important for the conversion rates of polyols. The order of promotional effects of cations in the alkalis is $Ba^{2+} > K^{+} > Na^{+} > Ca^{2+}$. It is clear that the promotional effects increase with increasing radius of cations [$Ca(OH)_2$ has low water solubility].

Detailed modeling work following experimental studies reveals the possible reaction mechanism on Pt/C catalysts: (a) the activation barrier of polyols (*e.g.* glycerol) on Pt surface is significantly lower (57.4 kJ/mol) than hydrothermal conversions (128.2 kJ/mol) thus DH can occur at much lower reaction

temperature. Alkalis act as a promoter here (metal-catalysis) rather than a reactant (in hydrothermal conversion) for the DH step. (b) Intermediates from DH quickly undergo reconstruction of molecules thus the overall HDO of these species is also easy to occur on Pt/C catalyst surface. A low activation energy for HDO (73.7 kJ/mol) is observed in our catalytic system, compared with 158.6 kJ/mol in the presence of external hydrogen for Pt/C catalysts. Therefore tandem DH/HDO occurs at a faster rate in the presence of Pt/C catalysts.

The activation barrier for C-C cleavage is very high (102~176 kJ/mol) compared with other reactions observed during tandem conversion of glycerol. The formation rates of methanol are enhanced dramatically as reaction temperature increases from 130 ^{o}C to 160 ^{o}C.

1.4 Lattice-matched Cu nanocatalysts for facile conversion of polyols to lactic acid

The surface morphologies of metal nanoparticles are critical for the catalytic performances in the conversion of polyols. Particularly several reactions, DH, dehydration, HDO and C-C cleavage occurring simultaneously on metal catalysts are very important reactions for catalytic upgrading of biomass feedstocks. However, limited activity and poor selectivity is the major problem plaguing current catalytic system. In collaboration Dr. Shenqiang Ren's group, design Cu-based nanocatalysts with well-defined structures was successfully achieved and evaluated for catalytic conversion of glycerol, xylitol and sorbitol to LA, 1,2-PDO, EG and other alcohols.

A key finding is the surface-dependent reactions on Cu catalysts during biomass upgrading. Conventional Cu-based nanocatalysts often exhibit mixed surface planes (*e.g.* [111], [100] and [101]), which promote several side reactions during polyols conversion, such as methanation, water gas shift reactions. Therefore the overall activity and selectivity towards useful liquid products are poor on the conventional catalysts. By exploiting lattice match engineering, Cu atoms are selectively deposited in [111] fashion on reduced graphene oxide (rGO) support at room temperature. The resultant Cu/rGO display a three-fold enhancement in catalytic DH of glycerol compared with conventional Cu catalysts. While conventional Cu catalysts show low activity for DH and poor selectivity towards LA (S < 52%), the Cu/rGO catalyst selectively promotes DH of glycerol at much milder reaction conditions compared with hydrothermal conversion with improve LA selectivity (S > 82%).

Further experimental studies show that bimetallic CuPd with cluster-in-cluster geometry on rGO support, exhibit significant synergistic effect on the activity for DH reactions of glycerol, while bimetallic CuPd nanoparticles only show slight increase in overall activity. A structure-activity relation is established for our catalytic system. In addition, the bimetallic CuPd/rGO catalysts display improved stability compared with monometallic Cu/rGO catalysts.

2. Recommendations

The results of this thesis pave the way for several follow-up studies:

(1) Investigating the reaction mechanism of C-C and C-O cleavage on metal catalysts *via* computational tools

Intermediates generated during DH and HDO reactions are often not stable thus cannot be detected quantitatively by experiments. Current *in situ* characterization techniques cannot be compatible with the majority of gas-liquid-solid reactions especially the key reactions involved in biomass conversion. Several unsolved problems can be potentially addressed with the aid from computational studies:

(a) The position where C-H and O-H bond breaks during DH step;

(b) The reaction paths of hydrogen formed *in situ* for HDO reactions;

(c) Reaction pathways of DH, HDO, C-C cleavage and WGS on selected surface facet including [111], [101], [100] and [110] of Pt, Pd and Cu metal nanoparticles.

The information derived from computational studies will provide insight on the reaction mechanism and further design of multi-functional catalysts. More importantly, the reaction pathways and intermediate species involved in biomass conversion will be considered for the development of micro-kinetic models.

(2) Collaboration with material scientists in designing nanocatalysts with well-defined structures

Based on the fundamental understanding on the possible reaction pathways of several important reactions, such as DH, HDO, C-C/C-O cleavage, water gas shift, designing multi-functional catalysts with selected active sites in one single catalyst is possible. In collaboration with material scientists, synthesis of well-defined nanocatalysts with wanted active sites should be carried out and will be tested using experimental results in order to establish the structure-activity relations. The following types of catalyst should be designed, synthesized and studied systematically:

(a) Monometallic Pt, Pd and Cu catalysts for DH, HDO, WGS reactions respectively using glycerol, xylitol and sorbitol as the model compounds;

(b) Electron interaction between catalyst supports, including carbon-based materials, zeolites, metal oxide (e.g. CeO_2, TiO_2, *etc*) and metal nanoparticles should be studied with details;

(c) Various bimetallic compositions, including random/structured alloy and core-shell should be studied for DH, HDO and WGS reactions respectively in order to understand the formulations of metal catalysts on their catalytic performances.

On the basis of the proposed work above, tandem conversion of biomass derived feedstocks (*e.g.* polyols, sugars, cellulose, *etc*) to high value chemicals

in one step, in other words, combing different reaction steps in one single pot should be carried out to evaluate the performances of synthesized nanocatalysts.

(3) Optimization of catalyst design and process modeling

Experimental studies described in this dissertation have shown promising results in converting glycerol, xylitol, mannitol and sorbitol to glycols and lactic acid in the presence of metal-based catalysts. Optimizing the design of catalysts including the pretreatment conditions, activation parameters and the addition of promoters (*e.g.* a second metal) is important for the catalyst and process development.

Detailed kinetic modeling on these metal catalysts should be carried out in order to understand the effects of experimental conditions on the reaction pathways as well as possible reaction mechanism involved in C-C and C-O bond activation.

Further, continuous studies on the catalyst stability and mass transfer effects on the overall conversion of substrate and selectivity towards glycols, acids and alcohols should be carried out for further understanding of the roles reaction parameters on the catalyst performances. Specifically, reactor modeling on (a) HDO of glycerol, xylitol and sorbitol, and (b) tandem DH/HDO of polyols should be carried out using the best catalyst candidates for continuous studies in order to collect important data of reactor performances.

In addition, as described in this dissertation, currently the major research efforts have been focused on designing nanocatalysts in powder forms, which are not practical for continuous studies in a fixed bed reactor. Therefore, developing new strategies on immobilization active nanocatalysts on larger particles (*e.g.* pellet) will be a promising research direction, which demands the collaboration between material scientists and chemical engineers. The scale-up of nanocatalyst synthesis and evaluation of activity, selectivity and stability of immobilized nanocatalysts on industrial catalyst supports will be the key for the further development of active nanocatalysts for biomass conversion in an industrial scale.

References and Notes

1 An Estimate of Undiscovered Conventional Oil and Gas Reserves of the World. U. S. Department of Interior, U.S. Geological Survey, March **2012**.

2 The Availability and Price of Petroleum and Petroleum Products Produced in Countries Other Than Iran. U. S. Energy Information Adminstration, February **2014**.

3 Serrano-Ruiz, J. C.; Dumesic, J. Catalytic routes for the conversion of biomass into liquid hydrocarbon transportation fuels. *Energy Environ. Sci.* **2011,** *4,* 83-99.

4 Klass, D. L. *Biomass for Renewable Energy, Fuels, and Chemicals*. Academic press, **1998**.

5 Renewable Energy Consumption and Electricity Preliminary Statistics. U. S. Energy Information Adminstration, Jun. **2011**.

6 Kamm, B.; Gruber, P. R.; Kamm, M. Biorefineries-industrial processes and products: status quo and future directions. Wiley-VCH, Verlag GmbH & Co. KGaA, **2008**.

7 http://www.nrel.gov/biomass/proj_biochemical_conversion.html.

8 NREL/TP-580-28893. Determing the cost of producing ethanol from corn starch and lignocellulosic feedstocks, **2000**.

9 Wu, M.; Yang, T. J.; Miao, M. D.; Ni, J. B. Improvement of Cell Permeability on Bio-production of 1,3-Propanediol. *Acta Chim. Sinica*. **2009,** *67,* 2133-2138.

10 Gao, C. X.; Feng, E. M.; Wang, Z. T.; Xiu, Z. L. Nonlinear dynamical systems of bio-dissimilation of glycerol to 1,3-propanediol and their optimal controls. *J. Ind. Manag. Optim.* **2005,** *1,* 377-388.

11 Anex, R. P.; Ogletree, A. L. Life cycle assessment of a bio-based process for producing 1,3-propanediol. 227th ACS National Meeting, Anaheim, CA, March 28-April 1, **2004**.

12 Distel, K. A.; Zhu, G. Y.; Wang, P. Biocatalysis using an organic-soluble enzyme for the preparation of poly(lactic acid) in organic solvents. *Bioresour. Technol.* **2005,** *96,* 617-623.

13 Ebshish, A.; Yaakob, Z.; Taufiq-Yap, Y. H.; Bshish, A.; Tasirin, S. M. Review of hydrogen production via glycerol reforming. Proceedings of the Institution of Mechanical Engineers, Part A: *J. Power and Energy.* **2012,** *226,* 1060-1075.

14 Martin, A.; Armbruster, U.; Gandarias, I.; Arias, P. L. Glycerol hydrogenolysis into propanediols using in situ generated hydrogen - A critical review. *Eur. J. Lipid. Sci. Tech.* **2013,** *115,* 9-27.

15 Vaidya, P. D.; Rodrigues, A. E. Glycerol Reforming for Hydrogen Production: A Review. *Chem. Eng. Technol.* **2009,** *32,* 1463-1469.

16 Gallezot, P. Conversion of biomass to selected chemical products. *Chem. Soc. Rev.* **2012,** *41,* 1538-1558.

17 Werpy, T.; Petersen, G. Top Value Added Chemicals from Biomass. August, **2004**.

18 International, H. Glycerine market report. Montmorency, France, December, **2012**.

19 Karinen, R. S.; Krause, A. O. I. New biocomponents from glycerol. *Appl. Catal., A* **2006,** *306,* 128-133.

20 Ott, L.; Bicker, M.; Vogel, H. Catalytic dehydration of glycerol in sub- and supercritical water: a new chemical process for acrolein production. *Green Chem.* **2006,** *8,* 214-220.

21 Miyazawa, T.; Koso, S.; Kunimori, K.; Tomishige, K. Glycerol hydrogenolysis to 1,2-propanediol catalyzed by a heat-resistant ion-exchange resin combined with Ru/C. *Appl. Catal., A* **2007,** *329,* 30-35.

22 Yuan, Z. L.; Wu, P.; Gao, J.; Lu, X.; Hou, Z.; Zheng, X. Pt/Solid-Base: A Predominant Catalyst for Glycerol Hydrogenolysis in a Base-Free Aqueous Solution. *Catal. Lett.* **2009,** *130,* 261-265.

23 Vila, F.; Granados, M. L.; Ojeda, M.; Fierro, J. L. G.; Mariscal, R. Glycerol hydrogenolysis to 1,2-propanediol with Cu/gamma-Al_2O_3: Effect of the activation process. *Catal. Today* **2012,** *187,* 122-128.

24 Vasiliadou, E. S.; Lemonidou, A. A. Kinetic study of liquid-phase glycerol hydrogenolysis over Cu/SiO_2 catalyst. *Chem. Eng. J.* **2013,** *231,* 103-112.

25 Nakagawa, Y.; Shinmi, Y.; Koso, S.; Tomishige, K. Direct hydrogenolysis of glycerol into 1,3-propanediol over rhenium-modified iridium catalyst. *J. Catal.* **2010,** *272,* 191-194.

26 Bravo-Suarez, J. J.; Lu, J.; Dallos, C. G.; Fujitani, T.; Oyama, S. T. Kinetic study of propylene epoxidation with H_2 and O_2 over a gold/mesoporous titanosilicate catalyst. *J. Phys. Chem. C* **2007,** *111,* 17427-17436.

27 Jin, G. J.; Lu, G.; Guo, Y.; Guo, Y.; Wang, J.; Kong, W.; Liu, X. Effect of preparation condition on performance of Ag-MoO_3/ZrO_2 catalyst for direct epoxidation of propylene by molecular oxygen. *J. Mol. Catal., A: Chem.* **2005,** *232,* 165-172.

28 Thiele, G. F.; Roland, E. Propylene epoxidation with hydrogen peroxide and titanium silicalite catalyst: Activity, deactivation and regeneration of the catalyst. *J. Mol. Catal., A: Chem.* **1997,** *117,* 351-356.

29 Miyazawa, T.; Koso, S.; Kunimori, K.; Tomishige, K. Development of a Ru/C catalyst for glycerol hydrogenolysis in combination with an ion-exchange resin. *Appl. Catal., A* **2007,** *318,* 244-251.

30 Miyazawa, T.; Kunimori, K.; Tomishige, K. Glycerol hydrogenolysis in the aqueous solution under hydrogen over Ru/C plus an ion-exchange resin and its reaction mechanism. 232nd ACS National Meeting, San Francisco, CA, September 10-14, **2006**.

31 Kusunoki, Y.; Miyazawa, T.; Kunimori, K.; Tomishige, K. Highly active metal-acid bifunctional catalyst system for hydrogenolysis of glycerol under mild reaction conditions. *Catal. Commun.* **2005,** *6,* 645-649.

32 Ma, L.; He, D. H.; Li, Z. P. Promoting effect of rhenium on catalytic performance of Ru catalysts in hydrogenolysis of glycerol to propanediol. *Catal. Commun.* **2008,** *9,* 2489-2495.

33 Ma, L.; He, D. H. Influence of catalyst pretreatment on catalytic properties and performances of Ru-Re/SiO_2 in glycerol hydrogenolysis to propanediols. *Catal. Today* **2010,** *149,* 148-156.

34 Ma, L.; He, D. H. Effect of rhenium component and preparation methods of ZrO_2 support on catalytic performance of Ru-Re/ZrO_2 for glycerol hydrogenolysis. *Chin. J. Catal.* **2009,** *30,* 471-478.

35 Bienholz, A.; Schwab, F.; Claus, P. Hydrogenolysis of glycerol over a highly active CuO/ZnO catalyst prepared by an oxalate gel method: influence of solvent and reaction temperature on catalyst deactivation. *Green Chem.* **2010,** *12,* 290-295.

36 Bienholz, A.; Blume, R.; Knop-Gericke, A.; Girgsdies, F.; Behrens, M.; Claus, P. Prevention of catalyst deactivation in the hydrogenolysis of glycerol by Ga_2O_3-modified copper/zinc oxide catalysts. *J. Phys. Chem. C* **2011,** *115,* 999-1005.

37 Wang, S. A.; Zhang, Y. C.; Liu, H. C. Selective hydrogenolysis of glycerol to propylene glycol on Cu-ZnO composite catalysts: structural requirements and reaction mechanism. *Chem.-Asian J.* **2010,** *5,* 1100-1111.

38 Balaraju, M.; Rekha, V.; Prasad, P. S. S.; Prasad, R. B. N.; Lingaiah, N. Selective hydrogenolysis of glycerol to 1, 2-propanediol over Cu-ZnO catalysts. *Catal. Lett.* **2008,** *126,* 119-124.

39 Balaraju, M.; Jagadeeswaraiah, K.; Prasad, P. S. S.; Lingaiah, N. Catalytic hydrogenolysis of biodiesel derived glycerol to 1,2-propanediol over Cu-MgO catalysts. *Catal. Sci. Technol.* **2012,** *2,* 1967-1976.

40 Mizugaki, T.; Arundhathi, R.; Mitsudome, T.; Jitsukawa, K.; Kaneda, K. Selective hydrogenolysis of glycerol to 1,2-propanediol using heterogeneous copper nanoparticle catalyst derived from Cu-Al hydrotalcite. *Chem. Lett.* **2013,** *42,* 729-731.

41 Yuan, Z. L.; Wang, L.; Wang, J/ Xia, S.; Chen, P.; Hou, Z; Zheng, X. Hydrogenolysis of glycerol over homogenously dispersed copper on solid base catalysts. *Appl. Catal., B* **2011,** *101,* 431-440.

42 Meher, L. C.; Gopinath, R.; Naik, S. N.; Dalai, A. K. Catalytic hydrogenolysis of glycerol to propylene glycol over mixed oxides derived from a hydrotalcite-type precursor. *Ind. Eng. Chem. Res.* **2009,** *48,* 1840-1846.

43 Vasiliadou, E. S.; Eggenhuisen, T. M.; Munik, P.; de Jongh, P. E.; de Jong, K. P.; Lemonidou, A. A. Synthesis and performance of highly dispersed Cu/SiO_2 catalysts for the hydrogenolysis of glycerol. *Appl. Catal., B* **2014,** *145,* 108-119.

44 Vasiliadou, E. S.; Lemonidou, A. A. Investigating the performance and deactivation behaviour of silica-supported copper catalysts in glycerol hydrogenolysis. *Appl. Catal., A* **2011,** *396,* 177-185.

45 Wolosiak-Hnat, A.; Milchert, E.; Grzmil, B. Influence of parameters on glycerol hydrogenolysis over a Cu/Al_2O_3 catalyst. *Chem. Eng. Technol.* **2013,** *36,* 411-418.

46 Feng, Y.; Yin, H.; Shen, L.; Wang, A.; Shen, Y.; Jiang, T. Gas-phase hydrogenolysis of glycerol catalyzed by Cu/MO_x catalysts. *Chem. Eng. Technol.* **2013,** *36,* 73-82.

47 Zhao, L. L.; Chen, J. X. Effect of phosphorus on structure and performance of Cu/Al_2O_3 Catalysts for hydrogenolysis of glycerol. *Chin. J. Catal.* **2012,** *33,* 1410-1416.

48 Wolosiak-Hnat, A.; Milchert, E.; Lewandowski, G.; Grzmil, B. Influence of reduction time of copper based catalysts: Cu/Al_2O_3 and $CuCr_2O_4$ on hydrogenolysis of glycerol. *Pol. J. Chem. Technol.* **2011,** *13,* 71-76.

49 ten Dam, J.; Hanefeld, U. Renewable Chemicals: Dehydroxylation of Glycerol and Polyols. *ChemSusChem* **2011,** *4,* 1017-1034.

50 Bloom, P. D. Hydrogenolysis of glycerol and products produced therefrom, U.S. patent application: 20080103339, **2008**.

51 Suppes, G., Sutterlin, W. & Dasari, M. Method of producing lower alcohols from glycerol, U.S. patent: 8017816, **2002**.

52 Casale, B. & Gomez, A. M. A catalytic method of hyrogenating glycerol. European patent: 0523014, **1993**.

53 Ma, L.; He, D. H. Hydrogenolysis of glycerol to propanediols over highly active Ru-Re bimetallic catalysts. *Top. Catal.* **2009,** *52,* 834-844.

54 Balaraju, M.; Rekha, V.; Sai Prasad, P. S.; Prabhavathi Devi, B. L. A.; Prasad, R. B. N.; Lingaiah, N. Influence of solid acids as co-catalysts on glycerol hydrogenolysis to propylene glycol over Ru/C catalysts. *Appl. Catal., A* **2009,** *354,* 82-87.

55 Ma, L.; Li, Y. M.; He, D. H. Glycerol hydrogenolysis to propanediols over Ru-Re/SiO_2: acidity of catalyst and role of Re. *Chin. J. Catal.* **2011,** *32,* 872-876.

56 Torres, A.; Roy, D.; Subramaniam, B.; Chaudhari, R. V. Kinetic modeling of aqueous-phase glycerol hydrogenolysis in a batch slurry reactor. *Ind. Eng. Chem. Res.* **2010,** *49,* 10826-10835.

57 Maris, E. P.; Davis, R. J. Hydrogenolysis of glycerol over carbon-supported Ru and Pt catalysts. *J. Catal.* **2007,** *249,* 328-337.

58 Kwak, B. K.; Park, D. S.; Yun, Y. S.; Yi, J. Preparation and characterization of nanocrystalline CuAl2O4 spinel catalysts by sol-gel method for the hydrogenolysis of glycerol. *Catal. Commun.* **2012,** *24,* 90-95.

59 Mane, R. B.; Kondawar, S. E.; Niphadkar, P. S.; Joshi, P. N.; Patil, K. R.; Rode, C. V. Effect of preparation parameters of Cu catalysts on their physico-

chemical properties and activities for glycerol hydrogenolysis. *Catal. Today* **2012,** *198*, 321-329.

60 Zhao, B. B.; Li, C. C.; Xu, C. L. Insight into the catalytic mechanism of glycerol hydrogenolysis using basal spacing of hydrotalcite as a tool. *Catal. Sci. Technol.* **2012,** *2*, 1985-1994.

61 Xia, S. X.; Zheng, L.; Ning, W.; Wang, L.; Chen, P.; Hou, Z. Multiwall carbon nanotube-pillared layered $Cu_{0.4}/Mg_{5.6}Al_2O_{8.6}$: an efficient catalyst for hydrogenolysis of glycerol. *J. Mater. Chem. A* **2013,** *1*, 11548-11552.

62 Tan, H.; Hedhill, M. N.; Wang, Y.; Zhang, J.; Li, K.; Sioud, S.; Al-Talla, Z. A.; Amad, M. H.; Zhan, T.; Tall, O. E.; Han, Y. One-pot synthesis Of $Cu/ZnO/ZnAl_2O_4$ catalysts and their catalytic performance in glycerol hydrogenolysis. *Catal. Sci. Technol.* **2013,** *3*, 3360-3370.

63 Xia, S. X.; Nie, R.; Lu, X.; Wang, L.; Chen, P.; Hou, Z. Hydrogenolysis of glycerol over $Cu\text{-}_{0.4}/Zn_{5.6\text{-}x}Mg_xAl_2O_{8.6}$ catalysts: The role of basicity and hydrogen spillover. *J. Catal.* **2012,** *296*, 1-11.

64 Xiao, Z. H.; Li, C.; Xiu, J.; Wang, X.; Williams, C. T.; Liang, C. Insights into the reaction pathways of glycerol hydrogenolysis over Cu-Cr catalysts. *J. Mol. Catal. A-Chem.* **2012,** *365*, 24-31.

65 Xiao, Z. H. Xiu, J.; Wang, X.; Zhang, B.; Williams, C. T.; Su, D.; Liang, C. Controlled preparation and characterization of supported $CuCr_2O_4$ catalysts for hydrogenolysis of highly concentrated glycerol. *Catal. Sci. Technol.* **2013,** *3*, 1108-1115.

66 Wolosiak-Hnat, A.; Milchert, E.; Lewandowski, G. The Influence of Technological Parameters on Hydrogenolysis of Glycerol in the Presence of $CuCr_2O_4$ Catalyst. *J. Adv. Oxid. Technol.* **2012,** *15*, 405-417.

67 Xiao, Z. H. Jin, S.; Wang, X.; Li, W.; Wang, J.; Liang, C. Preparation, structure and catalytic properties of magnetically separable Cu-Fe catalysts for glycerol hydrogenolysis. *J. Mater. Chem.* **2012,** *22*, 16598-16605.

68 Zhu, S. H. *et al.* Promoting effect of boron oxide on Cu/SiO2 catalyst for glycerol hydrogenolysis to 1,2-propanediol. *J Catal* **303**, 70-79 (2013).

69 Xia, S. X.; Yuan, Z. L.; Wang, L. N.; Chen, P.; Hou, Z. Y. Catalytic production of 1,2-propanediol from glycerol in bio-ethanol solvent. *Bioresour. Technol.* **2012,** *104*, 814-817.

70 Wu, Z. J.; Mao, Y. Z.; Wang, X. X.; Zhang, M. H. Preparation of a Cu-Ru/carbon nanotube catalyst for hydrogenolysis of glycerol to 1,2-propanediol via hydrogen spillover. *Green Chem.* **2011,** *13*, 1311-1316.

71 Lee, S. H.; Moon, D. J. Studies on the conversion of glycerol to 1,2-propanediol over Ru-based catalyst under mild conditions. *Catal. Today* **2011,** *174*, 10-16.

72 Yuan, Z. L.; Wang, J.; Wang, L.; Xie, W.; Chen, P.; Hou, Z.; Zheng, X. Biodiesel derived glycerol hydrogenolysis to 1,2-propanediol on Cu/MgO catalysts. *Bioresour. Technol.* **2010,** *101*, 7088-7092.

73 Huang, Z. W. Cui, F.; Xue, J.; Zuo, J.; Chen, J.; Xia, C. Cu/SiO_2 catalysts prepared by hom- and heterogeneous deposition-precipitation methods: Texture, structure, and catalytic performance in the hydrogenolysis of glycerol to 1,2-propanediol. *Catal. Today* **2012,** *183*, 42-51.

74 Huang, Z. W.; Cui, F.; Kang, H. X.; Chen, J.; Xia, C. G. Characterization and catalytic properties of the CuO/SiO2 catalysts prepared by precipitation-gel method in the hydrogenolysis of glycerol to 1,2-propanediol: Effect of residual sodium. *Appl. Catal., A* **2009,** *366*, 288-298.

75 Zheng, J.; Zhu, W.; Ma, C.; Jia, M. Wang, Z.; Hou, Y.; Zhang, W. Hydrogenolysis of glycerol to 1,2-propanediol over Cu/SiO_2 catalysts prepared by ion-exchange method. *Pol. J. Chem.* **2009,** *83*, 1379-1387.

76 Huang, Z. W. Cui, F.; Kang, H.; Chen, J.; Zhang, X.; Xia, C. Highly dispersed silica-supported copper nanoparticles prepared by precipitation-gel method: A simple but efficient and stable catalyst for glycerol hydrogenolysis. *Chem. Mater*. **2008,** *20*, 5090-5099.

77 Zhou, Z. M.; Li, X.; Zeng, T.; Hong, W.; Cheng, Z.; Yuan, W. Kinetics of hydrogenolysis of glycerol to propylene glycol over $Cu\text{-}ZnO\text{-}Al_2O_3$ catalysts. *Chin. J. Chem. Eng.* **2010,** *18*, 384-390.

78 Kishida, H.; Jin, F. M.; Zhou, Z. Y.; Moriya, T.; Enomoto, H. Conversion of glycerin into lactic acid by alkaline hydrothermal reaction. *Chem. Lett*. **2005,** *34*, 1560-1561.

79 Roy, D.; Subramaniam, B.; Chaudhari, R. V. Cu-based catalysts show low temperature activity for glycerol conversion to lactic acid. *ACS Catal.* **2011,** *1*, 548-551.

80 King, D. L.; Zhang, L.; Xia, G.; Karim, A. M.; Heldebrant, D. J.; Wang, X.; Peterson, T.; Wang, Y. Aqueous phase reforming of glycerol for hydrogen production over Pt-Re supported on carbon. *Appl. Catal., B* **2010,** *99*, 206-213.

81 Coll, D.; Delbecq, F.; Aray, Y.; Sautet, P. Stability of intermediates in the glycerol hydrogenolysis on transition metal catalysts from first principles. *Phys. Chem. Chem. Phys.* **2011,** *13*, 1448-1456.

82 Lahr, D. G.; Shanks, B. H. Kinetic analysis of the hydrogenolysis of lower polyhydric alcohols: Glycerol to glycols. *Ind. Eng. Chem. Res.* **2003,** *42*, 5467-5472.

83 Lahr, D. G.; Shanks, B. H. Effect of sulfur and temperature on ruthenium-catalyzed glycerol hydrogenolysis to glycols. *J. Catal*. **2005,** *232*, 386-394.

84 Xi, Y. Y. Holladay, J. E.; Frye, J. G.; Oberg, A. A.; Jackson, J. E.; Miller, D. J. A kinetic and mass transfer model for glycerol hydrogenolysis in a trickle-bed reactor. *Org. Process. Res. Dev*. **2010,** *14*, 1304-1312.

85 Kim, N. D.; Park, J. R.; Park, D. S.; Kwak, B. K.; Yi, J. Promoter effect of Pd in CuCr2O4 catalysts on the hydrogenolysis of glycerol to 1,2-propanediol. *Green Chem.* **2012,** *14*, 2638-2646.

86 Wang, S.; Yin, K.; Zhang, Y.; Liu, H. Glycerol hydrogenolysis to propylene glycol and ethylene glycol on zirconia supported noble metal catalysts. *ACS Catal.* 2013, *9*, 2112-2121.

87 *Kirk-Othmer Encyclopedia of Chemical Technology*. Wiley, John & Sons, Inc. **2006**.

88 Zhao, L.; Zhou, J. H.; Sui, Z. J.; Zhou, X. G. Hydrogenolysis of sorbitol to glycols over carbon nanofiber supported ruthenium catalyst. *Chem. Eng. Sci.* **2010,** *65*, 30-35.

89 Banu, M.; Sivasanker, S.; Sankaranarayanan, T. M.; Venuvanalingam, P. Hydrogenolysis of sorbitol over Ni and Pt loaded on NaY. *Catal. Commun.* **2011,** *12*, 673-677.

90 Sun, J. Y.; Liu, H. C. Selective hydrogenolysis of biomass-derived xylitol to ethylene glycol and propylene glycol on supported Ru catalysts. *Green Chem.* **2011,** *13*, 135-142.

91 Jin, X.; Roy, D.; Subramaniam, B.; Chaudhari, R. V. Activity and selectivity of bimetallic catalysts for polyols hydrogenolysis. 243rd ACS National Meeting, San Diego, CA, March 25-29, **2012**.

92 Huber, G. W.; Cortright, R. D.; Dumesic, J. A. Renewable alkanes by aqueous-phase reforming of biomass-derived oxygenates. *Angew. Chem., Int. Ed.* **2004,** *43*, 1549-1551.

93 Li, N.; Huber, G. W. Aqueous-phase hydrodeoxygenation of sorbitol with Pt/SiO2-Al2O3: Identification of reaction intermediates. *J. Catal.* **2010,** *270*, 48-59.

94 Sohounloue, D. K.; Montassier, C.; Barbier, J. Catalytic hydrogenolysis of sorbitol. *React. Kinet. Catal. Lett.* **1983,** *22*, 391-397.

95 Kim, Y. T.; Dumesic, J. A.; Huber, G. W. Aqueous-phase hydrodeoxygenation of sorbitol: A comparative study of Pt/Zr phosphate and Pt-ReO_x/C. *J. Catal.* **2013,** *304*, 72-85.

96 Moreno, B. M.; Li, N.; Lee, J.; Huber, G. W.; Klein, M. T. Modeling aqueous-phase hydrodeoxygenation of sorbitol over Pt/SiO_2-Al_2O_3. *RSC Adv.* **2013,** *3*, 23769-23784.

97 Li, N.; Tompsett, G. A. & Huber, G. W. Renewable high-octane gasoline by aqueous-phase hydrodeoxygenation of C_5 and C_6 carbohydrates over Pt/Zirconium phosphate catalysts. *ChemSusChem* **2010,** *3*, 1154-1157.

98 Zhang, Q.; Jiang, T.; Li, B.; Wang, T.; Zhang, X.; Zhang, Q.; Ma, L. Highly selective sorbitol hydrogenolysis to liquid alkanes over Ni/HZSM-5 catalysts modified with pure silica MCM-41. *ChemCatChem* **2012,** *4*, 1084-1087.

99 Tronconi, E. Feriazzo, N.; Forzatti, P.; Pasquon, I.; Casale, B. Marini, L. A mathematical-model for the catalytic hydrogenolysis of carbohydrates. *Chem. Eng. Sci.* **1992,** *47*, 2451-2456.

100 Ye, L. M.; Duan, X. P.; Lin, H. Q.; Yuan, Y. Z. Improved performance of magnetically recoverable Ce-promoted Ni/Al_2O_3 catalysts for aqueous-phase hydrogenolysis of sorbitol to glycols. *Catal. Today* **2012,** *183,* 65-71.

101 Werpy, T. A.; Frye, J. G.; Zacher, A. H.; Miller, D. J. Hydrogenolysis of sugars and sugar alcohols. European patent: 1939161, **2008**.

102 Blanc, B.; Bourrel, A.; Gallezot, P.; Haas, T.; Taylor, P. Starch-derived polyols for polymer technologies: preparation by hydrogenolysis on metal catalysts. *Green Chem.* **2000,** *2,* 89-91.

103 Clark, I. T. Hydrogenolysis of sorbitol. *Ind. Eng. Chem.* **1958,** *50,* 1125-1126.

104 Montassier, C.; Menezo, J. C.; Hoang, L. C.; Renaud, C.; Barbier, J. Aqueous polyol conversions on ruthenium and on sulfur-modified ruthenium. *J. Mol. Catal.* **1991,** *70,* 99−110.

105 Wang, K. Y.; Hawley, M. C.; Furney, T. D. Mechanism study of sugar and sugar alcohol hydrogenolysis using 1,3-Diol model compounds. *Ind. Eng. Chem. Res.* **1995,** *34,* 3766-3770.

106 Chopade, S. P. Frye, J. G. Jr.; Jackson, J. E., Miller, D. J.; Werpy, T. A.; Zacher, A. H. Catalysts and process for hydrogenolysis of sugar alcohols to polyols. World patent: 2001066499, **2001**.

107 Banu, M.; Venuvanalingam, P.; Shanmugam, R.; Viswanathan, B.; Sivasanker, S. Sorbitol hydrogenolysis over Ni, Pt and Ru supported on NaY. *Top. Catal.* **2012,** *55,* 897-907.

108 Huber, G. W.; Li, N. Aqueous-phase hydrodeoxygenation of sorbitol with Pt/SiO_2-Al_2O_3: Identification of reaction intermediates. *J. Catal.* **2010,** *270,* 48-59.

109 Dumesic, J. A.; Simonetti, D. A.; Kunkes, E. L. Gas-phase conversion of glycerol to synthesis gas over carbon-supported platinum and platinum-rhenium catalysts. *J. Catal.* **2007,** *247,* 298-306.

110 Byrd, A. J.; Pant, K. K.; Gupta, R. B. Hydrogen production from glycerol by reforming in supercritical water over Ru/Al_2O_3 catalyst. *Fuel* **2008,** *87,* 2956-2960.

111 Beltramini, J. N.; Tanksale, A.; Zhou, C. H.; Lu, G. Q. Hydrogen production by aqueous phase reforming of sorbitol using bimetallic Ni-Pt catalysts: metal support interaction. *J. Incl. Phenom. Macro.* **2009,** *65,* 83-88.

112 Wen, G. D.; Xu, Y. P.; Ma, H. J.; Xu, Z. S.; Tian, Z. J. Production of hydrogen by aqueous-phase reforming of glycerol. *Int. J. Hydrogen Energy* **2008,** *33,* 6657-6666.

113 Chaminand, J. Djakovitch, L.; Gallezot, P.; Marion, P.; Pinel, C.; Rosier, C. Glycerol hydrogenolysis on heterogeneous catalysts. *Green Chem.* **2004,** *6,* 359-361.

114 Perosa, A.; Tundo, P. Selective hydrogenolysis of glycerol with Raney nickel. *Ind. Eng. Chem. Res.* **2005,** *44,* 8535-8537.

115 Miyazawa, T.; Kusunoki, Y.; Kunimori, K.; Tomishige, K. Glycerol conversion in the aqueous solution under hydrogen over Ru/C plus an ion-exchange resin and its reaction mechanism. *J. Catal.* **2006,** *240,* 213-221.

116 Davis, R. J.; Maris, E. P. Hydrogenolysis of glycerol over carbon-supported Ru and Pt catalysts. *J. Catal.* **2007,** *249,* 328-337.

117 Liu, H. C.; Wang, S. Selective hydrogenolysis of glycerol to propylene glycol on Cu-ZnO catalysts. *Catal. Lett.* **2007,** *117,* 62-67.

118 Tomishige, K.; Miyazawa, T.; Koso, S.; Kunimori, K. Glycerol hydrogenolysis to 1,2-propanediol catalyzed by a heat-resistant ion-exchange resin combined with Ru/C. *Appl. Catal., A* **2007,** *329,* 30-35.

119 Huang, Z.; Cui, F.; Kang, H.; Chen, J.; Zhang, X.; Xia, C. Highly dispersed silica-supported copper nanoparticles prepared by precipitation-gel method: A simple but efficient and stable catalyst for glycerol hydrogenolysis. *Chem. Mater.* **2008,** *20,* 5090-5099.

120 Jin, X.; Subramaniam, B.; Chaudhari, R. V. Activity and Selectivity of Base Promoted Mono and Bimetallic Catalysts for Hydrogenolysis of Xylitol and Sorbitol. ACS Symposium Series 1132. American Chemical Society: Washington, DC, **2013**; pp 273-285.

121 D'Hondt, E.; de Vyver, S. V.; Sels, B. F.; Jacobs, P. A. Catalytic glycerol conversion into 1,2-propanediol in absence of added hydrogen. *Chem. Commun.* **2008,** 6011-6012.

122 Roy, D.; Subramaniam, B.; Chaudhari, R. V. Aqueous phase hydrogenolysis of glycerol to 1,2-propanediol without external hydrogen addition. *Catal. Today* **2010,** *156,* 31-37.

123 Barbelli, M. L.; Santori, G. F.; Nichio, N. N. Aqueous phase hydrogenolysis of glycerol to bio-propylene glycol over Pt-Sn catalysts. *Bioresour. Technol.* **2012,** *111,* 500-503.

124 Mane, R. B.; Rode, C. V. Simultaneous glycerol dehydration and in situ hydrogenolysis over Cu-Al oxide under an inert atmosphere. *Green Chem.* **2012,** *14,* 2780-2789.

125 Auneau, F.; Michel, C.; Delbecq, F.; Pinel, C.; Sautet, P. Unravelling the mechanism of glycerol hydrogenolysis over rhodium catalyst through combined experimental-theoretical investigations. *Chem.-Eur. J.* **2011,** *17,* 14288-14299.

126 Kunkes, E. L. Simonetti, D. A.; Dumesic, J. A.; Pyrz, W. D.; Murillo, L. E.; Chen, J. G.; Buttrey, D. J. The role of rhenium in the conversion of glycerol to synthesis gas over carbon supported platinum-rhenium catalysts. *J. Catal.* **2008,** *260,* 164-177.

127 Xia, S. X.; Yuan, Z. L.; Wang, L. N.; Chen, P.; Hou, Z. Y. Hydrogenolysis of glycerol on bimetallic Pd-Cu/solid-base catalysts prepared via layered double hydroxides precursors. *Appl. Catal., A* **2011,** *403,* 173-182.

128 Auneau, F.; Noel, S.; Aubert, G.; Besson, M.; Djakovitch, L.; Pinel, C. On the role of the atmosphere in the catalytic glycerol transformation over iridium-based catalysts. *Catal. Commun.* **2011,** *16,* 144-149.

129 Auneau, F.; Arani, L. S.; Besson, M.; Djakovitch, L.; Michel, C.; Delbecq, F.; Sautet, P.; Pinel, C. Heterogeneous transformation of glycerol to lactic acid. *Top. Catal.* **2012,** *55,* 474-479.

130 Liu, B.; Greeley, J. A density functional theory analysis of trends in glycerol decomposition on close-packed transition metal surfaces. *Phys. Chem. Chem. Phys.* **2013,** *15,* 6475-6485.

131 Liu, B.; Greeley, J. Decomposition pathways of glycerol via C-H, O-H, and C-C bond scission on Pt(111): A density functional theory study. *J. Phys. Chem. C* **2011,** *115,* 19702-19709.

132 Liu, B.; Greeley, J. Density functional theory study of selectivity considerations for C-C versus C-O bond scission in glycerol decomposition on Pt(111). *Top. Catal.* **2012,** *55,* 280-289.

133 Musolino, M. G.; Scarpino, L. A.; Mauriello, F.; Pietropaolo, R. Selective transfer hydrogenolysis of glycerol promoted by palladium catalysts in absence of hydrogen. *Green Chem.* **2009,** *11,* 1511-1513.

134 John, R. P.; Nampoothiri, K. M.; Pandey, A. Fermentative production of lactic acid from biomass: an overview on process developments and future perspectives. *Appl. Microbiol. Biot.* **2007,** *74,* 524-534.

135 Datta, R. Hydroxycarboxylic acids. *Kirk-Othmer Encyclopedia of Chemical Technology*. John Wiley & Sons, Inc. **2001**.

136 Datta, R.; Tsai, S. P.; Bonsignore, P.; Moon, S. H.; Frank, J. R. Technological and economic-potential of poly(lactic acid) and lactic-acid derivatives. *Fems. Microbiol. Rev.* **1995,** *16,* 221-231.

137 Shen, Z.; Jin, F.; Zhang, Y.; Wu, B.; Kishita, A.; Tohji, K.; Kishida, H. Effect of alkaline catalysts on hydrothermal conversion of glycerin into lactic acid. *Ind. Eng. Chem. Res.* **2009,** *48,* 8920-8925.

138 Jin, X., Roy, D., Subramaniam, B. & Chaudhari, R. V. One pot synthesis of lactic acid from sugars and polyols. AIChE Annual Meeting, Pittsburgh, PA, Oct. 28-Nov. 2, **2012**.

139 Shen, Y. H.; Zhang, S. H.; Li, H. J.; Ren, Y.; Liu, H. C. Efficient synthesis of lactic acid by aerobic oxidation of glycerol on Au-Pt/TiO_2 catalysts. *Chem.-Eur. J.* **2010,** *16,* 7368-7371.

140 Zope, B. N.; Hibbitts, D. D.; Neurock, M.; Davis, R. J. Reactivity of the gold/water interface during selective oxidation catalysis. *Science* **2010,** *330,* 74-78.

141 Onda, A.; Ochi, T.; Kajiyoshi, K.; Yanagisawa, K. A new chemical process for catalytic conversion Of D-glucose into lactic acid and gluconic acid. *Appl. Catal., A* **2008,** *43,* 49-54.

142 Onda, A.; Ochi, T.; Kajiyoshi, K.; Yanagisawa, K. Lactic acid production from glucose over activated hydrotalcites as solid base catalysts in water. *Catal. Commun.* **2008,** *9,* 1050-1053.

143 Sautet, P.; Auneau, F.; Michel, C.; Delbecq, F.; Pinel, C. Dehydrogenation vs. dehydration in the rhodium catalyzed glycerol hydrogenolysis from a combined theoretical and experimental study. 242nd ACS National Meeting, Denver, CO, August 28th-September 1st, **2011**.

144 Yan, X. Y.; Jin, F. M.; Tohji, K.; Kishita, A.; Enomoto, H. Hydrothermal conversion of carbohydrate biomass to lactic acid. *AIChE J.* **2010,** *56,* 2727-2733.

145 Kusserow, B.; Schimpf, S.; Claus, P. Hydrogenation of glucose to sorbitol over nickel and ruthenium catalysts. *Adv. Synth. Catal.* **2003,** *345,* 289-299.

146 Davda, R. R.; Shabaker, J. W.; Huber, G. W.; Cortright, R. D.; Dumesic, J. A. A review of catalytic issues and process conditions for renewable hydrogen and alkanes by aqueous-phase reforming of oxygenated hydrocarbons over supported metal catalysts. *Appl. Catal., B* **2005,** *56,* 171-186.

147 Vasiliu, M.; Guynn, K.; Dixon, D. A. Prediction of the thermodynamic properties of key products and intermediates from biomass. *J. Phys. Chem. C* **2011,** *115,* 15686-15702.

148 Ramachandran, P. A. C.; Chaudhari, R. V. Three Phase Catalytic Reactors. Gordon & Breach: New York ,**1983**.

149 Krichevsky, I. R.; Kasarnovsky, J. S. Thermodynamical calculations of solubilities of nitrogen and hydrogen in water at high pressure. *J. Am. Chem. Soc.* **1935,** *57,* 2168-2171.

150 Lide, D. R. *et al. CRC Handbook of Chemistry and Physics*. Taylor & Francis Group, **2010**.

151 Zhao, L.; Zhou, J.; Yang, G.; Ji, Y.; Zhang, M.; Chen, H.; Zhou, X. Sorbitol hydrogenolysis to glycols over carbon nanofibers/graphite-felt composite-supported Ru catalyst in a trickle bed reactor. *Energy Source Part A* **2012,** *34,* 430-438.

152 Zhou, J. H.; Zhang, M.; Zhao, L.; Li, P.; Zhou, X.; Yuan, W. Carbon nanofiber/graphite-felt composite supported Ru catalysts for hydrogenolysis of sorbitol. *Catal. Today* **2009,** *147,* S225-S229.

153 Bravo-Suarez, J. J.; Subramaniam, B.; Chaudhari, R. V. Vapor-phase methanol and ethanol coupling reactions on CuMgAl mixed metal oxides. *Appl. Catal.,A* **2013,** *455,* 234-246.

154 Chen, X. G.; Wang, X. C.; Yao, S. X.; Mu, X. D. Hydrogenolysis of biomass-derived sorbitol to glycols and glycerol over Ni-MgO catalysts. *Catal. Commun.* **2013,** *39,* 86-89.

155 Zhao, L.; Zhou, J.; Chen, H.; Zhang, M.; Sui, Z.; Zhou, X. Carbon nanofibers supported Ru catalyst for sorbitol hydrogenolysis to glycols: effect of calcination. *Korean J. Chem. Eng.* **2010,** *27,* 1412-1418.

156 Nagaraja, B. M.; Padmasri, A. H.; Seetharamulu, P.; Hari Prasad Reddy, K.; David Raju, B.; Rama Rao, K. S. A highly, active Cu-MgO-Cr_2O_3 catalyst for simultaneous synthesis of furfuryl alcohol and cyclohexanone by a novel coupling route - Combination of furfural hydrogenation and cyclohexanol dehydrogenation. *J. Mol. Catal. A-Chem.* **2007,** *278,* 29-37.

157 Mitsudome, T.; Mikami, Y.; Ebata, K.; Mizugaki, T.; Jitsukawa, K.; Kaneda, K. Copper nanoparticles on hydrotalcite as a heterogeneous catalyst for oxidant-free dehydrogenation of alcohols. Chem. Commun. **2008,** *39,* 4804-4806.

158 Peng, L. C.; Lin, L.; Zhang, J.; Zhuang, J.; Zhang, B.; Gong, Y. Catalytic conversion of cellulose to levulinic acid by metal chlorides. *Molecules* **2010,** *15,* 5258-5272.

159 Davis, M. E.; Roman-Leshkov, Y.; Moliner, M.; Labinger, J. A. Mechanism of glucose isomerization using a solid lewis acid catalyst in water. *Angew. Chem., Int. Ed.* **2010,** *49,* 8954-8957.

160 Jin, X.; Subramaniam, B.; Chaudhari, R. V. Hydrogenolysis of polyols over Cu/hydrotalcite catalysts to value-added chemicals: A new multifunctional catalyst. International Congress of Catalysis Meeting, Munich, Germany, July 1-6, **2012**.

161 Jin, X.; Subramaniam, B.; Chaudhari, R. V. One-pot conversion of sugars and sugar alcohols to value-added chemicals. Center for Environmentally Beneficial Catalysis Industry Advisory Board Meeting, Lawrence, KS, Oct. 3-4, **2011**.

162 Jin, X.; Dang, L.; Lohrman, J.; Subramaniam, B.; Ren, S.; Chaudhari, R. V. Lattice-matched bimetallic CuPd-graphene nanocatalysts for facile conversion of biomass-derived polyols to chemicals. *ACS Nano* **2013,** ***7***, 1309-1316.

163 Jin, X.; Roy, D.; Thapa, P. S.; Subramaniam, B.; Chaudhari, R. V. Atom economical aqueous-phase conversion (APC) of biopolyols to lactic acid, glycols, and linear alcohols using supported metal catalysts. *ACS Sustain. Chem. Eng.* **2013,** *1,* 1453-1462.

164 Ramirez-Lopez, C. A.; Ochoa-Gomez, J. R.; Fernandez-Santos, M.; Gomez-Jimenez-Aberasturi, O.; Alonso-Vicario, A.; Torrecilla-Soria, J. Synthesis of lactic acid by alkaline hydrothermal conversion of glycerol at high glycerol concentration. *Ind. Eng. Chem. Res.* **2010,** *49,* 6270-6278.

165 Davda, R. R.; Shabaker, J. W.; Huber, G. W.; Cortright, R. D.; Dumesic, J. A. Aqueous-phase reforming of ethylene glycol on silica-supported metal catalysts. *Appl. Catal., B* **2003,** *43,* 13-26.

166 Green, D. W.; Perry, R. H. *Perry's Chemical Engineers' Handbook*. McGraw-Hill, **2007**.

167 Mok, W. S. L.; Antal, M. J.; Jones, M. Formation of acrylic-acid from lactic-acid in supercritical water. *J. Org. Chem.* **1989,** *54,* 4596-4602.

168 Lira, C. T.; Mccrackin, P. J. Conversion of lactic-acid to acrylic-acid in near-critical water. *Ind. Eng. Chem. Res.* **1993,** *32,* 2608-2613.

169 Aguilera, A.; Alcantara, A. R.; Marinas, J. M.; Sinisterra, I. V. $Ba(OH)_2$ as the catalyst in organic-reactions .14. mechanism of claisen-schmidt condensation in solid liquid conditions. *Can. J. Chem.* **1987,** *65,* 1165-1171.

170 Roman-Leshkov, Y.; Moliner, M.; Labinger, J. A.; Davis, M. E. Mechanism of glucose isomerization using a solid lewis acid catalyst in water. *Angew. Chem., Int. Ed.* **2010,** *49,* 8954-8957.

171 Machell, G.; Richards, G. N. Mechanism of saccharinic acid formation .3. The alpha-keto-aldehyde intermediate in formation of D-glucometasaccharinic acid. *J. Chem. Soc*. **1960,** 1938-1943.

172 Assary, R. S.; Curtiss, L. A. Theoretical study of 1,2-hydride shift associated with the isomerization of glyceraldehyde to dihydroxy acetone by lewis acid active site models. *J. Phys. Chem. A* **2011,** *115,* 8754-8760.

173 ten Dam, J.; Kapteijn, F.; Djanashvili, K.; Hanefeld, U. Tuning selectivity of $Pt/CaCO_3$ in glycerol hydrogenolysis - A design of experiments approach. *Catal. Commun.* **2011,** *13,* 1-5.

174 Mori, K.; Yamada, Y.; Sato, S. Catalytic dehydration of 1,2-propanediol into propanal. *Appl. Catal., A* **2009,** *366,* 304-308.

175 Zhang, D. Z.; Barri, S. A. I.; Chadwick, D. Dehydration of 1,2-propanediol to propionaldehyde over zeolite catalysts. *Appl. Catal., A* **2011,** *400,* 148-155.

176 Salciccioli, M.; Chen, Y.; Vlachos, D. G. Density functional theory-derived group additivity and linear scaling methods for prediction of oxygenate stability on metal catalysts: adsorption of open-ring alcohol and polyol dehydrogenation intermediates on Pt-based metals. *J. Phys. Chem. C* **2010,** *114,* 20155-20166.

177 Wawrzetz, A.; Peng, B.; Hrabar, A.; Jentys, A.; Lemonidou, A. A.; Lercher, J. A. Towards understanding the bifunctional hydrodeoxygenation and aqueous phase reforming of glycerol. *J. Catal.* **2010,** *269,* 411-420.

178 Basaran, D.; Genest, A.; Rosch, N. Comment on "Towards understanding the bifunctional hydrodeoxygenation and aqueous phase reforming of glycerol" [*J. Catal.* **2010,** *269,* 411-420]. *J. Catal.* **2012,** *287,* 210-213.

179 Recasens, F.; Velo, E.; Larrayoz, M. A.; Puiggene, J. Endothermic character of toluene adsorption from supercritical carbon-dioxide on activated carbon at low-coverage. *Fluid Phase Equilibr.* **1993,** *90,* 265-287.

180 Chheda, J. N.; Huber, G. W.; Dumesic, J. A. Liquid-phase catalytic processing of biomass-derived oxygenated hydrocarbons to fuels and chemicals. *Angew. Chem., Int. Ed.* **2007,** *46,* 7164-7183.

181 Jacobs, G.; Williams, L.; Graham, U.; Thomas, G. A.; Sparks, D. E.; Davis, B. H. Low temperature water-gas shift: in situ DRIFTS-reaction study of ceria surface area on the evolution of formates on Pt/CeO_2 fuel processing catalysts for fuel cell applications. *Appl. Catal., A* **2003,** *252,* 107-118.

182 Shao-Horn, Y.; Sheng, W. C.; Chen, S.; Ferreira, P. J.; Holby, E. F.; Morgan, D. Instability of supported platinum nanoparticles in low-temperature fuel cells. *Top. Catal.* **2007,** *46*, 285-305.

183 Daw, M. S.; Foiles, S. M. Calculations of the energetics and structure of Pt(110) using the embedded atom method. *J. Vac. Sci. Technol., A* **1986,** *4*, 1412-1413.

184 Foiles, S. M.; Baskes, M. I.; Daw, M. S. Embedded-atom-method functions for the fcc metals Cu, Ag, Au, Ni, Pd, Pt, and their alloys. *Phys. Rev. B* **1986,** *33*, 7983-7991.

185 Petroski, J. M.; Wang, Z. L.; Green, T. C.; El-Sayed, M. A. Kinetically controlled growth and shape formation mechanism of platinum nanoparticles. *J. Phys. Chem. B* **1998,** *102*, 3316-3320.

186 Narayanan, R.; El-Sayed, M. A. Catalysis with transition metal nanoparticles in colloidal solution: Nanoparticle shape dependence and stability. *J. Phys. Chem. B* **2005,** *109*, 12663-12676.

187 Narayanan, R.; El-Sayed, M. A. Effect of colloidal nanocatalysis on the metallic nanoparticle shape: The Suzuki reaction. *Langmuir* **2005,** *21*, 2027-2033.

188 Parthasarathy, P.; Virkar, A. V. Electrochemical ostwald ripening of Pt and Ag catalysts supported on carbon. *J. Power Sources* **2013,** *234*, 82-90.

189 Simonsen, S. B.; Chorkendorff, I.; Dahl, S.; Skoglundh, M.; Sehested, J.; Helveg, S. Direct observations of oxygen-induced platinum nanoparticle ripening studied by in situ TEM. *J. Am. Chem. Soc.* **2010,** *132*, 7968-7975.

190 Aragane, J.; Urushibata, H.; Murahashi, T. Effect of operational potential on performance decay rate in a phosphoric acid fuel cell. *J. Appl. Electrochem.* **1996,** *26*, 147-152.

191 Hong, C.; Jin, X.; Harak, E.; Totleben, J.; Lohrman, J.; Subramaniam, B.; Chaudhari, R.V.; Ren, S. Graphene oxide stabilized Cu_2O for shape selective nanocatalysis. *J. Mater. Chem. A*, **2014,** DOI:10.1039/C4TA00599F.

192 Li, X. S.; Cai, W.; An, J.; Kim, S.; Nah, J.; Yang, D.; Piner, R.; Velamakanni, A.; Jung, I.; Tutuc, E.; Banerjee, S. K.; Colombo, L.; Ruoff, R. Large-area synthesis of high-quality and uniform graphene films on copper foils. *Science* **2009,** *324*, 1312-1314.

193 Huang, J. H.; Chen, H. J.; Hsieh, C. C.; Lee, G. H.; Peng, S. M. Synthesis and characterization five-coordinate molybdenum compounds bearing bi- or tridentate substituted pyrrole ligands: molecular structures of $\{Mo(NC_6H_3Pr^i_2\text{-}2,6)_2R[NC_4H_3(CH_2NMe_2)\text{-}2]\}$ and $\{Mo(NC_6H_3Pr^i_2\text{-}2,6)_2Cl[NC_4H_2(CH_2NMe_2)_2\text{-}2,5]\}$, where R = Cl, Me, Bu. *Inorg. Chim. Acta* **2001,** *321*, 142-148.

194 Chen, S. S.; Brown, L.; Levendorf, M.; Cai, W. W.; Ju, S. Y.; Edgeworth, J.; Li, X. S.; Magnuson, C. W.; Velamakanni, A.; Piner, R. D.; Kang, J. Y.; Park, J.; Ruoff, R. S. Oxidation resistance of graphene-coated Cu and Cu/Ni alloy. *ACS Nano* **2011,** *5*, 1321-1327.

195 Rioux, R. M.; Vannice, M. A. Hydrogenation/dehydrogenation reactions: isopropanol dehydrogenation over copper catalysts. *J. Catal.* **2003,** *216,* 362-376.

196 Kirkeminde, A.; Retsch, M.; Wang, Q.; Xu, G.; Hui, R.; Wu, J.; Ren, S. Surface-passivated plasmonic nano-pyramids for bulk heterojunction solar cell photocurrent enhancement. *Nanoscale* **2012,** *4,* 4421-4425.

197 Balogh, L.; Tomalia, D. A. Poly(amidoamine) dendrimer-templated nanocomposites. 1. Synthesis of zerovalent copper nanoclusters. *J. Am. Chem. Soc.* **1998,** *120,* 7355-7356.

198 Chan, G. H.; Zhao, J.; Hicks, E. M.; Schatz, G. C.; Van Duyne, R. P. Plasmonic properties of copper nanoparticles fabricated by nanosphere lithography. *Nano. Lett.* **2007,** *7,* 1947-1952.

199 Rao, R. S.; Bansil, A.; Asonen, H.; Pessa, M. Electronic-structure of copper-rich copper-palladium alloys. *Phys. Rev. B* **1984,** *29,* 1713-1721.

200 Toshima, N.; Wang, Y. Preparation and catalysis of novel colloidal dispersions of copper noble-metal bimetallic clusters. *Langmuir* **1994,** *10,* 4574-4580.

201 Gokhale, A. A.; Dumesic, J. A.; Mavrikakis, M. On the mechanism of low-temperature water gas shift reaction on copper. *J. Am. Chem. Soc.* **2008,** *130,* 1402-1414.

202 Contescu, C. I.; Brown, C. M.; Liu, Y.; Bhat, V. V.; Gallego, N. C. Detection of hydrogen spillover in palladium-modified activated carbon fibers during hydrogen adsorption. *J. Phys. Chem. C* **2009,** *113,* 5886-5890.

Appendix I General operation procedures and data analysis

Operation procedures of GC

(a): Turn on helium gas supply to GC, and then the power of GC was turned on. The software was then opened and a beep sound comes out from the system indicating the instrument was connected with the software. Start the GC by pressing “System” followed by “PF1” button in the instrument; (b): Select the method that would be used for quantifying the gas composition. Then confirm both detectors, “DFID1” and “DTCD1” are controlled by pressing “DET”; (c): The FID detector needs hydrogen and air supplies to be turned on. Once the temperature of detector is above 150 ^{o}C, hydrogen and air supplies could be turned on. The FID could be ignited manually by pressing “DET” followed by “PF1”. Then check the status of FID by pressing “DET”; (d): Once desired detector and oven temperature was reached, the monitor screening on the instrument would display “Ready”. It is strongly suggested that another 30~60 min waiting time should be added to let the base line stabilize; (e): Check the sampling loop to make sure the outlet of the fixed bed reactor (besides GC) was shut off and by-pass valve is opened. Then connect the reactor with GC sampling loop, open the outlet valve of the reactor to flush the loop before starting the analysis. The flow rate of gas was set at roughly 25~35 mL/min, as indicated by the flow meter; (f): After about 2 min flushing, start analysis by clicking “Run” on the toolbar of the software. Entering information about sample ID, file paths, and sample information (in description) and press submit;

(g): A beep sound would come out from the software followed by the sound of opening the inlet valve of GC. It would take about 3 min to collect enough gas samples for analysis. Then the valve was switched to a by-pass line; (h): The reactor could be disconnected at this stage. First close the outlet valve of the reactor to deplete the gas remaining in the loop. Once there is no gas flow in the loop (indicated by the flow meter), close the controlling valve on the loop line, disconnect the reactor and seal the loop. It would take 35 min to complete the whole analysis process.

Calibration of HPLC (Examples)

Detailed procedures of calibration for sorbitol and xylitol (as examples) are described as follows: (a): Certain amounts of sorbitol and xylitol were measured carefully and charged into a 25 mL volumetric flask; (b): deionized water was added to the flask slowly until the liquid level reached 25 mL line; (c): The flask was shaken vigorously at room temperature for at least 1 min; (d): The solution was set still at room temperature at least 4 h before analysis; (e): The exact weight of measured sorbitol and xylitol was noted in the textbook and the corresponding concentration was calculated; (f): Another three solution of sorbitol, xylitol and 1,2-butanediol were prepared repeating (a) to (e); (g): About 1 mL of the aqueous solution was added to HPLC vials accordingly, which was then injected into HPLC for calibration.

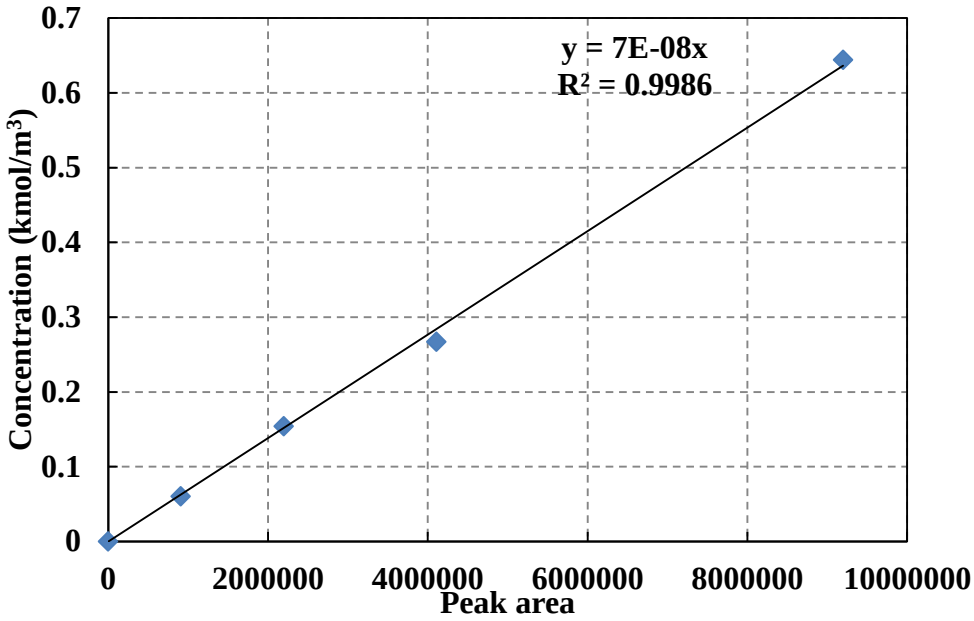

Figure 1-1 Sorbitol calibration at 0.5 mL/min (mobile phase) and 60 ^{o}C (oven temperature)

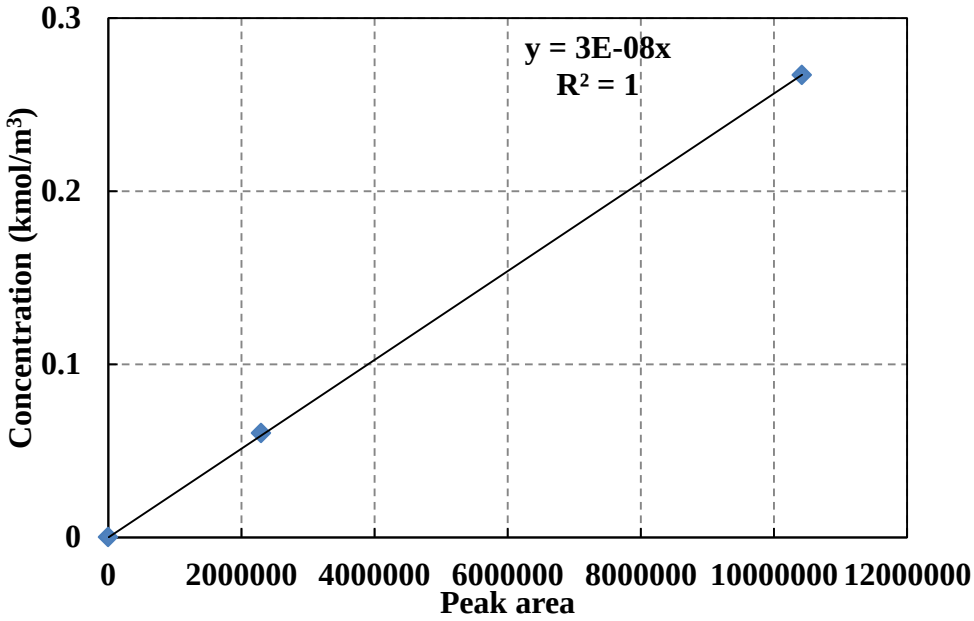

Figure 1-2 Sorbitol calibration at 0.2 mL/min (mobile phase) and 60 ^{o}C (oven temperature)

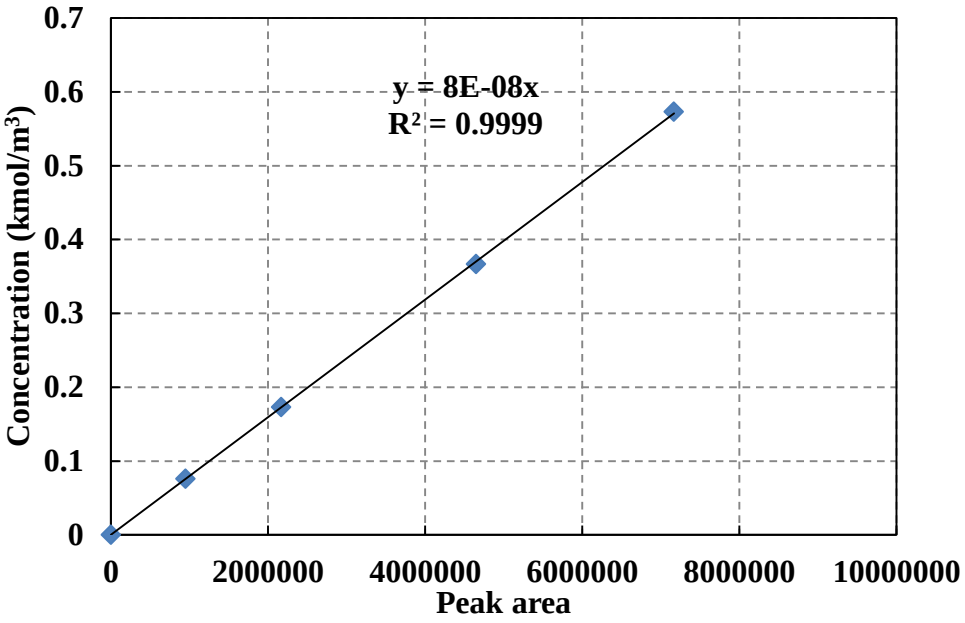

Figure 1-3 Xylitol calibration at 0.5 mL/min (mobile phase) and 60 ^{o}C (oven temperature)

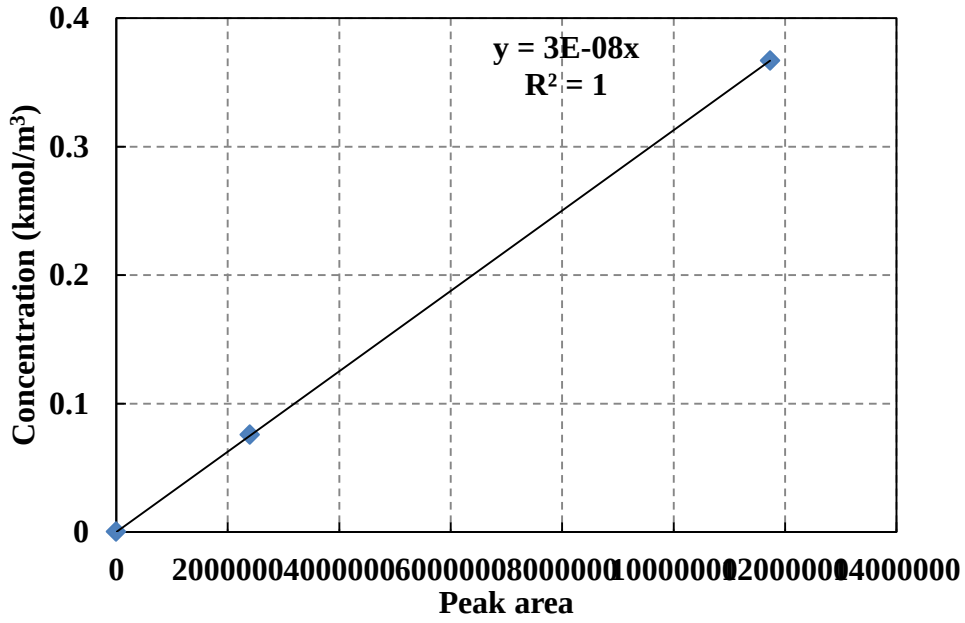

Figure 1-4 Xylitol calibration at 0.2 mL/min (mobile phase) and 60 ^{o}C (oven temperature)

Calculation of material balance (An example)

Table 1-1. A typical spreadsheet for material balance

Initial Concentration	Co (kmol/m^3)	C (×10^3) mol	C*	X (%)
Sorbitol	0.59	329.22		64.220
Final Liquid Products	**Co (mol/L)**	**C (×10^3) mol**	**C**	**S (%)**
Sorbitol	0.2170	117.086	6	
C6		0.000	6	0.000
Xylitol		0.000	5	0.000
Pentanediol		0.000	5	0.000
C5		0.000	5	0.000
1,2-Butanediol	0.0470	17.484	4	8.400
1,3 or 2,3-Butanediol		0.000	4	0.000
C4		0.000	4	0.000
Pyruvaldehyde	0.0600	16.740	3	8.043
Glycerol	0.0300	8.370	3	4.021
1,2-Propanediol	0.3450	96.255	3	46.247
Lactic Acid	0.0730	20.367	3	9.786
IPA		0.000	3	0.000
1-Propanol		0.000	3	0.000
Ethylene Glycol	0.1670	31.062	2	14.924
Ethanol	0.0170	3.162	2	1.519
Methanol	0.1430	13.299	1	6.390
Acetic Acid		0.000	2	0.000
SUM		327.825		99.330
Final Gas Products	**Co (mol/m3)**	**C (×10^3) mol**	**C**	**X or S (%)**
Methane		0.000	1	0.000
Ethane		0.000	2	0.000
Propane		0.000	3	0.000
n-butane		0.000	4	0.000
n-pentane		0.000	5	0.000
Carbon Monoxide		0.000	1	0.000
Carbon Dioxide		0.000	1	0.000
SUM		0.000		0.000
Carbon Balance		0.996		99.330

As shown in Table 1-1, a typical spreadsheet for the calculation of conversion, selectivity and carbon balance is summarized. After a batch test, the final liquid volume can be measured in a graduated cylinder. Thus the conversion of sorbitol can be calculated accordingly. It is important to note that the total amounts of carbon in sorbitol in the initial solution can be calculated based on the amounts of sorbitol charged into reactor and total carbon number of sorbitol (6 carbon atoms):

$$Total\ carbon\ of\ sorbitol\ in\ initial\ solution = \frac{10\ g\ of\ sorbitol \times 6}{182.1\ g\ sorbitol/mol}$$

$$= 0.329\ mol$$

The total amounts of carbon of sorbitol in the final solution can be calculated based on sorbitol concentration, volume of solution (90 mL = 0.09 L) and total carbon number of sorbitol (6 carbon atoms):

$$Total\ carbon\ of\ sorbitol\ in\ final\ solution$$

$$= 0.217\ kmol/m^3 \times 0.09 \times 10^{-3} m^3 \times 6$$

$$= \ 0.117\ \times 10^{-3} kmol$$

Therefore conversion of sorbitol is

$$Conversion = \frac{329 - 117}{329} \times 100\% = \ 64\%$$

The selectivity for each product is also calculated based on the carbon numbers. For example, the selectivity for 1,2-propanediol is

$$S = \frac{0.345\ kmol/m^3 \times 0.09 \times 10^{-3} m^3 \times 3}{(329 - 117) \times 10^{-3} kmol} \times 100\% = \ 46.3\%$$

There exist two methods of calculating carbon balance, one using the total amounts of carbon detected in the product solution (including unreacted substrate and generated products), another calculating the sum of the selectivity of each product. The latter one is used throughout the whole thesis because it reflects the actual carbon distribution and accuracy of experiments and analysis.

The total carbon (carbon balance) detected in products is

$$C\% = (8.4 + 8.04 + 4.02 + 46.2 + 9.8 + 14.9 + 1.5 + 6.4) = \ 99.3\%$$

Calculation of material balance for synthesis of lactic acid (example)

Table 1-2. A typical spreadsheet for material balance

Initial Concentration	Co (mol/L)	C (×10^3) mol	C*	X (%)	
Glycerol	1.15	34.528		22.671	shown in HPLC
Final Liquid Products	**Co (mol/L)**	**C (×10^3) mol**	**C**	**S (%)**	
Glycerol	0.890	26.700	3		0.445
Propanediol	0.002	0.060	3	0.767	0.001
Lactic Acid	0.214	6.420	3	82.017	0.107
Pyruvaldehyde	0.000	0.000	3	0.000	
Glyceraldehyde	0.000	0.000	3	0.000	
1-Propanol	0.000	0.000	3	0.000	
Ethylene Glycol	0.000	0.000	2	0.000	
Ethanol	0.000	0.000	2	0.000	
Methanol	0.016	0.160	1	2.044	0.008
Acetic Acid	0.000	0.000	2	0.000	
Glycolic acid	0.000	0.000	2	0.000	

SUM	33.340	84.827
Carbon %	96.560	84.827

If alkalis which are soluble in water was added, such as CaO, $Ba(OH)_2$, and NaOH, liquid products needed to be further treated before injected to HPLC for quantitative analysis. Lactic acid was usually formed in large amounts with the addition of soluble alkalis. Lactic acid was present in the form of lactate salts in the presence of these alkalis. And pH values of final products were usually higher than 11. However, the mobile phase (sulfuric acid solution) and HPLC column can only work under acidic conditions. Therefore acidification of samples is necessary. The detailed description of acidifying reaction liquids have been discussed in the main text. The acidified solution was injected into HPLC and liquid chromatography could be obtained after 35 min analysis.

Because the reaction mixture was diluted, the measured concentration of substrate (*e.g.* glycerol, sorbitol) and products (*e.g.* lactic acid) is lower than actual ones. For example, the measured concentration of glycerol and lactic acid is 0.445 mol/L (kmol/m^3) and 0.107 mol/L (kmol/m^3), respectively, and the volume of liquid products is 30 mL. About 30 mL dilute sulfuric acid solution was mixed completely with 30 mL of the reaction liquid and the final total volume is 60 mL. Thus the concentration was half of the original one. Therefore the actual concentration of glycerol and lactic acid is about 0.890 mol/L (kmol/m^3) and 0.214 mol/L (kmol/m^3). The conversion of glycerol and selectivity towards lactic acid is about 22.7% and 82% respectively.

The methods of calculating conversion and selectivity have been already shown in Appendix I.

Recycle of solid catalysts

The catalyst candidates with leading performances were selected for recycle studies. The experimental procedure is described as follows: (a): A fresh reaction mixture (*e.g.* glycerol+NaOH+water, sorbitol+water) was already prepared before the recycle study. The total volume of the mixture should be about 5~10 mL smaller than required volume of reaction mixture; (b): After reaction liquid was taken out, the remaining solid in the PTFE liner was washed several times, each time with only 1~3 mL of deionized water, and the slurry was collected in a 20 mL vial for centrifuge; (c): The remaining solid catalysts in reaction product mixture were also collected. After liquid samples were taken out for HPLC analysis, the remaining slurry was immediately put into centrifuge at 3000 RPM for 1~10 min. Then the upper layer of the liquid was removed and about 10 mL of fresh deionized water was mixed with the solids and centrifuged for 1~10 min. Same procedure was repeated twice. Identical procedure was also carried out for the solid catalyst obtained in (b); (d): The collected catalysts from (b) and (c) were sealed in the 20 mL vial. The total volume of solid and liquid (water) is about 2~5 mL; (e): For recycle tests, the solid catalyst sample was charged to the cleaned PTFE liner. Then the vial containing solid catalyst was washed several times using fresh reaction mixture prepared in (a), after which the vial was washed by small amount of fresh

deionized water. The total volume of solid catalyst sample slurry, fresh reaction mixture and deionized water is equal to the required volume of reaction mixture. Then the whole mixture was stirred vigorously for 2 min before the recycle study; (f): After the first recycle tests were finished, same procedure from (a) to (e) were repeated as required.

Calculation of mass transfer limitation

Take sorbitol hydrogenolysis on RuRe/C catalyst for example, the calculation of the significance of gas-liquid, liquid-solid and intraparticle mass transfer is described as follows. The equations used in this section are found in reference [1]~[4].

(1) Gas-liquid mass transfer resistance is considered negligible if

$$\alpha_{g-l} = \frac{R_{H_2}}{k_{g-l} \cdot a_b \cdot C_{H_2}^g} < 0.1$$

Where R_{H_2} is the measured rate of hydrogen consumption (kmol/m^3/h), $k_{g-l} \cdot a_b$ is the gas-liquid mass transfer coefficient (1/h) and calculated based on the correlation given by the following equation

$$k_{g-l} \cdot a_b = 1.48 \times 10^{-3} (N)^{2.18} (V_g / V_l)^{1.88} (d_i / d_t)^{2.16} (h_g / h_l)^{1.16}$$

$C_{H_2}^g$ is the hydrogen concentration in gas phase (kmol/m^3).

(2) Liquid-solid mass transfer

Liquid-solid mass transfer will be considered not significant if

$$\alpha_{l-s} = \frac{R_{sor}}{k_{l-s} \cdot a_p \cdot C_{sor}} < 0.1$$

where R_{sor} is the reaction rate of sorbitol (kmol/m^3/h), and a_p, surface area of catalyst particles (m^2/m^3, not metal particle size) per unit volume for spherical shapes is given by $a_p = \frac{6}{d_p}$, d_p is particle diameter (m). C_{sor} is sorbitol concentration.

k_{l-s} is liquid-solid mass transfer coefficient estimated by the following equation.

$$\frac{k_{l-s} \cdot d_p}{D} = 2 + 0.4 \cdot \left[\frac{e \cdot (d_p)^4 \cdot \rho_l^3}{\mu_l^3} \right]^{0.25} \cdot \left[\frac{\mu_l}{\rho_l \cdot D} \right]^{0.333}$$

D is the molecular diffusivity (diffusion coefficient, m^2/h) predicted the following equation

$$D = \frac{7.4 \times 10^{-8} T (\chi M_{sor})^{0.5}}{\mu_l \upsilon_{sor}^{0.6}}$$

(3) Intraparticle mass transfer

The significance of pore diffusion is negligible if

$$\psi = \frac{6}{d_p} \left[\frac{(m+1) \cdot \rho_p \cdot R_{sor}}{2 \cdot D_e \cdot \omega \cdot C_{sor}^l} \right]^{0.5} < 0.2$$

Where is the effective diffusion coefficient and calculated by

$$D_e = D(\varepsilon/\tau)$$

Table 1-3. Evaluation of mass transfer limitation in HDO experiments in Chapter 2

Mass transfer step	Criteria	Calculated values
Gas-liquid	$\alpha_{g-l} = \frac{R_{H_2}}{k_{g-l} \cdot a_b \cdot C^g_{H_2}} < 0.1$	$7\times10^{-4} \sim 1\times10^{-3}$
Liquid-solid	$\alpha_{l-s} = \frac{R_{sor}}{k_{l-s} \cdot a_p \cdot C_{sor}} < 0.1$	$1.27\times10^{-8} \sim 2.55\times10^{-7}$
Intraparticle	$\psi = \frac{6}{d_p}\left[\frac{(m+1)\cdot \rho_p \cdot R_{sor}}{2 \cdot D_e \cdot \omega \cdot C^l_{sor}}\right]^{0.5} < 0.2$	$5.4\times10^{-4} \sim 2.1\times10^{-3}$

Calibration of ICP (An example)

Table 1-4. Preparation of Pt standard for ICP analysis

Item	S1	S2	S3
Pt ICP standard (g)	0.1220	0.4085	1.7957
Total amounts of solution (g)	15.0863	15.3086	15.1883
Pt^{4+} concentration (ppm)	8.09	26.68	118.23

Pt^{4+} concentration (ppm) was calculated by Pt ICP standard (g)/Total amount (g) × 1000

The calibration procedure of ICP for Pt element is shown below: (a) standard Pt^{4+} solution in aqueous phase was prepared by adding known amounts of Pt ICP standard (Sigma-Aldrich, 1000±2 ppm in HCl solution) to 20 mL sample

vials at room temperature. Then DI water was added to the corresponding vial to approximately 15 g of total weight. Three Pt standard solutions were prepared for calibration (Table 1-4). (b) The calibration results of Pt element in JY-2000 are shown in Figure 1-5. The selected wavelength for Pt analysis is 224 nm because the level of deterrence (LOD) is lowest compared with other wavelengths. (c) Reaction mixtures after catalytic tests were taken (about 15 mL) for ICP analysis without further treatment. The Pt content in the aqueous phase was measured in order to evaluate the leaching ratio of Pt during reactions. The measured value of metal content (ppm) in the solution was divided by dilution ratio to calculate the actual metal leaching ratios.

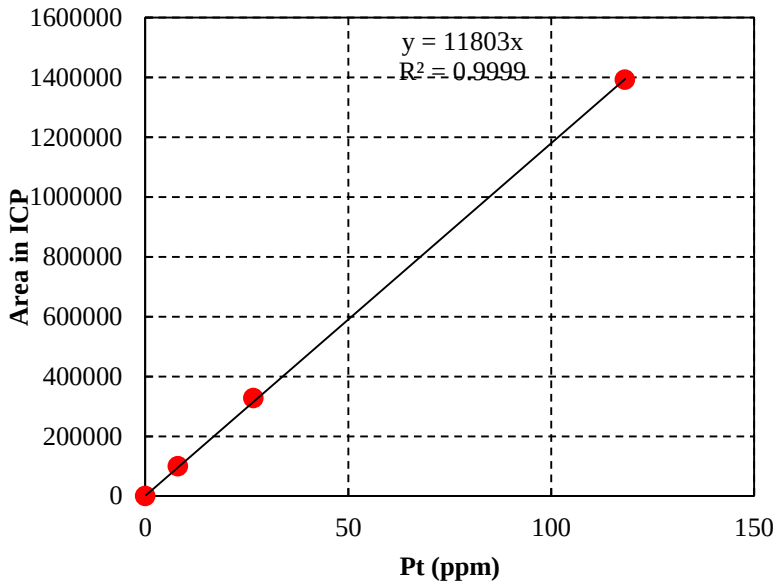

Figure 1-5. Calibration of Pt element for ICP analysis

Calculation of metal content in reaction solution

Cu catalysts (an example)

The measured Cu content from ICP analysis is about 1.97 ppm. The total volume of diluted solution is about 15 mL (See Chapter 5 for details). Therefore the total Cu amounts in the ICP sample is

$$m_{Cu} = 1.97\ ppm \times 0.015\ L = 0.0296\ \text{mg}$$

Because 2 mL sample was taken from the reaction solution. The Cu content in the reaction medium is

$$C_{Cu} = \frac{0.0296\ \text{mg}}{0.002\ L} = 14.8\ ppm$$

The reaction solution was acidified from 30 mL to 50 mL after reaction. The total amount of Cu leached in the reaction solution is

$$m'_{Cu} = 14.8\ ppm \times 0.05\ L = 0.74\ \text{mg}$$

It is known that 0.2 g fresh catalysts with 2w% Cu loading were charged to the reaction medium, therefore the total amounts of Cu on the fresh catalysts are

$$m''_{Cu} = 0.2\ g \times 0.02\ = 0.004\ \text{g} = 4\ \text{mg}$$

The percentage of Cu leached during reaction is about

$$\Delta_{Cu} = \frac{m'_{Cu}}{m''_{Cu}} = \frac{0.74\ mg}{4\ mg} \times 100\% = 18.5\%$$

Error analysis

(1) Experimental error

Key experiments in sorbitol hydrogenolysis (Figures 15~17 in Chapter 2) and tandem glycerol conversion (Figures 8 and 9 in Chapter 4) were repeated and mean values of substrate/product concentration were calculated (see Table 4-4-13 in Appendix IV), the error of which was taken into account when parameter estimation was carried out.

(2) Measuring error

As mentioned in Chapter 2, the maximum error for HPLC analysis (repeated injection of one sample) is only 0.08%, which is much lower compared with experimental error (approximately 3~12%).

(3) Error analysis of reaction parameters-weighted least squares

The goal of suing weighted least squares is to ensure that each data point has an appropriate level of influence on the final parameter estimation. However, it is difficult to evaluate the appropriate level of each component (*e.g.* glycerol, lactic acid, *etc*), therefore the weight factor for each species and replicates (repeated experimental results) were considered is 1.0 during estimation of reaction parameters.

(4) Error analysis in calculation of activation energy

The activation energy was estimated based on reaction rate constants at each temperature. The uncertainty of activation energy for sorbitol hydrogenolysis and tandem glycerol conversion is summarized in Tables 1-5 and 1-6 respectively. The equation for activation energy is $k=k_o \times e^{(-Ea/RT)}$.

Table 1-5. Error analysis for activation energy in sorbitol hydrogenolysis

k_i	T (°C)			E_a (kJ/mol)	ln(k_o)	R^2	Error in E_a			err
	200	215	230				err (200)	err (215)	err (230)	
k_1 (×10^4)	3.22±0.22	4.60±0.40	5.75±0.22	38.33	1.72	0.987	0.40	0.37	0.22	0.33
k_2 (×10^4)	2.53±0.02	5.02±0.25	10.5±1.63	93.39	15.45	0.999	0.57	0.59	5.85	2.34
k_3 (×10^4)	2.44±0.18	4.92±0.16	9.72±0.38	75.98	11.04	0.989	0.54	0.46	1.03	0.68
k_4 (×10^5)	0.77±0.12	2.56±0.36	5.12±0.57	125.98	20.18	0.982	1.21	1.42	1.35	1.33
k_5 (×10^5)	2.37±0.16	5.16±0.28	9.98±0.49	94.78	13.47	0.999	0.63	0.63	0.97	0.73
k_6 (×10^4)	0.51±0.04	1.55±0.39	10.1±3.11	195.81	39.78	0.973	1.23	4.00	13.61	6.28
k_7 (×10^4)	0.74±0.21	1.24±0.08	3.54±2.62	103.26	16.65	0.958	2.76	0.64	36.57	13.32
k_8 (×10^2)	0.87±0.09	1.25±0.44	2.71±0.49	74.64	14.16	0.953	0.54	3.85	1.56	1.99

The unit for error is kJ/mol

Table 1-6. Error analysis for activation energy in tandem glycerol conversion

k_i	T (°C)			E_a (kJ/mol)	ln(k_o)	R^2	Error in E_a			err
	130	145	160				err (130)	err (145)	err (160)	
$k_{s1}\times10^0$	1.33±0.09	1.97±0.15	4.09±0.59	53.0	23.82	0.958	0.42	0.76	0.30	0.49
$k_{s2}\times10^{-1}$	6.09±0.51	10.8±0.50	22.8±3.04	63.7	26.24	0.991	0.53	5.38	1.57	1.88
$k_{s3}\times10^{-2}$	6.48±0.98	24.8±3.38	55.6±14.0	104.2	36.19	0.985	5.57	13.22	5.07	7.14
$k_{s4}\times10^{-2}$	5.95±0.53	12.9±1.48	39.3±4.23	104.2	35.81	0.967	1.55	13.30	4.47	5.25
$k_{s5}\times10^{-2}$	7.00±1.87	24.2±1.64	131.6±9.01	141.6	47.25	0.988	1.37	0.93	2.21	3.14
$k_{s6}\times10^{-1}$	1.12±0.48	2.85±0.39	9.32±2.02	102.3	36.04	0.992	1.64	4.71	1.88	2.84
$K_{gly}\times10^{-2}$	3.83±0.47	3.75±0.25	3.50±0.48	4.3	3.21	0.902	-0.04	0.19	0.09	0.15
$K_{OH^-}\times10^{-3}$	2.21±0.17	1.81±0.22	1.33±0.29	24.5	-5.65	0.980	-0.32	0.77	0.28	0.41
$K_{1,2\text{-}PDO}\times10^{-1}$	3.72±0.08	2.02±0.45	1.01±0.48	63.0	-12.01	0.997	1.80	6.82	2.40	3.19
$K_{EG}\times10^{-2}$	4.00±0.37	2.50±0.48	1.13±0.12	60.9	-15.89	0.972	1.25	0.51	0.55	0.86

The unit for error is kJ/mol

Error analysis in calculation of activation energy (example)

(a) Functions for error propagation are listed in Table 1-7, which will be used to calculate the error (uncertainty) of activation energy.

Table 1-7. Functions for propagation of error

Function	Propagated error
$z = a + b$	$\Delta z = [(\Delta a)^2 + (\Delta b)^2]^{1/2}$
$z = a \times b$	$\frac{\Delta z}{z} = \left[\left(\frac{\Delta a}{a}\right)^2 + \left(\frac{\Delta b}{b}\right)^2\right]^{1/2}$
$z = lna$	$\Delta z = \frac{\Delta a}{a}$

Δa is the uncertainty of a.

(b) The uncertainty for activation energy is determined by the following equation:

$$\ln(k_T) = \ln(k_o) - {}^{E_a}/_{RT}$$

After rearrangement,

$$E_a = RT[\ln(k_o) - \ln(k_T)]$$

Therefore, the uncertainty for activation energy,

$$\frac{\Delta E_a}{E_a} = \left[\left(\frac{\Delta RT}{RT}\right)^2 + \left(\frac{\Delta[\ln(k_o) - \ln(k_T)]}{[\ln(k_o) - \ln(k_T)]}\right)^2\right]^{1/2}$$

$$\frac{\Delta E_a}{E_a} = \left[\left(\frac{\Delta T}{T}\right)^2 + \left(\frac{\Delta[\ln(k_o)] + \Delta\,[\ln(k_T)]}{[\ln(k_o) - \ln(k_T)]}\right)^2\right]^{1/2}$$

$$\frac{\Delta E_a}{E_a} = \left[\left(\frac{\Delta T}{T}\right)^2 + \left(\frac{(\Delta k_o)/k_o + (\Delta k_T)/k_T}{[\ln(k_o) - \ln(k_T)]}\right)^2\right]^{1/2}$$

To calculate the average error for E_a based on different temperature,

$$\Delta E_a = \left[\left(\Delta E_{a_{T1}}\right)^2 + \left(\Delta E_{a_{T2}}\right)^2 + \left(\Delta E_{a_{T2}}\right)^2\right]^{1/2}$$

(c) Take k_7 at 200 ^{o}C (473K) in sorbitol hydrogenolysis for example.

$$\Delta E_{a_{T1}} = E_a\left[\left(\frac{\Delta T}{T_1}\right)^2 + \left(\frac{(\Delta k_o)/k_o + (\Delta k_{T_1})/k_{T_1}}{\left[\ln(k_o) - \ln\left(k_{T_1}\right)\right]}\right)^2\right]^{1/2}$$

$$= 103.26\frac{kJ}{mol} \times \left[\left(\frac{1\ K}{473\ K}\right)^2 + \left(\frac{\left(1 - 0.958^{\frac{1}{2}}\right) + \frac{0.21}{0.74}}{[16.65 - \ln(0.74 \times 10^{-4})]}\right)^2\right]^{\frac{1}{2}}$$

$$= 2.76\ kJ/mol$$

(d) Similarly, error at 215 ^{o}C and 230 ^{o}C is 0.64 kJ/mol and 36.57 kJ/mol respectively.

(e) The average error for activation energy is calculated based on the following equation:

$$\left(\frac{\Delta E_a}{E_a}\right)^2 = \left[\frac{\Delta E_{a_{T1}} + \Delta E_{a_{T2}} + \Delta E_{a_{T3}}}{(3 \times E_a)}\right]^2$$

$$\Delta E_a = \frac{\Delta E_{a_{T1}} + \Delta E_{a_{T2}} + \Delta E_{a_{T3}}}{3} = \frac{2.76 + 0.64 + 36.57}{3} = 13.32\ kJ/mol$$

Sensitivity analysis

(1) False compensation

If reaction rates are measured over only a fairly small range of temperature and the activation energy is determined based on the reaction rate constants derived from Arrhenius plot, the value determined may be subject to considerable error.

In other words, the sensitivity of obtained activation energy to temperature may be much more significant compared with the maximum error from reaction constants. Therefore, it is necessary to analyze the sensitivity of activation energy derived from kinetic modeling. The sensitivity of activation energy is calculated based on the temperature range and error of reaction constants within the investigated temperature. The general equation is

$$\delta E_a = \frac{2 \times R \times T_1 \times T_2}{|T_1 - T_2|} \times err_{max}\%$$

Where δE_a is maximum error (sensitivity) of activation energy (kJ/mol), R is the gas constant (kJ/mol.K), T_1 and T_2 are investigated temperature (K) and $err_{max}\%$ is the maximum error in reaction constants (determined from 95% confidence level from Tables 1-5 and 1-6).

(2) Sensitivity of activation energy

Table 1-8. Sensitivity of activation energy in sorbitol hydrogenolysis

k_i	relative error at T (°C)			δE_a (kJ/mol)
	200	215	230	
k_1	0.07	<u>0.09</u>	0.04	11.5
k_2	0.01	0.05	<u>0.16</u>	20.5
k_3	<u>0.07</u>	0.03	0.04	9.7
k_4	<u>0.16</u>	0.14	0.11	20.6
k_5	<u>0.07</u>	0.05	0.05	8.9
k_6	0.08	0.25	<u>0.31</u>	40.6
k_7	0.28	0.06	<u>0.74</u>	97.6
k_8	0.10	<u>0.35</u>	0.18	46.4

<u>Maximum error</u>

Table 1-9. Sensitivity of activation energy in tandem glycerol conversion

k_i	relative error at T (°C)			δE_a (kJ/mol)
	130	145	160	
k_{s1}	0.07	0.08	<u>0.14</u>	14.0
k_{s2}	0.08	0.05	<u>0.13</u>	12.9
k_{s3}	0.15	0.14	<u>0.25</u>	24.4
k_{s4}	0.09	<u>0.11</u>	0.11	11.1
k_{s5}	<u>0.27</u>	0.07	0.09	25.8
k_{s6}	<u>0.43</u>	0.14	0.22	41.5
K_{gly}	0.12	0.04	<u>0.14</u>	13.3
K_{OH-}	0.08	0.12	<u>0.26</u>	25.3
$K_{1,2\text{-}PDO}$	0.02	0.22	<u>0.48</u>	46.0
K_{EG}	0.09	<u>0.19</u>	0.11	18.6

<u>Maximum error</u>

For example, the maximum error for k_{s1} is 0.14 in tandem glycerol conversion (see Tables 1-7 and 1-9), while the temperature difference is 433 K (160 °C)-403 K (130 °C) = 30 K. Therefore the sensitivity of E_a for k_{s1} is

$$\delta E_a = \frac{2 \times 8.314 \times 433 \times 403}{1000 \times 30} \times 0.14 = 14.0\ kJ/mol$$

Reference

[1] Gholap, R.V.; Chaudhari, R.V.; Hofmann, H. *Can. J. Chem. Eng.* **1987**, *65*, 744.

[2] Sano, Y.; Yamaguchi, N.; Adachi, T. *J. Chem. Eng. Jpn.* **1974**, *1*, 255.

[3] Wilke, C.R.; Chang, P. *AIChE J.* **1955**, *1*, 264.

[4] Calderbank, P. H. *Trans. Inst. Chem. Eng.* **1958**, *36*, 443.

[5] Taylor, J. R. An Introduction to Error Analysis: The Study of Uncertainties if Physical Measurements. *University Science Books*, **1982**.

[6] Bork, P. V.; Grote, H.; Notz, D.; Regler M. Data Analysis Techniques in High Energy Physics Experiments. *Cambridge University Press*, **1993**.

[7] Athena Visual Studio Help File.

[8] Satterfield, C. N. Heterogeneous Catalysis in Industrial Practice (2nd edition). *McGraw Hill*, **1991**.

Appendix II Surface characterization

Preparation of Cu and Ru catalyst samples for TEM

The solid catalyst samples were smashed before TEM characterization. Small amounts of solid samples were then mixed with anhydrous ethanol and dispersed in a ultrasound bath for 10 min. Next, one drop of the slurry was put on the surface of TEM grid (Figure 2-1, left), which is held with tweezers (Figure 2-1, right). Then the sample was dried at room temperature. Ethanol was dried after about 10 min. TEM grid and tweezers were purchased from Ted Pella Inc. Pt/C, Ru/C and RuRe/C catalysts were prepared on Cu-based grids. Different the grid used for RuRe/C catalysts, Cu samples were prepared on grids made from nickel materials.

Figure 2-1. TEM grid (left) and tweezers (right)

Electron backscatter diffraction (EBSD) from SEM analysis

The crystal structure of Cu/CaO-Al_2O_3-1 sample is clearly seen from TEM characterization. But TEM only show 2-D structure of crystallized species. The actual lattice structure information is still not clear. Therefore, further characterization was carried out to obtain detailed crystal information from our

catalysts. EBSD spectra of Cu/CaO-Al_2O_3-1 sample were also carried out, the picture of which is shown in Figure 2-2.

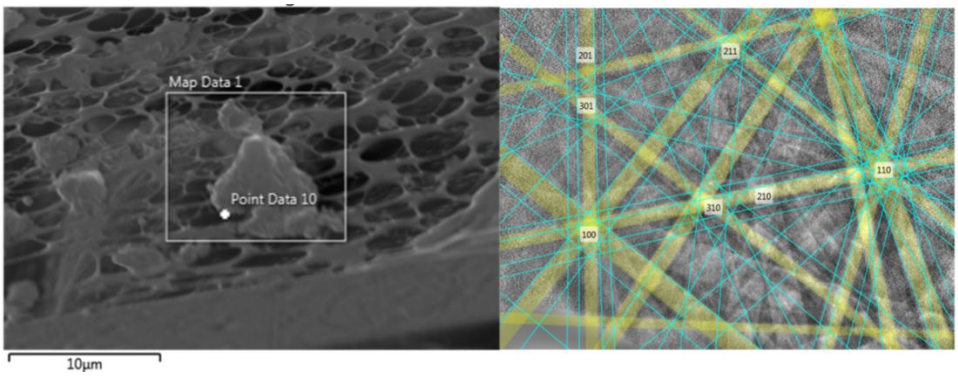

Figure 2-2. EBSD characterization of Cu/CaO-Al_2O_3-1 sample

Preparation of TPR samples and temperature program

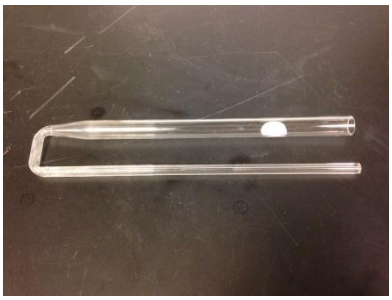

Figure 2-3. U-shape tube for temperature programmed techniques

Preparation of TPR samples were described as follows: (a) Cu catalysts for TPR were obtained directly from calcination, before activated (reduced) in a tube furnace. Cu, Ca and Al elements were thus all in oxidation states. Since Cu catalyst samples would be reduced at 300 ^oC at a ramping rate of 5 ^oC/min, in order to simulate the reduction process of Cu catalysts, identical temperature program were set up for AutoChem 2920 II instrument; (b): Preparation of Cu catalysts, CuO/CaO-Al_2O_3 for example was conducted at room temperature

once calcination of $CuO/CaO-Al_2O_3$ was finished. The solid particle was filtered and particle of 50~100 mesh in size would be collected for TPR characterization; (c): Small volume of glass cotton were obtained and put at the bottom of one side of the U-shape with larger diameter to hold the solid samples. The cotton was made into a ball shape and should be enough to avoid solid samples going through; (d): About 0.05 g of solid samples was charged into the U-shape quartz tube. Two important points needs to be noted. The tube could not be touched by bare hands since the tube would experience high temperature (> 500 ^{o}C) and the salts on hands would deteriorate the quartz materials. More importantly, the solid sample could not be allowed to stick on the inner wall of the tube. The sample should be directly pushed to the top of glass cotton "ball" in the tube using a straight stick rod quickly; (e): Then the sample tube would be finger-tightened and connected to AutoChem instrument. Certain amounts of ice would be placed in the cooling container. It is important to note that the amounts of ice should be enough to cool the cold coil; (f): Once the sample tube was set up, corresponding program could be edited on the software user interface. After the instrument was cooled down to room temperature, the sample tube could be disconnected and the used sample could be taken out, after which the tube was cleaned using deionized water and iso-propanol several times and dried in a drying oven.

Brunauer-Emmett-Teller (BET) analysis

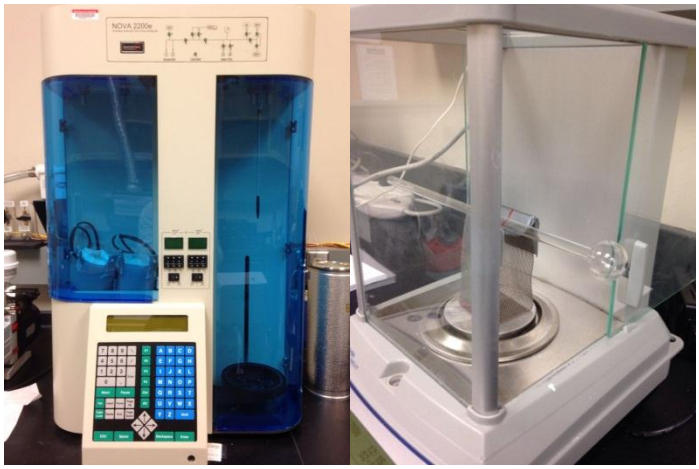

Figure 2-4. NOVA instrument for BET analysis (left) and sample tube (right)

Measurement of surface areas of solid catalyst samples were carried out in NOVA 2200e Instrument, as shown in Figure 2-5. The operation procedure is summarized as follows: (a): Solid catalyst samples were filtered and particle of >200 mesh in size were collected for BET measurement; (b): Before the introduction of solid sample, the weight of the measurement tube was noted as m_1 in lab book. Then the solid samples were carefully transferred to the sample tube, shown in Figure 2-6. A piece of paper sheet was foiled to "V" shape as used to transport sample to the bottom of the measurement tube. Then the total weight of sample and tube was measured and denoted as m_2; (c): The sample tube was then connected to the instrument and vacuumed at 200 ^{o}C for at least one hour to remove the humid content remaining on the solid sample. After the tube was cooled down, the total weight was measured again and denoted as m_3. $\Delta m = m_3-m_1$ is the amount of dried sample; (d): The sample tube was then

connected to the equipment and liquid nitrogen was introduced to the container below the sample tube. Sample information was input to the system and the data collection began; (e): After a certain range of measuring time (about 20 h), the analysis was finished. The sample tube was disconnected and washed with is-propanol several times and dried by purging air to the tube.

Table 2-1. Surface area of solid catalysts

Catalyst	Surface area (m^2/g)
Cu/CaO-Al_2O_3-1	30.25
Cu/CaO-Al_2O_3-2	50.98
Pt(5w%)/C-P	879.8
Pt(5w%)/C	2008.1
Ru/C	872.1
RuRe/C	812.2

X-ray diffraction (XRD) analysis

(1) Pt/C catalysts

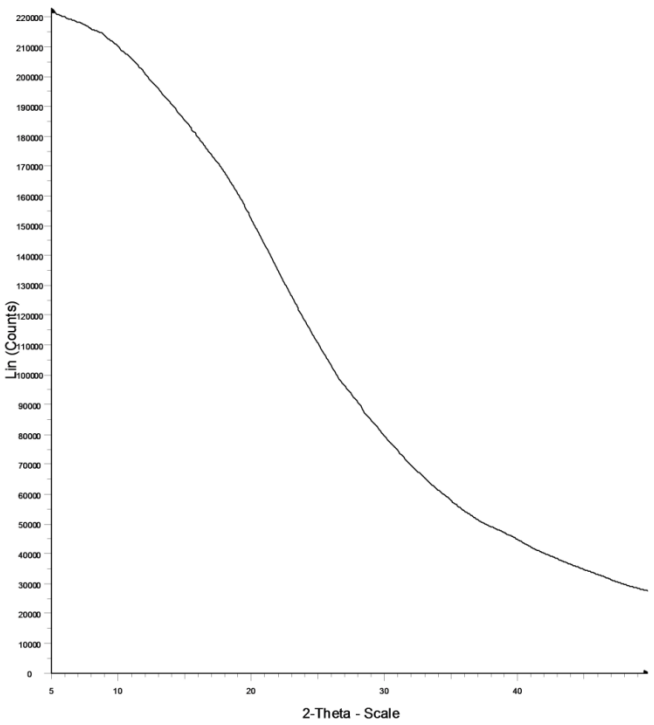

Figure 2-5. XRD characterization of fresh Pt/C catalyst

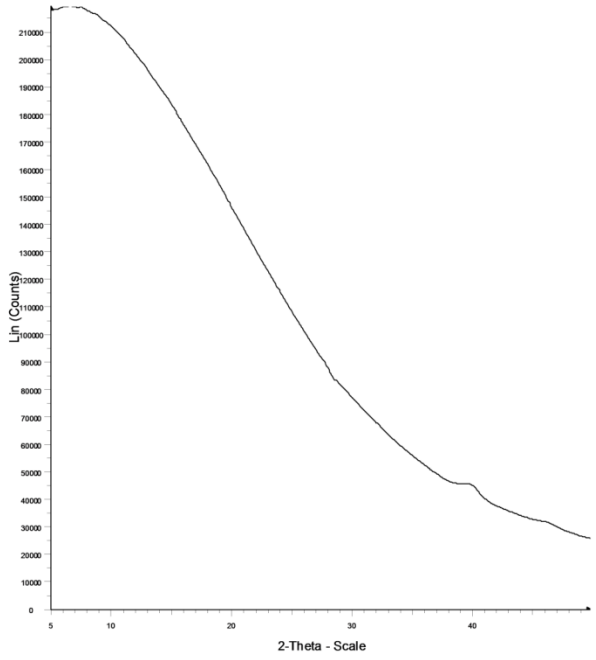

Figure 2-6. XRD characterization of used Pt/C catalyst from Entry#1 of Table 4-4-4 in Appendix IV

Appendix III Notation and programming codes

Notation

Symbol	Unit	Physical meaning
r_{gly}	kmol/m^3/h	Reaction rate of glycerol
$r_{1,2-PDO}$	kmol/m^3/h	Reaction rate of 1,2-propanediol
k_{gly}	1/h	Reaction constant of glycerol
C_{gly}	kmol/m^3	Concentration of glycerol in liquid phase
K_{gly}	-	Adsorption constant of glycerol on catalyst surface
K_{EG}	-	Adsorption constant of ethylene glycol on catalyst surface
C_{EG}	kmol/m^3	Concentration of ethylene glycol in liquid phase
$K_{1,2-PDO}$	-	Adsorption constant of 1,2-propanediol on catalyst surface
$C_{1,2-PDO}$	kmol/m^3	Concentration of 1,2-propanediol in liquid phase
C_{H_2}	kmol/m^3	Concentration of hydrogen in liquid phase
$\left(C_{H_2}\right)_g$	kmol/m^3	Concentration of hydrogen in gas phase
H_{H_2}	atm/(kmol/m^3)	Henry's constant for hydrogen solubility in water
K_{Ace}	-	Adsorption constant of acetol on catalyst surface
C_{Ace}	kmol/m^3	Concentration of acetol in liquid phase
C_{OH^-}	kmol/m^3	Concentration of OH^- in liquid phase
K_{H_2}	-	Adsorption constant of hydrogen on catalyst surface
k_{DH}	1/h	Reaction constant of dehydrogenation
P_{H_2}	MPa	Partial pressure of hydrogen in gas phase
w	kg/m^3	Catalyst charged
C_{Sor}	kmol/m^3	Concentration of sorbitol in liquid phase
E_a	kJ/mol	Activation energy

A	mol/mol/h	Pre-exponential factor
ΔH	kJ/mol	Reaction/adsorption heat (< 0: exothermic; > 0: endothermic)

Abbreviation

MeOH: methanol

EtOH: ethanol

PrOH: propanols

2-PrOH: 2-propanol

1,2-PDO: 1,2-propanediol

1,3-PDO: 1,3-propanediol

EG: ethylene glycol

LA: lactic acid

1,2-BDO: 1,2-butanediol

Glo-acid: glycolic acid

GLA: glyceraldehyde

DHA: dihydroxyacetone

1,2,3-BTO: 1,2,3-butanetriol

1,2,4-BTO: 1,2,4-butanetriol

DH: dehydrogenation

HDO: hydrogenolysis

DHD: dehydration

HPLC: high performance liquid chromatography

GC: gas chromatography

GC-MS: gas chromatography coupled with mass spectrometry

NPs: nanoparticles

CR: conversion rate

TOF: turnover frequency

X: conversion

S: selectivity

Y: yield

TEM: transmission electron microscopy

HRTEM: high resolution transmission electron microscopy

SEM: scanning electron microscopy

EDX: energy dispersive X-ray spectroscopy

ICP: inductively coupled plasma

XRD: x-ray diffraction

UV-Vis: ultraviolet-visible spectra

CP: coprecipitation

IWI: insipient wetness impregnation

HE: HDO efficiency

WGS: water gas shift

APC: aqueous phase conversion

fcc: face-centered-cubic

rGO: reduced graphene oxide

GO: graphene oxide

MC: mesoporous carbon

AC: activated carbon

SWCNT: single wall carbon nanotube

Programming codes for ATHENA

Example (1) Kinetic modeling in Chapter 2

```
Global Temp,Tref,RxnTime As Real
Global kB(Nrx),EB(Nrx),kRATE(Nrx) As Real
Parameter Nrx=8 As Integer    ! number of chemical reactions
Parameter R=8.314 As Real     !J/mol.K
!constant data
Tref=298.0       !reference temperature, K

@Initial Conditions
U(1:10)=Xu(4:13)

@Model Equations
Dim C1,C2,C3,C4,C5,C6,C7,C8,C9,C10 As Real
!                                    concentration                                    of
1:sorbitol,2:BDO,3:GLY,4:LA,5:PDO,6:EG,7:MeOH,8:EtOH,9:PtOH,10:Glyacid
Dim Alpha As Real
C1=U(1)
C2=U(2)
C3=U(3)
C4=U(4)
C5=U(5)
C6=U(6)
C7=U(7)
C8=U(8)
C9=U(9)
C10=U(10)
Alpha=1.0-Tref/Temp
kRATE(1:Nrx)=kB*exp(EB*Alpha)
F(1)=-kRATE(1)*C1-kRATE(5)*C1-kRATE(2)*C1-kRATE(1)*C1        !sorbitol reaction rate
F(2)= kRATE(5)*C1                                            !BDO      reaction rate
F(3)=-kRATE(8)*C3+2*kRATE(1)*C1                              !glycerol reaction rate
F(4)= +2*kRATE(2)*C1                                         !LA       reaction rate
F(5)=-kRATE(4)*C5+2*kRATE(3)*C1                              !PDO      reaction rate
F(6)=-kRATE(6)*C6-kRATE(7)*C6+kRATE(5)*C1+kRATE(8)*C3        !EG       reaction rate
F(7)= kRATE(8)*C3                                            !MeOH     reaction rate
F(8)= kRATE(6)*C6                                            !EtOH     reaction rate
F(9)= kRATE(4)*C5                                            !IPA      reaction rate
F(10)=kRATE(7)*C6                                            !Gly-acid reaction rate

@Response Model
Y(1:10)=U(1:10)

@Connect Parameters and Settings
RxnTime=Xu(3)
Temp=Xu(2)
kB(1:Nrx)=Par(1:Nrx)
EB(1:Nrx)=Par((Nrx+1):(Nrx+Nrx))
```

```
@Solver Options
Headers=BlockId;Temp;RxnTime;C1o;C2o;C3o;C4o;C5o;C6o;C7o;C8o;C9o;C10o;C1;C2;C3;
C4;C5;C6;C7;C8;C9;C10;w1;w2;w3;w4;w5;w6;w7;w8;w9;w10;Replicate
```

Example (2) Kinetic modeling in Chapter 4

```
Global Temp,Tref,RxnTime As Real
Global kB(Nrx),EB(Nrx),kRATE(Nrx) As Real
Parameter Nrx=9 As Integer    ! number of chemical reactions
Parameter R=8.314 As Real     !J/mol.K
!constant data
Tref=298.0       !reference temperature, K

@Initial Conditions
U(1:8)=Xu(4:11)

@Model Equations
Dim C1, C2, C3, C4, C5, C6, C7, C8 As Real     !1:Glycerol, 2:LA, 3:PDO, 4:EG, 5:MeOH,
6:EtOH, 7:PrOH, 8:OH-
Dim Alpha As Real
Dim NaOH_to_Gly_ratio As Real
Dim ads_gly, ads_PDO, ads_OH As Real
Dim N As Real
NaOH_to_Gly_ratio=1.1
N=2
C1=U(1)
C2=U(2)
C3=U(3)
C4=U(4)
C5=U(5)
C6=U(6)
C7=U(7)
C8=U(8)

Alpha=1.0-Tref/Temp
kRATE(1:Nrx)=kB*exp(EB*Alpha)
ads_gly=(1+kRATE(7)*C1+kRATE(8)*C8)
ads_PDO=(1+kRATE(9)*C3)

F(1)=-kRATE(1)*kRATE(7)*C1*C8/(ads_gly)^N-kRATE(2)*kRATE(7)*C1*C8/(ads_gly)^N-
kRATE(4)*kRATE(7)*C1*C8/(ads_gly)^N-kRATE(5)*kRATE(7)*C1*C8/(ads_gly)^N-
kRATE(6)*kRATE(7)*C1*C8/(ads_gly)^N
F(2)=kRATE(1)*kRATE(7)*C1*C8/(ads_gly)^N
F(3)=kRATE(2)*kRATE(7)*C1*C8/(ads_gly)^N-kRATE(3)*kRATE(9)*C3*C8/(ads_PDO)^2
F(4)=kRATE(4)*kRATE(7)*C1*C8/(ads_gly)^N
F(5)=kRATE(4)*kRATE(7)*C1*C8/(ads_gly)^N+kRATE(5)*kRATE(7)*C1*C8/(ads_gly)^N+3*k
RATE(6)*kRATE(7)*C1*C8/(ads_gly)^N
F(6)=kRATE(5)*kRATE(7)*C1*C8/(ads_gly)^N
F(7)=kRATE(3)*kRATE(9)*C3*C8/(ads_PDO)^2
F(8)=-kRATE(1)*kRATE(7)*C1*C8/(ads_gly)^N

@Response Model
Y(1:8)=U(1:8)
```

```
@connect variables
RxnTime=Xu(3)
Temp=Xu(2)
kB(1:Nrx)=Par(1:Nrx)
EB(1:Nrx)=Par((Nrx+1):(Nrx+Nrx))

@Solver Options
Headers=BlockId;Temp;RxnTime;C1o;C2o;C3o;C4o;C5o;C6o;C7o;C8o;C1;C2;C3;C4;C5;C6;
C7;C8;w1;w2;w3;w4;w5;w6;w7;w8;Replicate
```

Appendix IV Additional experimental results

Chapter 2

(1) Concentration-time profiles of sorbitol conversion in RuRe/C+MgO system

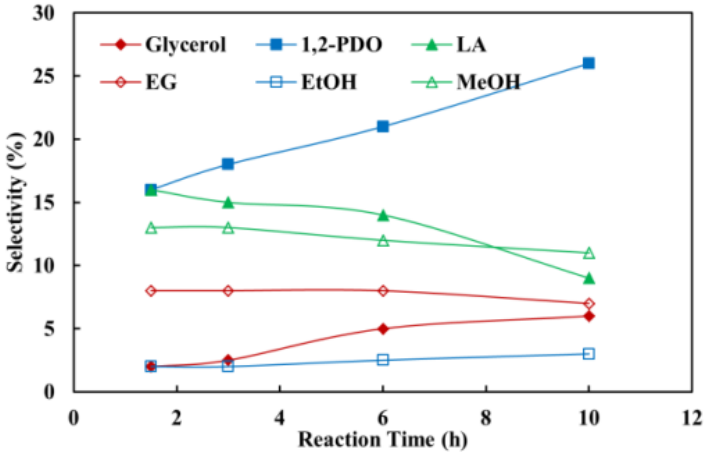

(a)

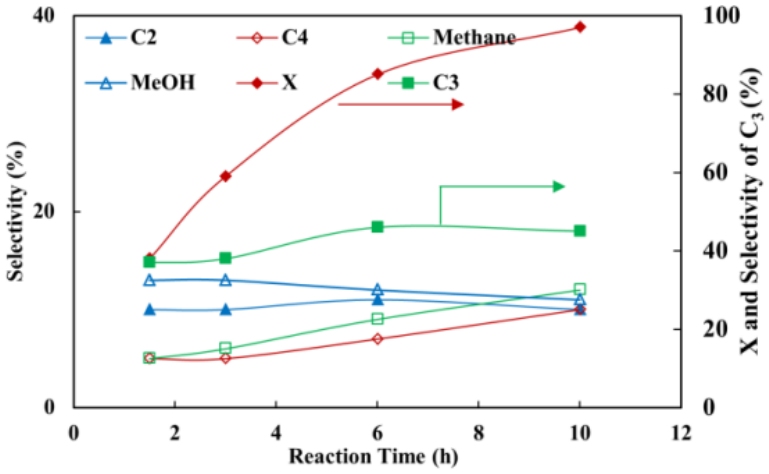

(b)

Figure 4-2-1. Reaction profiles for HDO of sorbitol on RuRe/C catalyst (experimental conditions same as described in Figure 9 of Chapter 1)

In order to establish the product distribution during HDO of sorbitol and xylitol, several experiments were carried out using the RuRe/C catalyst at 230 ^{o}C and 7.6 MPa hydrogen pressure. The results (Figure 4-2-1) show that with sorbitol as the substrate, the selectivities of the major products including glycerol, EG, EtOH and MeOH display only slight changes with time except for 1,2-PDO and LA. From the product distribution in Figure 8, it is clear that the major products are C_1, C_2 and C_3, which indicates that sorbitol molecules tend to undergo C_3-C_3 or C_1-C_2-C_3 cleavages, the former of which might undergo C_1-C_2 cleavage further. From the structure of the sorbitol molecule, it is clear that C-C and C-O cleavage can occur at multiple locations during HDO, producing C_5 and C_6 polyols, triols, and diols in addition to lower aliphatic alcohols. The large number of products makes accurate analysis of C_5 and C_6 products difficult. Similar challenges are associated with xylitol conversion. At higher conversion levels, most of the C_5 and C_6 intermediates are further converted and hence it was possible to obtain a more complete carbon balance.

(2) Different solid bases

Table 4-2-1. Major products during sorbitol conversion

#	1	2	3	4
Catalyst	Ru/C	RuRe/C	RuRe/C	RuRe/C
Base	MgO	MgO	NaOH	$Ca(OH)_2$
TOF (mol/mol/h)	480.0	546.0	1619.4	2006.4
Selectivity to major products (%)				
Glycerol	11.1	10.0	5.9	8.1

LA	48.5	35.0	38.9	40.4
Glycols	10.2	24.9	14.3	24.9
Alcohols	0.1	0.1	11.0	5.4
Gas alkanes	10.2	6.0	-	0.6
CO_2	10.1	4.0	2.0	1.8

T: 200 ^oC; P_{H2}: 3.5 MPa; sorbitol: 0.55 kmol/m^3; solvent: H_2O; Catalyst: Ru/C or RuRe/C, 0.05 g; base: 0.10~0.15 g; conversion < 25%; Glycols: PDO and EG; Alcohols: MeOH, EtOH and 2-PrOH.

The performances of various based promoters for Ru/C and RuRe/C catalysts in sorbitol conversion are compared at 200 ^oC and 3.5 MPa hydrogen pressure, the major products of which are presented in Table 4-2-1. As seen from entries#1 and #2, RuRe/C displays improved performance in terms of activity and selectivity, compared with Ru/C catalyst. In particular, Ru/C only exhibits limited activity (TOF = 480.0 mol/mol/h) while RuRe/C shows higher activity (TOF = 546.0 mol/mol/h) under the same reaction conditions. Furthermore, Ru/C gives an initial selectivity of 38% to LA and 8% to glycols (1,2-PDO and EG) with high gaseous phase products selectivity (20% totally, mainly methane and CO_2), which indicates its strong activity for methanation and decarboxylation reactions, as proposed by the reaction pathways in Scheme 1. In contrast, RuRe/C shows selectivity to LA and glycols of 26% and 18%, respectively and lower selectivity to gaseous products (10%) compared with Ru/C catalyst. Obviously the addition of Re enhances the overall performance of Ru catalyst in terms of C-O cleavage. Furthermore, comparing Entries#2 and #3, another enhancement in the activity of RuRe/C (TOF = 1619.4 mol/mol/h) in the presence of NaOH promoter. More importantly, gaseous products

(methane and CO_2) formation was almost completely restrained in the presence of NaOH. Among all three investigated bases, $Ca(OH)_2$ (Entry#4) shows highest promotional effect in RuRe/C activity (2006.4 mol/mol/h). Besides, RuRe/C gives highest selectivity to alcoholic compounds in the presence of $Ca(OH)_2$, compared with other base promoters.

Chapter 3

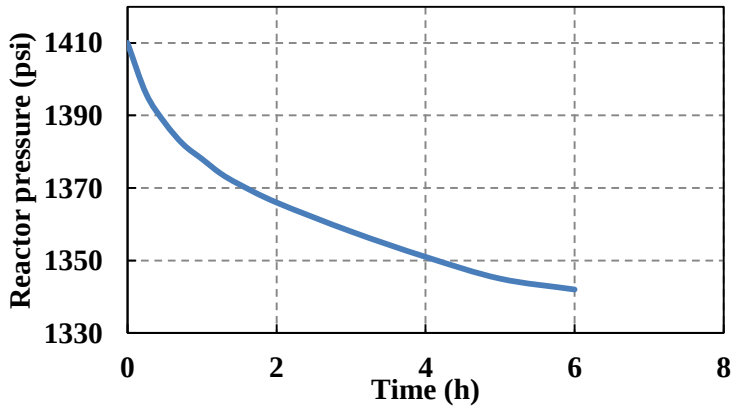

Figure 4-3-1. A typical pressure~time profile for sorbitol conversion on Cu/CaO-Al_2O_3-1 catalysts at 230 ^oC and 7.6 MPa hydrogen pressure

Chapter 4

Table 4-4-1. Activity of different supported metal catalysts for glycerol conversion

	Ru(5w%)/C	Rh(5w%)/C	Pt(5w%)/C	Pd(5w%)/C
Conversion (%)	24.6	17.9	21.6	24.6
	Product Selectivity (%)			
LA	48.2	26.6	69.8	27.4
1,2-PDO	25.9	40.4	9.1	11.2
EG	2.4	-	-	0.4

MeOH	7.8	Trace	4.7	Trace
EtOH	2.4	2.3	4.7	3.3
PrOH	-	-	2.1	-
Methane	1.6	4.2	0.5	0.2
C^{2+} alkanes	~0.1	Trace	Trace	-

T: 160 ^{o}C, P_{N2}: 1.4 MPa, reaction time: 0.5 h, glycerol: 1.1 kmol/m^3, solvent: H_2O, NaOH/glycerol molar ratio: 1.1, catalyst charge: 6.7 kg/m^3.

Table 4-4-2. Activity of Pt/C for conversion of different polyols at 160 ^{o}C

	Glycerol	Xylitol	Sorbitol	Mannitol
Conversion (%)	12.1	10.2	12.0	13.5
Product Selectivity (%)				
LA	71.1	56.7	51.9	69.1
1,2-PDO	8.6	4.4	2.5	5.1
EG	-	4.1	2.1	1.9
MeOH	3.2	10.8	8.0	8.8
EtOH	2.2	3.5	1.3	1.5
PrOH	1.6	1.7	-	-
Formic acid	-	6.7	6.1	8.6
Glycolic acid	-	-	1.7	1.9
Acetic acid	-	-	7.6	3.7

P_{N2}: 1.4 MPa, reaction time: 0.25~0.5 h, substrates: 1.1 kmol/m^3, solvent: H_2O, NaOH: 1.2 kmol/m^3, Pt/C catalyst charge: 6.7 kg/m^3.

Table 4-4-3. Conversion of sorbitol on Pt/C catalyst

Temperature (^{o}C)	115	130	160
Conversion (%)	22.3	54.8	97.9
Product Selectivity (%)			
LA	54.5	49.9	43.4
1,2-PDO	5.5	4.7	4.0
EG	3.2	3.3	2.5

MeOH	8.4	8.8	12.9
EtOH	4.5	2.8	2.3
PrOH	2.0	1.4	1.2
Formic acid	11.4	9.6	7.4
Glycolic acid	2.3	1.3	1.3
Acetic acid	3.6	2.8	2.4

P_{N2}: 1.4 MPa, reaction time: 4 h, sorbitol: 100 kg/m^3, solvent: H_2O, NaOH: 1.2 kmol/m^3, Pt/C catalyst charge: 6.7 kg/m^3.

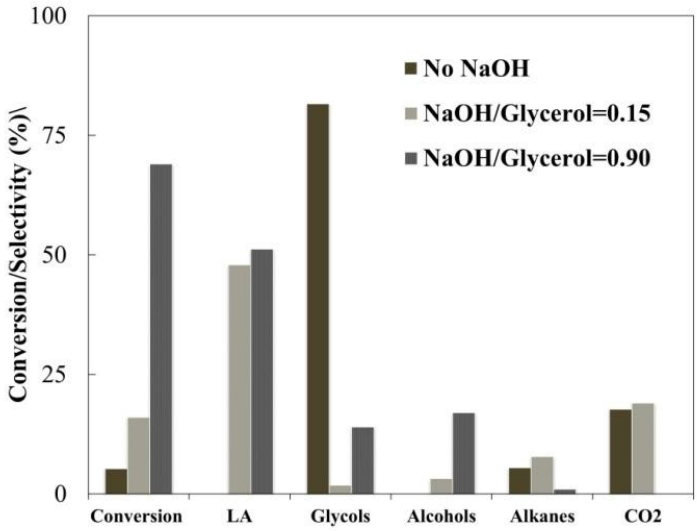

Figure 4-4-1. Effect of NaOH/Glycerol ratio on conversion and product selectivity with Pt/C catalyst (Reaction time: 4 h, T: 160 ^{o}C, P_{N2}: 1.4 MPa, glycerol: 1.1 kmol/m^3, solvent: H_2O, Pt/C catalyst charge: 6.7 kg/m^3)

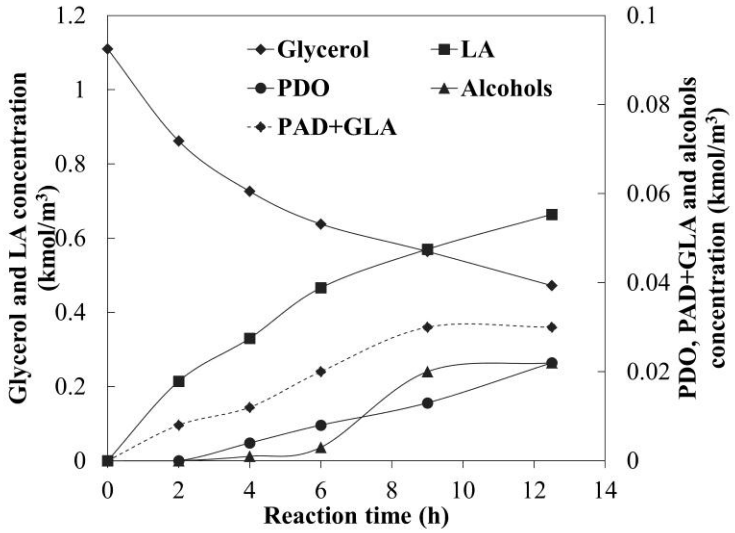

Figure 4-4-2. Glycerol conversion and product selectivity with Cu_2O catalyst (Reaction time: 4 h, T: 180 ^oC, P_{N2}: 1.4 MPa, glycerol: 1.1 kmol/m^3, solvent: H_2O, Cu_2O catalyst charge: 6.7 kg/m^3)

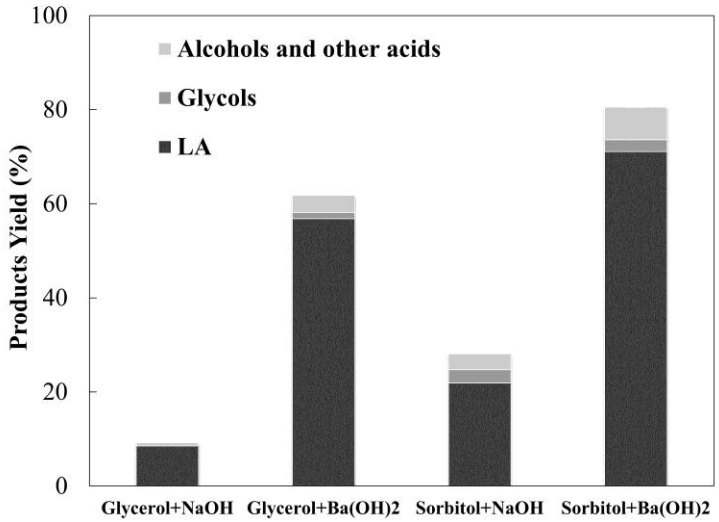

Figure 4-4-3. Glycerol and sorbitol conversion and product selectivity with Cu_2O catalyst with different bases (Reaction time: 1.5 h, T: 180 ^oC, P_{N2}: 1.4 MPa, glycerol: 1.1 kmol/m^3, solvent: H_2O, Cu_2O catalyst charge: 6.7 kg/m^3)

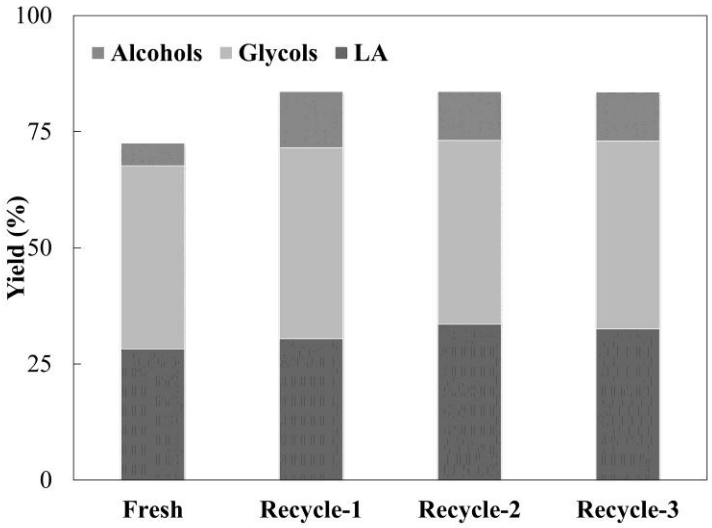

Figure 4-4-4. Recycle of Pt/C+$Ba(OH)_2$ catalyst for aqueous phase conversion of glycerol (T: 160 ^oC, P_{N2}: 1.4 MPa, glycerol: 100 kg/m^3, solvent: H_2O, OH^-: 1.2 $kmol/m^3$, reaction time: 6 h, Pt/C catalyst charge: 6.7 kg/m^3).

Table 4-4-4. Rate equations for Model *ii*

$$r_1 = \frac{k_{s1} \cdot K_{gly} \cdot C_{gly} \cdot K_{OH^-} \cdot C_{OH^-}}{\left(1 + K_{gly} \cdot C_{gly} + K_{EG} \cdot C_{EG} + K_{OH^-} \cdot C_{OH^-}\right)^2}$$

$$r_2 = \frac{k_{s2} \cdot K_{gly} \cdot C_{gly} \cdot K_{OH^-} \cdot C_{OH^-}}{\left(1 + K_{gly} \cdot C_{gly} + K_{EG} \cdot C_{EG} + K_{OH^-} \cdot C_{OH^-}\right)^2}$$

$$r_3 = \frac{k_{s3} \cdot K_{1,2-PDO} \cdot C_{1,2-PDO} \cdot K_{OH^-} \cdot C_{OH^-}}{\left(1 + K_{1,2-PDO} \cdot C_{1,2-PDO}\right)^2}$$

$$r_4 = \frac{k_{s4} \cdot K_{gly} \cdot C_{gly} \cdot K_{OH^-} \cdot C_{OH^-}}{\left(1 + K_{gly} \cdot C_{gly} + K_{EG} \cdot C_{EG} + K_{OH^-} \cdot C_{OH^-}\right)^2}$$

$$r_5 = \frac{k_{s5} \cdot K_{gly} \cdot C_{gly} \cdot K_{OH^-} \cdot C_{OH^-}}{\left(1 + K_{gly} \cdot C_{gly} + K_{EG} \cdot C_{EG} + K_{OH^-} \cdot C_{OH^-}\right)^2}$$

$$r_6 = \frac{k_{s6} \cdot K_{EG} \cdot C_{EG} \cdot K_{OH^-} \cdot C_{OH^-}}{\left(1 + K_{gly} \cdot C_{gly} + K_{EG} \cdot C_{EG} + K_{OH^-} \cdot C_{OH^-}\right)^2}$$

Table 4-4-5. Rate equations for Model *iii*

$$r_1 = \frac{k_{s1} \cdot K_{gly} \cdot C_{gly} \cdot C_{OH^-}}{\left(1 + K_{gly} \cdot C_{gly} + K_{OH^-} \cdot C_{OH^-}\right)^2}$$

$$r_2 = \frac{k_{s2} \cdot K_{gly} \cdot C_{gly} \cdot C_{OH^-}}{\left(1 + K_{gly} \cdot C_{gly} + K_{OH^-} \cdot C_{OH^-}\right)^2}$$

$$r_3 = \frac{k_{s3} \cdot K_{1,2-PDO} \cdot C_{1,2-PDO} \cdot C_{OH^-}}{\left(1 + K_{1,2-PDO} \cdot C_{1,2-PDO}\right)^2}$$

$$r_4 = \frac{k_{s4} \cdot K_{gly} \cdot C_{gly} \cdot C_{OH^-}}{\left(1 + K_{gly} \cdot C_{gly} + K_{OH^-} \cdot C_{OH^-}\right)^2}$$

$$r_5 = \frac{k_{s5} \cdot K_{gly} \cdot C_{gly} \cdot C_{OH^-}}{\left(1 + K_{gly} \cdot C_{gly} + K_{OH^-} \cdot C_{OH^-}\right)^2}$$

$$r_6 = \frac{k_{s6} \cdot K_{gly} \cdot C_{gly} \cdot C_{OH^-}}{\left(1 + K_{gly} \cdot C_{gly} + K_{OH^-} \cdot C_{OH^-}\right)^2}$$

Table 4-4-6. Parameter estimation for Model *ii*

Constants	Model *ii*		
	130°C	145°C	160°C
k_1	44.0±3.17	6.61±1.69	14.3±1.48
k_2	20.0±1.66	3.72±0.95	1.29
$k_3 \times 10^{-1}$	3.76±0.89	1.37±0.44	28.9±5.83
k_4	3.68±0.43	0.43±0.18	0.56±0.07
k_5	< 0	0.37±0.14	3.49±0.26
$k_6 \times 10^{3}$	1.95±0.57	~ 0	~ 0
$K_{gly} \times 10^{-2}$	6.06	14.2	17.5
$K_{OH-} \times 10^{-2}$	2.05	14.5	11.6
$K_{1,2\text{-}PDO}$	8.31±7.12	27.0±29.4	16.5
$K_{EG} \times 10^{-3}$	7.54	25.5±22.8	>>4000

Table 4-4-7. Parameter estimation for Model *iii*

Constants	Model *iii*		
	130°C	145°C	160°C
k_1	1.33±0.10	1.98±0.16	10.2±0.42
$k_2 \times 10^{-1}$	6.05±0.53	10.8	5.32
$k_3 \times 10^{-2}$	6.47±0.96	24.8±3.37	241±16.9
$k_4 \times 10^{-2}$	6.75	11.7±1.5	23.0±2.77

$k_5\times10^{-2}$	9.77±1.67	24.4±1.68	144±11.9
$k_6\times10^{-2}$	3.42±1.61	>>600	2105±194
$K_{gly}\times10^{-2}$	3.80	3.75±0.22	2.93±1.23
$K_{OH\text{-}}\times10^{-3}$	1.00	~ 0	5.70±26.5
$K_{1,2\text{-}PDO}$	0.38	0.20	2.65

Table 4-4-8. Rate equations for Model *iv*

$$r_1 = \frac{k_{s1}\cdot K_{gly}\cdot C_{gly}\cdot C_{OH^-}}{\left(1+K_{gly}\cdot C_{gly}+K_{EG}\cdot C_{EG}\right)^2\cdot\left(1+K_{OH^-}\cdot C_{OH^-}\right)}$$

$$r_2 = \frac{k_{s2}\cdot K_{gly}\cdot C_{gly}\cdot C_{OH^-}}{\left(1+K_{gly}\cdot C_{gly}+K_{EG}\cdot C_{EG}\right)^2\cdot\left(1+K_{OH^-}\cdot C_{OH^-}\right)}$$

$$r_3 = \frac{k_{s3}\cdot K_{1,2-PDO}\cdot C_{1,2-PDO}\cdot C_{OH^-}}{\left(1+K_{1,2-PDO}\cdot C_{1,2-PDO}\right)^2}$$

$$r_4 = \frac{k_{s4}\cdot K_{gly}\cdot C_{gly}\cdot C_{OH^-}}{\left(1+K_{gly}\cdot C_{gly}+K_{EG}\cdot C_{EG}\right)^2\cdot\left(1+K_{OH^-}\cdot C_{OH^-}\right)}$$

$$r_5 = \frac{k_{s5}\cdot K_{gly}\cdot C_{gly}\cdot C_{OH^-}}{\left(1+K_{gly}\cdot C_{gly}+K_{EG}\cdot C_{EG}\right)^2\cdot\left(1+K_{OH^-}\cdot C_{OH^-}\right)}$$

$$r_6 = \frac{k_{s5}\cdot K_{EG}\cdot C_{EG}\cdot C_{OH^-}}{\left(1+K_{gly}\cdot C_{gly}+K_{EG}\cdot C_{EG}\right)^2\cdot\left(1+K_{OH^-}\cdot C_{OH^-}\right)}$$

Table 4-4-9. Rate equations for Model *v*

$$r_1 = \frac{k_{s1}\cdot K_{gly}\cdot C_{gly}\cdot K_{OH^-}\cdot C_{OH^-}}{\left(1+K_{gly}\cdot C_{gly}+K_{EG}\cdot C_{EG}\right)^2\cdot\left(1+K_{OH^-}\cdot C_{OH^-}\right)}$$

$$r_2 = \frac{k_{s2}\cdot K_{gly}\cdot C_{gly}\cdot K_{OH^-}\cdot C_{OH^-}}{\left(1+K_{gly}\cdot C_{gly}+K_{EG}\cdot C_{EG}\right)^2\cdot\left(1+K_{OH^-}\cdot C_{OH^-}\right)}$$

$$r_3 = \frac{k_{s3}\cdot K_{1,2-PDO}\cdot C_{1,2-PDO}\cdot K_{OH^-}\cdot C_{OH^-}}{\left(1+K_{1,2-PDO}\cdot C_{1,2-PDO}\right)^2}$$

$$r_4 = \frac{k_{s4}\cdot K_{gly}\cdot C_{gly}\cdot K_{OH^-}\cdot C_{OH^-}}{\left(1+K_{gly}\cdot C_{gly}+K_{EG}\cdot C_{EG}\right)^2\cdot\left(1+K_{OH^-}\cdot C_{OH^-}\right)}$$

$$r_5 = \frac{k_{s5}\cdot K_{gly}\cdot C_{gly}\cdot K_{OH^-}\cdot C_{OH^-}}{\left(1+K_{gly}\cdot C_{gly}+K_{EG}\cdot C_{EG}\right)^2\cdot\left(1+K_{OH^-}\cdot C_{OH^-}\right)}$$

$$r_6 = \frac{k_{s5}\cdot K_{EG}\cdot C_{EG}\cdot K_{OH^-}\cdot C_{OH^-}}{\left(1+K_{gly}\cdot C_{gly}+K_{EG}\cdot C_{EG}\right)^2\cdot\left(1+K_{OH^-}\cdot C_{OH^-}\right)}$$

Table 4-4-10. Rate equations for Model *vi*

$$r_1 = \frac{k_{s1} \cdot K_{gly} \cdot C_{gly} \cdot C_{OH^-}}{\left(1 + K_{gly} \cdot C_{gly}\right)^2 \cdot \left(1 + K_{OH^-} \cdot C_{OH^-}\right)}$$

$$r_2 = \frac{k_{s2} \cdot K_{gly} \cdot C_{gly} \cdot C_{OH^-}}{\left(1 + K_{gly} \cdot C_{gly}\right)^2 \cdot \left(1 + K_{OH^-} \cdot C_{OH^-}\right)}$$

$$r_3 = \frac{k_{s3} \cdot K_{1,2-PDO} \cdot C_{1,2-PDO} \cdot C_{OH^-}}{\left(1 + K_{1,2-PDO} \cdot C_{1,2-PDO}\right)^2}$$

$$r_4 = \frac{k_{s4} \cdot K_{gly} \cdot C_{gly} \cdot C_{OH^-}}{\left(1 + K_{gly} \cdot C_{gly}\right)^2 \cdot \left(1 + K_{OH^-} \cdot C_{OH^-}\right)}$$

$$r_5 = \frac{k_{s5} \cdot K_{gly} \cdot C_{gly} \cdot C_{OH^-}}{\left(1 + K_{gly} \cdot C_{gly}\right)^2 \cdot \left(1 + K_{OH^-} \cdot C_{OH^-}\right)}$$

$$r_6 = \frac{k_{s5} \cdot K_{gly} \cdot C_{gly} \cdot C_{OH^-}}{\left(1 + K_{gly} \cdot C_{gly}\right)^2 \cdot \left(1 + K_{OH^-} \cdot C_{OH^-}\right)}$$

Table 4-4-11. Parameter estimation for Model *iv*

Constants	Model *iv*		
	130°C	145°C	160°C
k_1	1.28±0.10	1.97±0.16	2.28±0.24
$k_2 \times 10^{-1}$	5.86±0.51	10.8	12.7±1.57
$k_3 \times 10^{-2}$	6.47±0.96	24.9±3.6	43.6±11.6
$k_4 \times 10^{-2}$	6.53	12.9±1.48	21.9±2.31
$k_5 \times 10^{-2}$	9.45±1.60	24.1±1.56	73.4
k_6	1.66	12.0	177
$K_{gly} \times 10^{-2}$	3.80	4.35±5.33	6.24±0.45
$K_{OH-} \times 10^{-3}$	1.00	18.6±137	< 0
$K_{1,2\text{-}PDO}$	0.37	0.20	0.11
$K_{EG} \times 10^{-2}$	5.21±2.50	1.50±4.93	1.14±2.00

Table 4-4-12. Parameter estimation for Model *v*

Constants	Model *v*		
	130°C	145°C	160°C
k_1	25.2±1.74	4.12±2.47	-
$k_2 \times 10^{1}$	1.15±0.09	0.23±0.14	-
$k_3 \times 10^{-1}$	5.52±1.30	7.03	-

k_4	1.37±0.17	0.27±0.17	-
k_5	< 0	0.51±0.31	-
k_6	8.59	0.03±0.04	-
$K_{gly}\times10^{-1}$	1.55	0.77	-
$K_{OH-}\times10^{-2}$	1.40	47.8±18.2	-
$K_{1,2\text{-}PDO}$	8.30±7.07	0.01±0.005	-
$K_{EG}\times10^{-3}$	1.08	4122±8719	-

Table 4-4-12. Parameter estimation for Model *vi*

Constants	Model *vi*		
	130°C	145°C	160°C
k_1	1.28±0.10	1.98±0.16	-
$k_2\times10^{1}$	5.86±0.51	1.08	-
$k_3\times10^{-2}$	6.47±0.01	24.9±3.60	-
$k_4\times10^{-2}$	6.52	12.9±1.48	-
$k_5\times10^{-2}$	9.45±1.63	24.1±1.57	-
$k_6\times10^{-2}$	3.41±1.63	12.1±33.1	-
$K_{gly}\times10^{-2}$	3.80	4.16±4.49	-
$K_{OH-}\times10^{-3}$	1.00	100.6±109	-
$K_{1,2\text{-}PDO}$	0.37	0.20	-

Table 4-4-13. Repeated experiments in glycerol conversion on Pt/C catalyst

T (°C)	Time (h)	C_{gly}	C_{LA}	$C_{1,2\text{-}PDO}$	C_{EG}	C_{MeOH}	C_{EtOH}	C_{PrOH}	C_{OH-}
130	1.0	0.92	0.086	0.029	0.004	0.019	0.008	0.002	1.070
130	1.0	1.001	0.075	0.034	0.004	0.016	0.006	0.002	1.112
130	4.5	0.758	0.190	0.067	0.005	0.023	0.012	0.005	1.050
130	4.5	0.886	0.182	0.063	0.004	0.020	0.012	0.004	0.919
145	1.0	0.861	0.108	0.032	0.015	0.022	0.011	0.004	0.108
145	1.0	0.910	0.127	0.034	0.018	0.019	0.014	0.003	0.027
145	4.0	0.540	0.303	0.124	0.010	0.046	0.028	0.019	0.954
145	4.0	0.518	0.265	0.109	0.009	0.040	0.024	0.017	0.835
160	0.5	0.591	0.265	0.109	0.009	0.040	0.024	0.017	0.835
160	0.5	0.615	0.303	0.124	0.010	0.045	0.028	0.019	0.954
160	4.0	0.361	0.301	0.144	0.011	0.206	0.071	0.028	0.848
160	4.0	0.337	0.342	0.164	0.012	0.234	0.081	0.032	0.964

Chapter 5

(1) Supported Cu nanocatalysts on rGO

Table 4-5-1. Activity and selectivity of Cu/rGO and CuPd/rGO catalysts

#	Catalysts on rGO	Time (h)	X (%)	Selectivity (%)			
				LA	1,2-PDO	Alcohols	Others
1	Cu(2w%)	6	28.8	87.0	4.2	-	-
2	Pd(0.01w%)	6	12.9	69.0	6.9	3.1	-
3	Pd(0.05w%)	6	29.8	70.0	6.2	2.4	-
4	Pd(0.1w%)	6	40.0	53.3	5.4	6.0	9.6
5	Cu(2w%)-Pd(0.01w%)	6	58.2	76.2	3.6	6.8	4.3
6	Cu(2w%)-Pd(0.03w%)	6	61.3	78.4	3.2	6.3	6.0
7	Cu(2w%)-Pd(0.05w%)	0.7	15.2	81.5	2.1	3.2	-
8	Cu(2w%)-Pd(0.05w%)	1.5	30.1	84.5	5.6	3.6	5.7
9	Cu(2w%)-Pd(0.05w%)	6	84.5	74.6	4.2	6.6	5.4
10	Cu(2w%)-Pd(0.1w%)	6	96.8	60.3	4.5	9.1	4.4
11	Cu(2w%)+Pd(0.05w%) admixture	6	63.0	68.0	10.1	3.6	3.2

Glycerol: 100.0 kg/m^3; solvent: H_2O; catalysts charge: 6.7 kg/m^3; T: 200 ^oC; P_{N2}: 1.4 MPa; NaOH/glycerol molar ratio: 1.1. LA: lactic acid, 1,2-PDO: 1,2-propanediol, Alcohols: methanol, ethanol and propanols, Others: mainly acetic acid.

(2) Rhombic Cu_2O and cubic Cu_2O catalysts

cCu_2O: cubic Cu_2O; cCu_2O/GO: cubic Cu_2O mixed with GO; cCu_2O-GO: cubic Cu_2O grown on GO. The catalytic activity and stability of Cu_2O nanocrystals (both Cu_2O and Cu_2O-GO) are evaluated through aqueous phase glycerol conversion. Shape dependent catalytic activity of the Cu_2O nanocrystals was observed in both cases. In aqueous phase conversion of bio-derived glycerol to LA, it was observed poor activity for the glycerol conversion using the

commercially purchased Cu_2O catalyst (2.3 mol/g atom Cu/h). A three folds increase in activity was found on cCu_2O/GO (7.5 mol/g atom Cu/h) and rCu_2O/GO (6.0 mol/g atom Cu/h) catalysts. Both types of Cu_2O catalysts display similar selectivity towards the LA. The selectivity to alcohols is relatively higher by using the cCu_2O nanocatalysts. The activity of GO passivated cCu_2O-GO catalyst is significantly enhanced compared to the cCu_2O/GO nanocatalyst. The catalytic activity of cCu_2O-GO is 25 mol/g atom Cu/h, almost four fold higher than that of the cCu_2O/GO nanocatalysts.

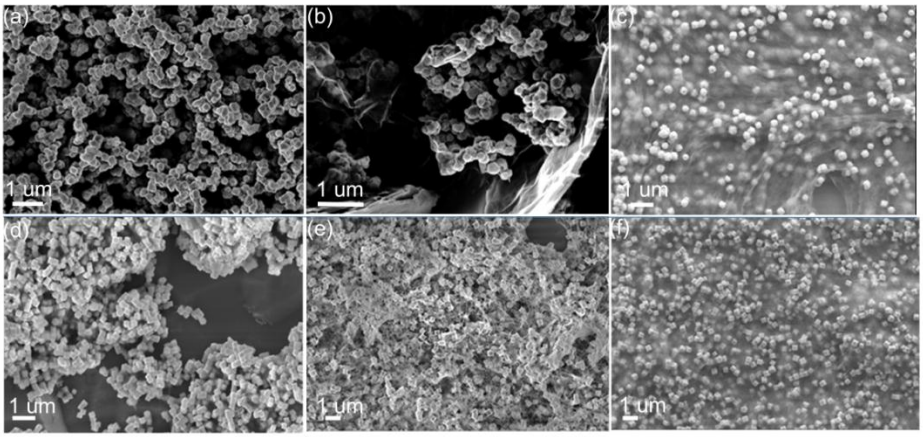

Figure 4-5-1. SEM images of (a)-(c) rCu_2O, rCu_2O/GO and hybrid rCu_2O-GO, (d)-(f) cCu_2O, cCu_2O/GO, and hybrid cCu_2O-GO (provided by Dr. Shenqiang Ren's group).

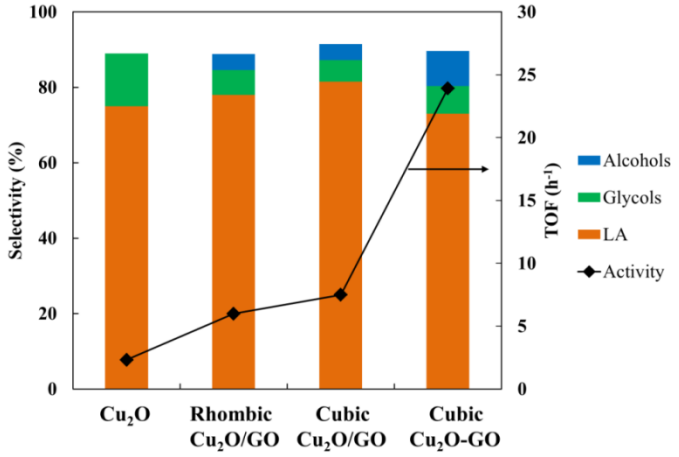

Figure 4-5-2. Activity tests of Cu_2O catalysts in catalytic conversion of glycerol to LA at 200 ^{o}C

List of Publications, Presentations and Awards

1. Publications/Manuscripts

(1) **Jin, X.**; Dang, L.; Lohrman, J.; Subramaniam, B.; Ren, S.; Chaudhari, R. V. Lattice-Matched Bimetallic CuPd Graphene Nanocatalysts for Facile Conversion of Biomass-Derived Polyols to Chemicals. ACS Nano, 2013, 7, 1309.

(2) **Jin, X.**; Roy, D.; Thapa, P.; Subramaniam, B.; Chaudhari, R. V. Atom Economical, Aqueous Phase Conversion (APC) of Biopolyols to Lactic Acid, Glycols and Linear Alcohols using Supported Metal Catalysts. ACS Sustainable Chemistry & Engineering, 2013, 1, 1453 (**Selected as Cover Page**).

(3) **Jin, X.**; Subramaniam, B.; Chaudhari, R. V. Activity and Selectivity of Bimetallic Catalysts for Polyols Hydrogenolysis. ACS Symposium Series 1132. American Chemical Society: Washington, DC, 2013; pp 273–285.

(4) Hong, C.; **Jin, X.**; Harak, E.; Totleben, J.; Lohrman, J.; Subramaniam, B.; Chaudhari, R.V.; Ren, S. Shape-Selective Cu_2O on Graphene as Hybrid Nanocatalysts. Journal of Materials Chemistry A, 2014 (accepted).

(5) Chaudhari, R.V.; Torres, A.; **Jin, X.**; Subramaniam, B. Multiphase Catalytic Hydrogenolysis/Hydrodeoxygenation Processes for Chemicals from Renewable Feedstocks: Kinetics, Mechanism & Reaction Engineering. Industrial & Engineering Chemistry Research, 2013, 52, 15226.

(6) **Jin, X.**; Thapa, P.; Subramaniam, B.; Chaudhari, R. V. Tandem Dehydrogenation and Hydrogenolysis of Polyols on Pt/C Catalysts: Reaction Mechanism and Kinetic Modeling. (In preparation)

(7) **Jin, X.**; Thapa, P.; Subramaniam, B.; Chaudhari, R. V. Hydrogenolysis of Sugar-Derived Polyols to Value-added Chemicals on Bi-Functional Cu Catalysts. (In preparation)

(8) Chaudhari, R. V. *et al*. 2012. Synergistic Nanocatalysts Using Cu-based Monometallic and Bimetallic Nanocrystals on Graphene Support. (invention disclosed to university)

(9) Chaudhari, R. V. *et al*. 2012. Catalytic conversion of sugars and sugar alcohols to lactic acid and glycols. (invention disclosed to university)

2. Conference oral presentations (presenting author)

(1) **Jin, X.**; Thapa, P.; Subramaniam, B.; Chaudhari, R. V. "Tandem Dehydrogenation/Hydrogenolysis of Bio-Derived Polyols to Valuable Chemicals on Pt/C Catalyst: Catalysis and Kinetic Studies". AIChE Annual Meeting, Nov. 2013 in San Francisco, CA.

(2) **Jin, X.**; Dang, L.; Lohrman, J.; Subramaniam, B.; Ren, S.; Chaudhari, R. V. "Graphene Supported Cu Nanocatalysts for Conversion of Bio-mass Derived Polyols to Chemicals". 23rd North American Catalysis Society Meeting, Jun. 2013 in Louisville, KY.

(3) **Jin, X.**; Subramaniam, B.; Chaudhari, R. V. "Kinetic Modeling of Hydrogenolysis of Sugar Based Polyols using a Bimetallic Ru-Re/C Catalyst in a Slurry Reactor". 3rd North American Symposium on Chemical Reaction Engineering, Mar. 2013 in Houston, TX.

(4) Chaudhari, R. V.; Torres, A.; **Jin, X.**; Subramaniam. B. Multiphase Catalytic Processes for Renewable Feedstocks to Chemical Intermediates: Kinetics, Mechanism and Reaction Engineering. 3rd North American Symposium on Chemical Reaction Engineering, Mar. 2013 in Houston, TX.

(5) **Jin, X.**; Subramaniam, B.; Chaudhari, R. V. "One Pot Conversion of Bio-derived Polyols to Lactic Acid". AIChE Annual Meeting Oct. 2012 in Pittsburgh, PA.

(6) **Jin, X.**; Roy, D.; Subramaniam, B.; Chaudhari, R. V. "Activity and Selectivity of Bimetallic Catalysts for Polyols Hydrogenolysis". ACS 243rd National Meeting, Mar. 2012 in San Diego, CA.

(7) **Jin, X.**; Subramaniam, B.; Chaudhari, R. V. "Activity and Selectivity of Bimetallic Catalysts for C_5 and C_6 Polyols Hydrogenolysis". AIChE Annual Meeting, Oct. 2011 in Minneapolis, MN.

(8) **Jin, X.**; Subramaniam, B.; Chaudhari, R. V. "One-pot Conversion of Sugars and Sugar Alcohols to Value-Added Chemicals". CEBC Industrial Advisory Board (IAB) Meeting, Oct. 2011 in Lawrence, KS.

3. Poster presentations

(1) **Jin, X.**; Subramaniam, B.; Chaudhari, R. V. "Making Renewable Chemicals from Biomass-Based Polyols by An Efficient Process". KU Center for Technology

Commercialization Innovation Fair, Apr. 2013 in Lawrence, KS.

(2) **Jin, X.**; Subramaniam, B.; Chaudhari, R. V. "Making Renewable Chemicals from Biomass-Based Polyols by An Efficient Process". 3rd Annual KU Energy Conference, Apr. 2013 in Lawrence, KS.

(3) **Jin, X.**; Dang, L.; Lohrman, J.; Subramaniam, B.; Ren, S.; Chaudhari, R. V. "Synthesis of Lactic Acid From Glycerol by Highly Cu-based Nanocatalysts". ACS Wakarusa Valley Symposium, Oct. 2012 in Lawrence, KS.

(4) **Jin, X.**; Subramaniam, B.; Chaudhari, R. V. "Atom Efficient Conversion of Biopolyols to High Value Chemicals: Part I and Part II". CEBC-IAB Meeting, Oct. 2012 in Lawrence, KS.

(5) **Jin, X.**; Dang, L.; Lohrman, J.; Subramaniam, B.; Ren, S.; Chaudhari, R. V. "2-D Cu Nanoclusters on Graphene as Remarkable Catalysts for Polyols Conversion". CEBC-IAB Meeting, Oct. 2012 in Lawrence, KS.

(6) **Jin, X.**; Subramaniam, B.; Chaudhari, R. V. "Hydrogenolysis of Polyols over Cu/Hydrotalcite Catalysts to Value-added Chemicals: A New Multifunctional Catalyst". 15th International Congress on Catalysis Jul. 2012 in Munich, Germany.

(7) **Jin, X.**; Dang, L.; Lohrman, J.; Subramaniam, B.; Ren, S.; Chaudhari, R. V. "Synthesis of Lactic Acid from Glycerol by Highly Cu-based Nanocatalysts". CEBC-IAB Meeting, Apr. 2012 in Lawrence, KS.

(8) **Jin, X.**; Subramaniam, B.; Chaudhari, R. V. "Catalytic Conversion of Sugars & Polyols to Lactic acid: Reaction Pathways". CEBC-IAB Meeting, Apr. 2012 in Lawrence, KS.

(9) **Jin, X.**; Subramaniam, B.; Chaudhari, R. V. "An Energy Efficient Route to Synthesizing Lactic Acid from Bio-based Sugars". 2nd Annual KU Energy Conference, Apr. 2012, in Lawrence, KS.

(10) **Jin, X.**; Subramaniam, B.; Chaudhari, R. V. "One-pot Conversion of Sugars and Sugar Alcohols to Value-Added Chemicals". CEBC-IAB Meeting, Oct. 2011 in Lawrence, KS.

(11) **Jin, X.**; Subramaniam, B.; Chaudhari, R. V. "Hydrogenolysis of Bio-Derived C_5 and C_6 Polyols with Bimetallic Catalysts". CEBC-IAB Meeting, Apr. 2011 in Lawrence, KS.

4. Awards

- **State-Sponsored Scholarship**
  China Scholarship Council (2009~2013)
- **Richard J. Kokes Award**
  North American Catalysis Society (2013)
- **Young Researcher Travel Award**
  North American Symposium on Chemical Reaction Engineering (2013)
- **Outstanding Teaching Assistant Award**
  Chemical & Petroleum Engineering Department, University of Kansas (2013)
- **Graduate Student Scholarship**
  University of Kansas (2009)
- **ACS Wakarusa Valley Student Research Symposium Award**
  American Chemical Society Wakarusa Valley Chapter (2012)
- **Graduate Scholar Presentation Travel Fund**
  University of Kansas Center for Research (2012)
- **2012 Energy Conference Best Poster Award**
  University of Kansas
- **2013 Energy Conference Best Poster Award**
  University of Kansas
- **3rd place in School of Engineering poster competition**
  School of Engineering, University of Kansas (2013)